A Finite Element Study of the Stress Distribution around Mechanical Fasteners in Composite Laminates

by

Matthew John Podbury

A dissertation submitted for the degree of Doctor of Philosophy in the Faculty of Engineering, University of London

Department of Mechanical Engineering
University College London

January 2002

ABSTRACT

A major concern when designing structures with polymer based composite laminates is the stress concentration developed around mechanically fastened joints. As composite laminates behave anisotropically, the design procedures available for metallic joints are not applicable, and hence a comprehensive guide for designing with these materials must be developed.

Experimental evaluation of joint strength is the most accurate, however, to provide a range of data for every joint configuration is both time consuming and very expensive. With the advent of powerful computers at relatively low cost and more sophisticated software tools, numerical methods have become more desirable in predicting the stress distribution and with appropriate failure criteria can provide accurate strength prediction.

In this study, commercially available finite element software was used to perform a three-dimensional stress analysis on mechanically fastened composite laminate double-lap joints. To enable accurate ply and inter-laminar stress prediction, a replica technique was adopted, whereby the material properties in each element were oriented according to the stacking sequence used. The model was developed so that the bolt assembly could be simulated accurately, by creating a mesh for each individual component, allowing contact to be modelled at every interface. A bolt preload was provided by applying an appropriate temperature drop to a beam element within the bolt shank.

The initial study concentrated on a single bolt composite laminate double lap joint, whereby the effects of clamping preload, bolt/hole clearance, bolt elasticity, laminate elasticity and stacking sequence, on the stress distribution in the vicinity of the fastener were analysed. The investigation was then continued by varying the outer diameter and stiffness of the washer and subsequently using these results to develop a multi-fastener model.

The results showed good agreement with previously published work and provide engineers with valuable guidance when designing mechanically fastened double lap joints of this type.

ACKNOWLEDGEMENTS

I would like to express my sincere gratitude to my supervisors Dr. Alvin Blackie and Dr. Kevin Drake for their valuable suggestions, guidance and encouragement throughout my study. I would also like to thank my family for their love, encouragement and support throughout my time at UCL.

I also gratefully acknowledge the financial support provided by the Engineering and Physical Sciences Research Council during my postgraduate time at UCL.

Finally, I would like to thank staff in the department of Mechanical Engineering, especially Mr. Phil Jeavons, Mr. David Bevan and the computer system manager Mr. Mark Iline for their help with the computer hardware and software.

CONTENTS

LIST OF TABLES

LIST OF FIGURES

Figure | **Title** | **Page**

NOMENCLATURE

Abbreviations and Acronyms

2D	two-dimensional
3D	three-dimensional
CFRP	carbon fibre reinforced polyester (or plastic)
d.o.f.	degree of freedom
FEA	finite element analysis
FEM	finite element model
GRP	glass fibre reinforced polyester (or plastic)
KFRP	Kevlar (aramid) reinforced polyester (or plastic)
RVE	representative volume element

Roman Symbols

C	experimentally derived parameter for determining the critical distance
c_a, c_b	circular plate coefficients
d	hole diameter
d_0	critical distance
d_{bo}	pin/bolt shank diameter
d_w	washer outside diameter
D	plate stiffness
$\mathbf{D}$	nodal displacement matrix
e	end distance (from centre of hole to edge of the laminate)
$\mathbf{e_1}$	unit vector parallel to the hitting surface in contact formulation
$\mathbf{e_2}$	unit vector parallel to the hitting surface in contact formulation
E	modulus of elasticity
F	force applied
F_a	axial force on beam element
F_{12}	interaction coefficient between two normal stresses
G	shear modulus
I	second moment of area
$\mathbf{K}$	structure stiffness matrix

k	torque coefficient
l_a, l_b	circular plate loading coefficients
L	laminate length
L_w	load on the washer
m	experimentally derived parameter for determining the critical distance
m	the last node layer for each laminate
n	the last node around the hole boundary
$\mathbf{n}$	normal vector, perpendicular to hitting surface
p	pitch distance (from centre of one hole to centre of the next)
p_e	penetration
p_{e0}	initial penetration
p_w	washer pressure
r, θ	polar co-ordinates
r_0	point of application of washer load
$\mathbf{R}$	structural load matrix
R	interlaminar shear strength
R_s	strength ratio
s	row spacing
S	in-plane shear strength
S_γ	allowable shear strain
t	laminate thickness
$\mathbf{t}$	tangential traction
t_n	contact pressure
$\mathbf{t_t}$	in-plane friction traction
t_w	washer thickness
T	bolt torque
$\mathbf{u_H}$	motion of hitting point
$\mathbf{u_t}$	tangential displacement
$\mathbf{u_T}$	motion of target point
w	laminate width
x, y, z	cartesian co-ordinates
X	lamina longitudinal strength

$X_{\varepsilon c}$, $X_{\varepsilon t}$	allowable compressive and tensile strain, respectively
Y	lamina transverse strength
$Y_{\varepsilon c}$, $Y_{\varepsilon t}$	allowable transverse compressive and tensile strain, respectively
Z	interlaminar normal strength

Greek Symbols

δ_{wz}	washer through thickness deflection
Δ	increment
ε	normal strain
ϕ	contact function
γ	shear strain
λ	clearance ratio
μ	coefficient of friction
ν	Poisson's ratio
σ	normal stress component
τ	shear stress component
$\Delta\xi$	magnitude of relative slip increment

Subscript

b	bearing
c	compressive
s	symmetric
t	tensile
x, y, z	global direction
1, 2, 3	material principle direction

n (representing an integer in e.g. $(0_n/90_n)$) number of plies in a particular direction

CHAPTER ONE

INTRODUCTION

1.1 – BACKGROUND

Composite materials are generally defined as a combination of two or more constituent materials and usually exist in the form of high strength polymer fibres set in a thermoplastic or thermoset resin matrix, although nowadays composite materials can be very much more diversified. The matrix exists simply to bind or support the reinforcing fibres, however, in unidirectional composites it also affects the properties in the transverse direction. In order to obtain specific material properties the constituent materials are chosen so that the benefits of each are combined in the composite, however, the resultant properties can also depend on other factors, such as the volume ratio of each constituent, the process by which the material is formed and the direction of fibres within the matrix. Hence designing a component utilising a composite material can be very complex.

With fibre reinforced composites short discontinuous or long continuous fibres may be used. Short fibres are usually randomly distributed within the matrix material to create chopped strand mat composite sheets, which behave essentially planar isotropically. Continuous fibres can be pultruded in a single direction or woven before applying the resin matrix, however the material properties are generally orthotropic. The anisotropic nature of these composites can make prediction of failure in composite materials very difficult and catastrophic failure can result in-service. In order to overcome the anisotropic nature of composites consisting of continuous fibre sheets, laminates can be constructed by joining several layers of orthotropic pultruded sheets at different orientations to one another, thus overall isotropic material properties can be simulated (quasi-isotropic).

Recently, as confidence in the reliability of composites has increased, engineers have been able to utilize composite materials more in the construction, aircraft and automobile industries and can, therefore, fully utilise the many advantages that these materials offer over metals, such as those listed in Table 1.1. As well as the high strength to weight ratio, one other major advantage is that structures can often be moulded easily to the finished shape with 'tailored' properties, however, there is still a need for joints to be included in the design of many structures. This is necessary when structures are too complicated to mould in one stage or when components of the structure need to be inspected or renewed at regular intervals.

Table 1.1 – Possible advantages and disadvantages of using composites

Advantages	Disadvantages
- High strength to weight ratio - Can be moulded easily to the required shape - Can reduce the number of components - Can tailor properties to suit application - Resistant to corrosion - Can provide thermal insulation - Can provide electrical insulation - Non magnetic	- Manufacturing without defects can be difficult - Strength depends heavily on manufacturing procedure - Can be elastic to failure which makes failure more difficult to predict - Anisotropy can make it difficult to predict failure

When joints must be included in a structure consisting of composite plates or panels several options are available to the engineer, the method adopted however depends upon the application. Components are normally joined using either mechanical methods or by adhesive bonding, but a combination of these methods may also be used. Both mechanical fastening and bonding possess their own advantages and disadvantages, as summarised in Table 1.2.

The main reason why adhesive joints are preferred over mechanically fastened joints is that they possess less of a stress concentration than the latter and, therefore, can be very strong under tension in comparison to mechanically fastened joints. However, there are major drawbacks with using adhesives in that perfect surface preparation is required for maximum strength and, more importantly, the components cannot be easily disassembled for inspection and replacement. Therefore, for structures such as aircraft wings, where inspection is mandatory, joining sections or panels is restricted to mechanical fastening.

Table 1.2 – Advantages and disadvantages of mechanically fastened and adhesive joints

	Advantages	Disadvantages
Bonded Joints	- Less stress concentration - Can provide smooth external surfaces - No weight penalty - Low cost - Can join very thin and complex shaped parts	- Cannot be disassembled easily - Strength depends upon surface preparation - Poor peel strength - Joint can be sensitive to environmental effects - Potential for creep - Some materials may not be bonded
Mechanically-Fastened Joints	- Can be disassembled for repair - Any material combination may be joined - Joints are not sensitive to environmental conditions - Easy joint preparation	- High stress concentrations exist at the hole edge - Possibility of galvanic corrosion - Hole generation may damage composites - Increase in weight - Increase in cost

Invariably with mechanically fastened joints the load is transferred through standard fasteners such as pins, rivets, screws or bolts, constructed using either a double lap or single lap arrangement, as detailed in Figure 1.1. Single lap joints are susceptible to transverse bending of the laps when the joint is under tension, making them weaker (Smith et al., 1986) and the failure of the joint more difficult to predict. With double lap joints, the load distribution and deflection of each lap is more uniform with the joint likely to fail in one of the ways detailed in Figure 1.2 or possibly through a combination of mechanisms. The mode by which failure occurs in a particular joint can be complex as it depends on parameters such as laminate lay-up, material properties and geometry of the joint (Hart-Smith, 1980).

In practice the more common mode of failure is one of bearing, where failure gradually occurs in a ductile manner. All of the other modes are more difficult to predict as they often occur catastrophically with little or no apparent external damage before final fracture. Hence, it is for this reason that engineers would usually design the joint so that bearing becomes the dominant mode of failure.

When using composite components engineers are therefore faced with many problems. They must be able to design joints which fail without catastrophic consequences by considering the fibre orientation or laminate lay-up as well as joint geometry, and they must also aim to reduce the stress concentration inherent with mechanically fastened joints and, thereby, improve the overall joint strength.

1.2 – DESIGN METHODS

Although experimental testing of joints provides more reliable data than any numerical analysis, to produce a thorough database of composite joint properties a large quantity of specimens would be required. Specimen quality testing would also have to be carried out before any tension or flexure testing to ensure reliability of the test data. This whole process then becomes very laborious and expensive. It is also very difficult to decide exactly where damage initiation occurs through the thickness of the specimens. As a consequence it is difficult for such studies to give guidelines on the type of joint, material or material stacking sequence necessary for a given application.

Two dimensional finite element analysis has been found to give reasonable agreement with experimental data for axial strain along the bearing plane (Eriksson, 1986), however, no stresses can be determined in the through thickness direction since average material properties are given to the model, rather than modelling the specific properties of each individual lamina, which is commonly known as replica modelling.

It is for these reasons, therefore, that many researchers are making the move towards the more comprehensive three-dimensional finite element analysis. Although this analysis is so much more complex, giving rise to extensive use of computational resources and time, a thorough stress analysis of composite joints can be carried out, as the interlaminar shear and through thickness stresses can be determined, so that a more realistic strength prediction can be made, once appropriate failure criteria have been applied.

1.3 – OBJECTIVES

The main objective of this study is to approach the optimum design of a mechanically fastened composite joint by conducting a more realistic and comprehensive stress analysis than has previously been reported. The stress results, together with a predicted failure index, derived using appropriate failure theories, will be used to provide valuable guidance for engineers when designing these types of joints.

1.4 – THESIS STRUCTURE

A review of recent work on mechanical fastened laminates, providing relevant details, is given in chapter two. The chapter is divided into an experimental section, which provides guidance to geometrical ratios and material combinations that should be used for joining composites, and an analytical section which provides details of accurate simulation techniques and an insight into the stress distribution in the joint/fastener as well as failure strength prediction.

Chapter three provides a brief overview of the finite element method, which has been used throughout the investigation, as well as details of the contact analysis incorporated in the I-DEAS (1993/1999) software.

Chapter four details the three-dimensional modelling technique used throughout the investigation and includes validation of the modelling technique by comparison with previously published work of Chutima (1996). Excellent agreement was found in this comparison, which provided confidence in the technique adopted in this study and hence the subsequent derived results.

A more realistic method of applying clamping preload than used previously is detailed in chapter five. The effects of changing the clamping preload, fastener elasticity, laminate elasticity, fastener/hole clearance and laminate stacking sequence on the stress distribution and failure are also reported.

An investigation into the effects of changing the washer material and size on the stress distribution and failure, while keeping the clamping pressure constant or the bolt torque constant, is detailed in chapter six.

The analysis was then applied to modelling multiple fastener joints and, thereby, to investigate the interaction between fastener assemblies. The details of this analysis are presented in chapter seven.

Finally, further discussion as well as overall conclusions from the work presented in this study, along with recommendations for further research are provided in chapter eight.

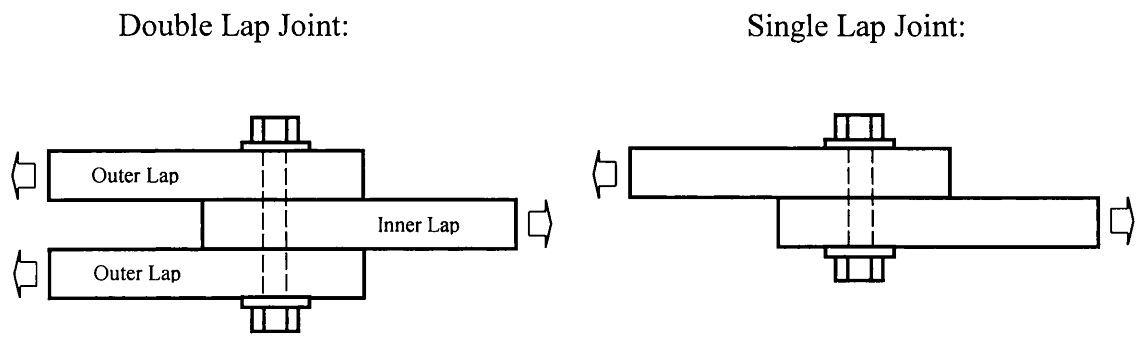

Figure 1.1 – Double lap and single lap joint configurations

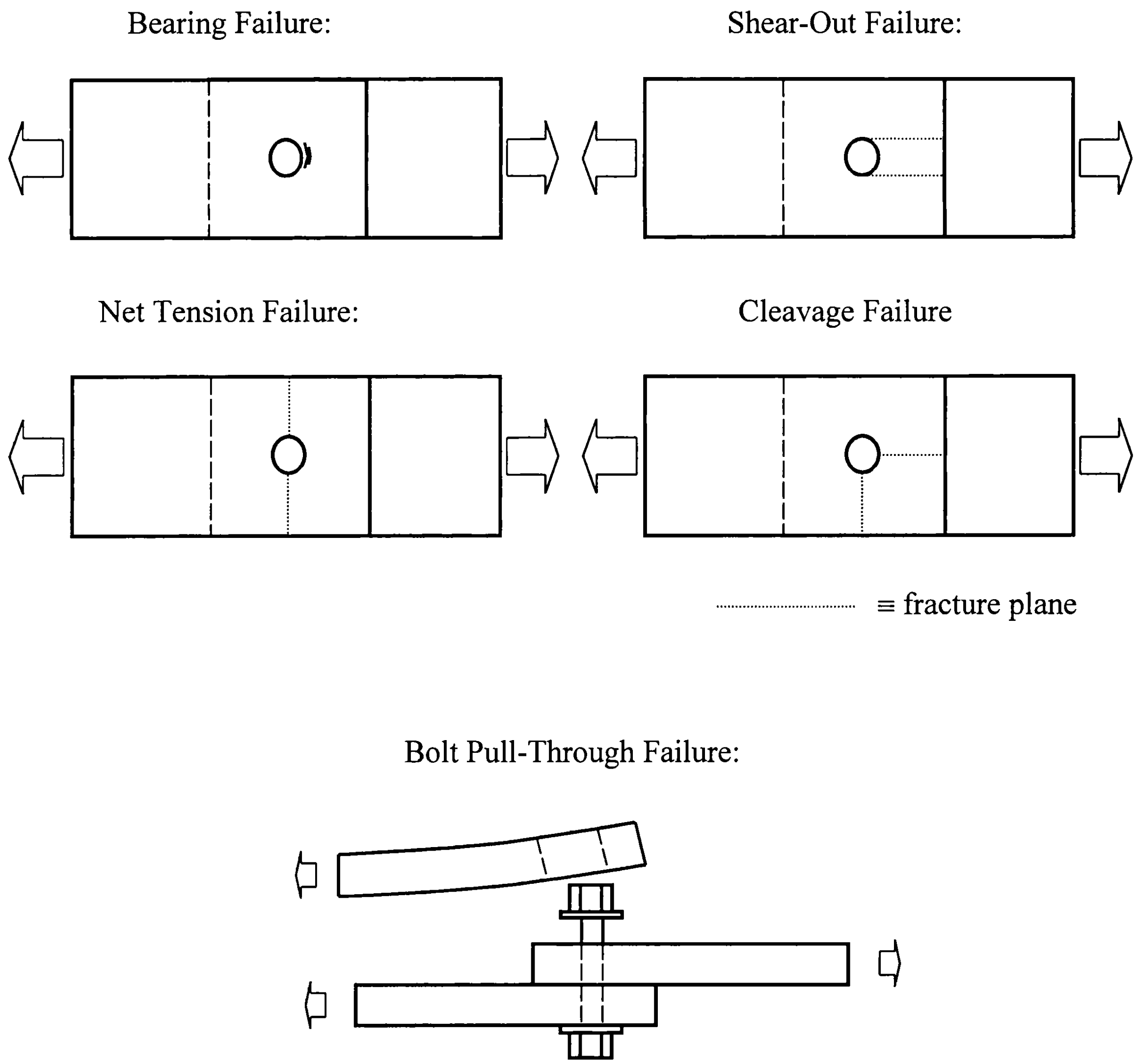

Figure 1.2 – Five possible failure modes of a mechanically fastened double lap joint

CHAPTER TWO

LITERATURE REVIEW

2.1 – INTRODUCTION

In order to approach the optimum design of a bolted joint in composite materials a vast amount of effort has been expended to date. The most accurate means of deriving joint strength is obviously through experimental evaluation, although this method of testing can be very expensive due to the size of possible combinations of material and geometrical parameters. Also estimating the stress distribution within the joint is very difficult. To overcome this engineers have adopted analytical and numerical methods such as the finite element method, in order to simulate the bolted joint geometries under load, with experimental data being used to validate sample results. Initial studies were conducted using two-dimensional modelling, although it is clear that three-dimensional finite element analysis is required for the most accurate simulation of joint strength, due to the complexity of the stress distributions. This chapter is therefore broken down into the two sections: experimental studies and analytical investigations, of mechanically fastened composite laminates.

2.2 – EXPERIMENTAL STUDIES

This section provides details of relevant experimental work carried out to date and describes important conclusions drawn from each investigation. In the main the results reported in sections 2.2.1 to 2.2.3 relate to work undertaken using double lap single fastener joints.

2.2.1 – Effects of laminate parameters

When designing a laminate composite joint the engineer must decide how the laminate should be constructed. There is a vast range of materials available for the reinforcing fibres and matrix systems that can be used to manufacture an individual lamina. The stacking sequence or angle of each lamina must then be chosen before completing the laminate. The following conclusions drawn from previous experimental work will thus be broken down into investigations concerned with fibre material and stacking sequence.

2.2.1.1 – Fibre material

In an early investigation, Matthews et al. (1982a) examined the effect of clamping pressures on the failure of carbon fibre and glass fibre laminates, as well as hybrid carbon and glass laminate composite joints with finger tight clamping. In terms of bearing strength the all carbon laminate joints were found to exhibit the highest strength followed by the all glass composite, with the hybrids being weakest.

In a subsequent study, Kretsis and Matthews (1985) also used CFRP and GRP laminate in single bolt joints with low clamping pressures and concluded that less delaminations were produced when using CFRP rather than GRP laminates. Oh et al. (1997) also carried out a similar analysis and confirmed the work of Kretsis and Matthews (1985), whereby the area of the laminate between the hole and the edge deformed considerably out of plane, due to the low modulus of the glass epoxy composite.

Ger et al. (1996) compared the dynamic and quasi-static strength of carbon/kevlar hybrid laminates with pure carbon laminates in a double lap joint configuration. Despite the difference in fibre moduli it was determined that the different laminates resulted in comparable strengths, and that dynamic loading weakened the joint slightly compared to static loading.

Other investigations have involved assessing the influence of joint geometry on performance and have incorporated different composite types in the studies, however, the effects attributed to the latter have not been thoroughly investigated.

2.2.1.2 – Stacking sequence

The stacking sequences used in a composite joint are considered to be of great interest, as they can significantly affect the stress distribution and hence failure mode and strength.

Hart-Smith (1978) concluded that even with specimens in which the fastener was located at a significant distance from the end of the laminate, shear-out failure occurred for highly orthotropic 0° laminates.

Collings (1982) tested clamped CFRP laminated single bolt joints under compression and came to the conclusion that the highest bearing strength was achieved with laminates consisting of 75% of ±45° plies in both (0/±45) and (90/±45) lay-ups, and 75% of 0° plies in (0/90) cross-ply laminates.

Eriksson (1990) also used CFRP laminates but tested joints under tension as well as compression to demonstrate that laminate lay-up significantly affected joint strength. He concluded that the highest bearing strength was reached with a high proportion of fibres aligned with the longitudinal axis, although laminates containing a high proportion of ±45° fibres exhibited near comparable strength. For toughened CFRP laminate joints the effects of fibre alignment were reversed.

Andreasson et al. (1998) measured bolt displacement as well as in-plane strains on the net tension and bearing planes of woven CFRP laminates under finger tight clamping. The quasi-isotropic laminate joints were found to exhibit higher bearing strengths than cross-ply laminate joints. Wang et al. (1996) also confirmed that quasi-isotropic specimens exhibited higher bearing strengths than cross ply CFRP joints, and concluded that by placing layers of 90° fibres on the outside of the laminate, e.g. $(90/\pm45/0)_s$, rather than 0° fibres, the bearing strength was maximised. This is because 0° plies on the surface lead to splitting, hence the plies break away from the laminate under bearing conditions.

Oh et al. (1997) determined that the bearing strength of their single bolt carbon and glass hybrid joint increased when ±45° plies were distributed evenly in the thickness direction, irrespective of the ratio of glass epoxy to carbon epoxy and the stacking pattern.

Turvey (1998) investigated the angle of pultrusion on joint strength with the end distance, e, to hole diameter, d, (shown in Figure 2.1), ratios between three and eight

($3 \leq e/d \leq 8$), and laminate width, w, to hole diameter of between four and ten ($4 \leq w/d \leq 10$). For each pultrusion angle tested the failure mode remained tensile, although the angle of crack propagation varied for each laminate.

The effects of stacking sequence on joint strength of single pinned double lap joints were investigated by Quinn and Matthews (1977). The GRP laminates were constructed using quasi-isotropic layups. It was concluded that the failure mode was dependent upon the stacking sequence and that by having 90° plies near the outer surface caused an improvement in the bearing strength.

Hamada et al. (1995) carried out a similar analysis using single pinned CFRP quasi-isotropic laminate joints. They also concluded that stacking sequence had a large influence upon bearing strength. From this work it was determined that the highest bearing strength was realised when the 0° plies were placed on the outer surfaces, with the 90° plies next to these and ±45° plies interspersed in the centre. This conclusion differs slightly to the findings of Wang et al. (1996).

2.2.2 – Effects of fastener parameters

The fastener configuration can also alter the joint strength quite significantly. To a varying degree, clearance exists at the fastener/hole interface to allow for insertion, which can affect the contact between hole and fastener and hence bearing strength. The material selected for the fastener can alter the friction and bending, hence also change the joint strength. The main concern for the engineer, though, is whether a pinned or clamped fastener is used, and whether the fastener should be a rivet, a protruding head bolt or a countersunk bolt, depending upon design limitations and resultant strength. A large number of experimental investigations have been conducted to examine the effects of these parameters and the conclusions drawn from these studies are detailed below.

2.2.2.1 – Clearance

The effects of clearance between the fastener and hole were investigated by Prabhakaran and Naik (1987), and Parida et al. (1997). Prabhakaran and Naik tested single pinned double lap quasi-isotropic CFRP joints under tension. They concluded, using a fibre optic technique, that when a small clearance existed the contact angle increased non-linearly with increasing load. Parida et al. used single and double lap joints with finger tight clamping and concluded that clearance did not significantly influence the joint strength.

Recently, Tong (2000) investigated the effects of clearance (up to 0.65mm) between the washer and bolt shank on joint strength. It was concluded that initial failure loads can be smaller when a clearance exists, however, the ultimate failure loads remained unaffected.

2.2.2.2 – Friction

Lucking (1990) used single bolt CFRP joints designed for bearing failure to investigate the effects of friction at the washer-laminate interface on bearing strength. It was concluded that higher friction changed the failure mode from bearing to tension. With a type of washer that induced less friction the strength increased with clamping pressure, with the joint failing in bearing only, however, the maximum strength was obtained with higher friction clamping.

2.2.2.3 – Fastener elasticity/type

Erki (1995) investigated the effects of bolt elasticity on laminate joint strength. In this study pultruded GRP laminate single bolt joints were tested with a small clearance at the fastener/hole interface. It was shown that the GRP fasteners failed before the laminates and that for steel bolts with clamping preload the failure mode was a combination of tensile and cleavage.

Whitworth (1998) used CFRP quasi-isotropic laminates joined with preloaded titanium and graphite/thermoplastic fasteners, and demonstrated that fastener elasticity did not significantly influence the bearing strength of a single bolt joint under tension.

This was also supported by the work of Parida et al. (1997) in their investigation on single and double lap joints with finger tight clamping. However, a slight improvement in strength was apparent when using steel rather than titanium alloy fasteners.

The effects of bolt type was investigated by Packman et al. (1993) where protruding head bolts were compared to countersunk bolts for single lap CFRP joints. In this study, the countersunk bolted joints were found to be the weakest.

2.2.2.4 – Fastener clamping/preload

Many experimental studies have investigated the effects of clamping upon the joint strength of double lap single bolt joints. Morgan and Beckwith (1985) demonstrated in their investigation of a single bolt composite joint that by introducing bolt torque the bearing strength increased. This was corroborated by Whitworth (1998) in his investigation of quasi-isotropic CFRP laminate single bolt joints under tension. He also determined that a fully tightened titanium bolt improved the fatigue life considerably.

Eriksson (1990) also determined that clamping significantly affected the joint strength, following an investigation of CFRP single bolt joints under both tension and compression. A clamping torque of 5.4 Nm increased the bearing strength by 2.4 times that of the simply pinned case, and by 1.5 times that of the finger tightened (0.6Nm torque) case, although the increase in strength was slightly reduced when using toughened CFRP laminates.

Collings (1982) investigated a clamped CFRP laminated single bolt joint under axial compression loading. A clamping torque of 3.4Nm was found to give better bearing strength than finger tightened bolts or simple pinned joints.

Cooper and Turvey (1995) used GRP single bolt joints, where the clamping pressure was applied using plates instead of washers, as recommended by Abd El Naby and Hollaway (1993a). The clamping pressure associated with a bolt torque of 3Nm was shown to increase the bearing failure load by 45% compared to the pinned case, while a 30Nm torque increased the failure load by approximately 80%. At low e/d and w/d ratios failure loads only increased slightly with increased torque. An increase in torque was also shown to increase the critical ratios, i.e. where mode of failure changes.

Akay and Kong-Ah-Mun (1995) investigated the effects of clamping on the strength of woven KFRP laminate joints. By finger tightening the bolt to a torque of approximately 0.2Nm, the bearing strength was found to increase by 100%, with a further increase in torque only slightly improving the bearing strength. They also showed that bolt clamping could produce a transition of failure mode from one of localised bearing failure to remote bearing or tensile modes. This effect was also shown by Lucking (1990), using a CFRP single bolt joint, where finger tight clamping and a clamping torque of 10.5Nm gave bearing failure under the washer, while a torque of 21Nm gave bearing failure outside the washer. A bolt torque of 31.5Nm and higher produced catastrophic failure through cleavage mechanisms.

In an earlier investigation Stockdale and Matthews (1976) conducted tests using (0/90) GRP composite double lap joints under tension and showed that failure load increased with increasing clamping pressure as well as washer contact area. It was suggested that the increase in failure load was not solely attributed to the friction but also to the suppression of out of plane deformations. At high clamping loads failure was found to occur from cracks at the hole boundary as well as compression at the washer edge.

Kretsis and Matthews (1985) carried out a similar analysis using GRP and CFRP laminates constructed from various stacking sequences. From this work it was found that shear cracks which initiated under the washer could not expand due to the clamping pressure, however, at the washer edge, where out of plane deformation could not be suppressed, delaminations occurred.

Wang et al. (1996) investigated the response of CFRP single bolt joints with low clamping pressures. They came to the conclusion that out of plane deformation occurs due to out of plane shear cracks and delaminations when the joint is simply pinned. When clamping was applied the bearing strength was shown to increase, as the shear cracks under the washer grew away from the hole rather than towards it, hence no delaminations formed. As the torque was increased further shear cracks under the washer were suppressed and the damage occurred at the washer edge, where shear cracks developed and propagated to the free edge of the laminate, an observation which confirmed the earlier work of Kretsis and Matthews (1985).

Oh et al. (1997) tested GRP, CFRP and hybrid composite joints under finger tight and clamped conditions in their investigation. Damage development and delaminations were found using C-scans and fracture surface inspection. Delaminations under the washer were found to develop first, with damage then occurring outside the washer edge. The bearing strength was found to increase with clamping pressure up to 71.1MPa, where the joint strength reached a maximum which was maintained as the clamping pressure increased further.

Packman et al. (1993) used single lap CFRP joints to demonstrate that joint strength improved with clamping pressures. The strength was found to improve when the clamping torque was increased from 1.13Nm to 4.52Nm, however, increasing the torque further to 8.47Nm, showed no significant increase in joint strength.

In addition to the studies confirming the beneficial effects of bolt clamping, Kallmeyer and Stephens (1997) found that an increase in bolt clamping torque decreased the creep rate associated with hole elongation of quasi-isotropic CFRP laminate joints.

2.2.3 – Effects of joint geometry

2.2.3.1 – End distance

The end distance, e, shown in Figure 2.1 and described as the distance between the centre of the hole and the end of the laminate, was considered an important parameter to investigate by many authors, as early work had shown the ratio of end distance to hole diameter significantly influenced the mode of failure and hence joint strength. As a consequence there are numerous reports of the minimum ratios of e/d to ensure bearing failure and high joint strength.

Rosner and Rizkalla (1995) used double lap joints with GRP laminates connected via a single pin in their study. The joint strength was found to improve when e/d increased to approximately 5. This work also showed that bearing failure gave more ductile behaviour than failure through tensile or shear-out mechanisms.

Matthews et al. (1982a) varied the end distance in their analysis of (0/90) cross-ply GRP laminate single bolt joints with low clamping pressures. This study showed that the maximum strength was obtained with the ratio of $e/d \geq 5$, as did the work of Turvey (1998) in an investigation into the effect of pultrusion angle on joint strength in single fastener configurations.

Kretsis and Matthews (1985) tested GRP and CFRP bolted laminates and supported earlier observations that maximum strength was obtained with $e/d \geq 5$ for cross-ply laminates, while in the case of quasi-isotropic laminates, the ratio of e/d should be greater than 3.

Cooper and Turvey (1995) tested pultruded GRP single bolt joints with low clamping pressures and recommended a ratio of $e/d \geq 3$ for maximum strength. Abd El_Naby and Hollaway (1993a) conducted tests on a similar material with the same joint configuration, but suggested a ratio of $e/w \geq 2$ for maximum strength, where w is the laminate width as shown in Figure 2.1. The former observation is apparently supported by Akay and Kong-Ah-Mun (1995) who recommended the ratio of $e/d > 3$ for optimum bearing strength of woven KFRP laminates under low clamping pressures.

Double lap joints and single lap joints were investigated by Smith and Pascoe (1985) and Smith et al. (1986), respectively, which were constructed using orthotropic cross-ply laminates with a 5.6Nm bolt clamping torque. In the former study, the ratio of e/d was varied between one and six, with the largest ratio tested resulting in the highest bearing strength. In the latter study, the ratio of e/d was varied between one and eight with the highest bearing strength obtained with an e/d ratio of 6, however, a reduction in strength was observed compared to the double lap joints due to plate bending.

Parida et al. (1997) carried out a similar analysis, using single and double lap CFRP joints with finger tightened bolts. The work concluded that the ratio of $e/d = 4$ provided the best bearing strength. In this work it was also apparent that single lap joints exhibited more non-linearity in their stress-strain response than the double lap joints, while also showing a reduction in strength. In a similar study, Packman et al. (1993) also showed that an increase in joint strength occurred as the ratio of e/d increased from 1 to 3.

2.2.3.2 – Laminate width

The width of the laps is also considered an important geometric parameter, as it too can affect the failure mode of a joint. Various workers have recommended minimum ratios of w/d so that either bearing failure, or maximum failure load results.

Rosner and Rizkalla (1995) ignored bolt clamping in their study which involved testing of double lap pinned GRP joints. It was suggested that width was the dominant parameter affecting the joint efficiency, as determined by stress concentration, and that strength increased as w/d increased up to a value of 5, approximately.

A similar study was carried out by Eriksson et al. (1995), using quasi-isotropic CFRP laminates subjected to tension loading. The load at failure was determined together with the gross section strain and bearing stress. This work showed that the ratio of w/d significantly affects the failure mode, with joints having $w/d < 2.5$ tending to tensile failure and those with $w/d \geq 2.5$ exhibiting bearing failure.

For double lap single fastener joints constructed using pultruded GRP, Cooper and Turvey (1995) recommended a ratio of $w/d \geq 4$ for the pinned condition, and $w/d \geq 8$ for bolt clamping torques of 3Nm and 30Nm. In subsequent work, Turvey (1998) used the same joint configuration with a 3Nm bolt clamping torque to investigate the effects of pultrusion angle and ratio of w/d on the joint strength. For laminates loaded along the pultrusion direction, maximum strength was obtained with a ratio of $w/d \geq 8$, which confirmed the former work, however with pultrusion along angles other than the load axis, the maximum strength was achieved with ratios of $w/d = 10$.

Using a double lap (0/90) cross-ply GRP laminate joint, with small clamping pressures applied to the bolt, Matthews et al (1982a) determined that the ratio of $w/d > 4$ should be used for maximum strength. In subsequent work, Kretsis and Matthews (1985) concluded that a ratio of $w/d > 3$ was required for maximum strength in quasi-isotropic GRP and CFRP laminates, whereas the (+45/-45) cross-ply attained maximum strength at a ratio of $w/d \geq 6$. The ratio of $w/d \geq 6$ was also recommended by Akay and Kong-Ah-Mun (1995) to obtain maximum bearing strength in clamped woven KFRP laminate joints.

Smith (1985) investigated the effects of width on bearing strength of quasi-isotropic CFRP double lap joints having 5.6Nm bolt clamping torque. The w/d ratio was varied between two and five, with the maximum bearing strength increasing with increasing ratio up to $w/d = 4$ before levelling off. In a subsequent report, Smith et al. (1986) investigated the same laminates in a single lap configuration by varying the ratio of w/d between two and five. The maximum bearing strength was obtained with the largest ratio tested, however, the magnitude was approximately 30% lower than that obtained in the former double lap study. The authors also suggested that with small end distances and widths final failure was controlled by events under the washer, thus the strength reductions were less significant due to bolt clamping suppressing some of the damage.

Ger et al. (1996) and Parida et al. (1997) carried out similar studies. Ger et al. concluded that a ratio of $w/d \geq 4$ was required for maximum bearing strength, however, the work conducted by Parida et al. confirmed the work of Smith et al. (1986) in which ratios of $w/d \geq 5$ were proposed to achieve maximum strength.

2.2.3.3 – Laminate thickness

Matthews et al. (1982a) found that by increasing the ratio of hole diameter, d, to laminate thickness, t, (as defined in Figure 2.1) of their (0/90) GRP joint, the bearing strength decreased. In subsequent work, Kretsis and Matthews (1985) also investigated the effects of laminate thickness on joint strength, and concluded that considerable buckling occurred when $d/t > 3$.

Ger et al. (1996) included the effects of laminate thickness in their experiments on single and double lap CFRP joints. They concluded that the ratio $d/t \leq 2$ was required for maximum strength. In a similar study Parida et al. (1997), however, concluded that a ratio of $t/d \geq 0.6$ should be used for maximum strength.

Rosner and Rizkalla (1995) also proposed that increasing the laminate thickness improved the joint strength of a pinned double lap GRP joint, but had little effect on the bearing stresses and mode of failure, however, by applying adequate bolt torque most of the influence from material thickness was removed.

2.2.3.4 – Washer Diameter

Abd El_Naby and Hollaway (1993a) assessed the failure strength of pultruded GRP single bolt joints under tension with low clamping pressures. In particular the effects of clamping area and washer type on bearing strength were investigated, using normal steel washers with d_w=2.2d, (where d_w represents the washer outside diameter, as shown in Figure 2.1), as well as steel plates and composite plates in place of the washer. The washer was found to suppress bearing failure mechanisms. Increasing the clamping area was found to increase the failure load, as the plates tended to spread the damaged area while keeping the degree of damage low.

Oh et al. (1997) used hybrid glass and carbon epoxy laminate single bolted joints to investigate the effects of clamping pressure and area on joint strength and failure mode. In this study the washer outside diameter was varied between 1.5 and 4.5 times the bolt diameter, d_{bo}, while keeping the inner diameter constant and the clamping pressure at 23.7MPa. The results showed that smaller washer diameters induced bearing failure modes but once the diameter reached a ratio of approximately d_w=3.0d_{bo}, the failure mode changed to the more catastrophic tensile mode.

2.2.4 – Multiple fastener joints

Several investigators have also examined the performance of multiple bolt joints as well as the simple single bolt case; Collings (1977) was one of the first, using CFRP laminates subjected to tensile loading with perfectly fitting fasteners. The net tensile and bearing strengths were measured for (0/±45), (0/60), (±45) and (0/90) laminate lay-ups. The most efficient joint tested within this limited group was the (0/±45) laminate with 50% plies in the ±45° direction, as some joint softening effects were experienced. In the absence of bolt clamping, a ratio of $d/t \leq 1$ was recommended by these workers to achieve maximum joint strength. However, when a clamping pressure of $22MN/m^2$ was applied it was found that laminate thickness did not significantly influence the bearing strength. Similarly, increasing bolt clamping further to $60MN/m^2$ had very little influence on the bearing strength. The multiple bolted joints containing two bolts side by side, as shown in Figure 2.2, were found to produce the weakest joints. This study also showed there was no adverse reaction on the efficiency of the joint as the number of bolts increased, however, the fasteners were generally well spaced so that single bolt strength was realised at each hole.

Reid et al. (1994) carried out a similar investigation using 3D braided CFRP single and multiple bolted joints subjected to tensile loading and compared load versus displacement plots in each case. The effects of clamping, pitch distance and hole pattern were also investigated while keeping the ratios of e/d for the following joint types: single bolt, two bolts in tandem (similar to the joint configuration shown in Figure 2.3) and two bolts side by side, as approximately 3, 2 and 3, respectively. The ratios for w/d for these joints were maintained at 3, 3 and 7, respectively. The highest tensile strength was obtained with two bolts in tandem, followed by the single bolt joint, with the two bolts side by side considered the weakest configuration. In the case of bearing strength the single bolted joint achieved the highest value, followed by the two bolts side by side, with the two bolts in tandem being the weakest. However, in the latter, the e/d distance was small, thereby promoting shear-out for the tandem joint rather than bearing failure.

Bailie et al. (1981) examined effects of temperature and moisture as well as laminate lay-up and bolt spacing on the strength of graphite cloth epoxy laminates, in single and double lap, single and multiple fastener joint configurations. The multiple pinned joints with large spacing were found to exhibit the same joint strength per unit area as the single pinned joints, confirming the work of Collings (1977). It was also found that when testing the lay-up containing 45° plies the radial stress was distributed around the hole by these plies, hence reducing the stress concentration at the hole boundary compared to the unidirectional laminates.

Starikov and Schön (2001) investigated the quasi-static behaviour of CFRP joints under tensile and compressive loading. The laminates used were both quasi-isotropic and 0°-dominated lay-ups fastened by two, four and six titanium bolts each having a 9Nm bolt torque. Double lap joints were used to test each fastener configuration and single lap joints were also included, fastened by six bolts. The highest quasi-static tensile and compressive strengths were obtained with the specimens containing six bolts (three rows), however, the joints failed catastrophically in a tensile mode. The specimens containing two bolts side by side failed in bearing at lower strength levels. This work also confirmed that different rows of fasteners transfer different amounts of load and that the compressive strength of bolted joints is generally higher than the tensile strength.

Saunders et al. (1993) also used CFRP laminates with a 10Nm clamping torque but restricted the investigation to joints incorporating multiple countersunk bolts under fatigue loading. C-scan and Shadow-Moire techniques were used to produce a 'damage' map. This study showed that initial damage occurred due to fastener/hole wear, which was then followed by delaminations, between the 0° and 45° plies, before developing at all interfaces.

Godwin et al. (1982) examined the mechanical response of woven roving GRP, with a (0/90) stacking sequence, in single and multiple bolted joint configurations, subjected to tensile loads, having either a 10Nm or finger tight bolt clamping torque. The joint strength was found to depend upon the degree of clamping pressure as well as the area of the clamped region. The joint geometry having e/d and w/d ratios of 4 was considered to exhibit the highest bearing strength in joints with a single fastener, with the 10Nm torque bolt providing approximately 35% more strength than the finger tight case. For joints incorporating two bolts in tandem, the pitch was varied between 3d and 6d, and when tightened to 10Nm bolt torque the bearing mode of failure was replaced by shear-out at each of the holes. These joints were found to be weaker than two bolts side by side, as confirmed by Reid et al. (1994). For two bolts side by side, the effect of varying the pitch, p, between 2d and 6d on the bearing strength was investigated and showed that the strength remained unchanged for the finger tightened bolt. However, an optimum strength was achieved with a ratio of p/d = 5, when the bolt was tightened to 10Nm. It was shown that joints containing bolts side by side with p/d = 5 and e/d = 5 resulted in the most efficient joint, however, at this pitch distance, the bearing strength of the joint was the same as the single bolted joint, and thus no interaction between the bolts was exhibited. Furthermore, it was observed that staggering the rows, as shown in Figure 2.4, did not seem to improve the joint strength.

Similar work was conducted by Abd-El-Naby and Hollaway (1993b), using pultruded GRP laminates. For those geometries in which bearing failure occurred, the load distribution was found to be uniform and hence, the load per bolt was equal to the strength of the single bolt joints. It was also recommended by these workers that the diameter of the bolts should be chosen so that the tensile strength of the cross section passing through the bolt closest to the point of loading is twice the bearing strength for single bolt specimens.

Hodgkinson et al. (1986) used both single lap joints containing single and multiple bolts, and double lap joints containing single bolts for their investigation of woven KFRP laminate joints, under tension with clamping forces applied to the bolts. Quasi-isotropic lay-ups showed a higher bearing strength than orthotropic lay-ups, with the highest bearing strength being reached when the 0° plies were positioned on the outer surface, with 90° plies adjacent and ±45° at the centre of the laminate. This finding is in agreement with the work of Hamada et al. (1995). Clamping pressures up to 30MPa (0.8Nm) were found to increase the strengths of all lay-ups, with thread stripping occurring at clamping pressures above 50MPa. To obtain maximum strength in multiple bolt joints it was recommended that the pitch distance should be greater than 4d with bolts in tandem and between 5-6d for bolts positioned side by side.

Walsh et al. (1989) carried out a similar investigation with single and double lap joints containing titanium bolts tightened with 3.34Nm clamping torque but in this case CFRP thermoplastic and thermoset laminates were used. From an analysis of the bearing strength and load to failure the thermoplastic laminates were found to give highest values in the former compared with the equivalent thermoset joints, although there appeared to be some inconsistency in the results for single lap joints.

Fracchia and Bohlmann (1994) carried out a similar analysis but instead tested single and multiple bolted joints, using near quasi-isotropic CFRP laminates in compression to assess the effects of delaminations. The C-scan method was used to detect any delaminations prior to loading which could cause loss of stiffness and strength. Stress and strain at failure were found using strain gauges. The thermoplastic joint was found to be the most delamination resistant, followed by the toughened thermoset, with the normal thermoset being most susceptible.

Zimmerman (1991) investigated multiple pin joints using Moire interferometry to find the stress and strain distribution near the holes. It was demonstrated that the joints containing two pins in tandem did not share the load equally. A staggered two row set-up was also found to give variable stress concentrations for each hole, with multiple hole arrays giving smaller stress concentrations than single bolt joints.

Rufin (1995) carried out experimental tests on multiple countersunk bolted CFRP joints to investigate the effects of different types of grommet on the overall joint strength. This study showed that the failure mode and load to fracture were the same, irrespective of the grommet type, since in every case examined the holes were undamaged during the insertion of bolts.

2.3 – ANALYTICAL AND NUMERICAL INVESTIGATIONS

Both analytical and numerical investigations are used mainly to assess the stress distributions around the holes in composite joints, however, if appropriate failure criteria are applied an approximate joint strength can also be obtained.

Several failure theories have been developed for use with anisotropic materials, a comparison of some of these was conducted by Reddy and Pandey (1987). Simple theories such as maximum stress and maximum strain were compared to mathematically derived Tsai-Hill, Tsai-Wu and Hoffman criteria for the strength prediction of composite laminates. Each criterion gave very similar results for in-plane tensile loads. Wilson and Tsujimoto (1986) also conducted a comparison between these criteria for bolted laminates and obtained good agreement between each method. The accuracy of joint strength prediction is considered therefore to be more dependent upon the method of stress analysis adopted rather than the theory used to predict failure.

A number of analytical investigations have employed classical methods based on two-dimensional theory of elasticity concerning anisotropic materials, as given by Lekhnitskii (1968). However, a vast amount of recent work has been conducted using more accurate numerical modelling techniques such as the finite element method.

2.3.1 – Classical Analyses

In an early investigation into the stress distribution around a pin loaded hole in orthotropic plates, de Jong (1977) used a method of complex functions as developed by Leknitskii (1968). The analysis was simplified by neglecting friction, clearance and pin elasticity. He concluded that the normal stress distribution around a hole in a plate of infinite width depends strongly upon the properties of the plate material and, that for elastically isotropic or slightly anisotropic materials, a sine function can be regarded as a good approximation.

In the work of Zhang and Ueng (1984), a compact analytical solution of stresses around a pin loaded hole in an orthotropic plate was obtained. Displacement expressions, which satisfied the displacement requirements around the hole were given then the stress functions were determined using Lekhnitskii's method. The analysis neglected pin elasticity, however, friction was included. It was determined that the distribution of stresses along the edge of the hole becomes more complex when friction is introduced, and that the method used gives reasonable results and was considered useful for estimating the stress distribution in pin loaded plates.

Wilson and Tsujimoto (1986) also used the classical technique developed by Lekhnitskii (1968) in their analysis of bolted laminate joints. A cosine pressure distribution was applied on the hole boundary to simulate a perfect fitting frictionless pin. The stress distributions were compared to finite element results and were found to agree well for geometries of $2 \leq w/d \leq 8$. To investigate failure, the point stress criterion developed by Whitney and Nuismer (1974) was adopted. This predicts failure once the stress of a notched laminate at a critical distance (d_0) along the net tension plane exceeds the un-notched laminate strength. The critical distance is a function of notch radius (d/2) and is defined as $1/C(d/2)^m$, where the parameters C and m are determined experimentally. In this study the characteristic distance at various angles around the hole boundary was used to predict the failure mode and rather than use maximum stress criterion, it was considered important to include stress interactions, hence stresses at the characteristic distance were used in the Tsai-Wu, Tsai-Hill and Hoffman criteria for comparison. The predicted strengths were found to be comparable for each failure criterion and agreed with the experimental work. However, failure modes were not in agreement for some geometries and hence these models cannot be applied to a wide range of laminate joints without appropriate calibration with experimental work.

Naidu et al. (1985) used an elastic continuum method to investigate a smooth rigid misfit pin in a finite plate under uniaxial loading. An inverse technique was used to develop continuum solutions for finite composite plates. The stresses and displacements were derived using complex potential functions as given by Lekhnitskii (1968). This work concluded that continuum solutions can be used to develop special hybrid finite element formulations, which eliminate the need for a large number of elements.

In a similar analysis, Mangalgiri and Dattaguru (1986) modelled a misfit pin in an orthotropic plate under biaxial loading using a classical technique. Friction and fastener elasticity were neglected in the analysis. The inverse technique with collocation points was used to model several contact conditions and derive the equivalent loads, in terms of complex potential functions as given by Lekhnitskii (1968). Significant differences in the nature of propagation of contact and separation regions were noticed between symmetrically loaded and arbitrarily oriented loaded joints.

Hyer et al. (1987) were able to investigate the effects of pin elasticity, clearance and friction in their analysis. They used a complex variable approach, where the unknown boundary tractions were expanded in terms of a complex Fourier series. The coefficients of the series were determined by using a collocation and an iterative technique. Clearance and friction were found to significantly affect the stress distribution while pin elasticity was shown to increase the joint strength marginally. It was also shown that the cosinusoidal loading assumption was inaccurate in describing the contact conditions.

Madenci et al. (1998) used a classical technique to investigate multiple fastener joints. They used boundary collocation with an iterative procedure to determine contact stresses and stress intensity factors required for strength prediction of the joints. The analytical method based on Lekhnitskii's (1968) solution method provided the capability to determine the contact stresses while capturing the effects of finite geometry, presence of edge cracks, interaction among fasteners, material anisotropy, fastener flexibility, clearance, friction and by-pass loading. The stress distribution derived using this method was found to agree well with finite element analysis results, however, converged solutions were not provided consistently, depending upon the number of bolts and their location.

Hanauska et al. (2001) continued this work where experimentally obtained bolt load distributions were used to validate analytical predictions based on the concept of virtual work in conjunction with the complex potential theory. Quasi-isotropic toughened CFRP outer laps were joined to a steel inner lap using five rigid, frictionless, finger tightened bolts in a staggered arrangement with a small clearance. The highest portion of the load was carried by each of the two bolts closest to the loaded end of the composite plate and reasonable agreement was obtained with experimental data.

Collings (1977) used a cosine pressure distribution to simulate the pin in his analysis of CFRP laminates which also included pin to hole friction. A semi-empirical method for predicting the bearing strength of typical composite laminate joints was developed using simple stress theory and experimental data. The predicted strengths were within 7% of experimental results, and the method was considered very useful for accurately predicting the strength of joints consisting of a variety of laminate lay-ups.

Ankara and Dara (1994) used a semi-empirical approach to model the mechanical behaviour of a single lap single fastener joint and developed a computer program so that when a tensile load is input the stress distribution in the laps and the mechanical behaviour of the fastener, together with the total displacement of the joint, could be calculated using an analytical theory by Barrois (1978). Clearance and friction effects were ignored, however, fastener flexibility was included by modelling it as a Timoschenko beam lying on an elastic foundation.

Hart-Smith (1978) used a semi-empirical approach to investigate the strength of several single and multiple bolted composite joint configurations. In this method a stress concentration factor was determined for an elastic isotropic material with the same geometry as the composite under consideration, using simple theory and experimental results. The stress concentration factor for the fibrous composite material was then deduced by using the elastic isotropic stress concentration factor, and an empirically determined correlation factor which accounts for laminate orthotropy, non-linear material behaviour and stress redistribution during final failure. This method was considered to be useful in predicting the strength of other joint geometries consisting of the same composite laminate and bolt size. It was also concluded that the strength of multiple row joints is only slightly improved compared to single row joints, however, more than two rows of bolts is not practical. It also seems apparent that even with a well designed joint the strength is only approximately half of the material failure strength.

Rosner and Rizkalla (1995) also used a semi-empirical analytical model to develop a mathematical model and design procedure capable of predicting ultimate failure load and mode of failure for a single bolt double lap joint. The prediction of ultimate tensile strength was based on the work of Hart-Smith (1978), and the bearing strength from experimental findings. It was reported that ultimate failure loads were predicted to within 10% of experimental findings.

2.3.2 – Two-Dimensional Finite Element Analyses

Due to the limited computer resources and time constraints the majority of numerical simulations of mechanically fastened composite joints have been carried out using simplified two-dimensional finite element analysis. However, in such analyses the complexity of models is limited by applying constraints and assumptions which can affect the reliability of results.

Essentially, the contact between the hole and fastener is non-linear with applied load, however, to simplify this many authors have modelled the contact by assuming boundary conditions at the interface. In the simplest analyses contact was simulated by restraining the nodal displacements around part of the hole boundary. Wilson and Pipes (1981) used this method to model a rigid frictionless pin. A range of geometries for e/d and w/d were investigated using a quasi-isotropic CFRP laminate lay-up. A slightly different version of the Whitney-Nuismer point stress criterion was used to predict failure, whereby the critical distance was determined as a function of the hole size and the shear-out strength was predicted once the shear stress at the characteristic distance exceeded the shear strength of un-notched laminates. It was concluded that the model could predict strength for various e/d and w/d geometries without the need for further empirical information, and excellent agreement with experimentally obtained joint strengths was achieved.

Soni (1981) also restrained nodal displacements around the hole boundary to simulate a rigid frictionless pin within CFRP laminates with various ply orientations and volume fractions. Three loading conditions were investigated: an unloaded hole, a loaded hole and a by-pass loaded hole. Failure strengths were predicted for each model using the tensor polynomial failure criterion (Tsai and Wu, 1971). The ultimate strength was determined as the failure strength of the strongest ply at the weakest point of the laminate. The strength predictions were consistently conservative, varying from 10% to 50% below the measured strengths, depending upon the laminate lay-up and geometry.

Lessard and Shokrieh (1995) carried out a similar analysis using non-linear and linear finite element analysis in a progressive damage model, which was utilised to determine first ply failure load, direction of failure propagation, residual strength and ultimate strength. With the linear solution the failure load was found to be within 10.7% of the experimental findings and the bearing strength was found to be a maximum when $e/d > 2$

and w/d > 3. The non-linear analysis determined the bearing strength with slightly more accuracy.

Agarwal (1980) used NASTRAN to model a frictionless pin in CFRP laminates with various stacking sequences. The average stress criterion developed by Whitney and Nuismer (1974) was applied at numerous positions around the hole boundary to predict ultimate failure strengths and failure modes. On average, the predicted strengths were higher than experimentally measured strengths, particularly for laminates with considerable shear deformation such as (0/90) and (45/-45) laminate sequences, however, the failure modes were predicted successfully. It was also concluded that the predicted strengths are very sensitive to the averaging distance.

Arnold et al. (1990) also assumed a rigid frictionless pin by using displacement restraints around the hole boundary of GRP and CFRP laminate joints. An extension of the Whitney-Nuismer point stress criterion (Whitney and Nuismer, 1974) was adopted to investigate the ultimate tensile and bearing failure strengths. Various characteristic distances were determined around the hole for predictiion of different failure modes. These were determined using experimentally derived pinned and bolted joint strengths rather than notched laminate strengths, as the characteristic distance was considered not to be a material property when applied to bolted joints. If the Hoffman or maximum stress criterion was then satisfied in the finite element model at a distance greater than the characteristic distance, then joint failure would be predicted and the mode of failure would be determined by correlation with the appropriate characteristic length. The strengths predicted using the Hoffman failure criterion were found to be in excellent agreement with experimental tests and this method enabled prediction of both pinned and bolted joint strength for other geometries.

Several investigations also used displacement restraints around the hole boundary and included friction at the interface between the hole and a perfect fit pin. Conti (1986) modelled a rigid pin using fixed radial displacements on nodes around the hole boundary, and introduced friction by using local tangential forces on the same nodes. An improvement was found in the laminate and bolt bearing strength when w/d = 2 and

$e/d \geq 2$. The optimum value of e/d and w/d varied with failure mode, which was also shown to depend upon stacking sequence and other material parameters. The predicted joint strength was found to be conservative compared to experimental results. It was also demonstrated for a three pin joint configuration that a non-uniform load distribution existed. Hollmann (1996) also modelled friction but by using zero tangential displacements around parts of the hole boundary. Three conditions were tested: frictionless, part friction and full friction, on a model designed for shear-out failure. The strength predictions derived from the damage zone model, for the most relevant boundary conditions, were within 5% of experimental results. The analysis indicated that minimum contact surface friction was preferred for optimum shear-out strength.

Several authors have also been able to model bolted connections using two-dimensional analysis. Webber et al. (1997) used displacement restraints around the hole boundary to describe the contact conditions in their analysis of a bolted joint. A rigid bolt and washers were used along with plane stress elements for the laminate plate while special interface finite elements were employed to represent frictional forces between the washer and plate. The washer with friction affected a uniformity in the strain distribution under uniaxial loading, while biaxial loading was found to give higher strains. This analysis was similar to Graham et al. (1994), where their novel two-dimensional finite element analysis allowed for washer friction and clamping but ignored interlaminar stresses. In this analysis a clamping ratio of 0.2 was found to reduce the magnitude of peak strains, without affecting their position. A clamping ratio of 0.4 was also found to reduce the strain but the position of the maximum axial strain around the hole boundary was found to shift from 90° to 75°, with respect to the loading direction. As the clamping ratio increased to 1.0, the positions of peak strain shifted from the hole boundary to the washer outer edge. Strains were found to increase after a ratio of 1.0, with failure likely to occur at the washer edge rather than from the bolt-hole interface. It should also be noted this study showed that at clamping ratios above 0.6 there was no contact between the bolt shank and hole boundary.

By adopting slightly different assumptions several researchers have tried to improve the accuracy of the finite element models by approaching a more realistic contact condition.

One such attempt was undertaken by Tsujimoto and Wilson (1986), who considered a cosine pressure distribution on the hole boundary as the most realistic contact condition for their elasto-plastic analysis of a perfect fitting rigid pin. Both frictional and smooth pin to plate contact conditions were analysed. The Hill yield criterion (Hill, 1950) was used in the progressive damage analysis. A characteristic distance was required for determining the tension failure mode as the mesh refinement was unable to accurately predict this type of failure. Laminate lay-up and joint geometry were found to influence the failure mode quite strongly and the elasto-plastic strength analysis did not offer any great improvement over the 2D elastic analysis using the characteristic distance for ultimate strength prediction. However, it did help identify the dominant failure mechanism as it gives an insight into the accumulation of damage up to final failure.

Chang et al. (1982) also used a cosine pressure distribution in their analysis of a rigid pin joint which neglected pin to hole friction. Failure was predicted using the Yamada-Sun failure criterion in conjunction with a characteristic curve. The characteristic curve was assumed to depend only upon the material properties and was determined experimentally from the tensile and compressive strengths of notched laminates. The strength predictions were found to be within approximately 10% of the experimental results given by Agarwal (1980). Chang et al. (1984a) continued this work for strength prediction of multiple pin composite joints and then constructed a program, BOLT, (Chang et al., 1984b) for the strength prediction of this type of composite laminate joint.

Chang and Chang (1987a) developed a progressive damage model to predict the strength of tensile loaded CFRP notched laminates with various stacking sequences. Material and geometrical non-linearity were included. The load was applied incrementally so that the laminate could be checked for failure at each step. Using the modified Yamada-Sun failure criterion from Chang et al. (1982) the laminate was checked for matrix cracking, fibre-matrix shearing and fibre breakage. If failure occurred from matrix cracking the transverse modulus and Poisson's ratio were set to zero before increasing the load further. When fibre-matrix shearing or fibre breakage occurred then the transverse modulus and Poisson's ratio were set to zero but the degree of degredation of the in-plane modulus and shear modulus were assumed dependent upon the size of the damaged area. This method was subsequently adopted for the analysis of pinned joints (Chang and Chang, 1987b) to determine the onset of tension and shear-out failure. The Yamada-Sun failure criterion was used to determine matrix cracking, fibre-matrix shearing and fibre breakage, while matrix compressive failure was determined using the Hashin criterion (Hashin, 1980). The strength predictions agreed within 20% of experimental work and the progression of failure was accurately predicted. It was concluded that no improvement in the predicted strength was obtained compared with the method used in Chang et al. (1982), (1984a) and (1984b), however, progressive failure analysis enabled an assessment of the redistribution of stress.

Naik and Crews (1986) used an inverse technique to model the pin to hole contact by applying constraint equations around the hole boundary and determining the equivalent bearing stress. This method described the contact conditions more realistically than the previously assumed radial displacements or stress distributions. They also allowed for clearance in the analysis of a rigid pinned joint. The results from the finite element analysis compared very well to previous numerical procedures. It was found that contact arc and peak stresses, as well as their location, were strongly influenced by clearance, although joint stiffness was not thought to be much affected.

Many investigators have chosen to model the contact condition between the fastener and the hole, rather than assume boundary conditions along the interface, in an attempt to gain increased simulation accuracy. The work reported by Rahman et al. (1984) was one of the first attempts to accurately model this interaction and used a rigid pin with an iterative procedure to account for the contact non-linearity. These results agreed well with previous work, with a refined finite element mesh giving superior results.

Wilkinson et al. (1981) also used an iterative procedure with a non-linear plane stress analysis to model their wooden joint. The plates were fastened using a rigid pin with frictional pin to hole contact and the material and geometrical parameters were varied. Their results were shown to agree well with experimental findings, however, the iteration procedure was found to be slow due in part to non-linearity in the analysis.

Murthy et al. (1990), (1991) used clearance with a rigid pin both normally and eccentrically loaded. The clearance non-linearities were accounted for by using an iterative approach to compare to the frequently assumed cosine pressure distribution. This study concluded that the cosine distribution was inaccurate and the contact angles, location and magnitude of maximum stress at contact, were all found to be functions of the fibre angle.

Kang and Lee (1997) also used a rigid fastener with gap/contact type elements, which could include friction and clearance, in their progressive failure analysis to investigate the influence of geometrical parameters on joint strength. Both compression and tension loads were used in this analysis and it was found that a combination of $e/d \geq 3$ with $w/d \geq 6$ was required to achieve maximum bearing strength.

In a similar analysis, Dano et al. (2000) also used a rigid pin with gap/contact type elements to determine the contact conditions. Friction and clearance were also included in their progressive failure analysis. Failure strengths were predicted by combining the maximum stress and Hashin (1980) failure criteria. Stress results were found to agree very well with experimental work and failure strengths were predicted to within 1-15% of experimental data.

Ko et al. (1996) carried out a similar analysis but also investigated the effects of an elastic pin with clearance and used isotropic composite plates in their study, which utilised the Yamada-Sun (1978) criterion to investigate failure of the joints. The non-linear analysis was found to be no better than linear analysis for predicting failure strengths and both sets of results agreed well with experiments.

Eriksson (1986) assessed the effects of: load magnitude, friction, bolt stiffness, interference and clearance fit pins, on the strength of double lap joints under tensile, compressive and tensile bypass loads. These investigations found that bolt stiffness (titanium compared to steel), has little effect on the radial contact stress at the hole boundary. Friction was found to decrease radial and shear stress due to equilibrium conditions at the hole boundary contact area. The contact area at the bolt-hole interface was found to vary with the magnitude of load applied. Clearance was found to reduce the contact area with magnitude of the peak stress remaining virtually constant but the location around the hole boundary varied. The method used involved determining the contact condition rather than using prescribed hole boundary conditions, and the results were found to be in good agreement with experimental work.

Arnold et al. (1989) also used gap elements to model the frictionless interaction between the pin and hole of a composite joint. A square CFRP laminate loaded via a perfect fit steel pin was tested under various biaxial loading conditions. Three laminate stacking sequences were examined: 0, 90 and quasi-isotropic lay-ups. It was concluded that the stresses arising from biaxial loading are significantly influenced by the laminate elastic properties. The transverse loads can improve the stress state local to the fastener hole, however, this is dependent upon the ratio between the transverse load and axial load. It was also concluded that a high ratio was detrimental to the joint strength.

Ireman et al. (1993) also used an iterative technique and an elastic bolt in their analysis. The results obtained from an analytical method and finite element analysis compared favourably, however, both methods incorrectly predicted a failure mechanism for one of the specimens. This was thought to be due to ignorance of the through thickness effects caused by fastener bending.

Hung and Chang (1996) modelled a bolted joint and allowed for friction between the washer and plate by decreasing the bearing load applied by an amount dependent upon an assumed friction coefficient at the laminate-washer interface. An iterative approach was adopted to accurately determine the contact boundary conditions. The predictions were found to agree very well with experimental data and quasi-isotropic laminates were found to exhibit higher bearing strengths than cross-ply laminates, confirming experimental work by Wang et al. (1996) and Andreasson et al. (1998).

Jurf and Vinson (1990) modelled contact in a bolted joint slightly differently, using truss elements between the bolt and hole. The objective of this work was to assess the effects of bolt clamping as well as various geometrical parameters on the mechanical response of kevlar/epoxy and graphite/epoxy laminates. The bolted conditions were investigated by introducing areas of plane strain in the model. The finite element analysis results compared well with experimental data and the washer outside diameter (d_w) was found to give optimum joint strength at ratios of d_w/d_{bo} = 1.8-2.6.

In many engineering applications composite laminate joints are constructed using multiple pins. A number of investigators have assumed in the analysis of these configurations that the bolt spacing is large enough so that the single fastener joint strength can be used in the prediction of multiple bolt joint strength. Clearly, this may be inaccurate if the fastener spacing is below a value where fastener interaction can be ignored. Consequently, investigators have more recently modelled multiple fastener joints to gain an insight into the fastener load distribution and its effect on the joint strength.

Hyer and Chastain (1988) applied different cosinusoidal loads to holes in a graphite/epoxy laminate joint to see whether the maximum joint strength was obtained when each hole carried the same load. They assumed that if tailoring the load proportion is beneficial then it could be done easily, so that the material around each of the holes in the joint fail at the same rate. With the load proportion shared equally between the bolts, the same failure rate was not observed by each hole.

One of the earlier investigations was carried out by Rowlands et al. (1982) in which they investigated the effects of load distribution, material properties, pin spacing, friction at the pin/hole interface, clearance and end distance in the performance of single and double rigid pinned joints. They used incremental loading in an iterative technique to determine the contact conditions. The friction and clearance results are in disagreement with later work reported by Eriksson (1986). Stiffer materials were found to give an increased maximum stress, and joint strength was found to alter substantially depending upon the load distributions between the pins. Similar work was also undertaken by Rahman and Rowlands (1993).

Cohen et al. (1995) modelled both single and multiple pinned thick CFRP joints with perfectly fitting rigid pins. Non-linear finite element analysis was used to model actual contact at the bolt-hole interface rather than use assumed boundary conditions. The average stress criterion was used in conjunction with average strain criterion to predict failure, as independently, the average stress criterion is inaccurate in predicting the failure location. This work showed that the highest portion of the load for each of the multiple pin configurations was carried by the holes closest to the application of tensile loading, and these results compared favourably to experimental data.

Chutima and Blackie (1996) also used an iterative contact technique in the form of gap elements. Friction was included between the face of the hole and both rigid and elastic perfect fitting pins in their multiple pin investigation. The effects of pitch distance, row spacing, end distance and pin diameter on the percentage of load transferred was investigated. For a pin diameter of 6.35mm, the optimum pitch distance, row spacing and end distance, was found to be 6d, 3d and 2d respectively. Friction was found to have a minor effect on the percentage load transferred in multiple pinned joints. When friction was introduced the stress along the bearing plane reduced, while the maximum stress on the inboard row was only marginally affected, and the maximum stress decreased at the holes on the outboard row.

Kim and Kim (1995) included friction and clearance in their investigation of multiple rigid pinned joints. Contact was modelled using an extended interior penalty method and variational principle. When friction was included it was found that the peak stress did not occur on the bearing plane, as with the non-frictional case, and the contact area increased for both single and double pinned joints. It was also found that for two holes in tandem the pin nearest to the point of load application carried a higher proportion of the load, and that the geometry of the plate, the row spacing and clearance, have a significant influence on the distribution of contact pressure. These results were found to agree well with the results obtained from experimental tests.

Wang and Han (1988) investigated multiple pinned joints using a linear elastic analysis. Clearance at the hole boundary was neglected, as were the bending effects. Oakeshott and Matthews (1994) also neglected friction and clearance in their multiple pinned model. Two dimensional laminated composite shell elements were used for the plates, with beam elements representing the elastic fasteners. It was found that the majority of the load was carried by the outermost bolts and that the optimum number of rows depended upon the geometry of the array. An interesting point to note was that when the outer pins had a smaller diameter than the inner pins, the load became more evenly distributed and hence the joint was considered to perform more efficiently. Although bending effects were considered, which were not included in the work of Wang and Han (1988), the beam elements did not represent the whole fastener length and the interface between the laps was not modelled, which could also affect the reliability of the results.

2.3.3 – Three-Dimensional Finite Element Analyses

Three-dimensional finite element analysis is still a relatively new approach to predicting the strength of mechanically fastened laminated composite joints because of limited computational resources and time restraints. More recently, with advances in computer technology, many investigators have used this approach to model the through thickness and interlaminar stresses of the joint, and thereby gain a greater accuracy in predicting joint strength.

Several authors have carried out 3D analyses on laminated composite laps without a mechanically fastened joint. Kim & Hong (1991) developed a 3D finite element analysis program with a substructure technique to investigate interlaminar stresses at the edges of thick composite laminate plates with and without holes, under tensile loads, having various thicknesses and stacking sequences. Barboni et al. (1995), Gamble et al. (1995), Hu et al. (1997) and Tsumara et al. (1995) have also carried out simple 3D analyses of laminates with notches/holes subjected to tensile loading. In the former study laminates with the lamina stacking sequences $(90/0)_s$ and $(-45/45)_s$ were studied, while Gamble et al. used $(0/90)_s$ laminates, with one finite element representing each layer of lamina and one for each layer of resin through the thickness. Hu et al. (1997) examined $(90/0)_s$ and $(0/90)_s$ laminates with multiple finite elements representing each lamina. Tsumara et al. (1995) developed a 3D Finite Element Analysis computer program, based on damage mechanics, to analyse the stress distributions in notched CFRP composite laminates under tensile loading. Three different stacking sequences were tested, $(0,15,-15)_s$, $(15,0,-15)_s$ and $(15,-15,0)_s$, each containing an open hole in the centre. The $(15,0,-15)_s$ laminate was found to give the highest fracture strength. The effect of stacking sequence on the fracture strength was caused by the differences in the occurrence and progression of damage.

In an early three-dimensional study of mechanically fastened joints, Matthews et al. (1982b) analysed a double lap joint under tensile loads. Clamping was included, however, clearance and friction were ignored, as pin jointed bars were placed around the hole to simulate the rigid fastener. These researchers developed a new finite element, based on a 20 noded iso-parametric brick element which was able to represent all the layers in a laminated composite, thereby reducing the computer time and work space required. This element was then validated using the results obtained using a separate element for each layer in the thickness direction; a good comparison was found for a $(0/45/-45/0)_s$ laminate. The displacement in the z- direction was fixed on the nodes under the washer area to simulate a 'finger tight' bolt and washer assembly. A compressive displacement, corresponding to a bolt tension of 10kN, was applied to simulate a fully tightened bolt. When loaded by a simple pin it was found that maximum through thickness tensile stresses of about 7% of the bearing stress occurred on the loaded side of the pin. For the 'finger tight' case, the through thickness tensile stress was found to decrease. For the fully tightened case, the axial compressive stresses increased significantly and high interlaminar shear stresses were observed at the washer edge, on the outer plies close to the axis of loading. This compared favourably with the findings of their experimental work where failure was observed due to delamination at the washer edge.

A similar analysis was carried out by Lessard et al. (1993). A composite plate with a bolt-loaded hole was analysed using I-DEAS FEA software with 20-noded iso-parametric elements. The rigid fastener was simulated by applying radial constraints to nodes around the hole boundary, however, the analysis did not account for friction between the bolt and the hole, only between the washer and the laminate. The clamp-up was modelled by applying a uniform pressure under the washer area. Three different

CFRP laminate lay-ups were examined: $(0/90)_s$, $(90/0)_s$ and $(+45/-45)_s$. By applying a bolt clamping load the normal and interlaminar shear stresses were found to reduce more significantly for the $(0/90)_s$ laminate than the $(90/0)_s$ laminate, with the normal stresses σ_{zz} all changing from positive (tensile), to negative (compressive).

In an attempt to reduce the stress concentration at the hole boundary, Camanho (1999) assessed the effects of including adhesively bonded metallic inserts on the strength of rigid bolt joints. A progressive damage model was constructed, which used a single element to represent each lamina of the CFRP laminate in the through thickness direction, and unidirectional gap elements were employed between the laminate and washer to provide finger tight clamping. The results were found to agree well with experimental work, which showed that an increase in joint strength occurred through using the insert. These workers concluded that not only did the metallic insert protect the laminate during insertion of the bolt into the hole but it also redistributed the stress more evenly around the hole boundary. Stiffer insert materials were found to give a more effective stress redistribution, however, the resulting higher tensile stresses in the insert adhesive lead to lower failure loads.

Benchekchou & White (1993) used fixed nodal displacements around a hole in a laminate to represent the fasteners in their three dimensional analysis of bolted joints under flexural loading and fatigue. The analysis, which neglected clearance and friction included a bolt tightening torque of 7Nm, as used in aircraft applications, which was applied as a constant pressure to the elements around the area representing the bolt head. One element was used to represent each laminate layer in the through thickness direction. Direct and shear stress values were found to be generally lower when bending the plate downwards rather than upwards. Joints containing countersunk bolts were found to fatigue more quickly than those containing cheese head bolts, due to the higher direct and shear stresses these induced. In subsequent work, Benchekchou and White (1995a), investigated the performance of CFRP laminates having material properties representing XAS/914 CUD, which were statically loaded in a cantilever arrangement. Three different laminate stacking sequences were used, $((\pm45/0/90)_2)_s$, $((0/\pm45/90)_2)_s$, and $((+45)_2/(-45)_2/(0)_2/(90)_2))_s$. A row of three cheese head bolts, (4mm and 6mm diameters), were used to clamp down one end, while the other end was subjected to alternating deflections having predetermined amplitudes. Again, one element represented one laminate layer in the through thickness direction and clamping pressures of 10, 50 and 100MPa were applied to the bolts, using constant pressure under the bolt head area. The same procedure was utilised by Benchekchou & White (1995b) using countersunk fasteners but with clamping pressures of 10, 65 and 100MPa. Comparisons were made with experimentally derived data, to demonstrate that the stresses and strains obtained were in good agreement, with differences not exceeding 8.11%. The experimental results were also used to determine the patterns of stresses in the simulation, which led to major damage in the experimentally tested coupons. Delaminations were found to occur between layers where direct stresses were high, particularly those in the through thickness direction, whilst cracks tended to occur in areas which exhibited high shear stresses. An increase in clamping pressure led to an increase in stress values, indicating the specimens would delaminate more quickly. However, a decrease in clamping increased the shear stresses and decreased the direct stresses, therefore it was proposed, more cracks should be found with fewer delaminations. Reducing the bolt size was found to give higher stresses, hence, inducing earlier damage initiation. As expected the authors confirmed that countersunk bolts induced larger stresses than cheese head bolts and hence joints incorporating these bolts failed by fatigue more rapidly.

Marshall et al. (1989) included both friction and bolt clamping in their three-dimensional analysis of a double lap joint under tension. A 3D analysis was carried out on pinned and bolted joints in $(0/90)_s$ and $(90/0)_s$ laminated composites. A rigid frictionless pin was modelled using fixed radial displacements around part of the hole boundary, and infinite friction was also modelled by fixing tangential displacements on those same nodes. Three elements were used to represent the thickness of a ply. The effects of clamping and stacking sequence on the stress distribution were investigated under four clamping conditions: pinned, finger tight washer, flexible washer (uniform pressure applied) and rigid washer (uniform displacement applied). The stresses in the $(0/90)_s$ layup were found to be significantly higher than in the $(90/0)_s$ lay-up. Clamping was found to reduce the fibre axial and transverse stresses as well as the shear stresses. Higher clamping pressures were produced when using a rigid washer, however, the benefits were reduced as the interlaminar shear stresses increased at the washer edge. Friction was shown to be beneficial in reducing the bearing stresses in pinned joints and placing 90° fibres at or near the surface improved the pin bearing strength. This study also found the strength of the $(90/0)_s$ lay-up higher as the interlaminar normal stresses, which influence delamination, are much lower for this lay-up.

Hassan et al. (1996) conducted a three dimensional analysis on both single and multiple-pin pultruded GRP composite double lap joints. Contact was modelled using interface elements to accurately determine the contact zone and one element was used to represent a single ply in the through thickness direction. High strength steel pins, approximating rigid pins, were incorporated in the model with a small degree of clearance at each interface with the laminate. The ultimate failure strength of the joint was predicted using the Tsai-Wu (1971) tensor polynomial failure criterion. The magnitudes of the net tensile stresses were found to be very high near the hole boundary but decreased rapidly away from the hole boundary at a distance equal to the hole diameter. An uneven distribution of bearing forces was found for the joints containing more than one row of pins. The Tsai-Wu (1971) failure criterion showed regions of failure in the vicinity of the pins but did not give an indication of the mode of failure.

Serabian (1991) carried out a similar analysis on pin loaded GRP composite joints, using two different stacking sequences. Interface elements were used with Lagrange theory to accurately model the contact area and classical laminate theory was used to apply the average laminate properties to each element. A small clearance was introduced between the pin and the hole boundary. Both linear and non-linear elastic 3D analysis was used to compare net, bearing and shearout sectional strains to experimentally derived results. Non-linear material behaviour was observed in both the net and bearing stress and strain components of the $(+45/-45)_{3s}$ laminate and also in the shearout section stress and strain components of the $((0/90)_3,0)_s$ laminate, at a relatively low load.

Chen et al. (1995) considered a double lap bolted composite joint constructed from a thin graphite epoxy $(45/0/-45/90)_s$ laminate as well as a thick glass reinforced polyester laminate having various stacking sequences, subjected to a tensile load and clamping torque. The effects of friction, clearance, bolt elasticity, stacking sequence and clamp-up on the contact tractions were investigated. The bolt to hole contact was modelled using an incremental restricted variational principle and using the Ye (1988) delamination criterion, the onset of delamination was predicted. The bolt tightening was simulated using a constant pressure over the washer contact area. The contact tractions of the elastic bolt were not very different to the rigid bolt, however, the cosine distribution assumption gave very different results and was therefore not considered appropriate for 3D analysis. Bolt clamp-up reduced the tensile normal interlaminar forces and increased the through thickness compressive forces. Friction reduced the axial strain but introducing clearance at the bolt interface had the converse effect. The strength of the composite laminate on the bearing plane decreased as the stacking sequence was changed from $(90/0)_s$ to $(0/90)_s$, which is in agreement with the work reported by Marshall et al. (1989).

Clamping and friction were both included in the analysis of Ireman (1998), who used I-DEAS and Abaqus to carry out an analysis on a single lap bolted joint in which laminate lay-up was varied in addition to the bolt diameter, bolt type (protruding head or countersunk), bolt pre-tension and lateral support. The bolt, washer, and nut were modelled as one component to reduce the contact surfaces. The bolt pre-load was applied using an orthogonal temperature drop on the bolt assembly elements. Bolt to hole contact was modelled using an iterative contact pair approach, which allowed for a friction coefficient of 0.2 to be introduced at every contacting surface. An experimental analysis was also performed to validate the FEM, the comparison being generally quite good. Tightening to higher torques was found to reduce the strain level on the surface of the laminate around the hole periphery compared to finger tight clamping, as did the protruding head bolt compared to countersunk bolt.

Chen & Lee (1995) investigated the effects of friction, stacking sequence and a countersunk bolt head on contact tractions of a single lap CFRP joint under bending loads. The bolt to hole contact was modelled using an incremental restricted variational principle. The progressive failure analysis, based on the maximum stress theory, Ye (1988) delamination criterion and complete ply failure, was undertaken for predicting the maximum load before catastrophic failure. The joint containing a laminate stacking sequence of $(90_8/0_8)_s$ was found to withstand a higher bending load before failure than a laminate sequence of $(0_8/90_8)_s$. The latter having the higher bending stiffness. An excellent comparison was made with experimental findings when the friction coefficient was set as 0.2.

An alternative to the application of three-dimensional finite element analysis to composite laminate joints was proposed by Iarve (1995), who used a spline variational method to solve the contact problems in a $(45/-45)_s$ CFRP composite double lap joint incorporating a single rigid fastener. This analysis was quite simple, no allowance was made for friction or clearance between the pin and the laminate and bolt clamping pressure was also neglected. An algorithm capable of adjusting the non-uniform through thickness contact zone was developed. The interlaminar stress results were found to be in good agreement with those derived from a single term asymptotic solution. An advantage of using this method is that stresses can be evaluated at any point on a surface rather than at nodal or integration points as with FEA. Iarve (1997) subsequently continued this work, where the laminate stacking sequences $(-45/90/45/0)_s$ and $(\pm 45)_s$ were also included in the analysis, along with fastener elasticity and a degree of clearance between the pin and hole. Good correlation was obtained between the results derived using the numerical and asymptotic solutions.

2.4 – CONCLUSIONS

The main conclusions that can be drawn from the numerous experimental studies are associated with the effects attributed to material and geometric parameters on joint strength. In the case of the analytical studies, conclusions may be drawn concerning the accuracy of the two-dimensional and three-dimensional finite element analyses for predicting the joint strength and stress distributions of composite joints.

Just as the fibre and matrix can affect the strength of a laminate they may also influence joint strength. It has been shown that when carbon is used as the reinforcing fibre not only does this lead to an improvement in joint strength, but it also results in fewer delaminations compared with GRP. Thermoplastic resins, being less susceptible to delamination, also offer improved strength over thermoset resins.

Further, previous work has shown that the stacking sequence has a major influence on the joint strength and failure mode. Higher strengths have been observed with quasi-isotropic materials rather than cross ply or unidirectional laminates and by utilising 90° and/or 0° fibres at the surface of the laminate, with ±45° plies interspersed in the mid-section, the maximum joint strength may be reached. It was also observed that if the laminate is highly orthotropic the joint may fail catastrophically, even with a large end distance and width.

Clearance has been shown to have a significant influence on the joint strength, however, it was concluded that the fastener and hole interaction is a non-linear process for joints loaded in tension.

Friction between contacting surfaces was found to have an important role in affecting the failure strength, with a higher friction coefficient increasing the joint strength, however, the failure mode may change due to the redistribution of stresses.

The fastener material itself does not appear to contribute significantly to the joint strength, with only a slight increase in joint strength observed when a steel rather than titanium fastener was used due to reduced fastener bending. However, the type of fastener employed can have a more significant effect, i.e. it has been shown that a protruding head bolt offered a great improvement in strength over a countersunk head bolt as well as a simple pin.

The clamping force was found to be one of the major influences on joint strength, with even small clamping pressures improving the joint strength considerably, when compared to a simply pinned joint. Increasing the clamping area also exhibited an improvement in joint strength, however, consideration should be given in selecting a clamping pressure and area as the failure mode can also be affected. Experimental studies have shown that damage which initiates under a washer can be suppressed by an appropriate clamping pressure. Consequently, damage occurs at the washer edge where delaminations can not be suppressed and then spreads to the free edge of the joint. This effect may lead to a catastrophic tensile failure mode.

The critical values for the geometric parameters of the joint have been reported by many authors to induce bearing failure and/or high strength. These vary quite considerably, especially with the ratios suggested from two-dimensional finite element analyses. From experimental tests on GRP joints, the minimum value advised for both e/d and w/d was 5, however, a value of 2 was recommended from two-dimensional FEA. For CFRP joints minimum e/d, w/d and p/d were recommended as 3, 3 and 6, respectively, for double lap joints and $e/d \geq 6$ and $w/d \geq 5$ for single lap joints. However, there have not been many experimental studies of the single lap joints so these values have been recommended based on two-dimensional analyses. For KFRP double lap joints the recommended ratios were $e/d \geq 3$, $w/d \geq 6$ and $p/d \geq 5$.

Work conducted on multiple bolted joints has produced some varied results. In many instances joints were designed with a large inter-spacing so that no stress interference occurred between the fasteners. The results for this type of joint demonstrated a similar strength was achieved compared to that attained from single bolt joints. However, when joints were designed so that interference existed a change in load distribution between each fastener was demonstrated, hence affecting the joint strength and failure mode. The highest tensile strength was obtained in a joint with two fasteners in tandem, compared with a single fastener joint or one containing two fasteners side by side, the latter was observed as the weakest. The highest bearing strength was obtained with a joint consisting of a single fastener followed closely by one having two fasteners side by side, while a joint with two fasteners in tandem is considered much weaker. However, these observations may not be universally applicable dependent upon the end distance and width employed; in this particular case the approximate ratios were: $w/d = 3$, 3 and 7 and $e/d = 3$, 2 and 3 for joints containing a single bolt, two bolts in tandem and two bolts side by side, respectively.

With two-dimensional modelling the accuracy in derivation of stress values and hence strength prediction largely depends upon the method used to model the contact condition between the fastener and hole. The simplest method which restrains nodal displacements around part of the hole boundary was found to give results in close agreement to those obtained experimentally. A cosine pressure distribution applied to the hole boundary was found to give improved results compared with using restraints on selected positions around the hole boundary. Inverse techniques, where boundary conditions were assumed and the resultant load derived, were found to describe the contact more realistically. However, the closest approximation appears to be obtained by actually modelling the contact using an iterative technique, rather than assume boundary conditions. Using the iterative technique authors generally found that non-linear and linear analyses agreed very well with experimental work, especially when friction, clearance and pin elasticity were included.

Semi-empirical approaches have proved to be very useful for predicting the joint strength of composite laminates and seem to be more accurate than using simple failure theories. Although these methods require some experimentally derived calibration constants, the non-linear material behaviour at the hole, prior to ultimate failure, can be taken into account. Even with simple two-dimensional stress analysis an accurate ultimate failure strength can be determined rather than the conservative strengths predicted from the entirely theoretical models.

Three-dimensional finite element modelling is the best method to use for analysing the stress distributions in laminate joints as the through thickness and interlaminar stresses can be examined as well as the out of plane deformation associated with bearing failure. However, the bolt-hole contact condition should be modelled rather than assumed as the area of contact interface varies through the thickness of the laminate and the cosine pressure distribution has proven to be inaccurate in three-dimensional modelling. Also, the laminate should be modelled using the replica layer-wise technique, as interlaminar stresses can not be determined accurately when classical lamination theory is employed to provide average material properties to the laminate.

As three-dimensional modelling increases the complexity of the simulation the running time and computer resource requirements are greatly affected, hence a limited amount of work has been carried out using this technique and a number of areas have not been fully investigated. The current study attempts to reduce the assumptions used in previous analyses of single and multiple fastener joints, hence deriving more accurate and reliable results for typical composite joints.

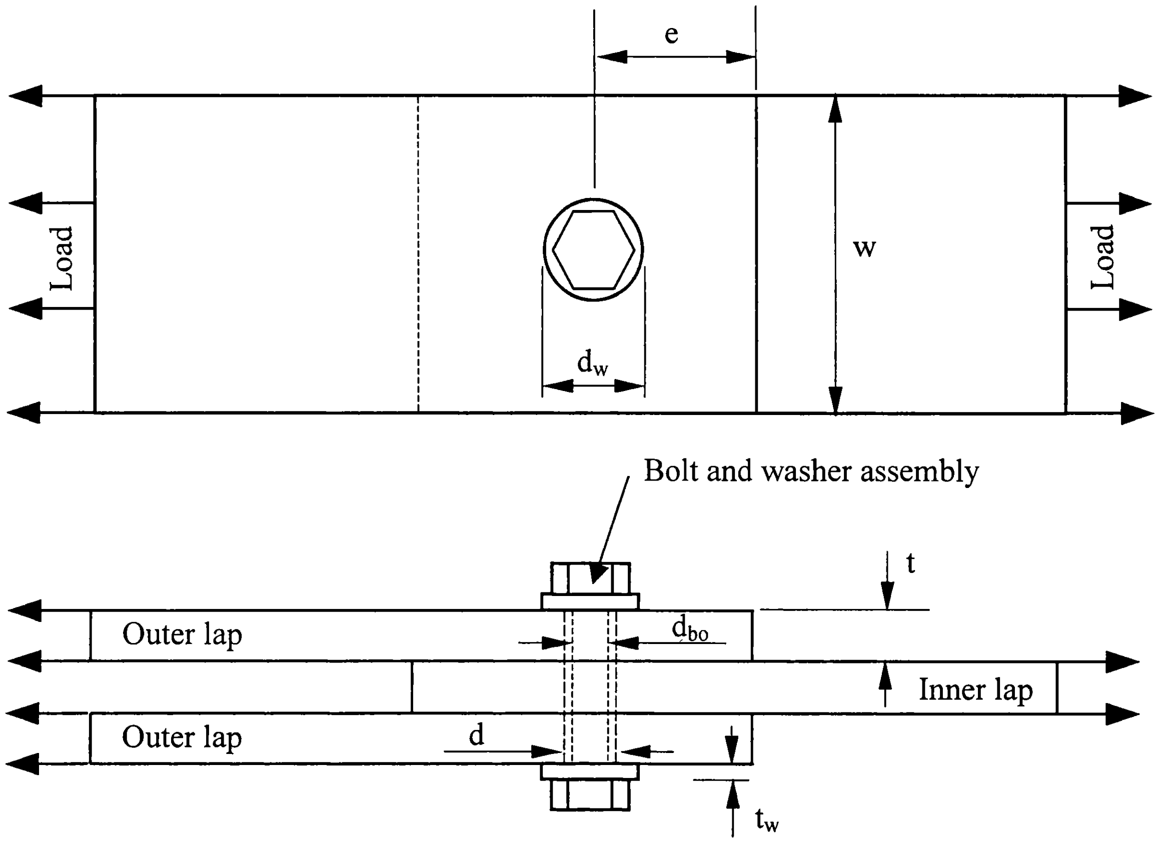

Figure 2.1 – Double lap single bolt joint configuration

d = hole diameter	p = bolt pitch
d_{bo} = bolt diameter	t = laminate thickness
d_w = washer diameter	t_w = washer thickness
e = end distance	w = laminate width
L = laminate length	

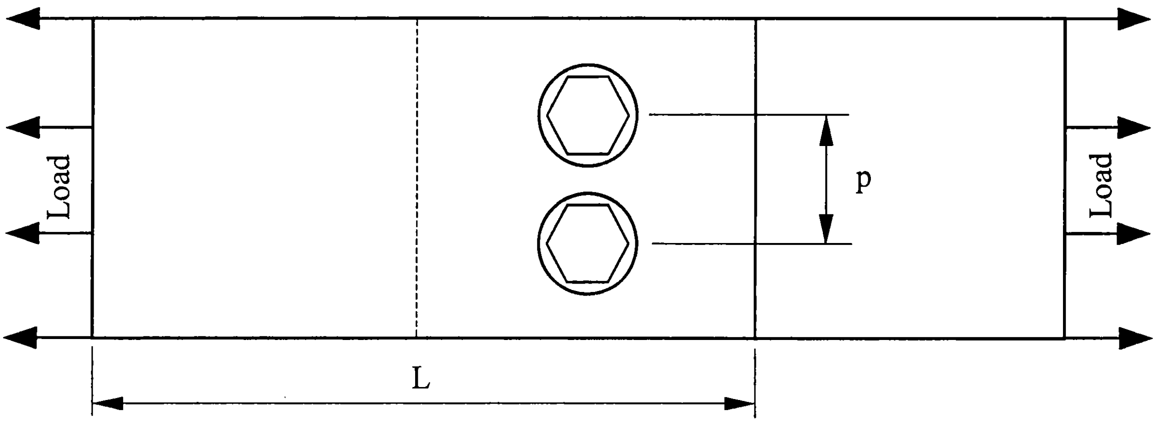

Figure 2.2 – Double lap multi-fastener joint arrangement showing two bolts side by side

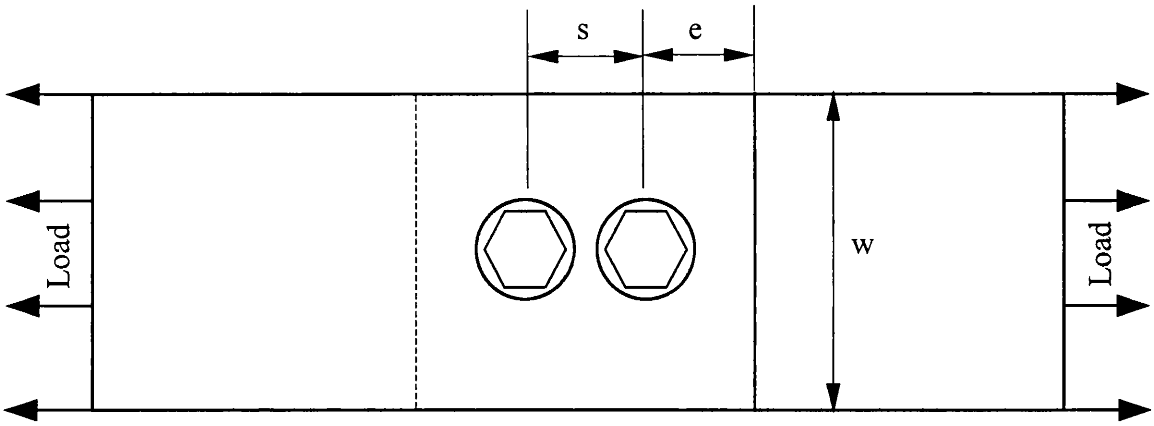

Figure 2.3 – Double lap multiple fastener joint arrangement showing two bolts in tandem

d_w = washer diameter	p = pitch spacing
e = end distance	s = row spacing
L = laminate length	w = laminate width

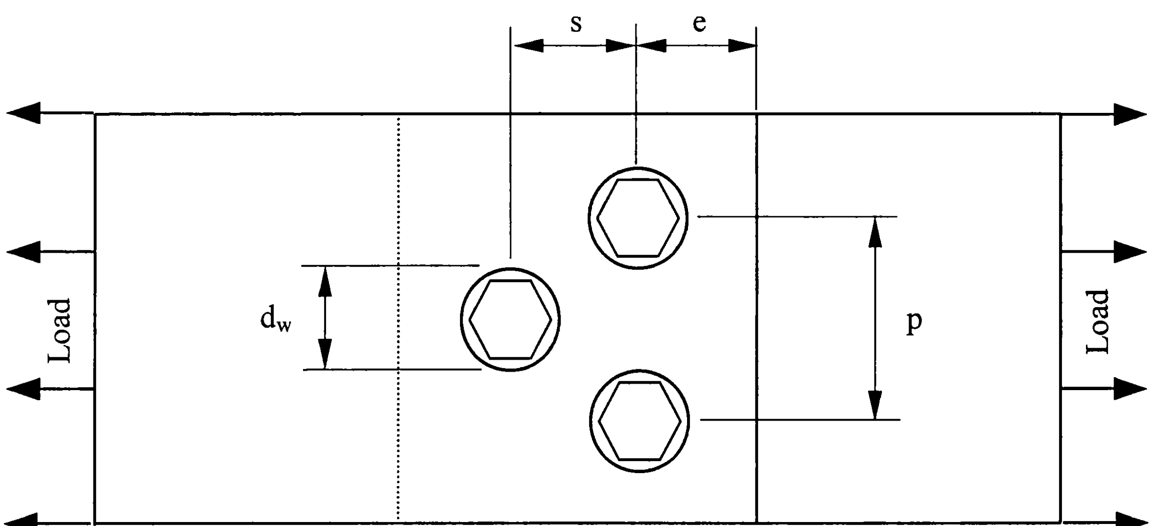

Figure 2.4 – Double lap multiple fastener joint arrangement showing staggered bolts

CHAPTER THREE

FINITE ELEMENT FORMULATIONS FOR CONTACT MECHANICS

3.1 – INTRODUCTION

The finite element method has been used extensively in simulating mechanically fastened joints in composite laminate materials so that the stress and strain sustained by the material under load may be evaluated. It is an approximate numerical solution to stress analysis problems, the accuracy of which depends upon the assumptions adopted in construction of the model. This chapter gives a brief overview of the finite element procedure and describes its application to contact mechanics. As I-DEAS (1993/1999) software has been used throughout the work reported here, the method of contact used by this software is described.

3.2 – OVERVIEW OF THE FINITE ELEMENT METHOD

The finite element method is now the most popular numerical technique used for the stress analysis of composite structures (Wood, 1994). Many commercial systems are now available incorporating this numerical technique and are becoming more accurate and more widely used with the development of better hardware and software. Each of the packages available have their own methods of data input and solution method, however, the general process by which an engineer carries out an analysis remains the same and follows the simple flow chart given in Figure 3.1.

In a broad sense the finite element method involves three processes. The first is the pre-processing stage, whereby the data is input, the mesh is constructed and the boundary conditions applied. The next stage is the solution, which the software carries out without any further input from the user. The final stage is post-processing, whereby the results of the analysis can be either extracted to external packages for analysis or can be displayed within the package used, depending upon the capabilities of the chosen software.

I-DEAS (1993/1999) software has been chosen for the simulations throughout the work reported in this thesis as it provides accurate results, as demonstrated in previous work such as Chutima (1996), and quite importantly, it also provides an excellent user interface with good graphics in both the pre- and post-processors. The stages of a simulation are as detailed in the following sections.

3.2.1 Pre-Processing

The first step in finite element modelling is to create the replica geometry of the structure being simulated. The geometry is then discretized into many elements to create a group of elements known collectively as a mesh. Each element in the mesh is connected to the next at nodal points, the number of which depends upon the required mesh refinement, which is usually determined from the shape of the structure, the type of elements used, and the desired accuracy.

To model laminated composites a three-dimensional analysis must be carried out by using a Representative Volume Element (RVE) approach or a replica approach. With the RVE approach global properties are applied to all the brick elements of the structure and are derived from individual fibre/matrix/ply properties using classical laminate theory. With the replica approach orthotropic brick elements are used for each lamina in the structure, whereby the orientation of the material properties is altered for each element of each lamina depending upon the stacking sequence used. This replica modelling method is useful for determining interlaminar and through thickness stresses (Wood, 1994), and will therefore be used throughout the analysis.

Once an appropriate mesh has been constructed boundary conditions such as restraints and loading must be applied, so that the model simulates the problem as accurately as possible. Restraints can be applied to limit nodes from movement in any one or more of their assigned degrees of freedom (the number of d.o.f. assigned to a node, depends upon the type of element attached to that node), to simulate for example symmetry or clamped conditions. Loads are applied to nodes in order to simulate the tension or compression applied to the joint. In the latest version of the I-DEAS software, contact parameters must also be set at this stage, whereby the maximum distance that I-DEAS must search for possible contact between elements must be set, and also the coefficient of friction between contacting surfaces. This is required, as the contact elements are not created physically, as gap elements were in earlier versions of the software but are created using these boundary conditions within the solve routine.

3.2.2 Solution

As detailed in Cook(1995), the finite element method is described as a piecewise polynomial interpolation, which can be carried out on an element, so that a certain quantity for that element can be interpolated from values of that quantity at each node. As each element is connected in the mesh the quantity can then be interpolated over the entire structure in a piecewise fashion using all the polynomial expressions. The whole process generates a set of simultaneous algebraic equations for values of the field quantity at nodes. The matrix construction, which represents the equations is as follows:

$$\mathbf{KD} = \mathbf{R} \tag{3.1}$$

where:

$\mathbf{K}$ = the stiffness matrix

$\mathbf{D}$ = the nodal displacement matrix

$\mathbf{R}$ = matrix of load on the mesh

The method for solving the simultaneous equations in I-DEAS is Gaussian elimination with a Cholesky decomposition. With Cholesky decomposition the matrix of equations is factorised into a lower and upper triangular matrix, which are a transpose of each other. After factorisation the equations are solved for the unknowns by performing a forward and backward substitution upon the load vector.

3.2.2.1 – Finite element application to contact mechanics

The solution to Equation 3.1 is non-linear in the analysis of a bolted joint connection, as the contact between the bolt and hole changes throughout the application of loading. The non-linear aspect of this analysis is dealt with by the contact solution within the I-DEAS software, whereby an iterative procedure is adopted until the contact conditions have converged.

There are two methods of contact available in the I-DEAS software, the first, which was the only method available in earlier releases of the software, is the 'gap element' method and the method more recently available is the 'contact element' approach. The method by which the equations are solved is the same in each contact simulation, however, they do differ slightly, as the constraint equations can only be imposed on nodes in the gap element approach, but in the contact element approach, the constraint equations are imposed at the integration points of each element in contact.

In determining the contact conditions during simulations, the I-DEAS software carries out four main stages in the following sequence:

(i) Kinematic equations describing the relative motion between each contacting surface are determined.
(ii) Equilibrium equations containing boundary conditions and contact constraints are then developed.
(iii) The two sets of equations are then transformed into equivalent finite element matrix equations.
(iv) The resulting matrix equations are then solved

Each process is described below:

(i) With reference to Figure 3.2, the penetration of the hitting point into the target surface occurs at the target point and is given by:

$$\mathrm{p_e} = \mathrm{p_{e0}} + \left(\mathbf{u}_{\mathrm{H}} - \mathbf{u}_{\mathrm{T}}\right) \cdot \mathbf{n} \qquad (3.2)$$

where:

$\mathrm{p_{e0}}$ = the initial penetration or separation

$\mathbf{u}_H$ = the motion of the hitting point

$\mathbf{u}_T$ = the motion of the target point

$\mathbf{n}$ = the normal vector, perpendicular to the hitting surface

When friction forces are also present, kinematic equations must also be determined to compute the relative tangential displacement increment, given by:

$$\Delta\mathbf{u}_t = (\Delta\mathbf{u}_H - \Delta\mathbf{u}_T) - [\mathbf{n}\cdot(\Delta\mathbf{u}_H - \Delta\mathbf{u}_T)]\mathbf{n} \tag{3.3}$$

where:

$\mathbf{u}_t$ = the tangential displacement

(ii) The contact constraints are imposed at the integration points on the finite element faces of the hitting region. The normal contact constraints are given by:

$$p_e \leq 0 \tag{3.4}$$

which states that the penetration must be less than or equal to zero, therefore, surfaces cannot interpenetrate,

$$t_n = -\mathbf{n}\cdot\mathbf{t} \geq 0 \tag{3.5}$$

which states that the contact pressure 't_n', which is defined as the negative of the normal surface traction component, cannot be tensile,

$$t_n p_e = 0 \tag{3.6}$$

which states that if the contact pressure is greater than zero, then the surfaces are in contact and if the penetration is less than zero, then the contact pressure is zero,

where:

p_e = the penetration

$\mathbf{t}$ = tangential traction

t_n = the contact pressure

When friction forces are also present constraint equations must also be developed for Coulomb friction conditions. The additional constraint conditions between the hitting and target surfaces are given as:

$$\phi = |\mathbf{t}_t| - \mu t_n \leq 0 \tag{3.7}$$

which imposes the constraint that the magnitude of the in-plane friction traction cannot exceed the coefficient of friction times the contact pressure. When the magnitude of friction force reaches its maximum allowable value, then the function ϕ will be equal to zero. Also,

$$\Delta \mathbf{u}_t = \Delta\xi \left(\frac{\mathbf{t}_t}{|\mathbf{t}_t|} \right) \tag{3.8}$$

which relates the relative tangential displacement increment between the hitting surface and the target surface, to the magnitude of the relative slip increment, which must be non-negative. When,

$$\Delta\xi \geq 0 \tag{3.9}$$

$$\phi \Delta\xi = 0 \tag{3.10}$$

the equations imply that if the magnitude of the relative slip increment is greater than zero, then there is slipping and the function ϕ must equal zero, and if the relative slip increment is zero, then the surfaces are sticking and the function ϕ must be less than zero.

where:

$\Delta\xi$ = the magnitude of the relative slip increment

$\mathbf{t}_t$ = the in-plane friction traction

$\Delta\mathbf{u}_t$ = the relative tangential displacement increment

In summary, as demonstrated in Figure 3.3:

- The maximum tangential traction equals the coefficient of friction times the normal traction force.

- Contacting surfaces stick if the tangential traction is less than the coefficient of friction times the normal traction force.

- Contacting surfaces will slide in the direction of tangential traction if the tangential traction equals the coefficient of friction times the normal traction force.

(iii) The kinematic and equilibrium equations described above for contact must then be transformed into finite element matrix equations using interpolation equations for each element face, so that the equations can be solved with the rest of the model.

(iv) The set of equations are then solved globally using an augmented Lagrangian procedure. This method offers advantages over previously used pure penalty methods and Lagrangian multiplier methods. A penalty stiffness is added but unlike pure penalty methods, the contact constraint solutions can be achieved with almost any required degree of accuracy through a series of contact traction updates. The penalty number can, therefore, be lower than in the penalty method, resulting in better conditioned equations.

An iterative procedure is adopted consisting of an inner loop and an outer loop. The inner loop iteratively updates the contact pressure (using the penalty number) for each active contact element to enforce the zero penetration constraint. The outer loop determines the contact element status, whereby inactive contact elements are activated if penetration between surfaces occurs, and active contact elements are set as sticking or sliding depending upon contact tractions, or are disabled if tensile forces exist.

The contact solution finishes once the contact tractions have converged and the contact status remains unchanged during an iteration.

The steps involved in the overall contact solution are as shown in Figure 3.4.

3.2.3 Post-Processing

The post processing stage involves extracting sample results such as stress or strain, which can be compared to previous work or simple calculations in order to validate the model. If the results are satisfactory, the rest of the results can be extracted or displayed for analysis. This can be carried out within the software used, or the results can be exported to another software package for analysis. However, as the I-DEAS software has an excellent post-processor the results were extracted and displayed within the software throughout this investigation.

The actual value of stress or strain is computed at the integration points of an element within the solution routine, however, during post-processing the values can be extracted at nodes, whereby the values from the integration points of a particular element have been extrapolated, or they can be taken from the element, which is the average between the values at each integration point of that element.

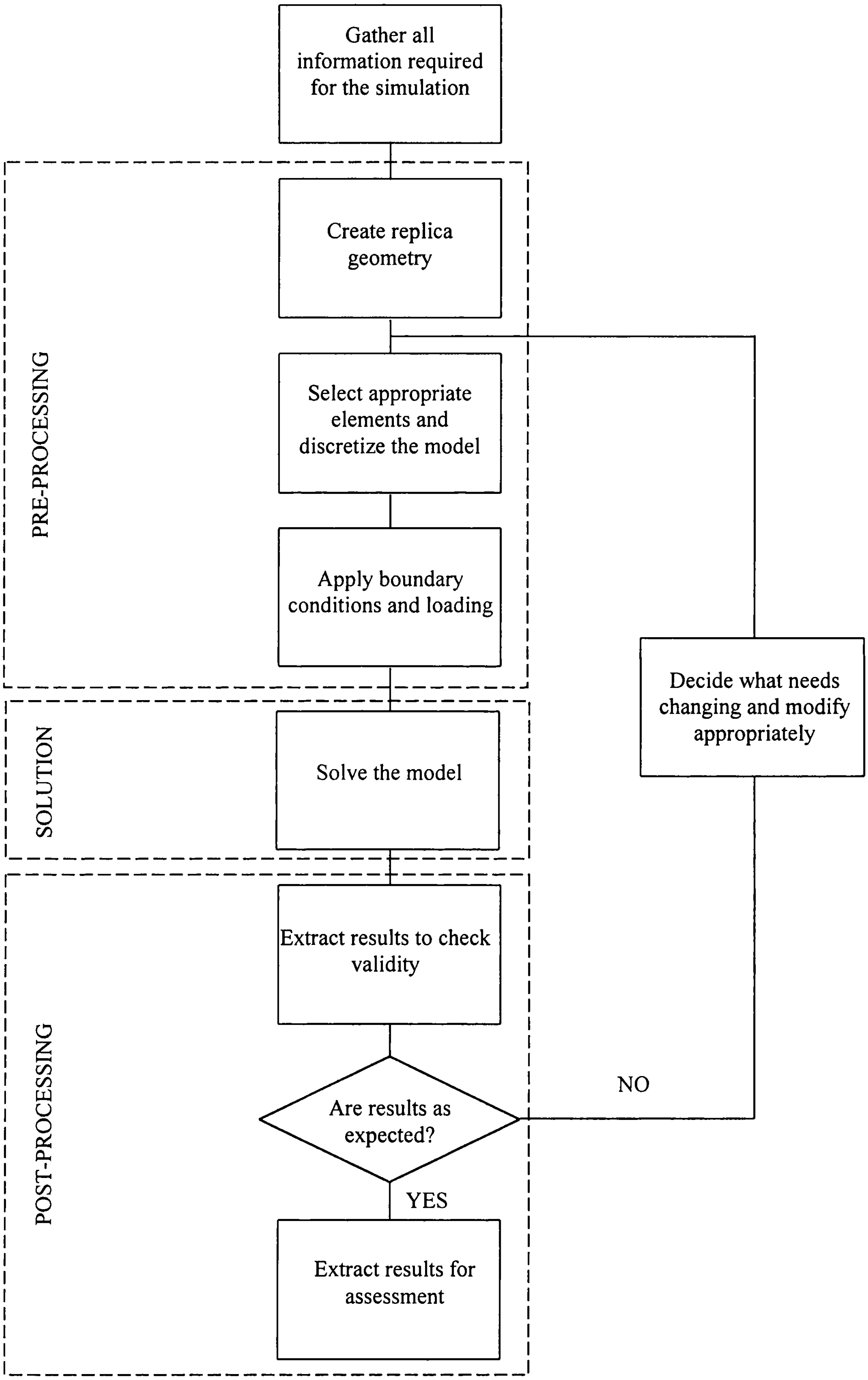

Figure 3.1 – Flowchart describing the finite element process

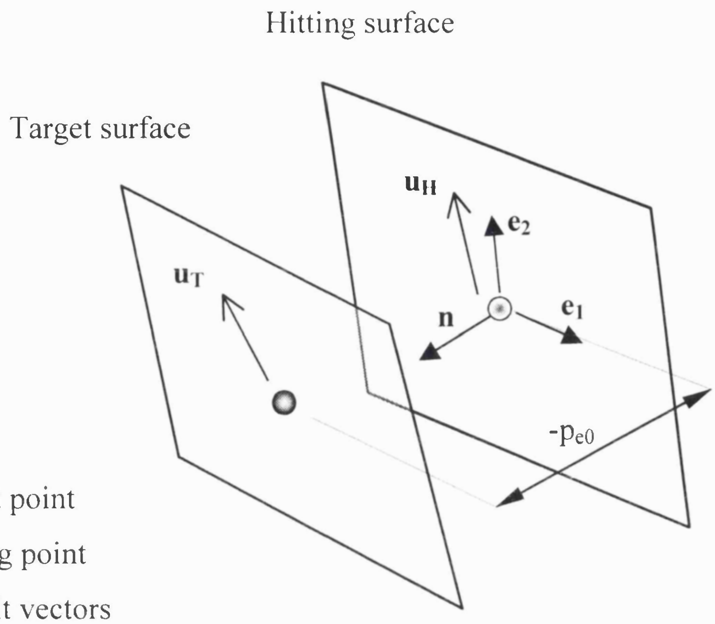

● = target point

⊙ = hitting point

$\mathbf{e}_1/\mathbf{e}_2$ = unit vectors

$\mathbf{n}$ = normal vector

p_{e0} = initial penetration

$\mathbf{u}_H$ = motion of hitting point

$\mathbf{u}_T$ = motion of target point

Figure 3.2 – Diagram showing notation used for the contact algorithm

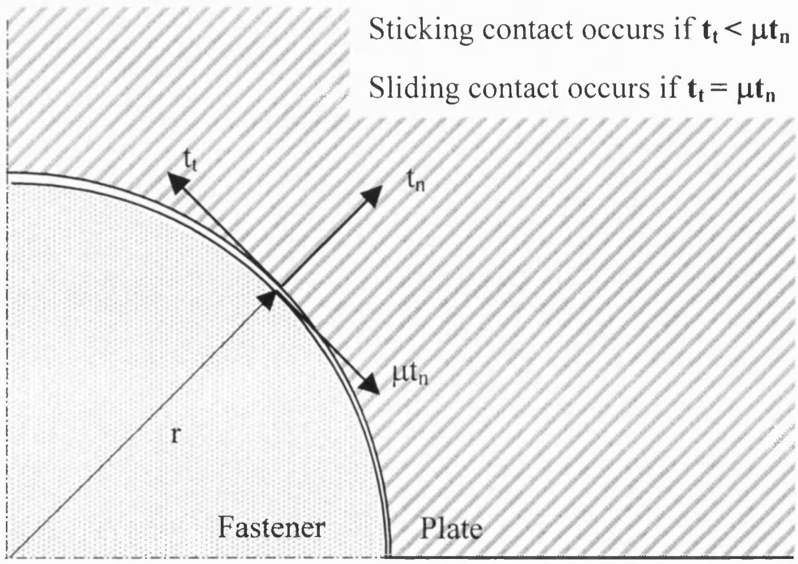

Figure 3.3 – Summary of contact between elements of the fastener and plate

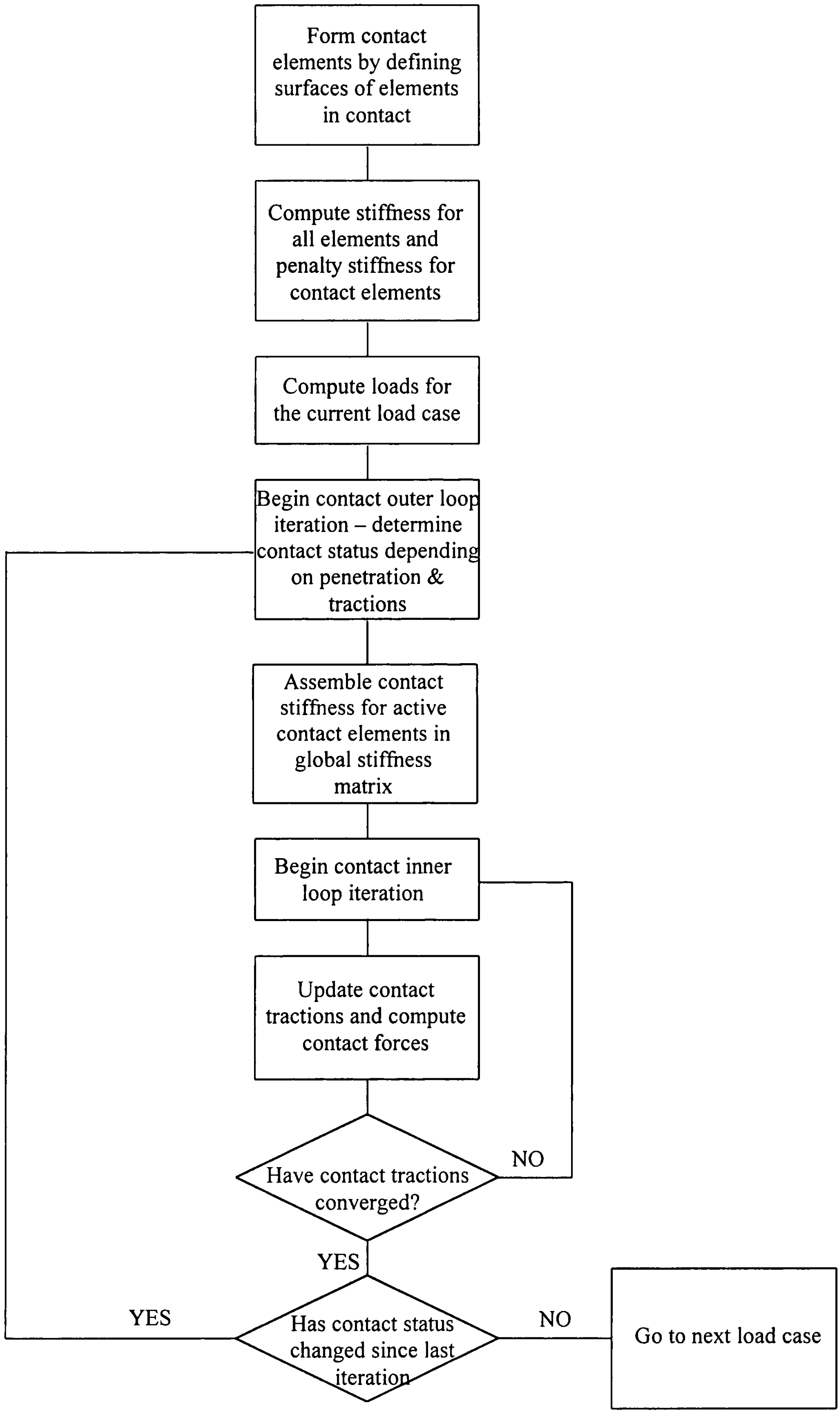

Figure 3.4 – Flowchart describing the contact solution process

CHAPTER FOUR

VERIFICATION OF MODELLING TECHNIQUE

4.1 – INTRODUCTION

In order to accurately predict the stress distribution in a composite laminate double lap joint, a comprehensive three-dimensional finite element analysis must be performed so that through thickness effects can be examined. In this chapter, three-dimensional models were constructed using I-DEAS Master Series versions 1.3c and 7.0 (1993/1999), to validate results with published three-dimensional work reported by Chutima (1996), which was validated against experimental results.

The first model was constructed using I-DEAS version 1.3c. With this version of the software, the only method for modelling contact was using gap elements, which are placed between coincident nodes of the pin and the hole and between each plate. This version of the software was used by Chutima (1996), therefore a direct comparison could be made between the results obtained in the current study.

Using the latest release of I-DEAS (1999) subsequent models were constructed using contact elements, which are connected between coincident element faces of the pin and hole and at the interface of each plate. This new modelling technique was also validated using the results of Chutima (1996). This particular version of the software also has no restrictions on the number of elements available for modelling contact, therefore mesh refinement could be carried out without restrictions.

4.2 – CONSTRUCTION OF MODEL

Common aspects of each model construction are described in this section, with version specific aspects detailed in separate sub-sections.

A double lap composite joint, consisting of two outer laps and a single inner lap was modelled in the investigations reported in this chapter. The inner lap was chosen to be twice as thick as the outer lap and was restrained from movement in all directions at the end furthest from the fastener. The end of each outer lap furthest from the fastener was subjected to a 2kN tensile load. Each laminate plate was constructed using GRP material properties, the outer laps having a $(0/45/-45/90)_s$ stacking sequence, and the inner lap having $((0/45/-45/90)_s)_s$. The load was transferred through the plates via an aluminium pin with no clamping force applied. The physical joint layout can be seen in Figure 4.1, the laminate lay-up can be seen in Figure 4.2 and the material properties used are shown in Table 4.1.

Table 4.1 – Material properties for each unidirectional lamina and the fastener (Chutima,1996)

Material	E_{11} (GPa)	E_{22} (GPa)	E_{33} (GPa)	G_{12} (GPa)	G_{23} (GPa)	G_{31} (GPa)	ν_{12}	ν_{23}	ν_{31}
GRP	31.8	10.2	7.14	2.14	2.14	2.14	0.328	0.199	0.045
Aluminium T6061-T6	68.3	68.3	68.3	25.7	25.7	25.7	0.33	0.33	0.33

When simulating the joint, symmetry permitted the modelling of only a quarter of the physical joint, as demonstrated in Figure 4.1. Although this is physically acceptable, the use of angle plies such as 45° within the laminate sequence, would create antisymmetric conditions in the xz- plane, thus requiring half of the model to be analysed. However, if symmetry in this plane is used a significant difference in stress would only occur on the bearing plane, and work conducted by Matthews et al. (1982b) using a half model and a quarter model has shown that this difference is only 5%, approximately. Work conducted in the present study confirmed this and since the only difference in stress is on the bearing plane of the 45° plies, which are not areas of highest stress, it was considered appropriate to simplify the model by using both planes of symmetry to significantly reduce the running time. Restraints were therefore placed on nodes along the bottom edge of the plates and the pin, by fixing the y- direction displacement as zero, thereby simulating the lower portion of the model. Where symmetry was modelled on the inner lap, the nodes were restrained by fixing the z- direction displacement as zero. At the far end of the inner lap the nodal displacements were fixed in the x-, y-, and z- directions, thereby simulating clamped conditions. On the outer lap, at the end furthest from the pin, the nodes were loaded in the negative x- direction to simulate the 4kN tensile load on the joint. A typical finite element mesh used for this investigation can be seen in Figure 4.3.

The laminate stacking sequence was applied to the model using a replica approach, whereby the GRP unidirectional material properties were assigned to the plate elements, and then the material axes for every element in a lamina were oriented to give the desired stacking sequence as shown in Figure 4.2.

4.2.1– Gap Element Model

Models incorporating gap elements were constructed using I-DEAS Master Series version 1.3c, having the mesh as outlined in Figure 4.3, with 1667 elements in total. The GRP plates were constructed using 1248 eight-node solid linear brick elements. These elements use serendipity interpolation functions with incompatible internal interpolation functions, details of which can be found in Cook (1995). This results in good performance when applied in bending and will not lock for nearly incompressible materials. The aluminium pin was constructed using 216 six-node solid linear triangular elements. The contact was modelled by connecting the nodes, expected to come into contact with each other, using 203 node-to-node type gap elements. This allowed for a coefficient of friction (μ=0.2) to be introduced at the plate interfaces and around the portion of pin in contact with the plates. With this method, a local cylindrical co-ordinate system had to be constructed to define the contact and friction directions for the nodes attached to the gap elements.

4.2.2 – Contact Element Model

Subsequent models were constructed using I-DEAS Master Series version 7, enabling the use of contact elements rather than gap elements. The first model constructed using this method consisted of 1724 elements, having 1248 eight-node solid linear brick elements for the laminate plies and 216 six-node solid linear triangular for the aluminium pin. For this method of contact a global search was applied by the software, whereby 260 contact elements were automatically placed between all coincident element faces to model possible contact during the solve. A friction coefficient of μ=0.2 was applied to all contacting surfaces, as many investigators such as Chen and Lee (1995) have considered this as a realistic representation of interfacial friction for this type of joint.

In an attempt to obtain more reliable approximations, two models were constructed using more refined meshes in the through thickness direction. For each ply of the laminate, three elements and eight elements were used in the through-thickness direction. The model containing three elements, consisted of a total of 5012 elements, 3744 eight-node solid linear brick elements for the plates, 624 six-node solid linear triangular for the pin and 644 contact elements. The model containing eight elements consisted of a total of 13232 elements, 9984 eight-node solid linear brick elements for the plates, 1644 six-node solid linear triangular for the pin and 1604 contact elements.

The model was then refined around the hole periphery, whereby nodes on the hole boundary subtended angles of 9°, 5° and 3° rather than 15°. Three elements were used for each ply in the through thickness direction for each of these models.

4.3 – RESULTS AND DISCUSSION

For all the investigations using the double lap joint shown in Figure 4.2, the radial stress results were extracted from each node on the hole boundary and for each layer of nodes through the thickness. These results were then normalized using the average bearing stress, where:

$$\text{Normalized radial stress} = \frac{\sigma}{\overline{\sigma}_b} \tag{4.1}$$

Where, the average bearing stress $\overline{\sigma}_b$ is given by:

$$\bar{\sigma}_b = \frac{\text{Load}}{d_{bo} \times t} \tag{4.2}$$

where:

d_{bo} = bolt diameter

t = laminate thickness

The results calculated for the normalized radial contact stress around the hole boundary of the outer and inner laps were then plotted against their respective angular position. The description of each notation used for all graph plotting can be seen in Figure 4.4. The curve produced using the results from nodes around the hole on the outer surface of each lap is labelled as '1'. Each label then increases consecutively with each set of nodes through the thickness of the laminate. For clarity, the following symbols '*' and '#' are given next to the node layer number representing the outer surface and laminate interface nodes respectively for the outer lap, and the laminate interface and the laminate mid-plane respectively for the inner lap.

Figures 4.5 and 4.6 show the radial stress results for the outer and inner lap respectively, produced using the same method as Chutima (1996) for a direct comparison. From these figures it can be seen that the radial contact stress results are in very close agreement with the reported data. Any slight discrepancy between the results at the bearing plane may be attributed to a slightly different tolerance between the pin and the hole. Although the pin is tight fitting in the hole, there must still be a very small physical gap to enable insertion of the gap elements. It is also demonstrated that the normalized stress reaches its highest value on the bearing plane on the ninth layer of nodes of the outer lap and on the first layer of nodes on the inner lap, corresponding to the interface between the outer and inner laps. This arises from pin bending as the outer lap moves toward the direction of loading while the inner lap is restrained from movement.

It may also be observed from these figures that at 90° around the hole boundary the radial stress seems to become minimal and tensile as there is no contact between the pin and the plate Hence, the stresses in this area are due to the deformation of the hole being constrained by the contact at the laminate interface.

For the analyses using the contact element method the same results were extracted by the same method as described for the model incorporating gap elements. Figures 4.7 and 4.8 show the variation in the normalized radial contact stress obtained around the hole boundary for the model having one element per lamina thickness for the outer and inner laps, respectively. For comparison, the results obtained for the outer and inner laps using three elements per lamina and eight elements per lamina thickness, are given in Figures 4.9 and 4.10 and Figures 4.11 and 4.12, respectively. Mesh convergence results showing the difference between the magnitudes of the through thickness stress components and percentage difference for each refinement level can be seen in Table 4.2.

Table 4.2 – Mesh convergence results (refinement through the thickness)

Refinement through the thickness	Maximum Stress (MPa)			% Change		
	σ_r	σ_z	τ_{xy}	σ_r	σ_z	τ_{xy}
1 Element per ply	-120.9	4.81	64.6	-	-	-
3 Elements per ply	-163	13.2	78.3	34.8	174.4	21.2
8 Elements per ply	-164	11.8	80.4	0.6	-10.6	2.7

By comparing the results in Figures 4.7 and 4.8 to those in Figures 4.5 and 4.6, the effects of changing the method of contact can be seen. The figures demonstrate that both methods give very similar results, although the results from the contact element approach should be slightly more accurate as the revised software is more refined and adopts a better approach to modelling the contact condition. The improvement in contact method is described in Chapter 3.

As can be seen from Figures 4.9 and 4.10, the more refined mesh using three elements per layer results in higher peak stress values. Figure 4.9 shows a peak normalized stress of approximately 3.3 compared to the peak stress of approximately 2.3 given in Figure 4.7. This effect is explained by Cook (1995) where a less refined mesh will give lower stresses compared with a more accurate highly refined mesh. An important feature of Figure 4.9 is that the second ply from the inner lap/outer lap interface shows the peak stress to appear at an angle of 45°, which coincides with the fibre direction. This effect is not observed in Figure 4.5 or Figure 4.7 using one element per lamina thickness. The results given in Table 4.2 show that there is a large difference between the maximum stresses obtained by refinement of the model and in particular a 174% difference was observed in the z- direction stress.

The results obtained using the more refined mesh of eight elements per lamina, shown in Figures 4.11 and 4.12, do not include the stress results for five of the eight plies furthest from the inner/outer lap interface, as the results for these were considered insignificant. The results shown in these figures and in Table 4.2 demonstrate that the mesh refinement need not exceed three elements through the thickness, as the results compare well with those presented in Figures 4.9 and 4.10 and the peak radial and shear stresses vary insignificantly. Although there is approximately a ten percent difference between the z-direction stresses obtained from models having three and eight elements per ply, the improvement is very small when considering the threefold increase in computational time. These results also show that the stresses throughout the plate are higher than those in Figures 4.5 and 4.6, indicating that the refined mesh is more appropriate for determining the highest stresses in the plate and that the joint is in fact weaker than previously thought from the evaluation by Chutima (1996).

With both three and eight elements representing each ply thickness, the mesh aspect ratios are 7 and 18 respectively, which are very high, and could lead to inaccurate stress results at regions of high stress concentration. Refinement of the mesh around the hole boundary may reduce the aspect ratio, thereby increasing the reliability of the results. Figures 4.13 and 4.14 demonstrates that with a more refined mesh, having 20 elements around half the hole boundary, compared with 12 elements, and 3 elements per lamina thickness, the peak radial stresses do not change very much but a smoother stress distribution is obtained. The same effect was observed with the radial stress results for both 36 elements around half the hole boundary (Figures 4.15 and 4.16) and 60 elements around half the hole boundary (Figures 4.17 and 4.18). From Table 4.3 it can be seen that by refining the mesh to one element every 9° around the hole boundary, the maximum z-direction and xy- shear stresses change by approximately 12% and 14%, respectively. The percentage change reduces to approximately 8% and 4%, respectively, with a further refinement of one element every 5° around the hole boundary. With one element every 3° around the hole boundary the z- direction stress changes only marginally and is considered negligible when taking into account the increased computational time. Hence, the mesh constructed with 36 elements around half the hole boundary (one element every 5°) will be used in the subsequent work. It was also observed from the results in Table 4.3 that the angle of contact between the pin and the hole, at the outer surface of the outer lap, remained almost unchanged for meshes with 20, 36 and 60 elements around half the hole boundary.

Table 4.3 – Mesh convergence results (refinement around the hole)

Refinement around the hole periphery	Contact Angle (°)	Maximum Stress (MPa)			% Change		
		σ_r	σ_z	τ_{xy}	σ_r	σ_z	τ_{xy}
Element every 15°	120	-163	13.2	78.3	-	-	-
Element every 9°	108	-152.2	11.6	89.2	-6.6	-12.1	13.9
Element every 5°	110	-156.6	10.7	92.8	2.89	-7.8	4
Element every 3°	108	-159.6	10.3	94.5	1.9	-3.7	1.8

4.4 – CONCLUDING REMARKS

The modelling technique developed in this chapter has been verified using the previously published three-dimensional stress results of Chutima (1996). The results obtained using both the 'gap element' and 'contact element' method of contact compared extremely well to the previously reported work. The more recent version of this software will therefore be used for subsequent studies, as the 'contact element' method available in this release is easier to use and has improved contact formulations.

By using three and eight elements per ply thickness to refine the mesh the magnitude of maximum radial stress was shown to increase slightly compared to one element per lamina, indicating that the mesh used by Chutima (1996) was not optimised. The more refined meshes were also able to demonstrate features not shown previously, such as a peak radial stress at an angle of 45° to the loading direction for the ply oriented at 45° to the loading direction. The refinement of three elements per ply thickness was therefore adopted for all further work.

By using 20, 36 and 60 elements around half the hole boundary rather than 12, so that each node around the hole boundary subtended angles of 9°, 5° and 3° rather than 15°, the mesh was further refined. As a result of this refinement, the resultant radial stress curves exhibit less marked changes from point to point and, compared to the initial unrefined mesh, indicate slightly different positions of the peak stress around the hole boundary. Considering the running times and the results obtained from the mesh convergence tests, the mesh constructed using one element every 5° around the hole boundary will be used in the subsequent work.

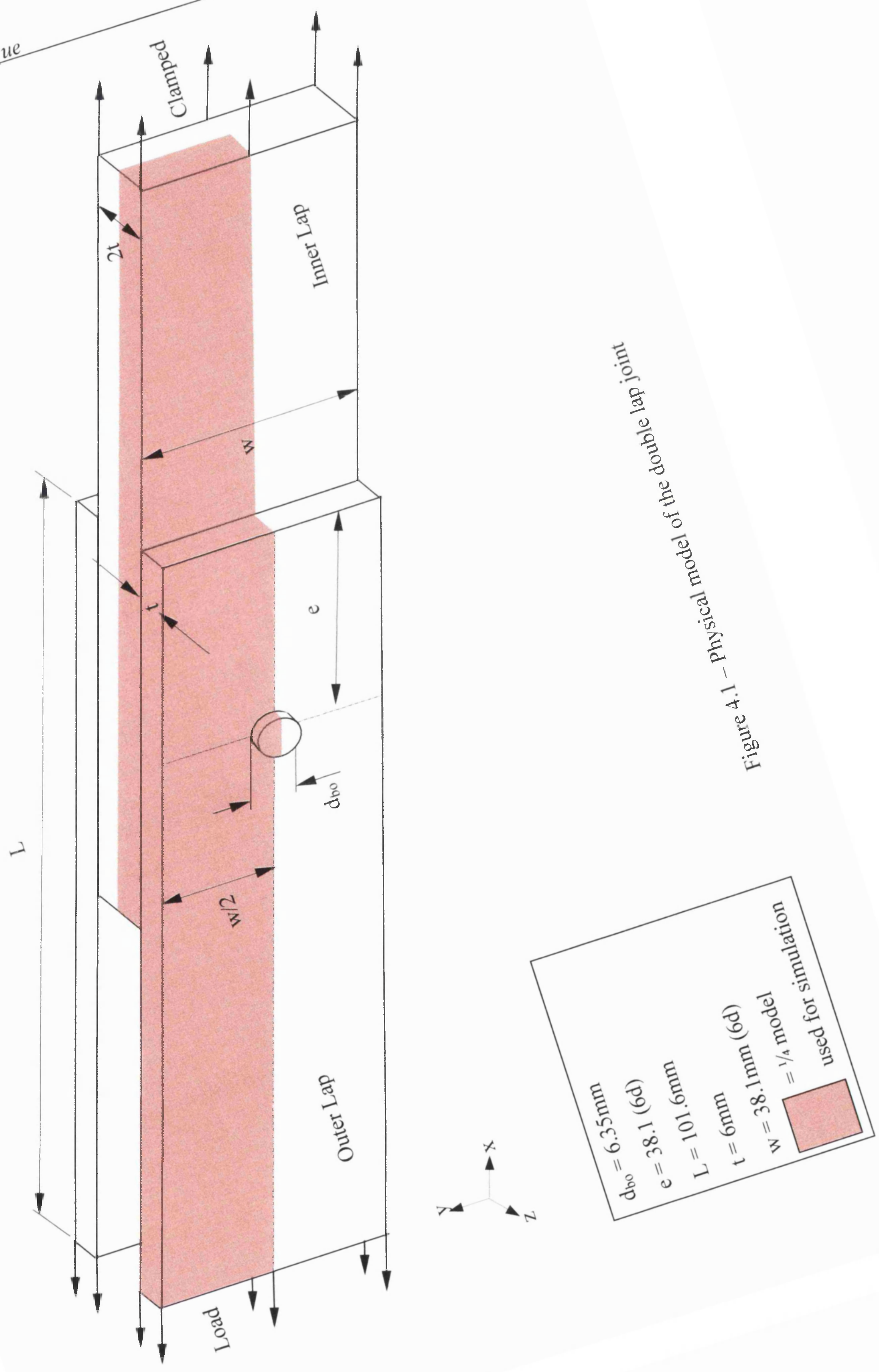

Figure 4.1 – Physical model of the double lap joint

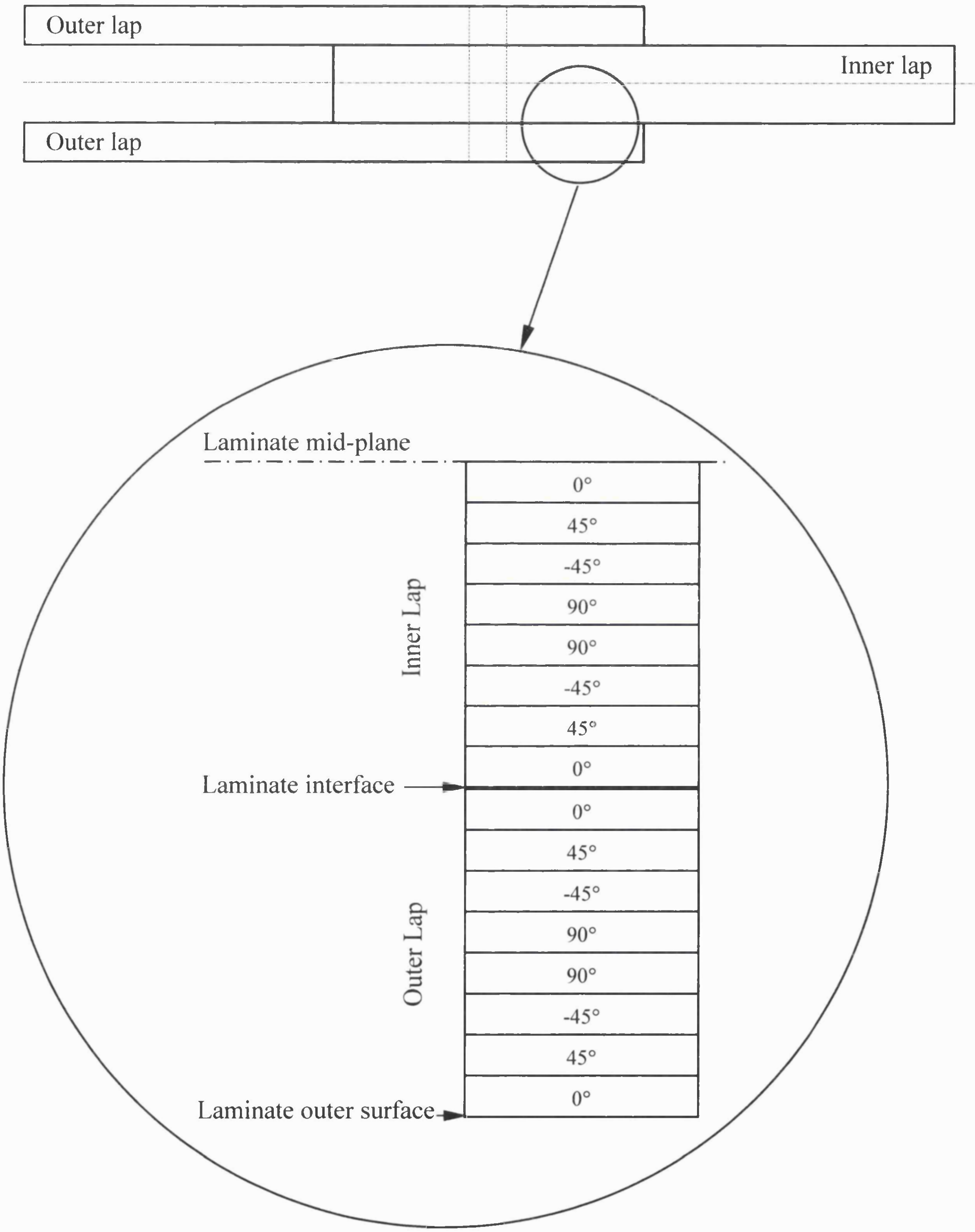

Figure 4.2 – Laminate lay-up for the stacking sequence $(0/45/-45/90)_s$

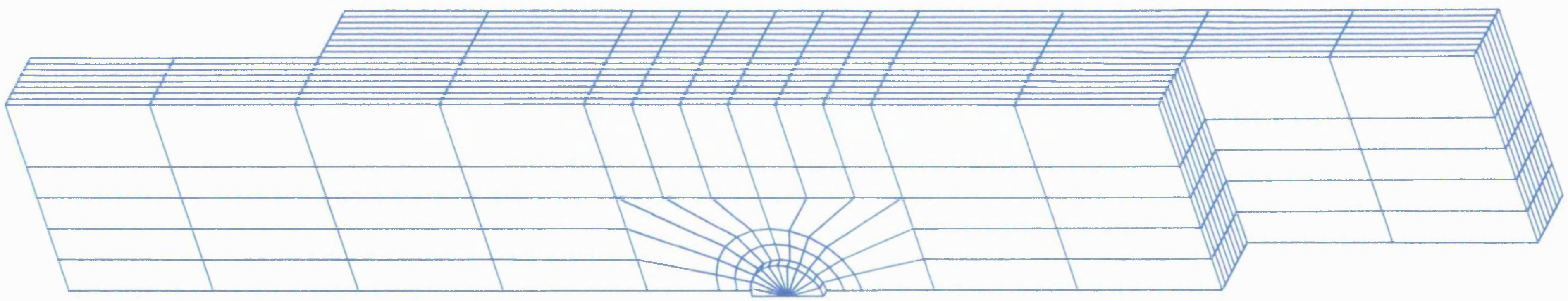

Figure 4.3 – Element layout for the three-dimensional model

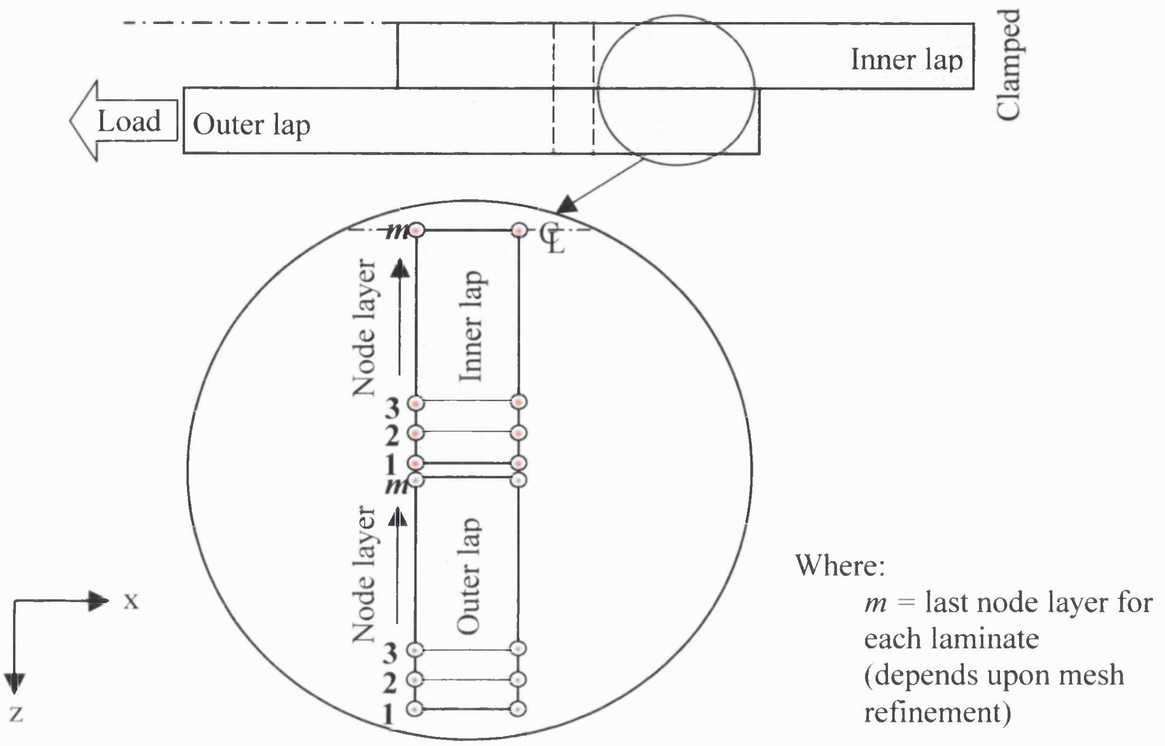

Figure 4.4a – Description of 'node layer' notation used for graph plots

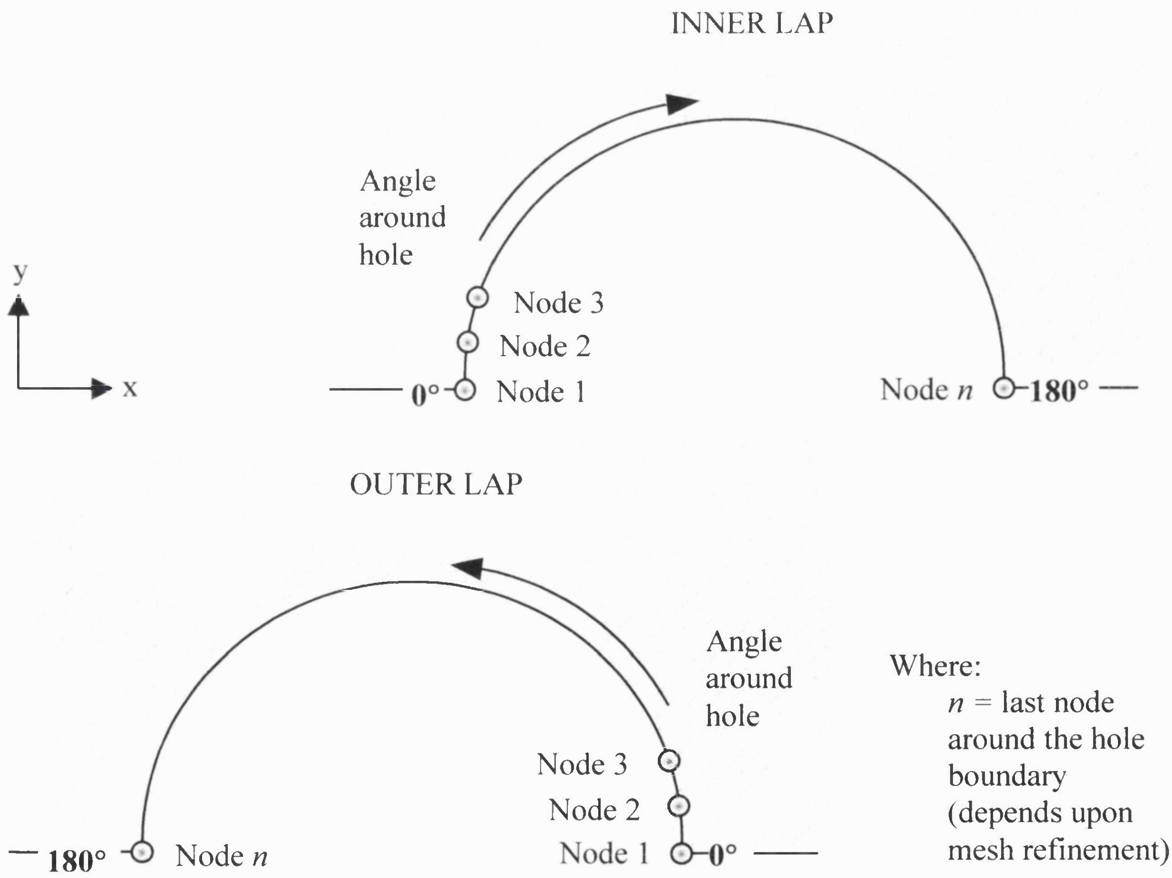

Figure 4.4b – Description of 'angle around the hole' notation used for all graph plots, for both the inner and outer laps

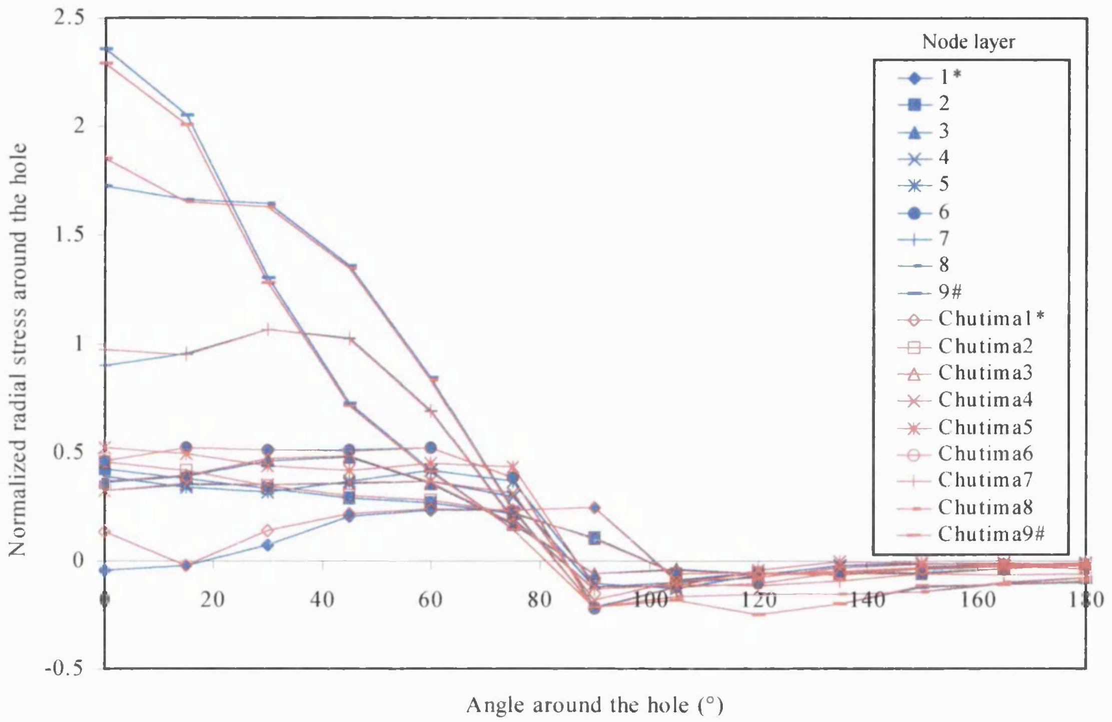

Figure 4.5 – Comparison of normalized radial stress of the outer lap with Chutima (1996)

* = Outer surface, # = Laminate interface

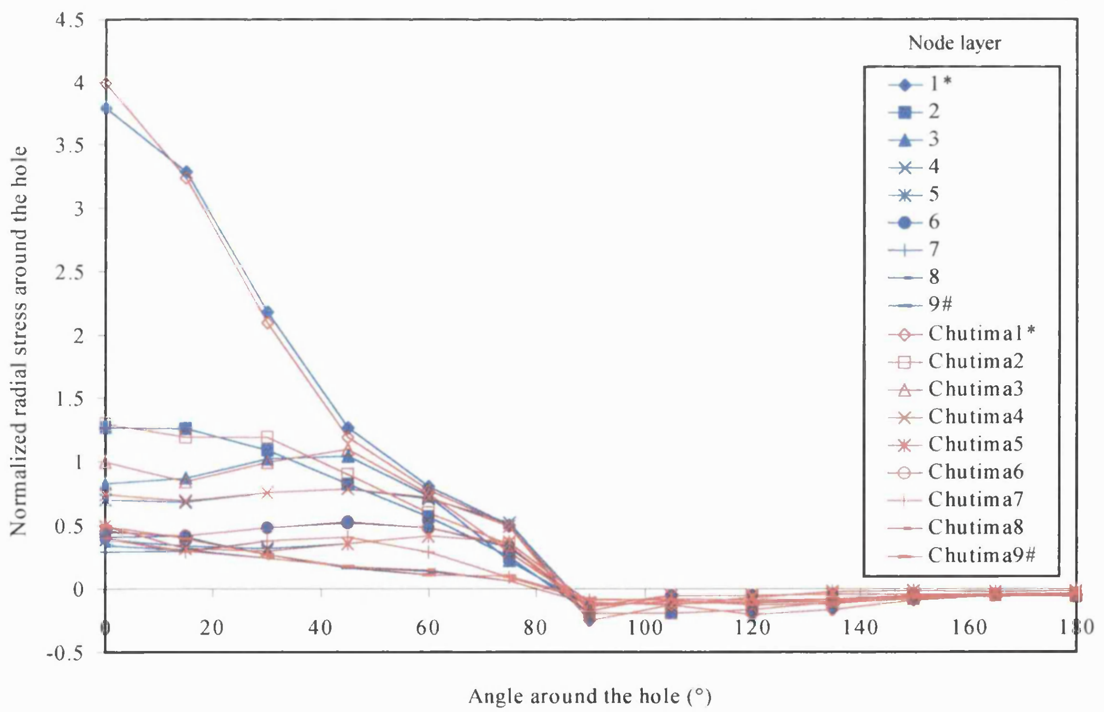

Figure 4.6 Comparison of normalized radial stress of the inner lap with Chutima (1996)

* = Laminate interface, # = Laminate mid-plane

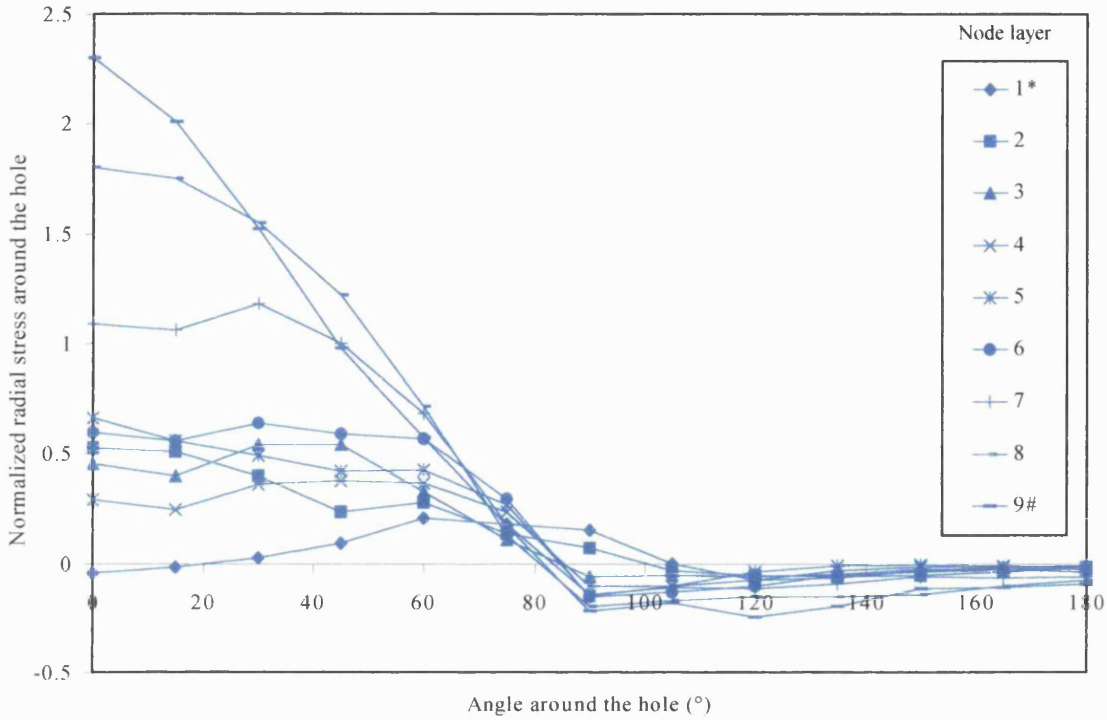

Figure 4.7– Normalized radial stress results of the outer lap for contact element method (1 element per lamina thickness, 12 elements around the half hole)

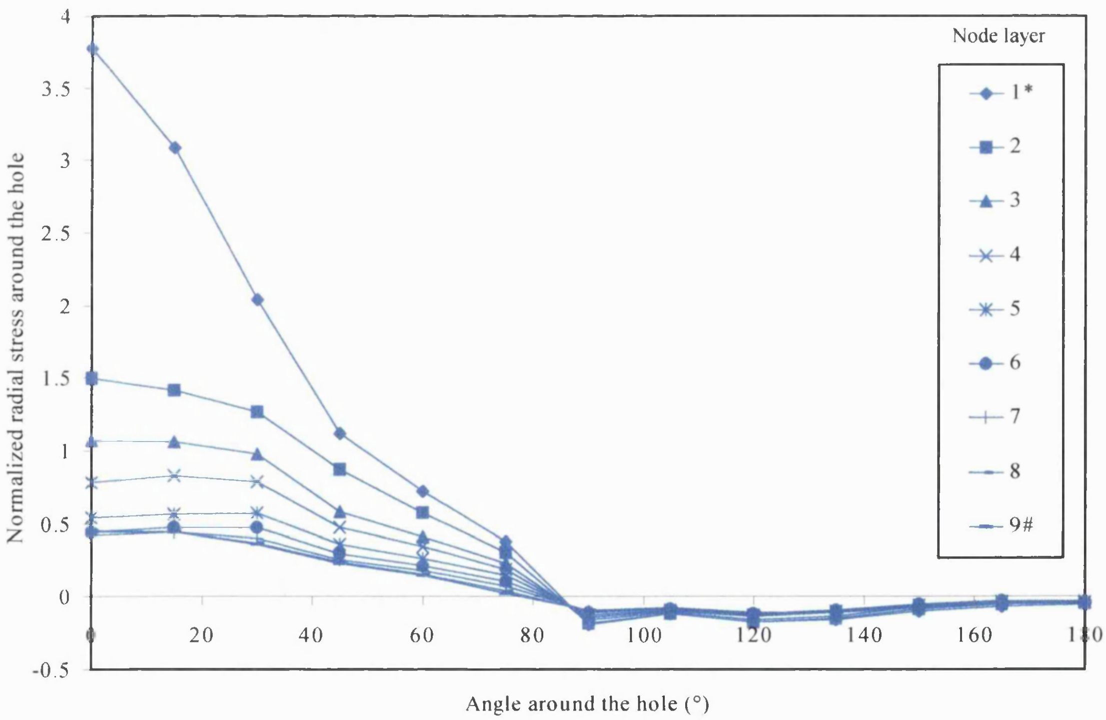

Figure 4.8– Normalized radial stress results of the inner lap for contact element method (1 element per lamina thickness, 12 elements around the half hole)

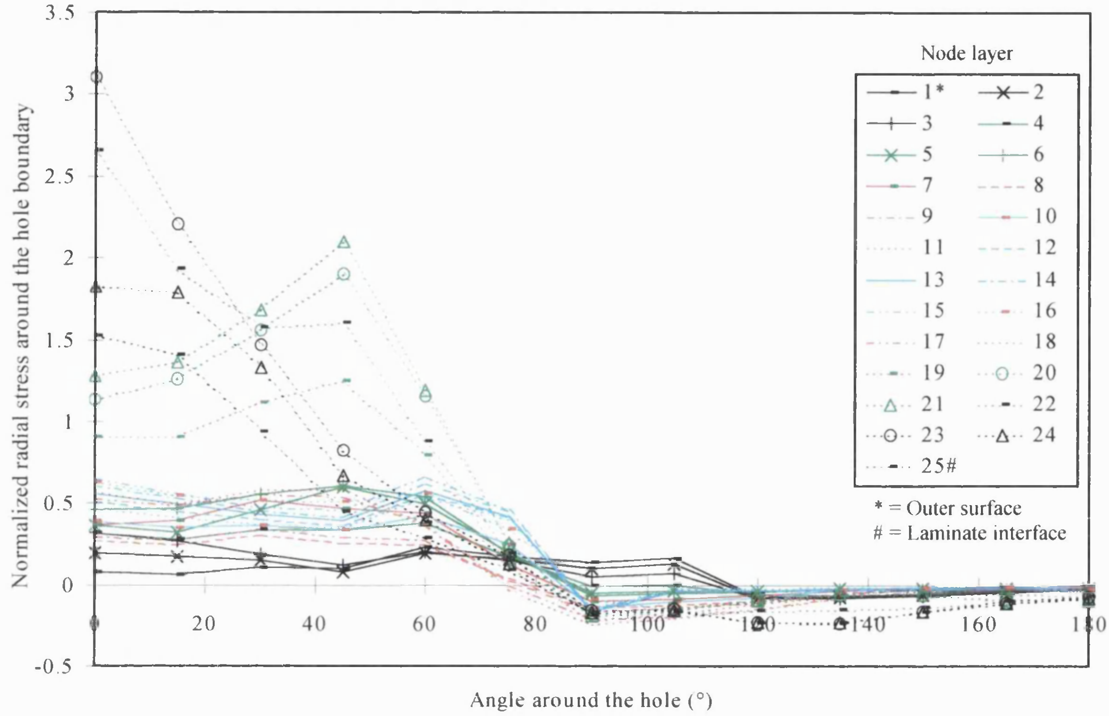

Figure 4.9– Normalized radial stress results of the outer lap - contact element method (3 elements per lamina thickness, 12 elements around the half hole)

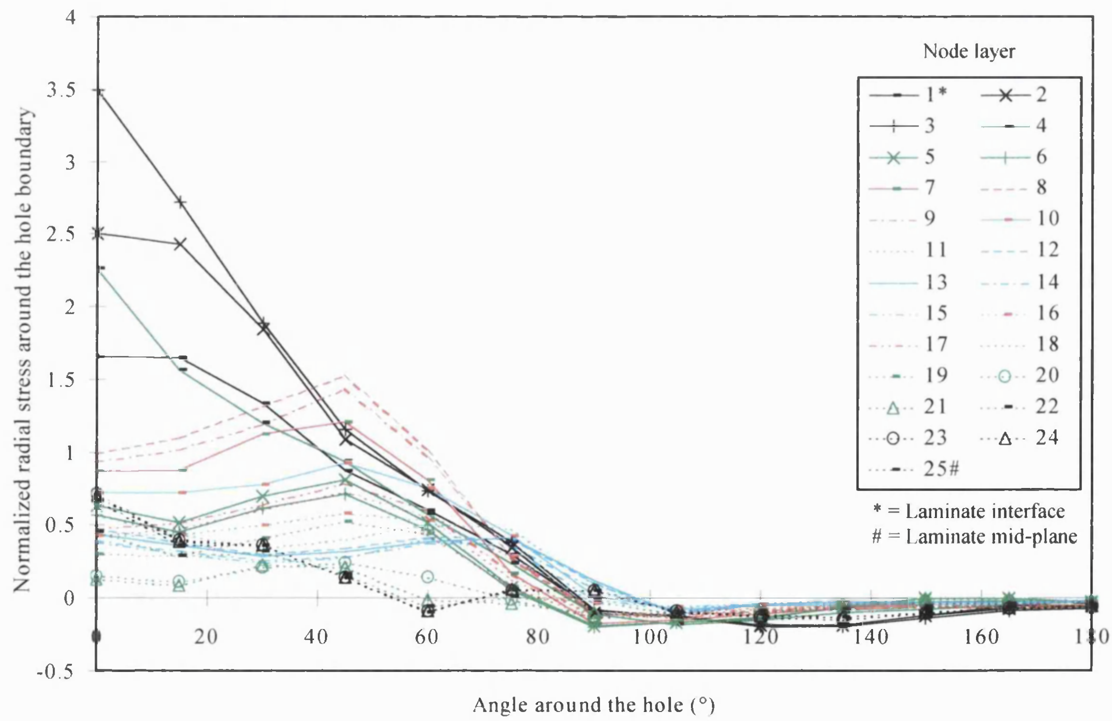

Figure 4.10– Normalized radial stress results of the inner lap - contact element method (3 elements per lamina thickness, 12 elements around the half hole)

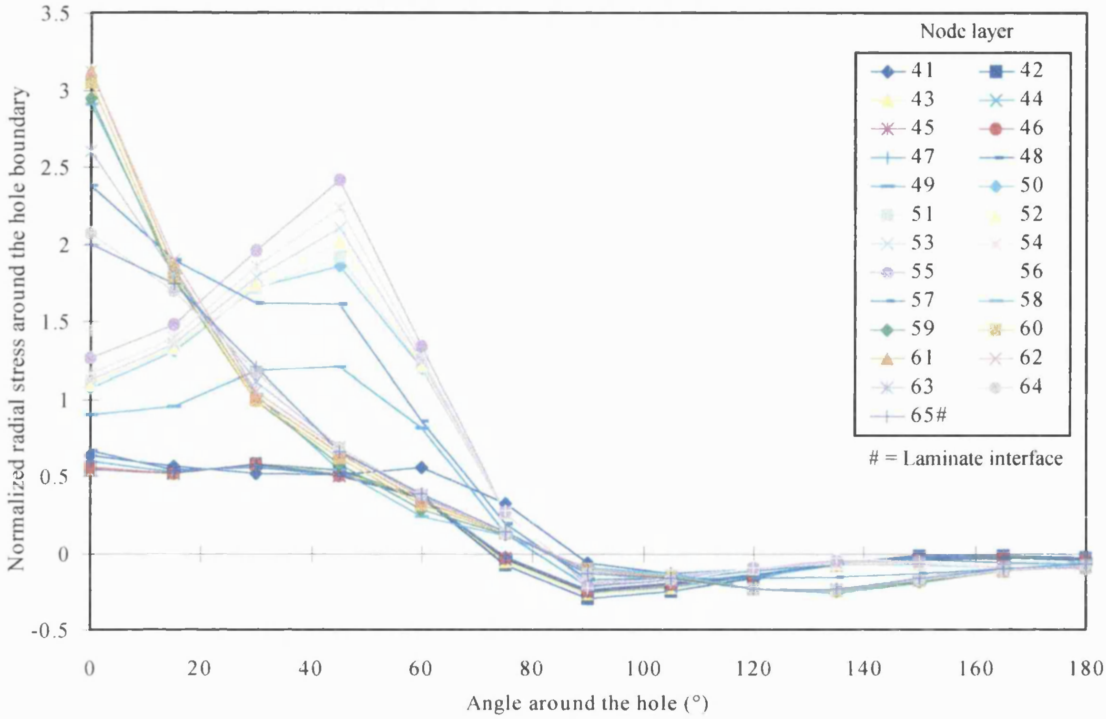

Figure 4.11 – Normalized radial stress results of the outer lap - contact element method (8 elements per lamina thickness, 12 elements around the half hole)

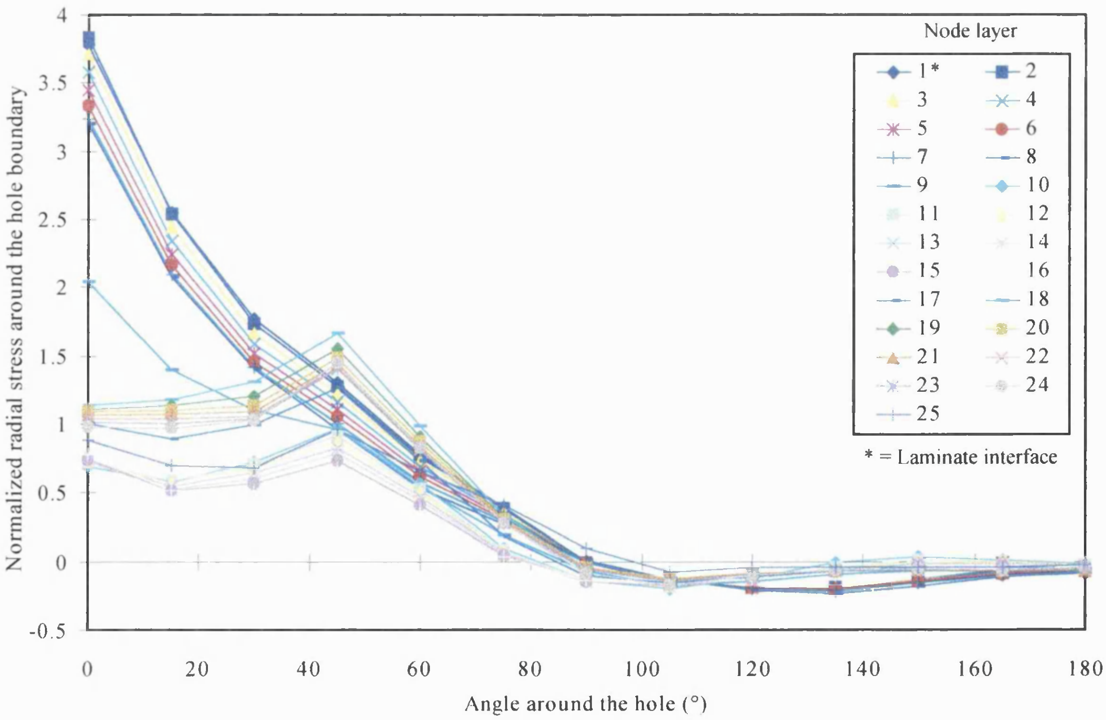

Figure 4.12– Normalized radial stress results of the inner lap - contact element method (8 elements per lamina thickness, 12 elements around the half hole)

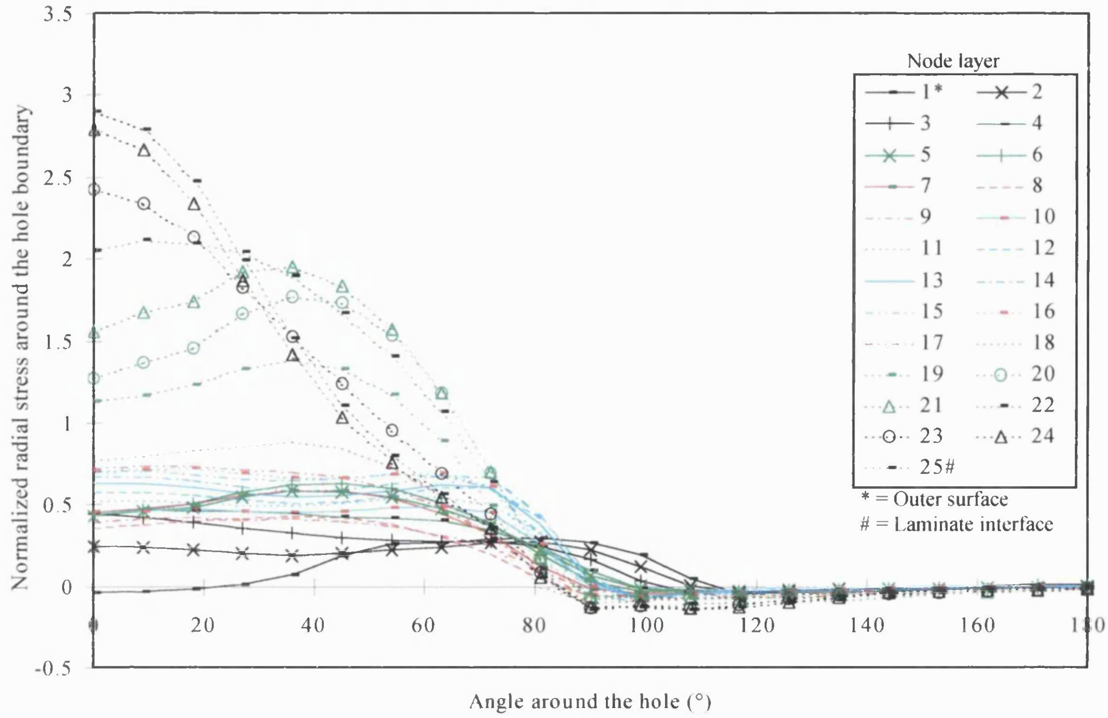

Figure 4.13– Normalized radial stress results of the outer lap - contact element method (3 elements per lamina thickness, 20 elements around the half hole)

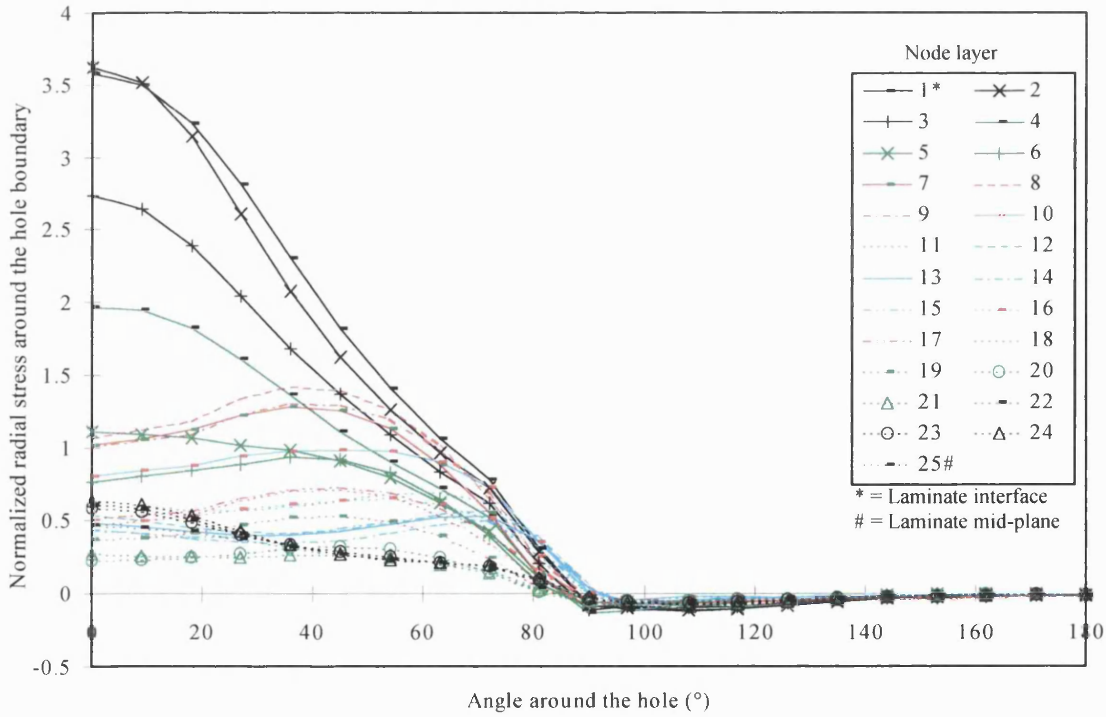

Figure 4.14– Normalized radial stress results of the inner lap - contact element method (3 elements per lamina thickness, 20 elements around the half hole)

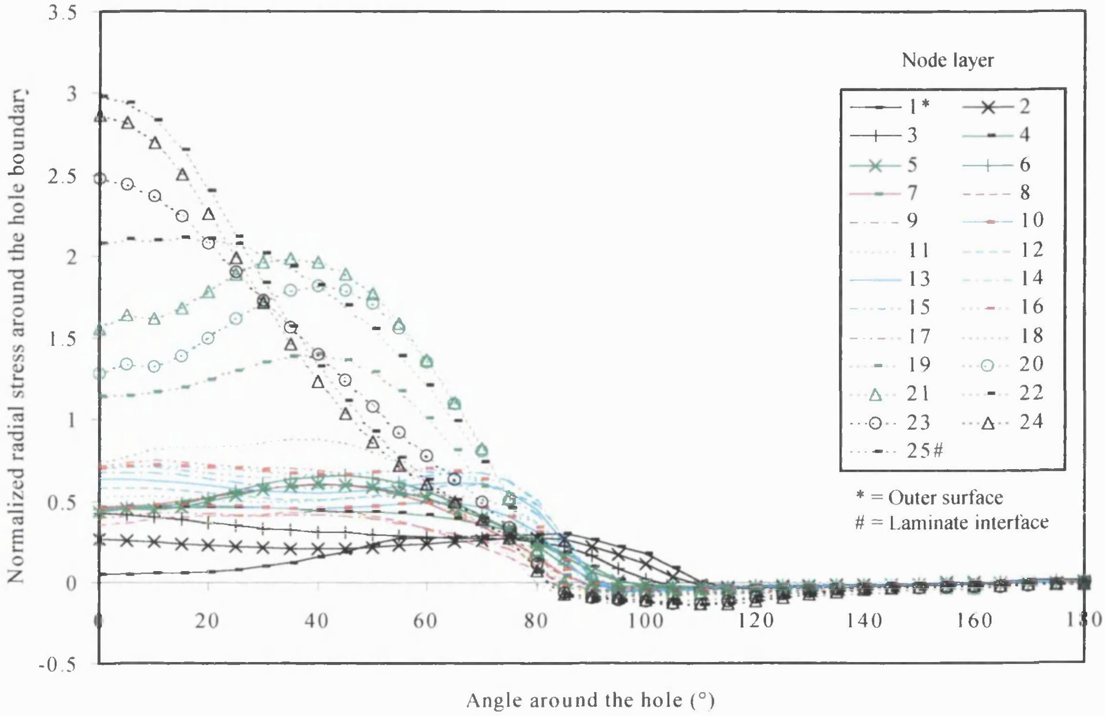

Figure 4.15– Normalized radial stress results of the outer lap - contact element method (3 elements per lamina thickness, 36 elements around the half hole)

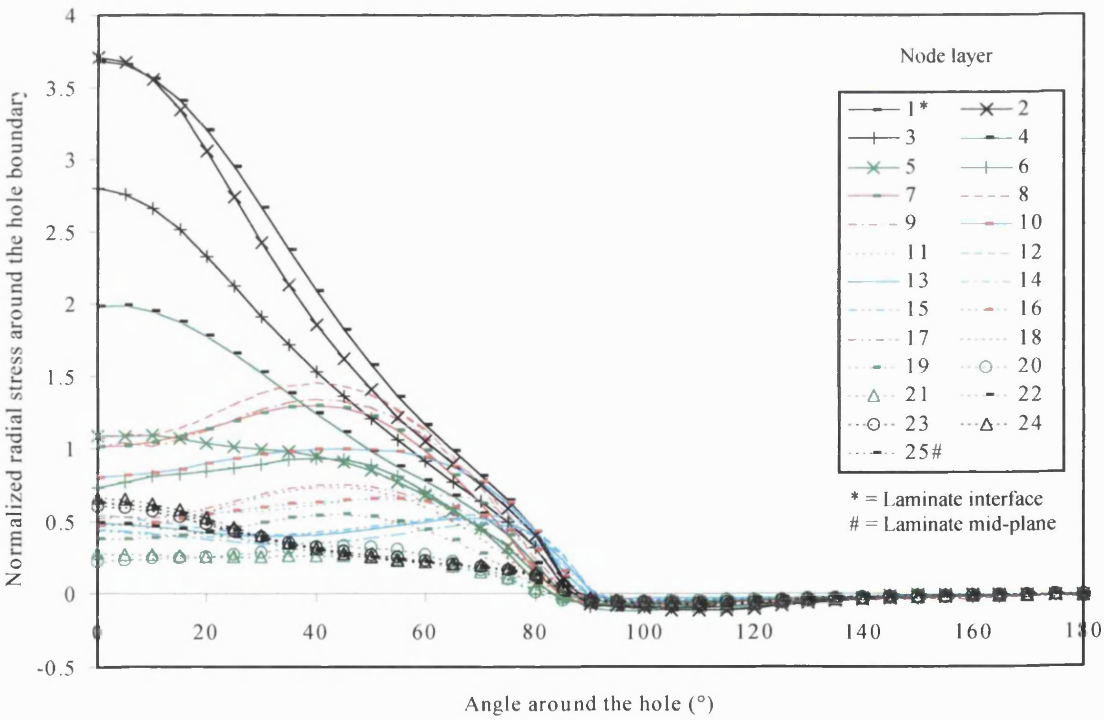

Figure 4.16– Normalized radial stress results of the inner lap - contact element method (3 elements per lamina thickness, 36 elements around the half hole)

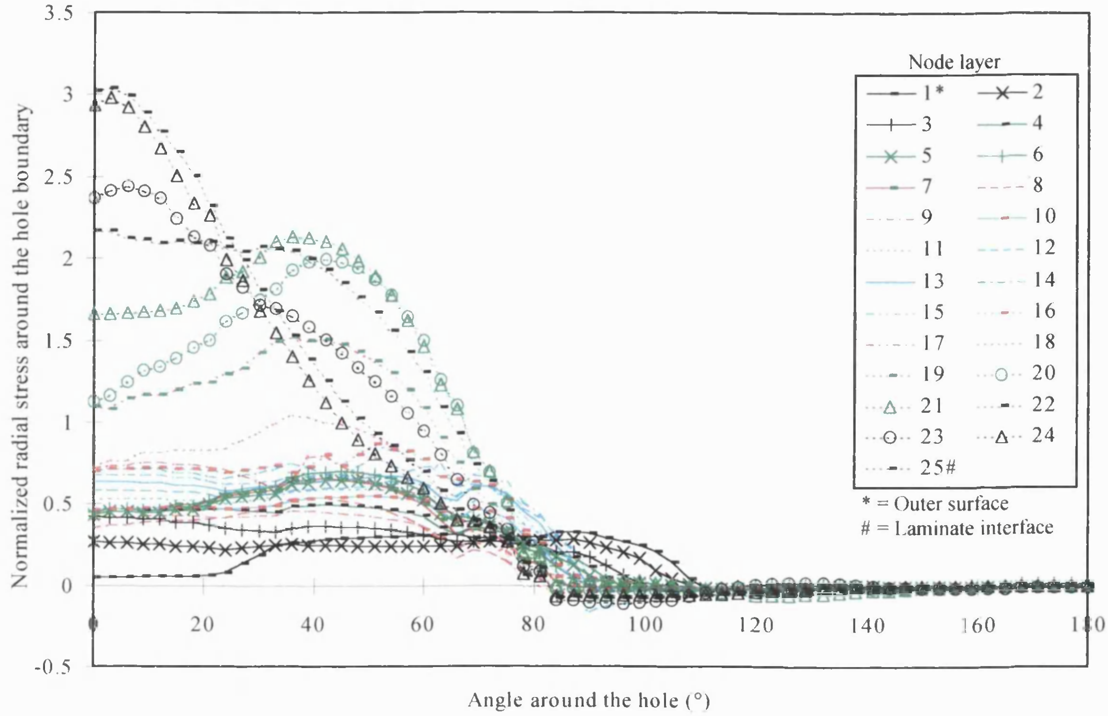

Figure 4.17– Normalized radial stress results of the outer lap - contact element method (3 elements per lamina thickness, 60 elements around the half hole)

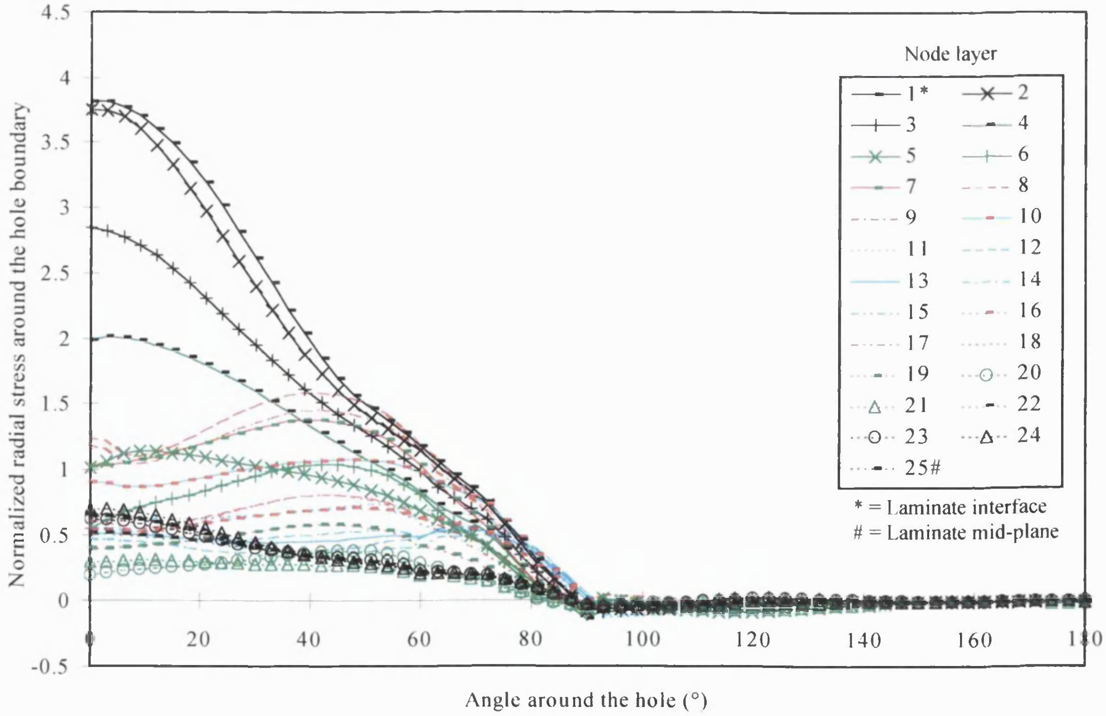

Figure 4.18– Normalized radial stress results of the inner lap - contact element method (3 elements per lamina thickness, 60 elements around the half hole)

CHAPTER FIVE

THREE-DIMENSIONAL MODELLING OF A SINGLE BOLT JOINT

5.1 – INTRODUCTION

Using the modelling techniques developed and validated in the previous chapter, the effects of varying clamping pressure and material properties on the stress distribution in double lap joints were investigated. I-DEAS Master Series version 7.0 was used throughout the analyses, which enabled the use of the contact element method for modelling contact, as this method is easier to use than the gap element contact method and results in a more reliable stress approximation, provided a suitably refined mesh is used.

In previous analyses such as Lessard et al. (1993) and Benchekchou and White (1993), clamping has been applied by using a constant clamping pressure over an area of the laminate surface representing the washer area. In this analysis, the washer and bolt were modelled physically as separate entities to enable a more realistic method for applying the bolt clamping preload.

Ply failure indices were calculated using the equation given by Tsai and Wu (1971) to provide details as to the location of ply failure. The onset of delamination was also determined using the equation given by Ye (1988).

5.2 – METHOD

A double shear joint was used for the investigations throughout this study. Each lap was constructed from GRP with the inner lap being twice as thick as the outer lap. The end of the inner lap was restrained from movement in all directions and a 2kN tensile load was applied to the end of each outer lap. The load was transferred by a bolt and washer assembly, which was constructed from either aluminium or steel. The physical representation of the joint can be seen in Figure 5.1. The material properties used can be seen in Table 5.1, with the corresponding material strengths given in Table 5.2.

Table 5.1 – Material properties for each unidirectional lamina and each fastener

Material	E_{11} (GPa)	E_{22} (GPa)	E_{33} (GPa)	G_{12} (GPa)	G_{23} (GPa)	G_{31} (GPa)	ν_{12}	ν_{23}	ν_{31}
GRP[1]	31.8	10.2	7.14	2.14	2.14	2.14	0.328	0.199	0.045
CFRP[2] T300/914	129	9.5	9.8	4.7	3.2	4.7	0.34	0.52	0.34
Aluminium[1] T6061-T6	68.3	68.3	68.3	25.7	25.7	25.7	0.33	0.33	0.33
Steel	206.8	206.8	206.8	80.2	80.2	80.2	0.29	0.29	0.29

Table 5.2 – Material strengths for each unidirectional lamina

Material	X_t (MPa)	X_c (MPa)	Y_t (MPa)	Y_c (MPa)	Z (MPa)	R (MPa)	S (MPa)
GRP	514[3]	240[3]	60[1]	70[3]	60[1]	60[1]	60[1]
CFRP[2] T300/914	1434	1318	98	215	76	79	79

[1] – Chutima (1996), [2] – Camanho (1999), [3] – Estimated from Hancox and Mayer (1994)

When simulating the joint, symmetry permitted the modelling of only a quarter of the physical joint, as demonstrated by the shaded portion of the drawing in Figure 5.1. This simplified the model and reduced running time. Restraints were therefore placed on nodes along the bottom edge of the plates as well as the bolt and washer, by fixing the y-direction displacement as zero, thereby simulating the bottom portion of the model. Where symmetry was modelled on the inner lap, the nodes were restrained by fixing the z- direction displacement as zero. At the far end of the inner lap the nodal displacements were fixed in the x-, y-, and z- directions, thereby simulating clamped conditions. On the outer lap at the end furthest from the bolt the nodes were loaded in the negative x-direction to simulate a 4kN tensile load on the whole joint.

To investigate the different clamping preloads the bolt had to be constructed slightly differently to the pinned model reported in Chapter 4. The bolt head, bolt shank and washer were all constructed as separate entities, so that the interaction could be modelled accurately. The bolt head was then joined to the bolt shank by a beam element which allowed for a temperature drop to be applied along its main axis. This will cause a contraction along the 'z' axis, pulling the bolt head and shank towards each other, which in turn pulls the washer against the laminate outer surface, hence clamping the joint. The physical and finite element representation of the bolt can be seen in Figure 5.2 and Figure 5.3, respectively.

Suitable mesh refinement was applied by using three elements per ply in the through thickness direction and an angle of 5° between each node around the hole periphery. This provided the mesh with a total of 28512 eight-node solid linear brick elements for the laminates. The bolt was constructed by using a short beam element to connect the 1764 six-node solid linear wedge elements of the bolt shank to the 108 six-node wedge and 324 eight-node brick elements of the bolt head. The washer was modelled using 216 eight-node solid linear brick elements. The interaction between every coincident surface was modelled using contact elements with a frictional coefficient of 0.2. The typical finite element mesh used for this investigation can be seen in Figure 5.4.

In order to provide the preload and hence torque to the bolt, the temperature drop applied to the beam element was determined by using Equation 5.1 given by Stewart (1965) of:

$$T = k d_{bo} p_w \left(\frac{\pi}{4} \left(d_w^{\ 2} - d_{bo}^{\ 2} \right) \right) \tag{5.1}$$

Which gives:

$$T = kd_{bo}F_a \tag{5.2}$$

Where:

T = Torque

k = Torque coefficient relative to μ (0.2)

d_{bo} = Bolt diameter

p_w = Pressure on washer

d_w = Washer outside diameter

F_a = Axial force of beam element

For each model, which included a clamping preload, the temperature drops required were calculated by estimating an initial temperature and comparing the resulting beam axial force to that required in Equation 5.2. The correct temperature drop for each torque was then calculated using the linear relationship between the temperature and axial force.

A range of stacking sequences were examined throughout the investigation, which were applied to the laminate by orienting the material property axes of each element in a ply so that the local 1-axis was rotated about the global z-axis by an amount determined by the stacking sequences given in Table 5.3.

Table 5.3 – Laminate stacking sequences used throughout the analysis

Sequence	Ply Orientation
A	$(0/45/-45/90)_s$
B	$(0_2/90_2)_s$
C	$(90_2/0_2)_s$
D	$(0/90/45/-45)_s$
E	$(90/45/-45/0)_s$
F	$(0)_8$

The first simulation was carried out to investigate the effects of clamping by applying preloads, equivalent to bolt torques of between 0Nm and 16Nm, to an aluminium bolt and washer assembly connecting GRP laminates. The bolt and washer assembly was then changed to steel to investigate the effects of fastener elasticity on the stress distributions. The next simulation was carried out to investigate the effects of laminate elasticity by changing the GRP laminates to a CFRP equivalent. Three small clearances were then introduced between the bolt and hole of a joint consisting of GRP laminates with an aluminium bolt assembly and, finally, the stacking sequences of the GRP laminates were varied using the orientations given in Table 5.3.

5.3 – RESULTS AND DISCUSSION

A description of the parameters investigated as well as the resulting stress distribution, contour and failure index plots, for each analysis of the bolted double lap joint, are given in this section.

As the load carried through bearing is an important aspect in the strength of mechanically fastened joints and can be used as a guide for comparative assessment of failure (Chutima, 1996), radial stress distribution around the hole boundary has been investigated for each model. In order to plot the distribution of radial stress around the hole boundary for each investigation, the stresses were extracted from each node on the hole boundary using a local cylindrical polar co-ordinate system. These results were then normalized using the average bearing stress, given by:

$$\bar{\sigma}_b = \frac{\text{Load}}{d_{bo} \times t} \tag{5.3}$$

Where:

d_{bo} = bolt diameter

t = laminate thickness

The results for each layer of nodes through the thickness were then plotted against the angle around the hole periphery, demonstrated previously in Figure 4.4b.

To provide ply failure indices for each ply in both the inner and outer laps of the joint, the failure criterion given by Tsai and Wu (1971) was used. By assuming that the thickness of a ply is very small compared with its lateral dimensions and that the material properties in directions transverse to the fibre direction are equal, the equation is simplified for use with orthotropic laminae, where failure occurs once the following relationship is satisfied:

$$\left(\frac{1}{X_t}-\frac{1}{X_c}\right)\sigma_1+\left(\frac{1}{Y_t}-\frac{1}{Y_c}\right)\sigma_2+\frac{\sigma_1^2}{X_tX_c}+\frac{\sigma_2^2}{Y_tY_c}+\frac{\tau_{12}^2}{S^2}+2F_{12}\sigma_1\sigma_2=1 \qquad (5.4)$$

F_{12} is an interaction coefficient, which accounts for the interaction between the two normal stresses, an approximation for which can be given by:

$$F_{12}\cong-\frac{1}{2\sqrt{X_cX_tY_cY_t}} \qquad (5.5)$$

Where:

σ_1 = direct stress component in the fibre direction

σ_2 = direct stress component in the transverse direction

τ_{12} = lamina shear stress

X_c, X_t = longitudinal compressive and tensile strength respectively of a lamina

Y_c, Y_t = transverse compressive and tensile strength respectively of a lamina

S = shear strength of a lamina

If Equation 5.4 is satisfied, then the stress state corresponds to failure. When the stress state does not result in failure it is possible to calculate a single factor, which may be applied to all the stress components to bring the state of stress up to failure. This factor 'R_s' can be referred to as a strength ratio. Since linear elastic behaviour to failure is assumed, the equation can therefore be rewritten in a way that is more convenient for design, (Barbero, 1998):

$$\left(\frac{\sigma_1^2}{X_t X_c}+\frac{\sigma_2^2}{Y_t Y_c}+\frac{\tau_{12}^2}{S^2}+2F_{12}\sigma_1\sigma_2\right)R_s^{\,2}+\left(\left(\frac{1}{X_t}-\frac{1}{X_c}\right)\sigma_1+\left(\frac{1}{Y_t}-\frac{1}{Y_c}\right)\sigma_2\right)R_s-1=0 \tag{5.6}$$

which can be rewritten as:

$$aR_s^{\,2}+2bR_s-1=0 \tag{5.7}$$

where:

$$a=\frac{\sigma_1^2}{X_t X_c}+\frac{\sigma_2^2}{Y_t Y_c}+\frac{\tau_{12}^2}{S^2}+2F_{12}\sigma_1\sigma_2 \tag{5.8}$$

and:

$$b=\left(\frac{1}{X_t}-\frac{1}{X_c}\right)\sigma_1+\left(\frac{1}{Y_t}-\frac{1}{Y_c}\right)\sigma_2 \tag{5.9}$$

Solving for the roots and taking the positive value gives the strength ratio:

$$R_s=\frac{1}{a}\left(-b+\sqrt{b^2+a}\right) \tag{5.10}$$

$$\text{Ply failure index}=1/R_s \tag{5.11}$$

The average element stresses were obtained for elements around the hole boundary of each ply and then used in Equation 5.11, along with the lamina strengths from Table 5.2, to determine the ply failure indices. Graphs of ply failure index versus element position around the hole boundary were then plotted for each simulation, giving an indication of ply failure if the curve exceeds 1 at any point.

The delamination onset was determined using the equations given by Ye (1988), where delamination failure is likely to occur when the following equations are satisfied:

When $\bar{\sigma}_3 > 0$:

$$\left(\frac{\bar{\sigma}_3}{Z}\right)^2 + \left(\frac{\bar{\tau}_{13}}{S}\right)^2 + \left(\frac{\bar{\tau}_{23}}{R}\right)^2 = 1 \tag{5.12}$$

When $\bar{\sigma}_3 \leq 0$:

$$\left(\frac{\bar{\tau}_{13}}{S}\right)^2 + \left(\frac{\bar{\tau}_{23}}{R}\right)^2 = 1 \tag{5.13}$$

Where:

R = the interlaminar shear strength

Z = interlaminar normal strength

In previous work such as Zhang & Ueng (1988), Brewer & Lagace (1988) and Raju & Crews (1982), it was reported that interlaminar stress singularities are known to exist at the hole boundary and between each lamina of angle ply laminates. Therefore it is more appropriate to use an average stress criterion rather than a point stress criterion, whereby the stress values are averaged over a small distance away from the singularity. The distance from the free edge over which the stress values must be averaged should be determined experimentally, however, in this analysis as the mesh is suitably refined around the hole boundary, it is assumed that the element average stress may be used in Equations 5.12 and 5.13. Chen and Lee (1995) obtained reasonable agreement with experimental work by using average element stresses in the maximum stress and Ye (1988) delamination criteria, however, such a correlation is clearly dependent upon the mesh refinement.

The average element stresses were thus obtained for the elements that were closest to each ply interface. These stresses were then used with Equation 5.12 or Equation 5.13 and the strength values from Table 5.2 to determine delamination failure indices.

5.3.1 – Investigation into the effects of clamping preloads

The model used in this investigation was constructed as detailed in section 5.2, with the ply orientation sequence A, $(0/45/-45/90)_s$. An aluminium bolt assembly, having an outside washer diameter equal to $2.0d_{bo}$ was used to join the GRP laminates, and the clamping preload was varied between finger tight (0Nm) and 16Nm, which hitherto will be expressed as the fully tightened condition.

The effect of clamping preload on the radial stress distribution for the outer lap and inner lap can be seen in Figures 5.5 and 5.6, respectively. From Figures 5.5a and 5.5b it can be seen that varying the clamping preload significantly affects the radial stress distribution of the outer lap. For each preload the maximum radial stress remains at the bearing plane (0° around the hole periphery), however, the through thickness position changes with increasing clamping pressure.

With the finger tight case, in Figure 5.5a(i), the maximum stress occurs at the interface between the outer and inner laps and has a normalized value of approximately 2.8. For the 2Nm case, shown in Figure 5.5a(ii), the maximum stress occurs just inside the laminate interface and has a normalized value of 2.9. However, as the clamping pressure increases further the magnitude of the maximum stress starts to fall and the position shifts from the laminate interface towards the outer surface of the outer lap. The radial stress near the outer surface increases in this way, as the stress is not just attributed to the bearing between the pin and the hole but also arises from the deformation and friction being induced by the clamping of the washer against the laminate.

At a clamping torque of 6Nm the stresses seem to average out, where it can be seen that the radial stresses at the interface with the inner lap, due to the bolt bearing, equal the radial stresses at the outer surface of the laminate, which arise predominantly due to friction. This particular clamping torque gives the lowest maximum radial stress and an even distribution around the hole boundary, which is preferred.

From Figure 5.5b, it can be seen that as the clamping torque increases to 8Nm and above, the maximum radial stresses remain on the outer surface of the outer lap but increase in magnitude with increasing clamping torque. The radial stress then reduces at all other locations until at a clamping torque of 16Nm they have diminished to such an extent that the bolt does not seem to be bearing up against the hole. In this case the tensile load is being carried by the friction between the washer and laminate interfaces only, under a sandwiching effect, which could then lead to a catastrophic failure mechanism, such as net tension, rather than simple progressive bearing failure.

The radial stress distribution for the inner lap, shown in Figures 5.6a and 5.6b, shows that the maximum value remains on the surface of the lap at the interface with the outer lap and is higher than the outer lap for clamping preloads between 0Nm and 6Nm. However, as the magnitude of stress continues to decrease with increasing torque the highest stress is obtained in the outer lap, at approximately 8Nm torque, and continues to rise with the degree of clamping.

It should also be noted from Figure 5.5 that pin to hole contact seems to occur beyond $\theta=90°$, up to approximately $\theta=105°$ on the outer surface of the outer lap, due to deformation of the laminates and the perfect fitting bolt. This demonstrates that the frequently assumed boundary conditions, such as fixed radial displacements around a section slightly less than 90° of the hole boundary, may be inaccurate in simulating this type of double lap GRP joint. However, this assumption would not be so inaccurate for the case of a single GRP inner lap under tension. Clamping also induces radial stresses past this angle which arises due to friction under the washer and the spreading of the laminate against the bolt shank.

Colour contour plots showing how the radial contact stress between the bolt shank and the hole varies as the clamping preload is increased are shown in Figure 5.8, with a description of this figure shown in Figure 5.7. Figure 5.8 confirms that the previously assumed cosine pressure distribution and fixed radial displacements around the hole would lead to inaccuracy in the assessment of this double lap GRP joint. When low preloads are applied the load is transferred mainly through bearing contact close to the interface between each lap. A small amount of contact is also shown to occur near the outer surface of the outer lap, up to approximately 105° around the hole boundary as the bolt is being bent by the high contact stresses that exist at the laminate interface. When the clamping preload is increased further up to 6Nm, the contact stress becomes more uniform through the thickness of each lap. Further increases in clamping torque beyond this value, and in particular reaching a value greater than 10Nm, reduces the bolt to hole contact area significantly, e.g. with a torque of 16Nm the load is carried almost entirely through the clamping mechanism.

Figure 5.9 shows the contact stress on the laminate surface in the through thickness direction under the washer for clamping preloads of 0Nm, 6Nm and 16Nm. This figure demonstrates that the aluminium washer is relatively compliant and does not transfer the bolt preload evenly over the entire washer area as some investigations have assumed, such as Lessard et al. (1993). The effects of the bolt bending can also be seen, whereby the finger tight condition results in limited contact between a segment of the washer and the laminate surface on the opposite side of the hole to the bearing surface. Although some clamping preloads investigated have been excluded from this figure, the trend can be seen whereby the contact stress distribution becomes more uniform around the hole as the clamping preload increases. However, the contact area between each surface, even at high preloads, is confined to an area that is similar in size to the bolt head. The narrow red zone at the hole boundary on the colour contour plots, even for higher clamping loads, may be attributed to a slight mismatch between the diameter of the laminate hole and the washer inside diameter, which may occur in practice and would be representative of a 'worst case' condition.

The effect of clamping preload on the through thickness contact stress at the interface of the outer and inner laps of the tensile loaded joint can be seen in the contour plots in Figure 5.10. Some results for intermediate clamping torques have been excluded from this figure, however, from the results shown (for clamping torques of 0Nm, 6Nm and 16Nm) it is clear that increasing the clamping torque increases the contact area between the inner and outer lap quite significantly. In the absence of bolt clamping contact mainly occurs on a small portion of the plate, as wide as the washer, around a quarter sector of the hole closest to the position of loading, with the highest stresses recorded at a small distance from the hole boundary. This is due to the pin bending in the direction of the load forcing the washer to compress a portion of the outer lap, as identified previously.

Clamping of 6Nm increases this contact area further to encompass the entire circumference, but with higher stresses obtained on the portion of the plate closest to the point of application of the load due to the effects already mentioned for the finger tight case. As the clamping preload increases further to a torque of 16Nm the contact area increases, so that it is slightly larger than the washer area, and higher through thickness stresses appear to be more evenly distributed around the hole. However, due to the elasticity of the washer the contact is not uniform in the radial direction at a discrete distance from the hole boundary. Beyond the contact region identified above, the laminates do not appear to be in contact and hence do not act to transfer the load through frictional effects.

The effects of clamping preload on the out-of plane deformation of the outer lap under tensile loading can be seen in Figure 5.11. For clarity, the deformation is exaggerated slightly on each of the contour plots. As can be seen in Figure 5.11a(i), the joint with no clamping (finger tight) permits the end of the outer lap, furthest from the application of the load, to deform by approximately 0.1mm (in the z-direction) away from the inner lap. As the clamping increases to 4Nm the magnitude of deformation at this point falls to approximately 0.04mm. However, as the clamping torque increases further the deformation at this point increases, but does not exceed the displacement recorded for the finger tight case. From Figure 5.11b, it can be seen that severe deformation may be noticed around the hole area for higher clamping preloads, which could possibly lead to ply failure in this area.

The ply failure index plots for the outer and inner lap, respectively, can be seen in Figures 5.12 and 5.13. From Figure 5.12a(i) it can be seen that without a clamping torque the ply failure index marginally exceeds unity for the 45° ply, close to the interface with the inner lap, at an angular displacement of 45° around the hole boundary from the loading axis. With a 2Nm torque the index increases slightly indicating that ply failure of the outer lap would occur for the 0° lamina on the bearing plane at the interface with the inner lap. With a further increase in torque to 6Nm the failure index reduces to approximately 0.7 indicating that the outer lap is not likely to fail at this level of torque. As the clamping increases beyond 6Nm the failure index starts to rise again with the highest indices obtained for the outer surface of the outer lap, at approximately 90° around the hole boundary with respect to the bearing plane. With a clamping torque of 16Nm the failure index exceeds unity around this same portion and consequently would be indicative of a tensile mode of failure. Figure 5.13 demonstrates that the magnitude of failure index is approximately the same for the inner lap as the outer lap for the joint without clamping, indicating that ply failure could also occur on the bearing plane of the inner lap surface. However, as the clamping is increased the failure index continues to fall. These figures demonstrate that failure may occur for the outer lap and inner lap without a clamping preload but may also occur for very high preloads, due to the washer damage on the surface of the outer lap.

Figures 5.14, 5.15 and 5.16 demonstrate the effects of using clamping torques of 0Nm, 6Nm and 16Nm, respectively on the interlaminar shear stress of the outer lap. It can be seen from the stress colour contour maps in Figures 5.14 and 5.15, that low clamping torque results in the maximum shear stress occurring near the hole boundary, which then decreases slowly with increasing radial distance from the hole. Figure 5.16 shows that with a clamping torque of 16Nm high shear stress develops within a finite distance from the hole boundary but is then suppressed under the washer area, until it increases again at the washer edge. This effect can be seen in particular, between ply 3 and 4 (-45° and 90° plies), where high shear stress occurs outside the washer edge and spreads towards the outside of the laminate, with high stresses also occurring very close to the hole boundary. This confirms the experimental work conducted by Kretsis and Matthews (1985), which concluded that shear cracks develop outside the washer area, which could be a major factor in the onset of delamination and subsequent failure of the joint.

Figures 5.17 and 5.18 demonstrate the effects of clamping preload on the delamination failure indices around the hole boundary of the outer lap and the inner lap, respectively. Results are presented for each layer of elements that form a ply interface. From these figures it can be seen that the delamination indices are much smaller than the ply failure indices, indicating that ply failure would be more likely to occur for this joint configuration with the clamping preloads tested. However, since average stresses were used to compute these indices, which can compromise the accuracy, the graphs may be more useful for a comparative assessment for each of the parameters tested. In this context the graphs do indicate that the delamination indices are higher for the elements either side of the 45°/0° interface of the outer lap (that is close to the inner lap) for nearly all of the clamping preloads tested. However for clamping torques above 6Nm the indices for other ply interfaces close to this critical region, as well as close to the outer surface, start to increase and in particular for 8Nm the elements at the 0°/45° interface near the outer surface exhibit higher indices than those nearer to the inner lap. The highest index of approximately 0.093 was obtained for a 2Nm clamping torque at an angle of approximately 25° around the hole boundary, with respect to the bearing plane. As the torque is increased the index then falls to a minimum value of approximately 0.013 at 8Nm before increasing again at higher torque level.

Figure 5.18 demonstrates that the highest index obtained for the inner lap is approximately 0.072 with no clamping, which then falls to a minimum value of approximately 0.017 at a torque of 4Nm before rising again with increasing clamping pressure. For all the torques tested the highest indices were obtained for the 0°/45° ply interface close to the outer surface, except for 2Nm torque where the highest index was obtained at the adjacent ply interface nearer to the centre of the lap. At torques above 8Nm it is also interesting to note that the index occurs at approximately 90° around the hole boundary with respect to the loading axis.

For a bolt clamping preload of 6Nm, Figure 5.19 shows the longitudinal strain obtained within the outer lap along the bearing and net-tension planes at each integration point through the thickness. The curves show that the strains at both the net-tension and bearing planes increase slightly near to the interface with the outer lap compared to the outer surface, indicating that for this clamping condition slightly more load is transferred from the plate to the bolt around this area.

For the same model, Figure 5.20 shows the xy- shear stress along the bearing and net-tension planes for each integration point through the thickness of the outer lap. From this figure it can be seen that high shear stresses exist near the interface of the +45° and –45° plies around the net tension plane and between the sixth and seventh ply at the bearing plane. It is also observed that the stresses in the elements adjacent to these ply interfaces change significantly across their integration points. This infers that using the average element stresses in the delamination failure equations may result in a higher strength prediction than would be expected in practice. As average element stresses have been used to obtain the delamination indices these results should be viewed with caution and used simply for a comparative assessment.

For the same 6Nm torque joint, Figure 5.21 shows the z- direction stress along both the bearing and net-tension planes for each integration point through the thickness of the outer lap. As a result of clamping the through thickness stress is higher at the outer surface of the outer lap and reduces slowly towards the interface with the inner lap. The curves are very similar for both the net tension plane and the bearing plane and, on the whole, the stress varies insignificantly between each integration point of the elements.

5.3.2 – Investigation into the effects of fastener elasticity

In this investigation the model was constructed as detailed in section 5.2 with laminate stacking sequence A, using a steel bolt and washer assembly having a washer outside diameter of $2.0d_{bo}$. The torque preloads were varied between 4Nm and 8Nm. Figures 5.22 and 5.23 show the normalized radial stress distribution for the outer lap and inner lap respectively. These may be compared with Figures 5.5 and 5.6, which show the stress distribution for a similar joint incorporating an aluminium bolt and washer assembly.

Figure 5.22 demonstrates that the stress distribution in the outer lap of the steel bolt model follows a similar pattern to that produced by the aluminium bolt model, whereby the position of the maximum stress moves from the inner/outer lap interface to the outer surface of the outer lap as the clamping torque is increased. It is also evident when comparing Figure 5.22 to Figure 5.5 that for low clamping torques the magnitude of stress appears to be much lower than for the aluminium bolt model. This may be due to less bolt bending and a slightly stiffer washer. This demonstrates that the often used assumption of a rigid pin is inaccurate when simulating a joint having both GRP inner and outer laps joined using an elastic fastener.

For the inner lap, Figure 5.23 demonstrates the similarity of the stress distributions to those shown in Figure 5.6, however, the steel bolt induces much lower stresses than the aluminium bolt, considered to arise from reduced bolt bending and a less compliant washer distributing the stress more uniformly.

Figure 5.24 shows the through thickness contact stress on the inner lap at the laminate interface. From this figure it can be seen that the contact area on the inner lap at the interface is very similar to the aluminium bolt and washer assembly at equivalent clamping preloads, however, the magnitude of the stress seems to be slightly lower when using the steel bolt and washer assembly. This is considered to be due to the stress being distributed more evenly over the contact area with a lower degree of fastener bending.

Figure 5.25 shows the through thickness contact stress under the washer on the surface of the outer lap for the joint having a steel bolt and washer assembly. By comparing the results obtained using the aluminium bolt assembly, shown in Figure 5.9, it is apparent that the contact areas under the washer are dissimilar. As the steel washer is stiffer than the aluminium, contact is evident at the washer edge as well as across a region close to the hole boundary demonstrated with the aluminium washer. However, it is evident that contact is still not uniform over the entire washer area.

For this particular joint configuration, Figures 5.26 and 5.27 show the ply failure indices for the outer and inner lap, respectively. It can be seen that the trend followed by each of the curves is almost identical to that produced by the aluminium bolt model, however, the values are lower as expected from observations made concerning the radial stress. The lowest index obtained by both the outer lap and inner lap was at a torque of 6Nm with a magnitude close to 0.5. For the range of torques investigated, the highest index was obtained on the bearing plane of the outer lap, at the interface with the inner lap, with a magnitude of 0.66, approximately for a 4Nm clamping torque. These results indicate that ply failure is not likely to occur for the range of clamping torques tested in this particular joint configuration.

Parida et al. (1997) concluded that for finger tight clamping different fasteners produced a small change in the strength. In the current study a difference in maximum ply failure index was found to exist between the aluminium bolt assembly and the steel bolt assembly. For example, at a small clamping torque of 4Nm on the outer lap the ply failure index was found to be close to unity, indicative of possible failure, for the aluminium bolt assembly, and approximately 0.66 for the steel bolt configuration. This shows a significant change in the likelihood of failure for GRP outer laps and demonstrates that if a stiff or rigid pin/bolt is used to simplify an analytical study then the predicted strength could easily be overestimated.

Delamination index plots have not been included as they show a similar trend to those provided by the aluminium bolt configuration but the values are smaller and are insignificant.

5.3.3 – Investigation into the effects of laminate elasticity

In this particular study both of the laps in a double lap configuration were constructed using the CFRP properties given in Table 5.1, having the ply orientation designated as sequence A. The load was transferred via a tight fitting steel bolt and washer assembly with a washer outside diameter of $2.0d_{bo}$. The clamping preload was varied between a bolt torque of 4Nm and 8Nm.

The normalized radial stress around the hole boundary for the outer and inner laps is shown in Figures 5.28 and 5.29, respectively. From these figures it is clear that the joints consisting of CFRP laminates with a steel bolt assembly exhibit higher bearing stresses than joints consisting of GRP laminates, with either aluminium or steel bolt assemblies, for each of the preloads tested. Figure 5.28 indicates that an optimum preload would be between 4Nm and 6Nm for the most even stress distribution, however, for the preloads tested, 8Nm gives the lowest magnitude of bearing stress when considering both the inner and outer laps.

Figures 5.30 and 5.31 show the ply failure index plots for the outer and inner laps respectively, for the CFRP double lap joint. These figures show that the likelihood of failure in the CFRP laminate is much lower than in the joints constructed using GRP, for equivalent clamping conditions. For the range of bolt torques tested the failure indices are shown to be higher on the outer lap than the inner lap, indicating that failure would be more likely to occur in the outer lap, however, the values are small, with a maximum magnitude of 0.26, approximately. From Figure 5.30(i) it can be seen that a torque of 4Nm results in the highest failure index on the bearing plane for the plies close to the interface with the inner lap. As the torque increases to 6Nm the index reduces to approximately 0.16 and the position changes to the elements on the outside of the laminate on the side of the hole that is closest to the point of load application. This may be due to the stiff laminate inducing a higher load through bearing onto the bolt, which in turn bends the bolt and hence the washer towards the load direction. With a further increase in torque the index rises due to the localised damage from the washer. Figure 5.31 shows that the failure indices for the inner lap remain low and reduce as the torque increases in the clamping range examined. These results indicate a 6Nm clamping torque may be an appropriate preload for CFRP laminate joints of this type.

Figure 5.32 shows that the through thickness displacement of the CFRP outer lap is lower than that obtained for the GRP laminate due to the higher stiffness of the material, however, as the clamping preload increases the plate still tends to move further away from the inner lap, although not as significantly as with the GRP laminate joint configuration.

Delamination index graphs were not included for this joint configuration as similar results were obtained as for the GRP joint although slightly lower, resulting in very low and insignificant results.

5.3.4 – Investigation into the effects of clearance fit bolts

In this model GRP plates were used having a laminate lay-up designated as sequence A, connected via an aluminium bolt assembly with the washer outside diameter as $2.0d_{bo}$. The clamping preload was kept constant at an equivalent torque of 6Nm and the hole diameter was varied in order to investigate the effects of clearance. Using the equation for clearance given by Hyer & Klang (1984) in Equation 5.6, the tolerances tested were calculated as λ=0.157%, 0.47% and 0.78%.

$$\lambda = \frac{d - d_{bo}}{d} \times 100 \qquad (5.6)$$

Figures 5.33 and 5.34 show the plots of normalized radial stress against angle around the hole boundary for the outer and inner laps, respectively. Both figures demonstrate that the magnitude of radial stress increases and the contact area decreases, as the clearance between the bolt shank and hole increases. Also, these figures show that the magnitude of the stress is higher in the inner lap when compared to the outer lap. For a clearance of λ=0.157%, as shown in Figure 5.33(i), the maximum normalized radial stress is approximately 1.32 and occurs on the bearing plane near to the centre of the outer lap. The lowest stresses were obtained at the outer surfaces and contact seems to occur up to about 90° around the hole circumference. The location of the maximum stress is maintained with an increase in bolt clearance to λ=0.47% although the normalized value rises to approximately 1.4. Contact was found to occur up to approximately 80° around the hole boundary for the –45° lamina closest to the outer surface of the outer lap. Contact for all of the other laminae occurs up to approximately 50° around the hole perimeter. With a higher clearance of λ=0.78%, the maximum radial stress occurs on the 0° and 45° plies on the outer surface of the outer lap, with the peak normalized radial stress reaching approximately 1.52. Contact for this case occurs up to 45° around the hole boundary.

In the case of the inner lap it can be seen in Figure 5.34 that the magnitude of maximum normalized radial stress increases from approximately 2.2 for 0.157% clearance, to 2.5 for 0.47% clearance and then to 3, approximately, for a clearance of 0.78%. The angle of contact around the hole decreases with increasing clearance as observed for the outer lap, however, the position of maximum stress remains at the outer surface of the inner lap, except for the largest clearance where the position moves slightly in towards the centre of the lap.

The ply failure index plots for the outer lap and inner lap are given in Figures 5.35 and 5.36, respectively. Figure 5.35 demonstrates that the failure index reaches a magnitude of approximately 0.76 on the bearing plane at the interface with the inner lap. As the clearance increases high indices are observed at the same position, however, the magnitude falls slightly. The indices obtained at the outer surface on the bearing plane close to the point of application of the load continue to increase with clearance. With a further increase in clearance, the highest index also occurs on the outer surface towards the point of load application and increases to approximately 0.86. Figure 5.36 demonstrates that the failure indices continue to increase with increasing clearance, with the magnitude reaching approximately 1.6 for the largest clearance tested, indicating that failure will occur for this particular applied load. However, the results for the largest clearance on the inner lap should be viewed with caution as they seem erratic. This may be due to the linear analysis not reforming contact elements as a change of element contact occurs through applied loading. Therefore for clearance fit joints, where contact is likely to change dramatically with applied loading, a non-linear analysis may be required.

5.3.5 – Investigation into the effects of laminate stacking sequence

The model was constructed as described in section 5.2. A perfect fitting aluminium bolt assembly with washer outside diameter of $2.0d_{bo}$ and clamping preload equivalent to a torque of 6Nm was used. The effect of changing the laminate lay-up on the stress distribution of the joint was investigated by applying the stacking sequences designated A through to F, as given in Table 5.3. Figures 5.37 and 5.38 show the plots of normalized radial stress around the hole boundary for the outer and inner laps, respectively, for each of the stacking sequences. These figures only show the results for the first and last two plies of each lap as the other results are insignificant.

From Figure 5.37 it can be seen that the maximum radial stress occurs on the bearing plane for stacking sequences A, B, D and F; in all these cases they have 0° plies on the outer surfaces of the laps. Laminates having stacking sequence C and E show maximum radial stress at about 90° around the hole boundary and in both cases these laminates have 90° plies on the outer surfaces. The level of maximum radial stress on the outer lap for all sequences seems to remain approximately constant, however, slightly higher stresses are provided by the quasi-isotropic specimens, sequences A, D and E. The magnitude of this stress appears to be marginally smaller when the 0° and 90° plies are adjacent to each other on the outer surfaces of the laminates.

Further, from Figure 5.38, the maximum radial stress is shown to occur on the inner lap rather than the outer lap, except for the sequences C $(90_2/0_2)_s$ and E $(90/45/-45/0)_s$ which have 90° layers on the outer surfaces.

The ply failure index plots for the outer lap and the inner lap can be seen in Figures 5.39 and 5.40, respectively. Figure 5.39 shows that the failure indices do not exceed unity for any of the laminate sequences examined, therefore failure of the outer lap is unlikely to occur. The maximum index occurs for sequence F $(0)_8$ with a magnitude of 0.72, approximately, which is followed by sequence A $(0/45/-45/90)_s$ with a magnitude of 0.7. The lowest failure index was obtained for sequence C (90/0)s, having a value of 0.57, approximately. It is therefore apparent that laminates constructed with 90° plies on the outer surface had the lowest failure indices and hence higher strength. Laminates with 0° plies on the outer surface have the lowest strength, however, it is evident that by placing 90° plies directly next to these the failure index is reduced. This confirms the experimental work of Hamada et al. (1995) and Quinn and Matthews (1977).

From Figure 5.40, it can be seen that the indices on the inner lap are higher than the outer lap for sequences C and E, which have 90° plies on the outer surface. The quasi-isotropic sequence having 0° plies on the outer surface and 90° plies adjacent has the lowest index, hence highest strength. Quasi-isotropic sequences having 45° plies next to the outer surface ply were observed to have the lowest strength. It is also apparent from both figures that the cross-ply, sequence C $(90/0)_s$ would be less likely to fail when considering both the outer lap and inner lap under these loading conditions.

5.4 - CONCLUDING REMARKS

From the results reported in the previous section, the following conclusions can be drawn.

5.4.1 – Effect of bolt clamping preload

For a GRP double lap joint having an aluminium bolt and washer assembly a clamping torque of 6Nm (equivalent to a clamping pressure of approximately 50MPa for a washer diameter of $2.0d_{bo}$) is considered optimum for the most favourable radial stress and ply failure index distribution.

Small clamping pressures are shown to reduce out-of-plane bending of the outer lap, however, if the clamping pressure is too high, the laminates are susceptible to damage around the washer periphery, with bolt bearing being eradicated. Also the out-of-plane deformation at the end of the outer lap increases with increasing torque levels above 4Nm. This can lead to catastrophic failure through other mechanisms such as tensile failure.

Clamping pressures are also shown to suppress interlaminar shear stress under the washer area, however, with higher preloads a high interlaminar shear stress occurs outside the washer edge as well as at the hole boundary, confirming experimental work of Kretsis and Matthews (1985), which can also affect the failure mode.

Ply failure is more likely to occur than delamination for this particular type of joint, however, the delamination index results should be viewed with caution, as average element stresses were used in the failure theory in conjunction with a linear elastic analysis which only provides a first approximation to shear stresses within the laminate.

It is also shown that the often assumed cosine and fixed radial displacement boundary conditions do not realistically represent the bolt to hole contact in a three-dimensional analysis of double lap composite joints.

5.4.2 – Effect of fastener elasticity

For the GRP double lap joint with a steel fastener assembly much lower radial stresses are exhibited at the hole boundary compared to the joint with an aluminium fastener. This is due to the higher bending stiffness of the steel fastener resulting in a more uniformly distributed load. A clamping torque of 6Nm offers the lowest failure indices, suggesting the same optimum clamping preload as the aluminium fastener joint. However, the steel fastener assembly results in lower failure indices for each bolt preload tested, thereby indicating that fastener elasticity should be included during analysis of joints having both composite inner and outer laps.

For double lap joint configurations constant pressure or constant displacement boundary conditions, representing the washer loading, are considered inaccurate in representing this type of joint, since with both aluminium and steel washers the pressure transferred to the laminate surface by the washer is by no means uniform.

5.4.3 – Effect of laminate elasticity

For a double lap CFRP joint with a steel fastener assembly, a good clamping torque is 6Nm, however a higher strength is exhibited compared to equivalent GRP joints due to higher laminate strength and reduced out-of-plane deformation of the outer lap.

5.4.4 – Effect of clearance fit bolts

For a double lap GRP joint having an aluminium bolt and washer assembly with a clamping torque of 6Nm, clearance between the bolt shank and the hole has been shown to affect the stress distribution and ply failure index significantly, indicating the likelihood of failure of the inner lap as the clearance increases. However, as a linear analysis was used the contact elements did not reform as the bolt to hole contact changed. This is thought to explain the erratic stress results obtained for the inner lap, and consequently the reliability of this data is considered questionable.

5.4.5 – Effect of laminate stacking sequence

For the GRP double lap joint configuration with a 6Nm clamping torque the variation in stacking sequence of the laminates does not confer significant changes in the stress distribution and hence strength of the joint.

Slightly higher radial stresses are exhibited at the hole boundary for the quasi-isotropic stacking sequences, especially for the laminates without 0° and 90° plies adjacent to each other at the surface of the laminates. With regards to the strength of the joint, the unidirectional $(0)_8$ laminate joint provides the highest likelihood of failure for the outer lap. By placing 90° plies adjacent to the 0° outer surface plies, the joint strength improves, however, laminates with 90° plies on the outer surface such as $(90/0)_s$ seem to offer the highest strength. For the inner lap, the laminates having 0° plies on the outer surface with 90° plies adjacent have the highest strength, whereas the quasi-isotropic laminates with 45° plies adjacent to the outer surface plies have the lowest strength. When considering the strength of both the outer and inner laps, a good laminate stacking sequence seems to be $(90_2/0_2)_s$, however, the failure indices for all sequences are less than unity, indicating that failure will not occur at the load level applied to these models.

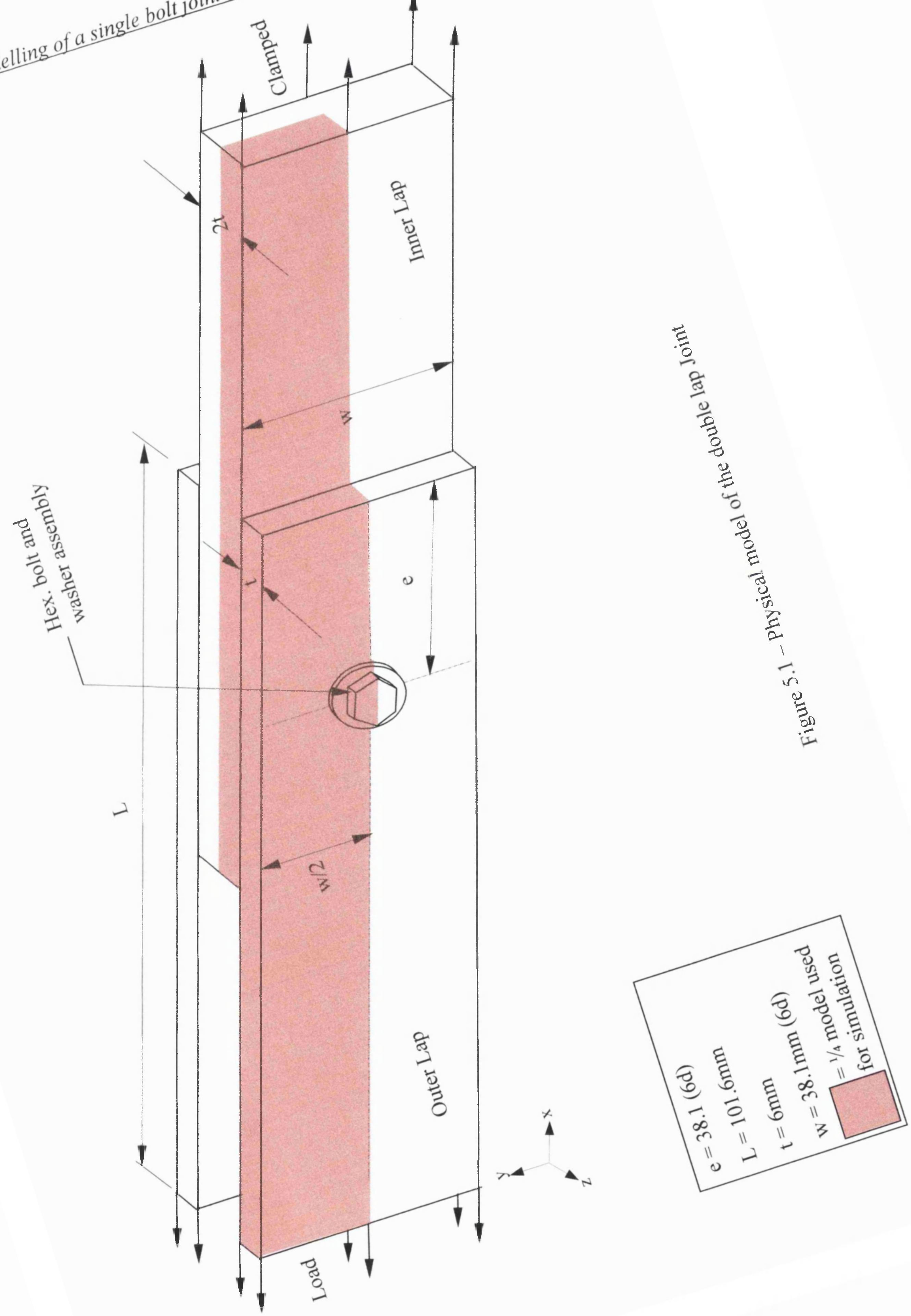

Figure 5.1 – Physical model of the double lap Joint

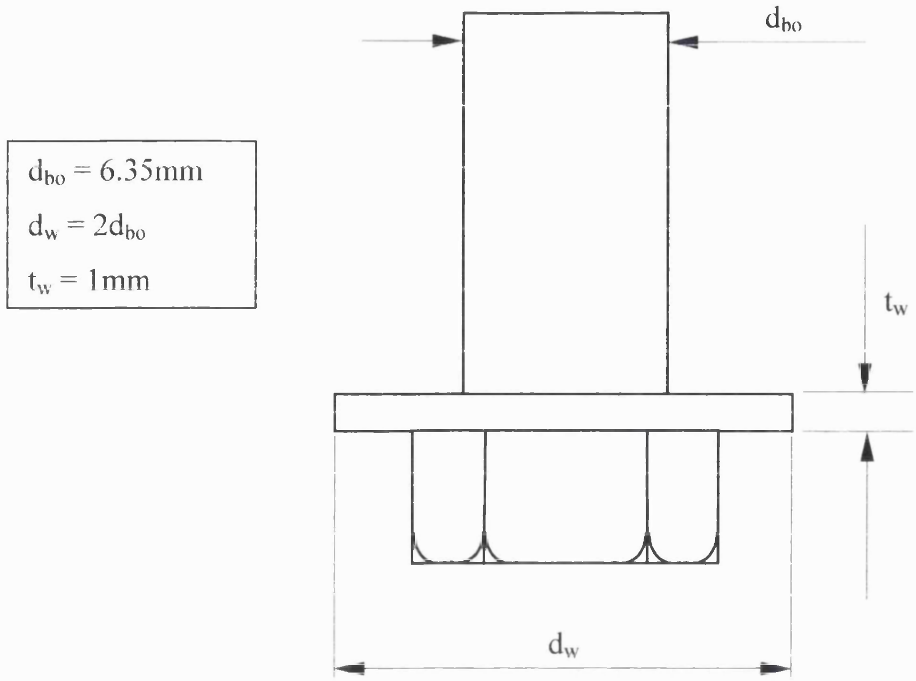

Figure 5.2 – Physical representation of the bolt and washer assembly

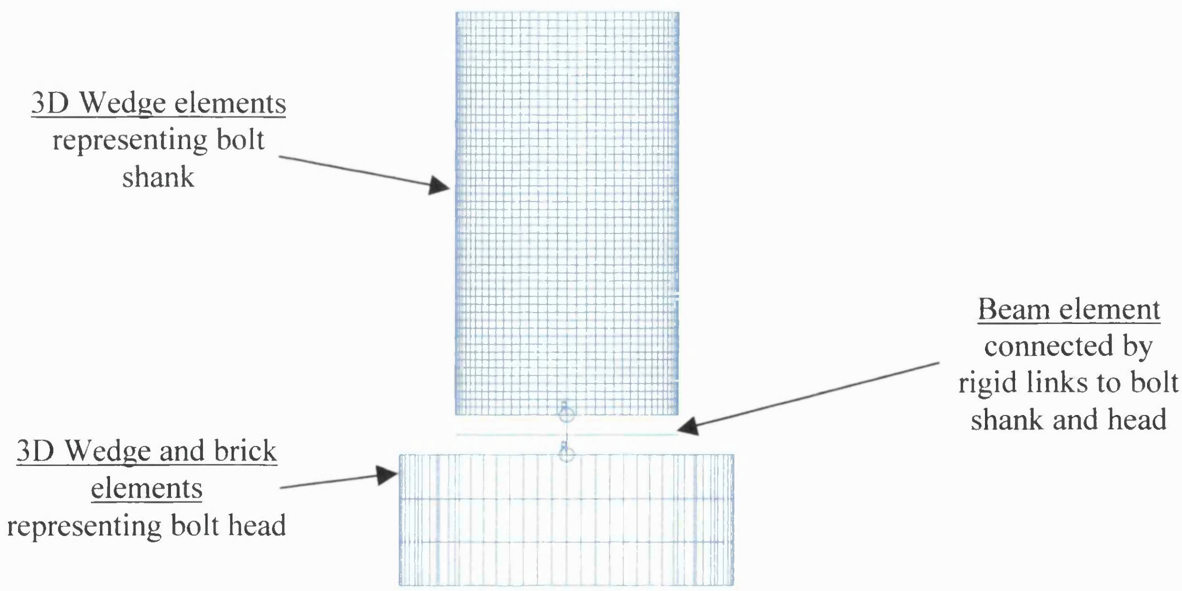

Figure 5.3 – Bolt mesh (not including the washer)

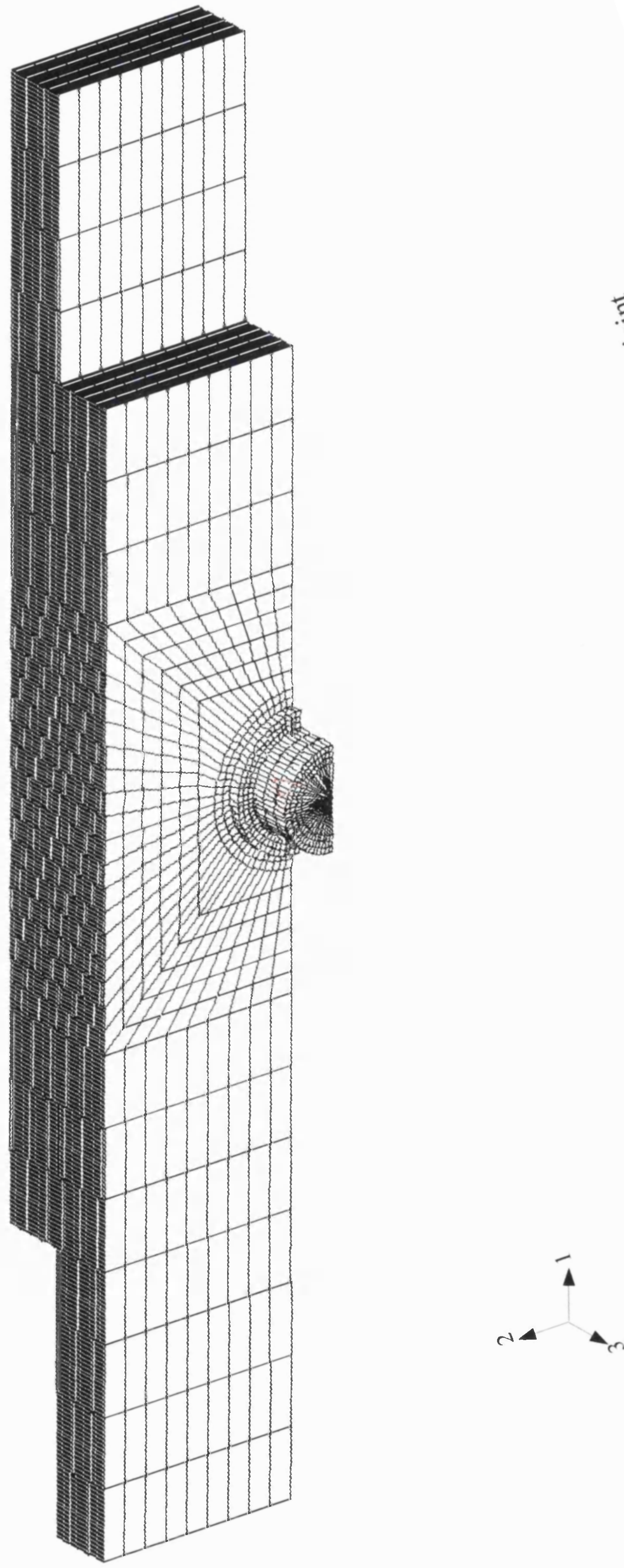

Figure 5.4– Typical element layout for the double lap joint

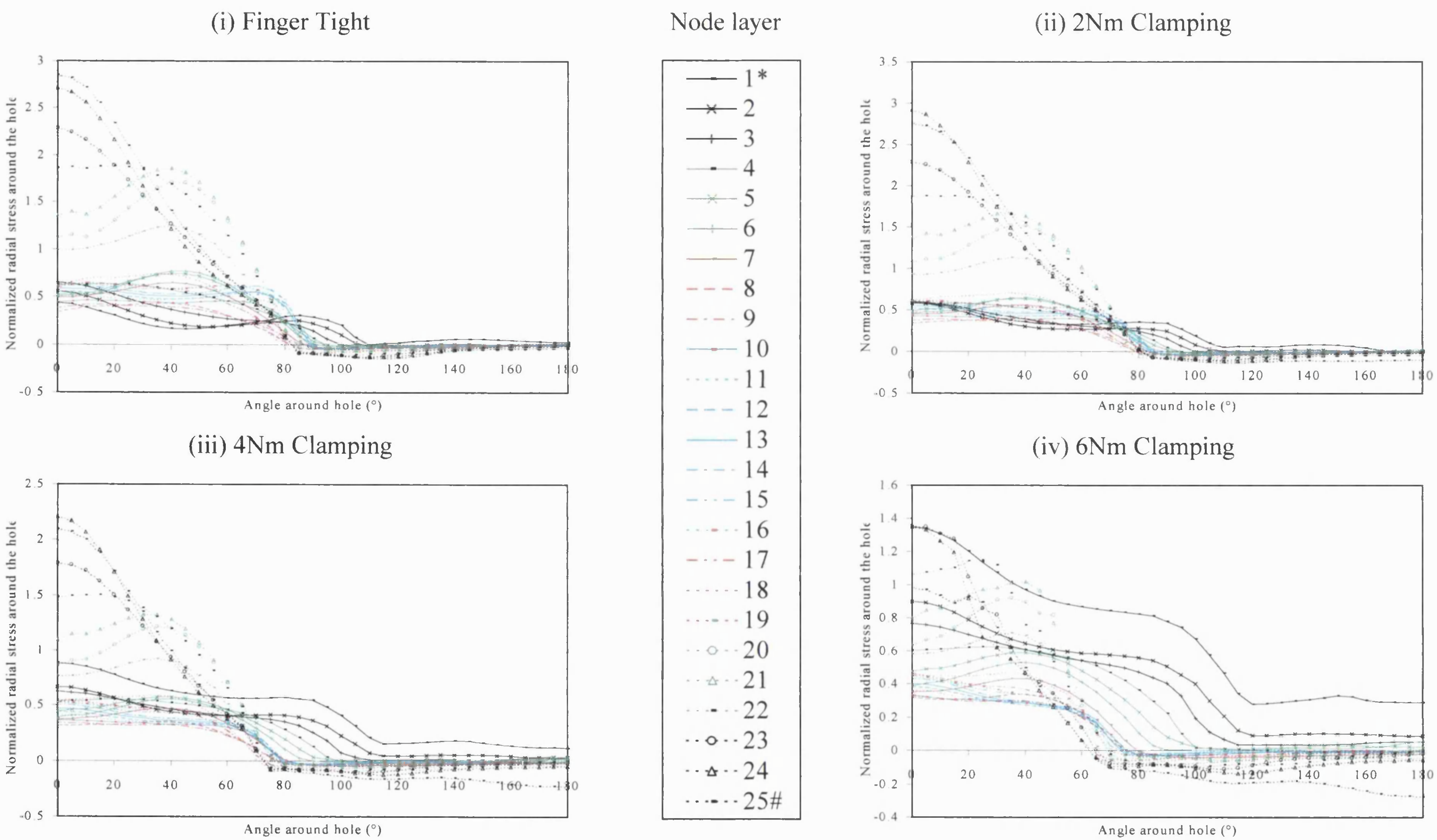

Figure 5.5a – Normalized radial stress around the hole boundary of the outer lap – aluminium bolt and washer assembly
0Nm, 2Nm, 4Nm and 6Nm clamping - * = Outer surface, # = Laminate interface

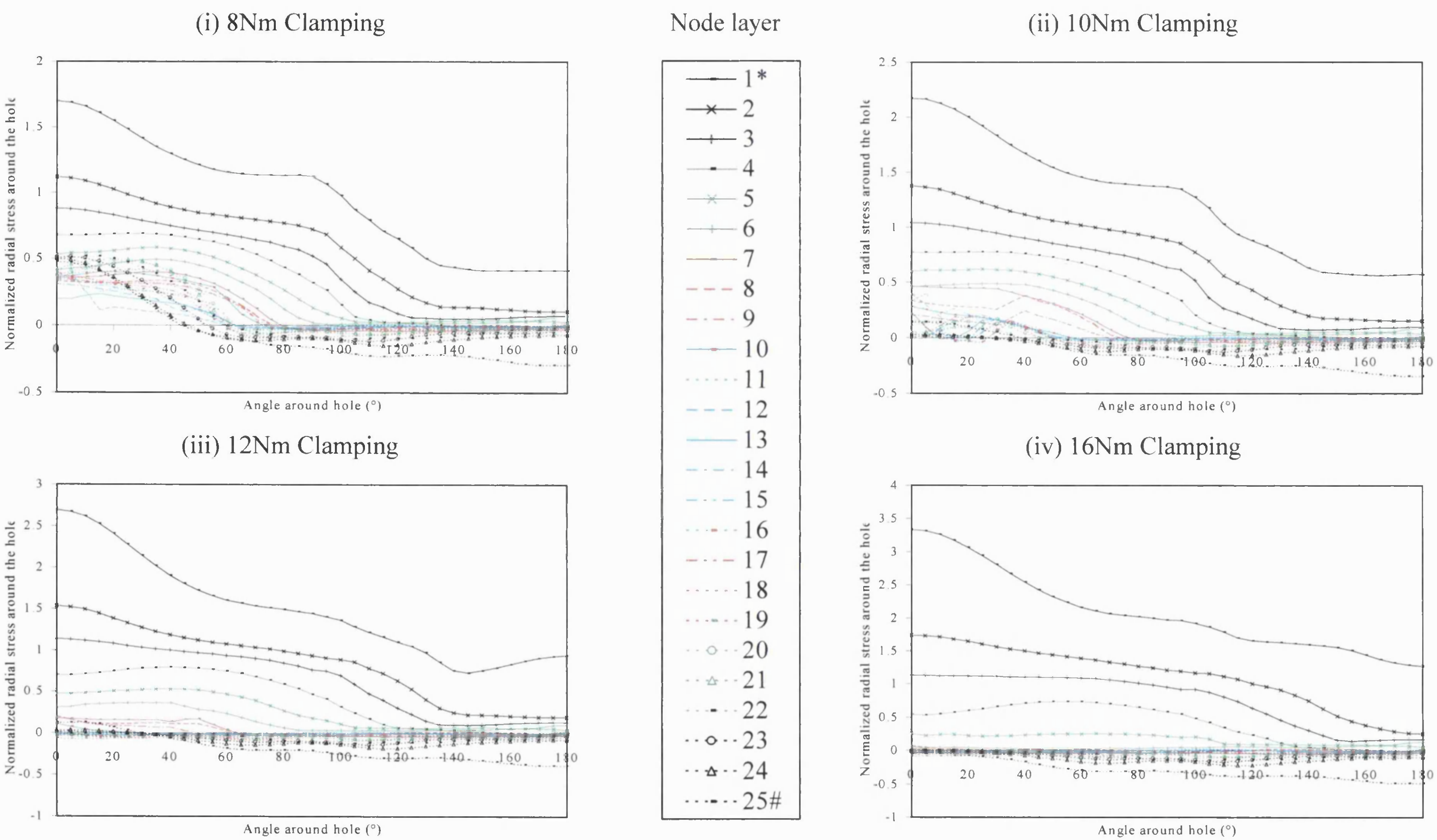

Figure 5.5b – Normalized radial stress around the hole boundary of the outer lap – aluminium bolt and washer assembly 8Nm, 10Nm, 12Nm and 16Nm clamping - * = Outer surface, # = Laminate interface

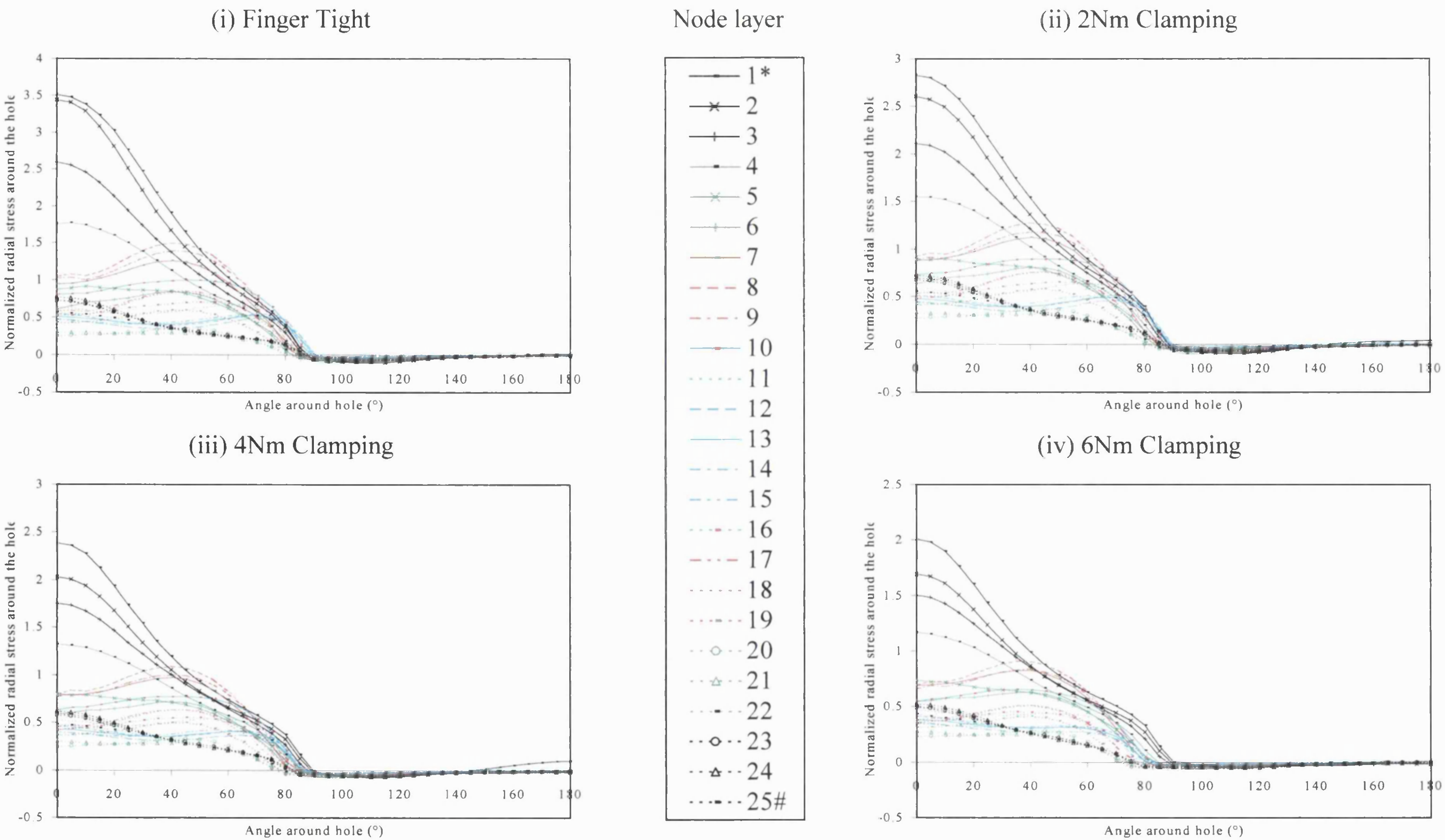

Figure 5.6a – Normalized radial stress around the hole boundary of the inner lap – aluminium bolt and washer assembly 0Nm, 2Nm, 4Nm and 6Nm clamping - * = Laminate interface, # = Laminate mid-plane

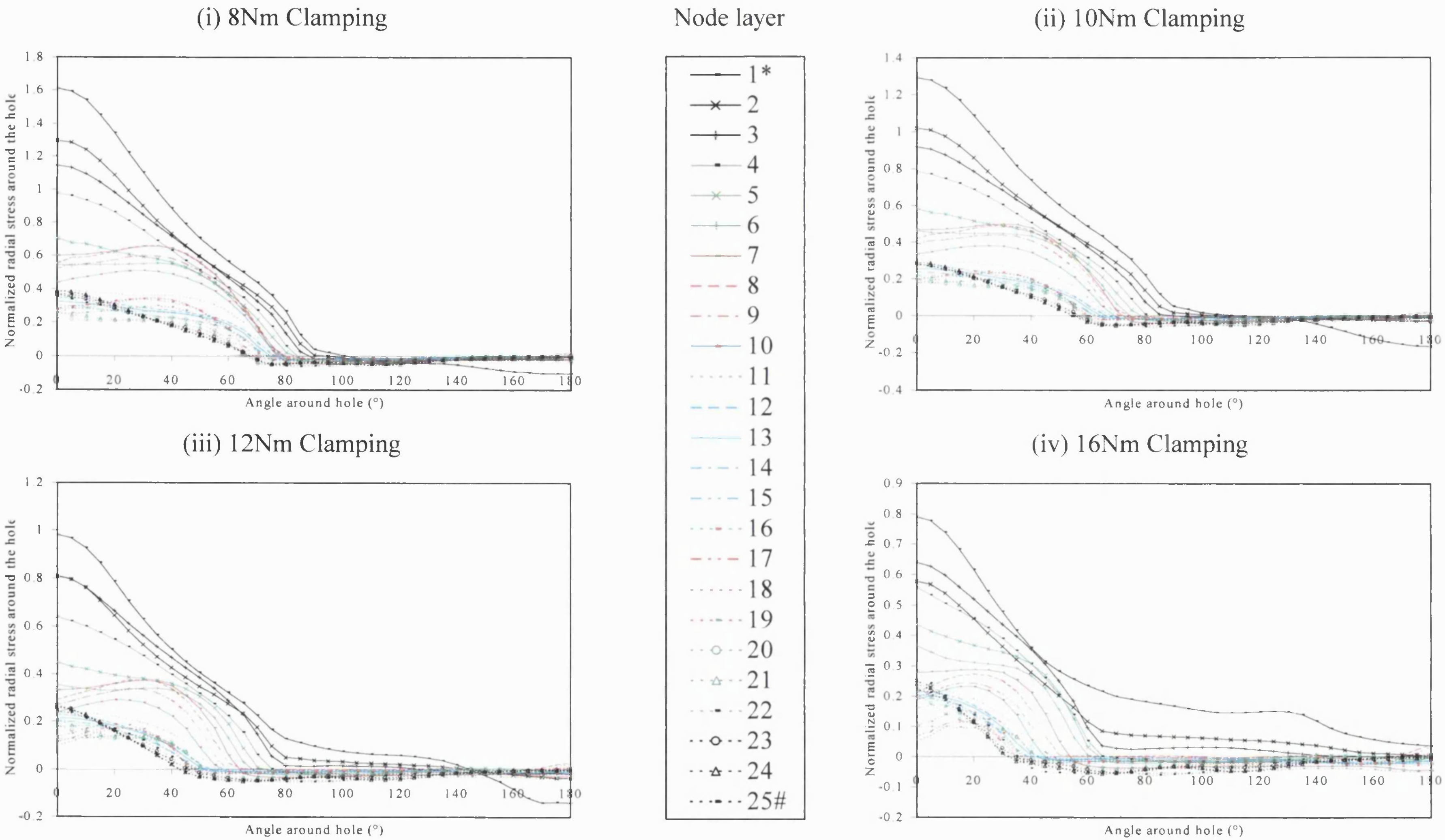

Figure 5.6b – Normalized radial stress around the hole boundary of the inner lap – aluminium bolt and washer assembly 8Nm, 10Nm, 12Nm and 16Nm clamping - * = Laminate interface, # = Laminate mid-plane

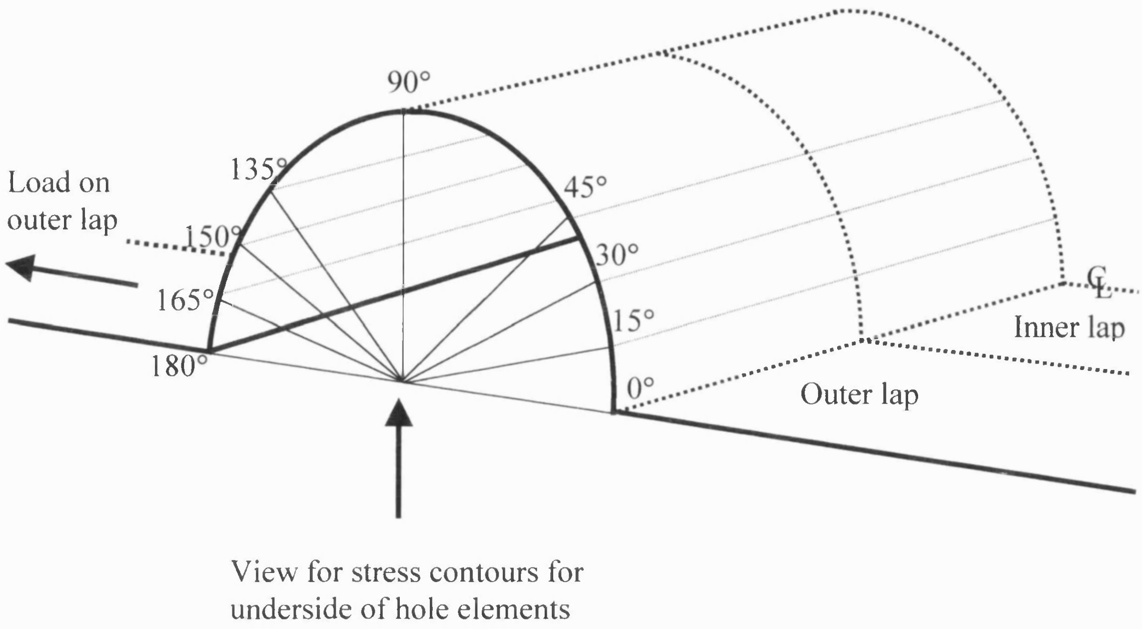

Figure 5.7a - Diagram showing the angular positions on the hole surface identified on the radial contact stress contour plots, as given below:

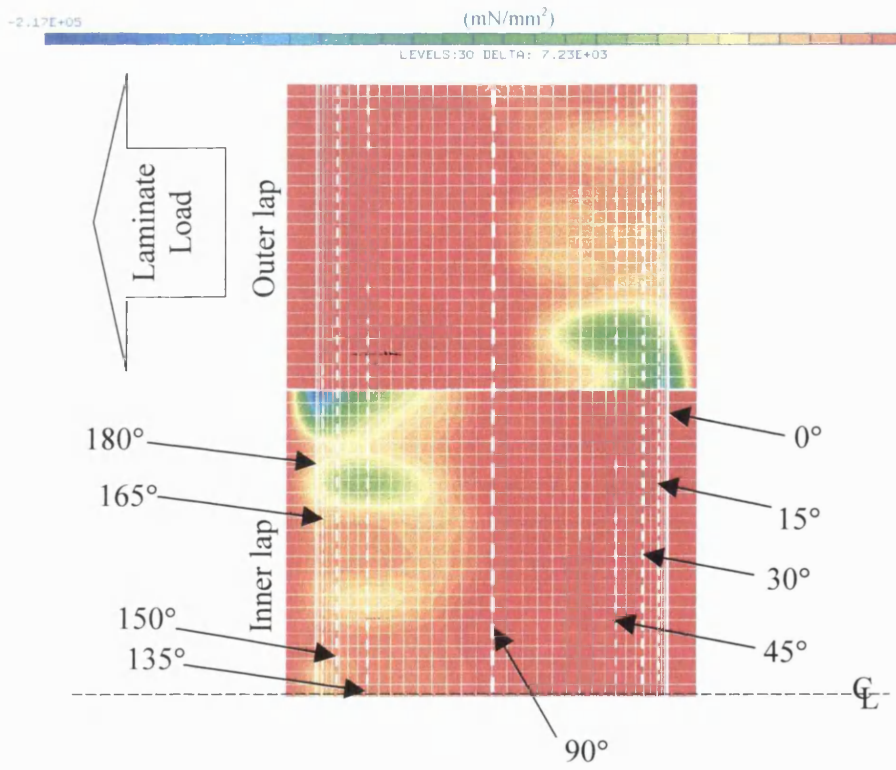

Figure 5.7b – A transverse view showing the angular positions on the contour plot of the radial contact stress at the hole surface

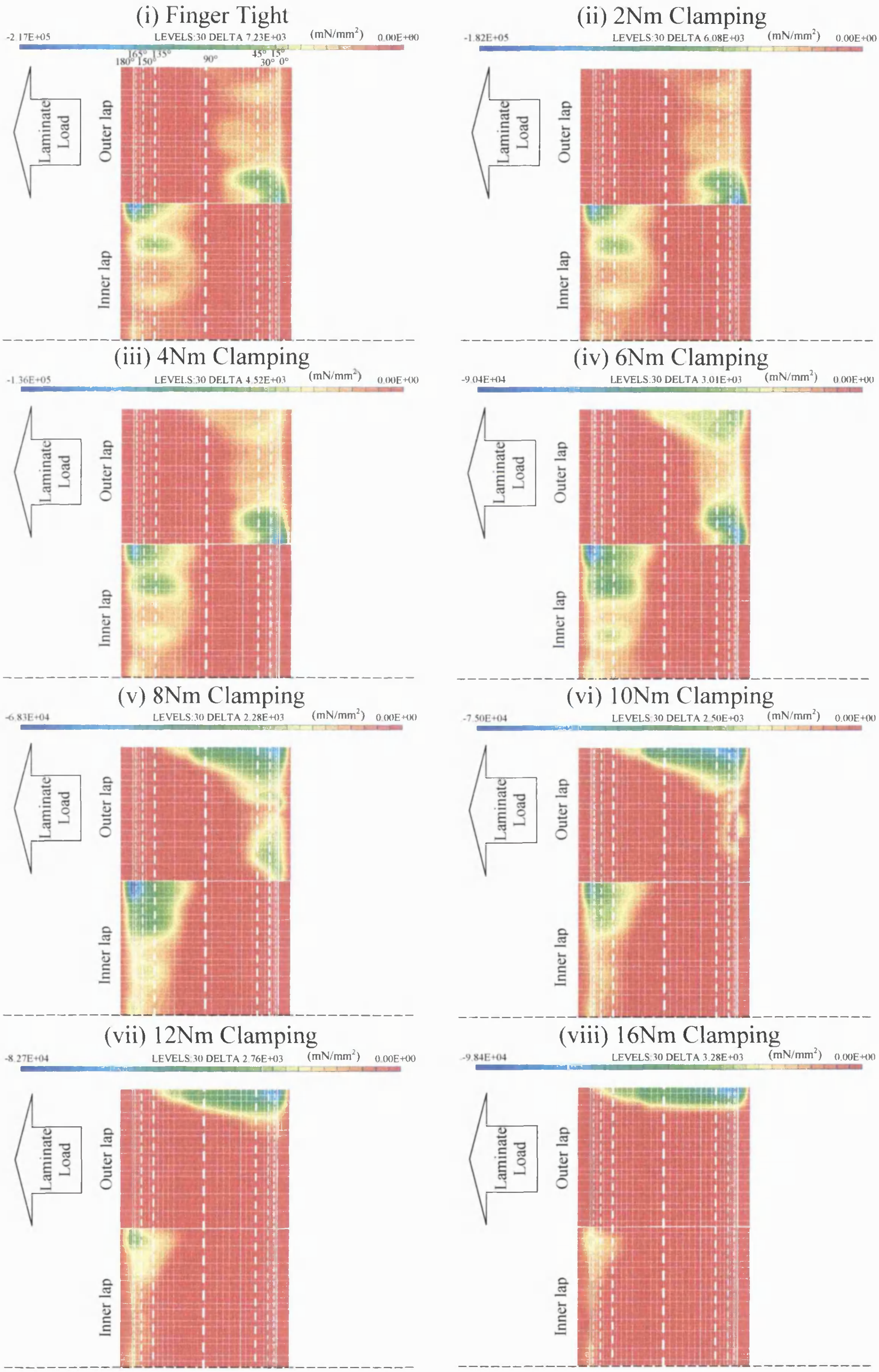

Figure 5.8 – Radial contact stress plots on the underside of the hole boundary 0Nm to 16Nm clamping

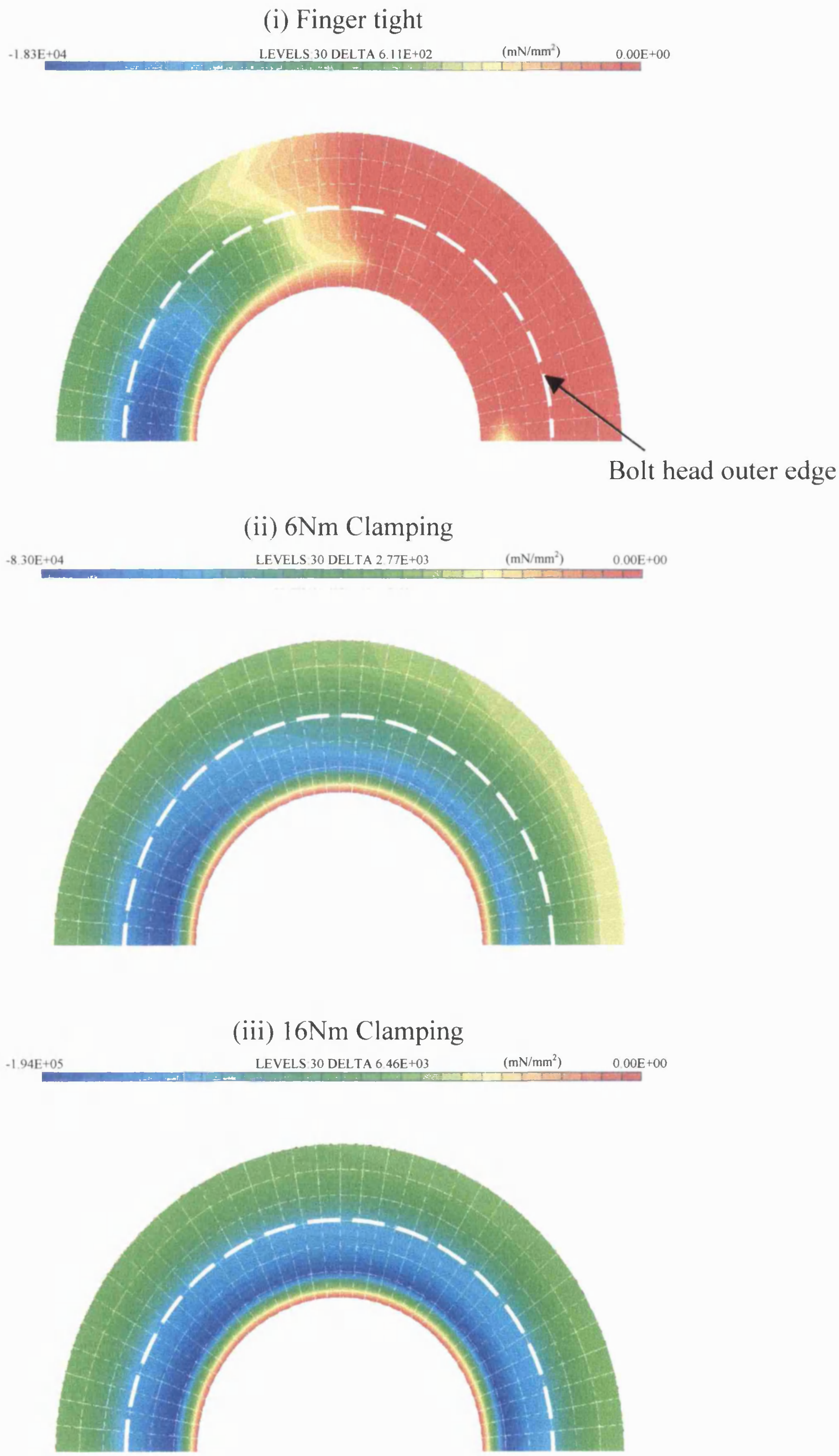

Figure 5.9 – Through thickness contact stress on the outer lap under the washer aluminium bolt and washer assembly – 0Nm, 6Nm and 16Nm clamping

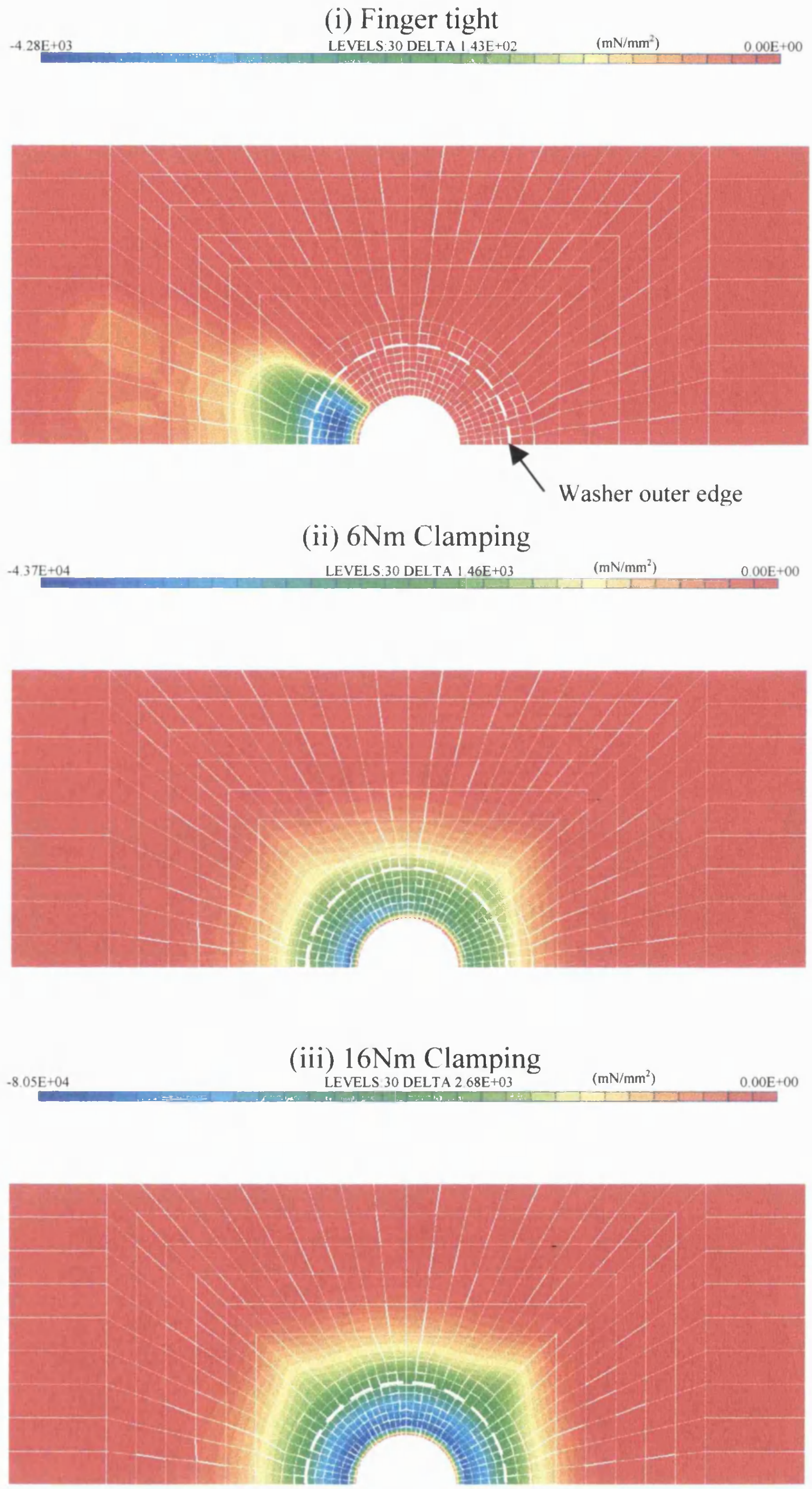

Figure 5.10 – Through thickness contact stress on the inner lap at the laminate interface aluminium bolt and washer assembly – 0Nm, 6Nm and 16Nm clamping

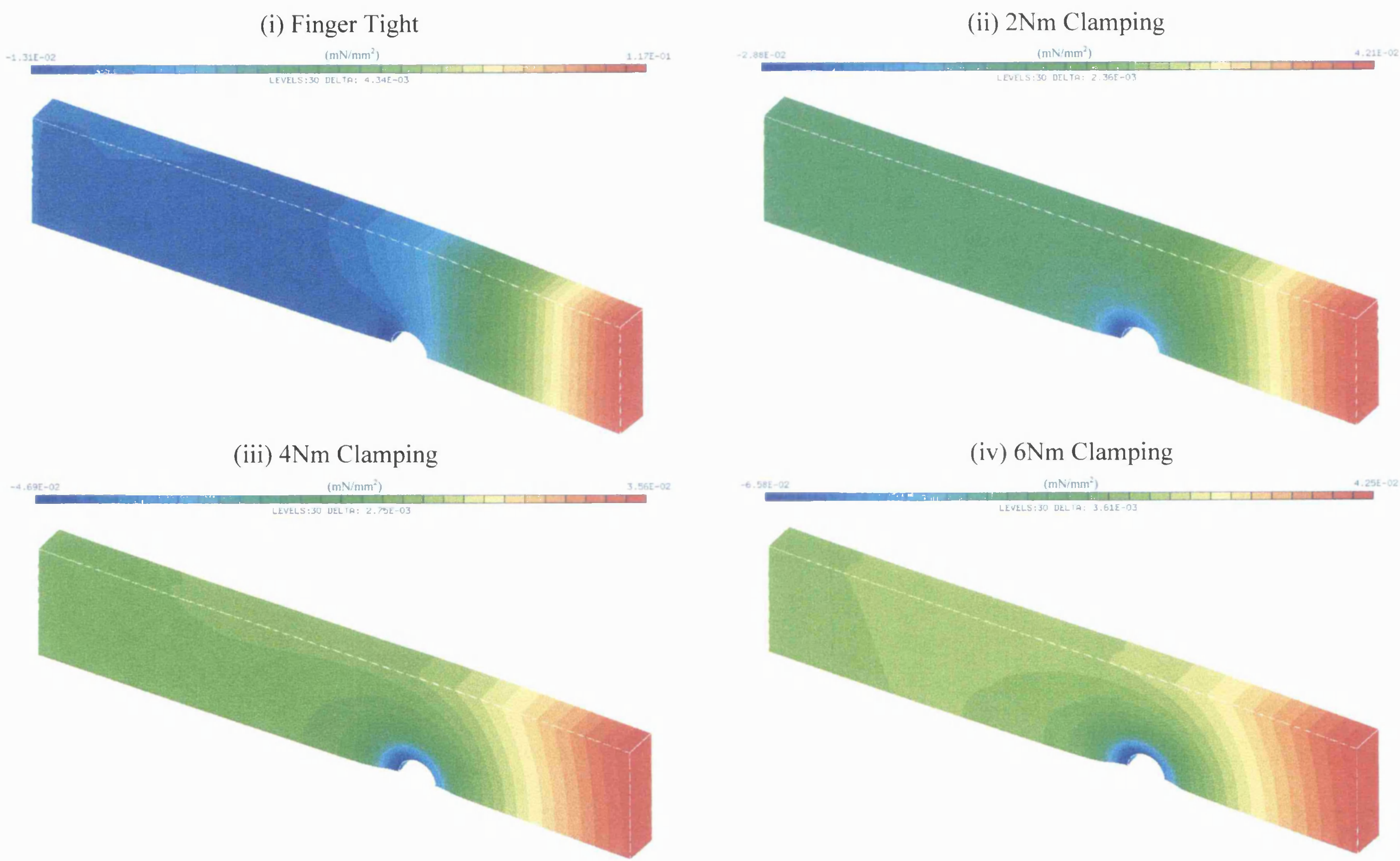

Figure 5.11a – Through thickness displacement of the outer lap – aluminium bolt and washer assembly 0Nm, 2Nm, 4Nm, and 6Nm clamping

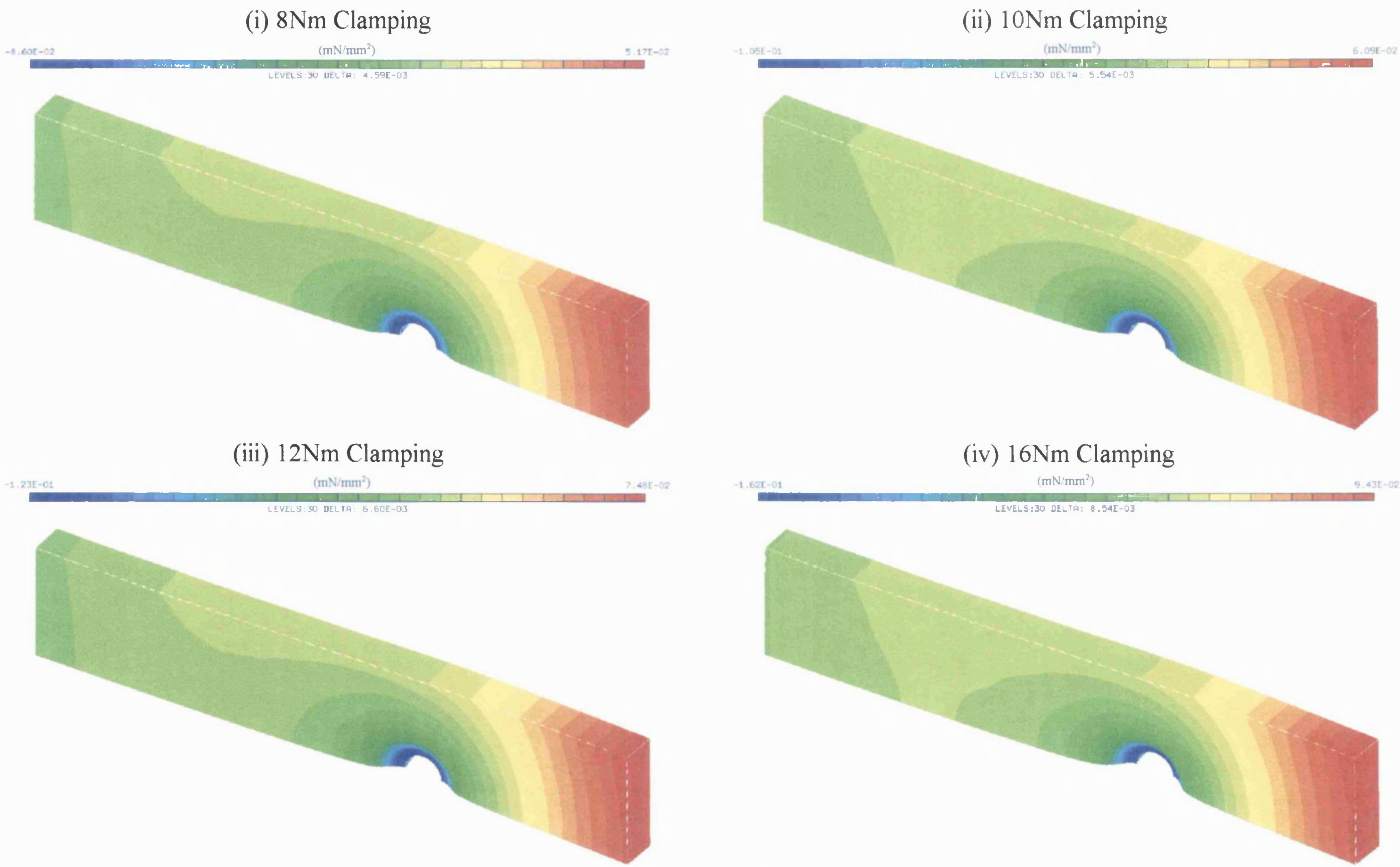

Figure 5.11b – Through thickness displacement of the outer lap – aluminium bolt and washer assembly
8Nm, 10Nm, 12Nm and 16Nm clamping

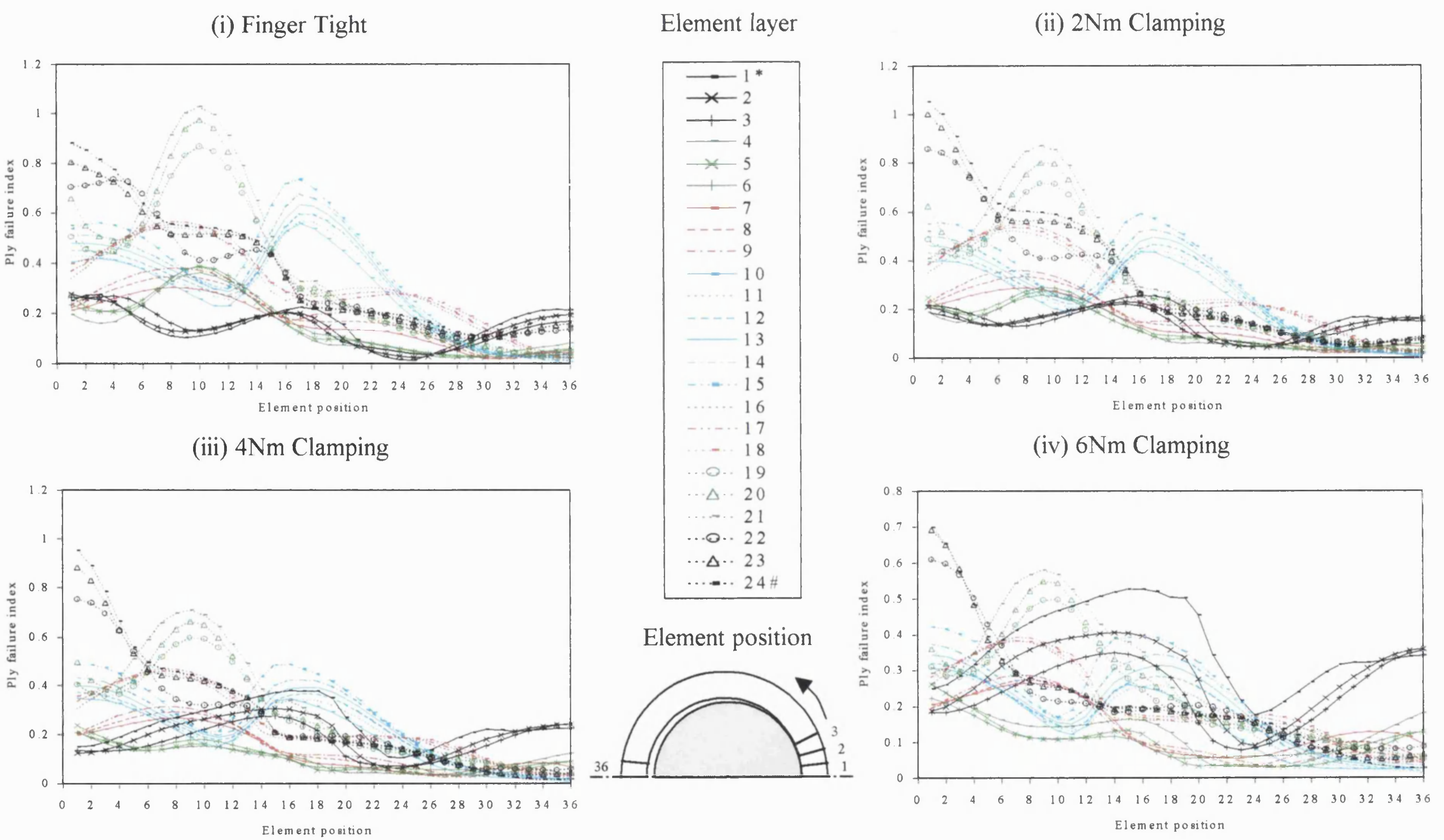

Figure 5.12a – Ply failure index plots for the outer lap – aluminium bolt and washer assembly
0Nm, 2Nm, 4Nm and 6Nm clamping - * = Outer surface, # = Laminate interface

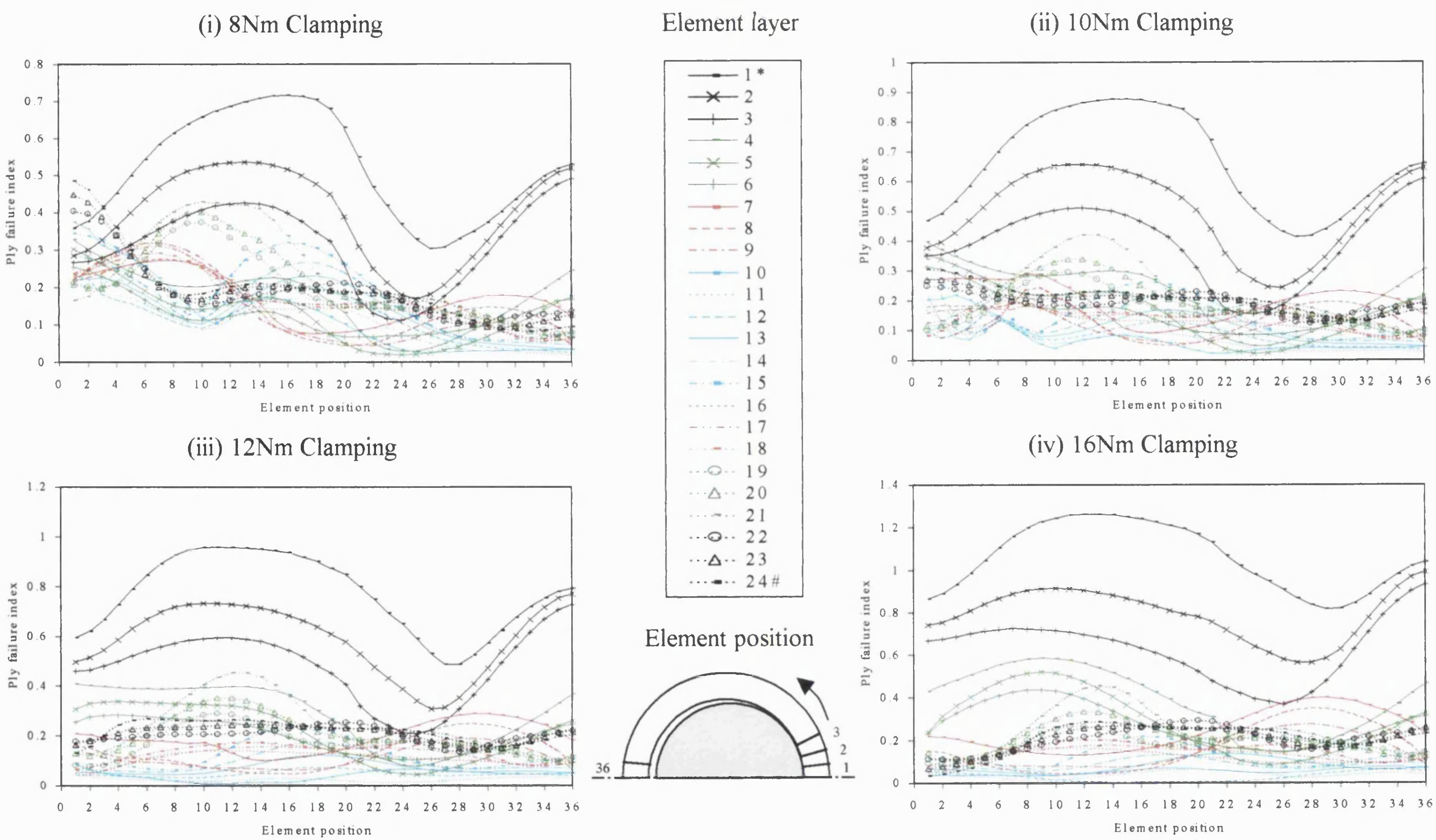

Figure 5.12b – Ply failure index plots for the outer lap – aluminium bolt and washer assembly
8Nm, 10Nm, 12Nm and 16Nm clamping - * = Outer surface, # = Laminate interface

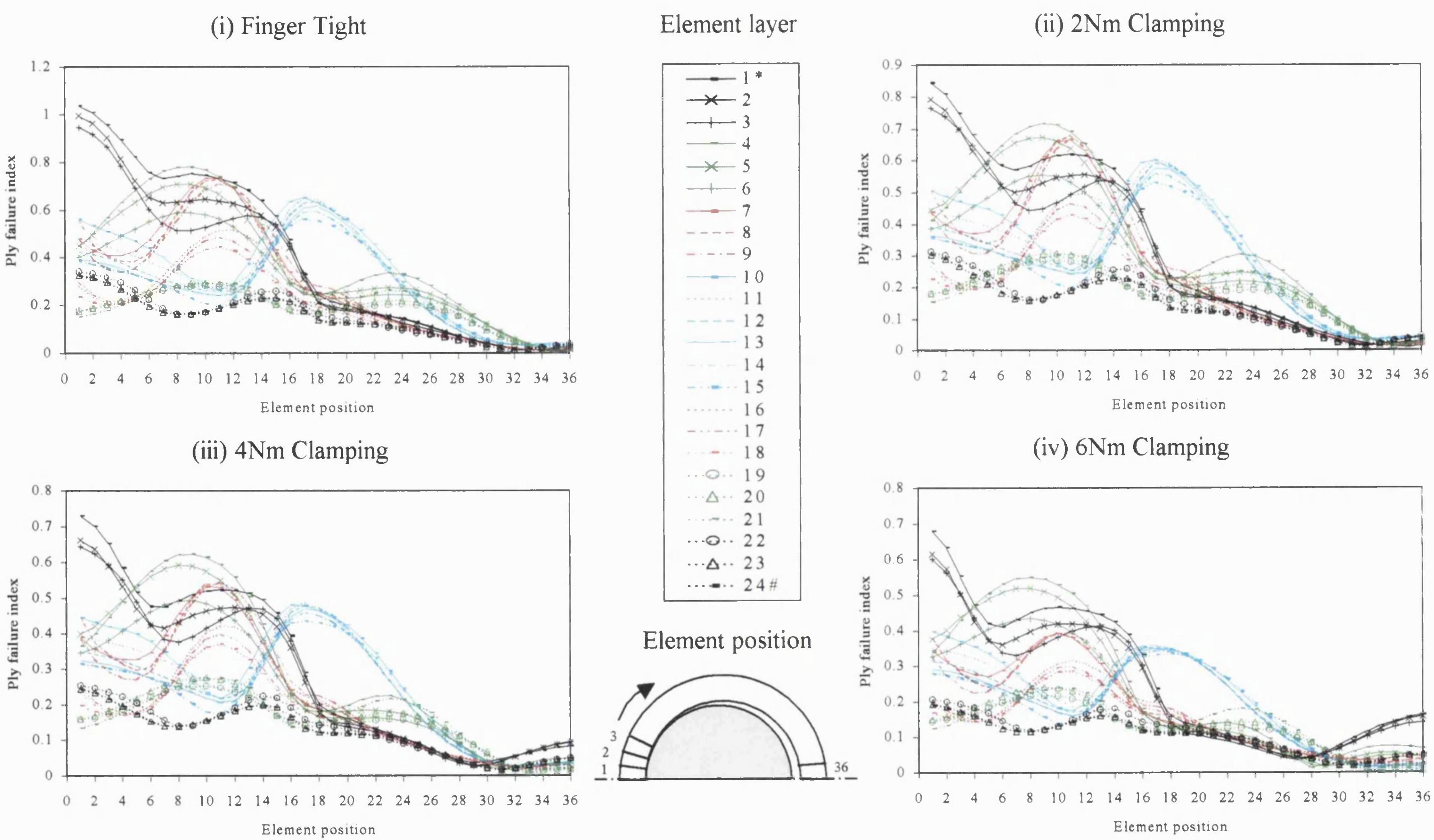

Figure 5.13a – Ply failure index plots for the inner lap – aluminium bolt and washer assembly 0Nm, 2Nm, 4Nm and 6Nm clamping - * = Laminate interface, # = Laminate mid-plane

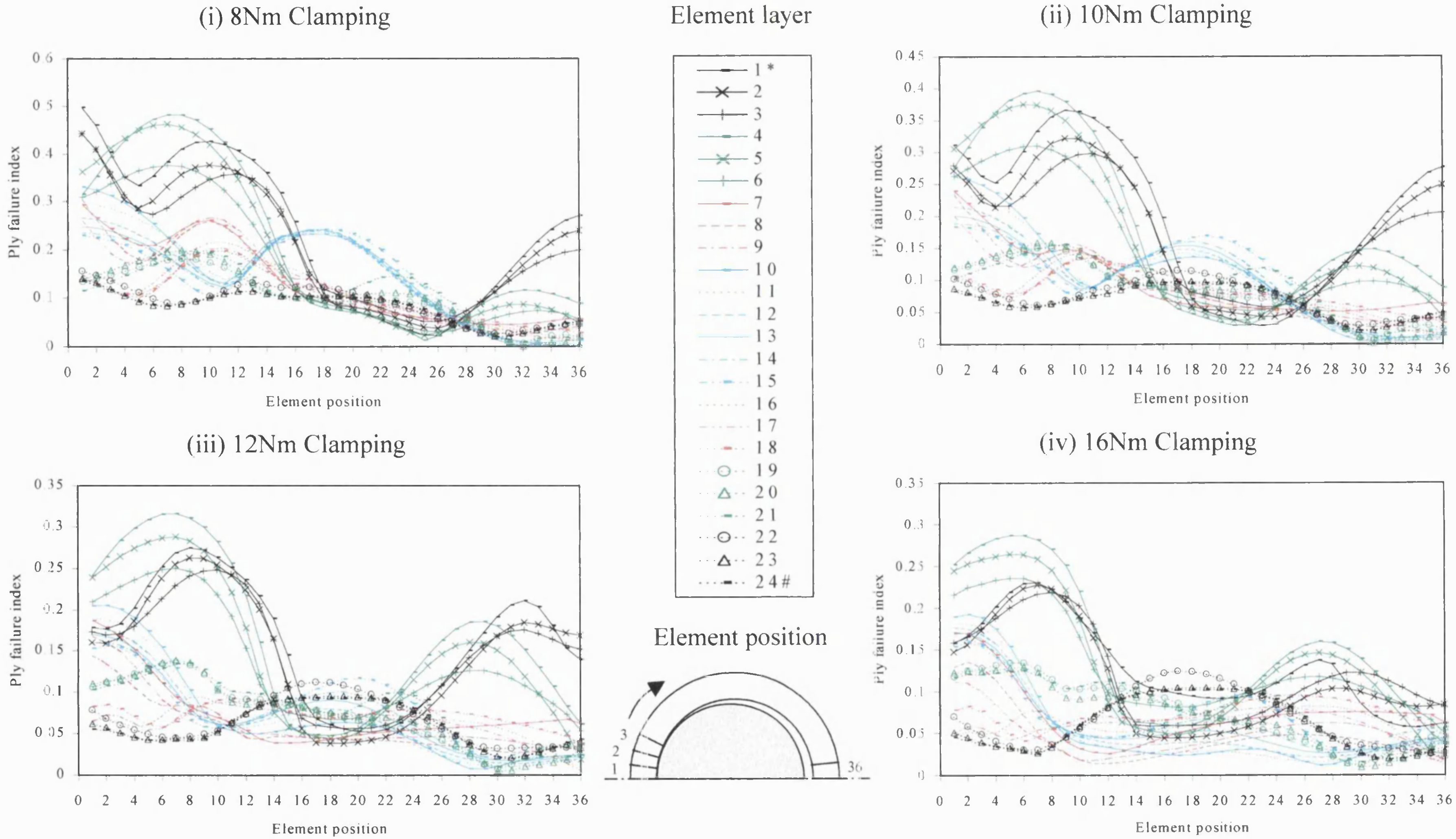

Figure 5.13b – Ply failure index plots for the inner lap – aluminium bolt and washer assembly 8Nm, 10Nm, 12Nm and 16Nm clamping - * = Laminate interface, # = Laminate mid-plane

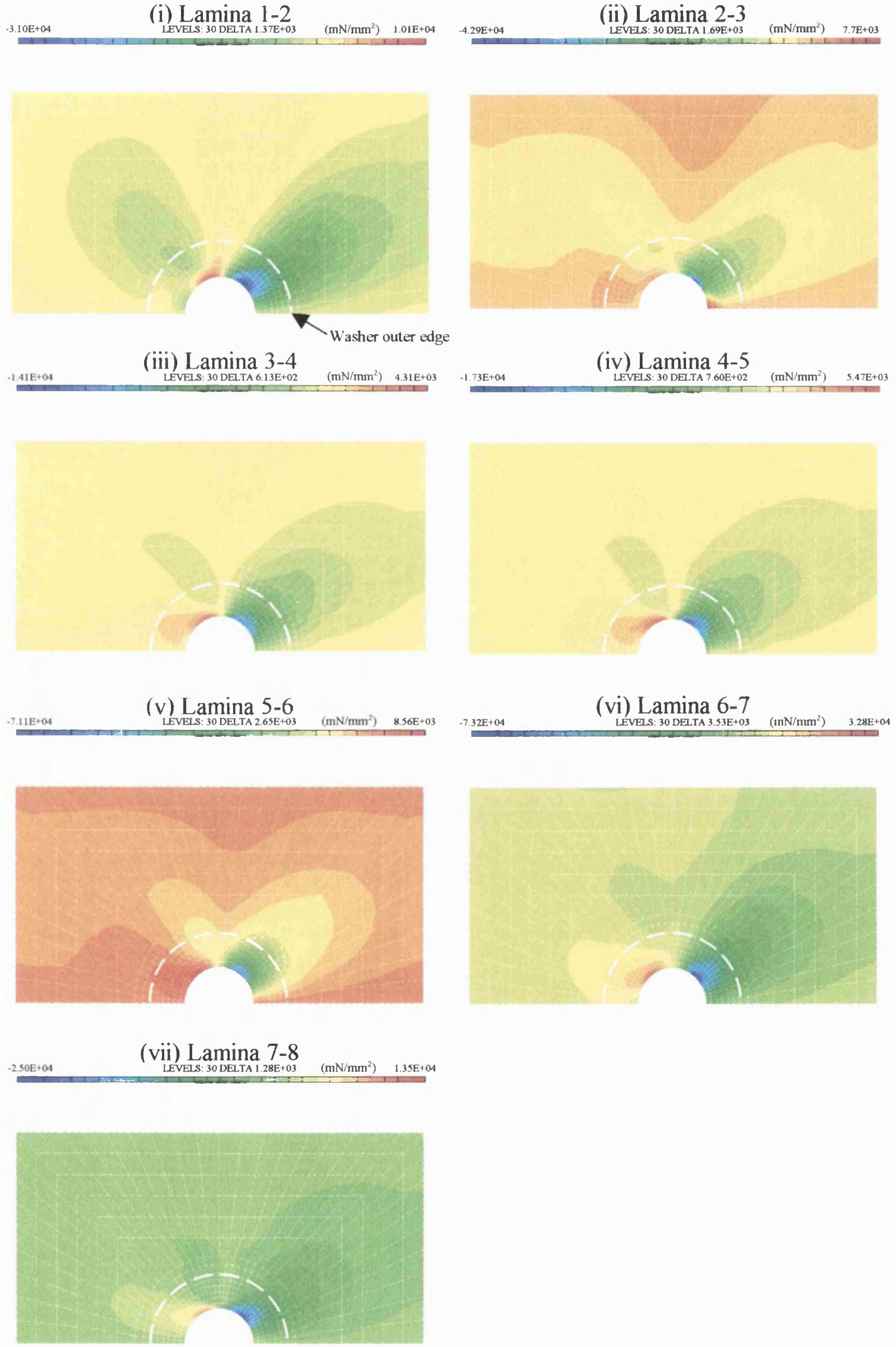

Figure 5.14 – Interlaminar shear stress between plies – outer lap – 0Nm clamping

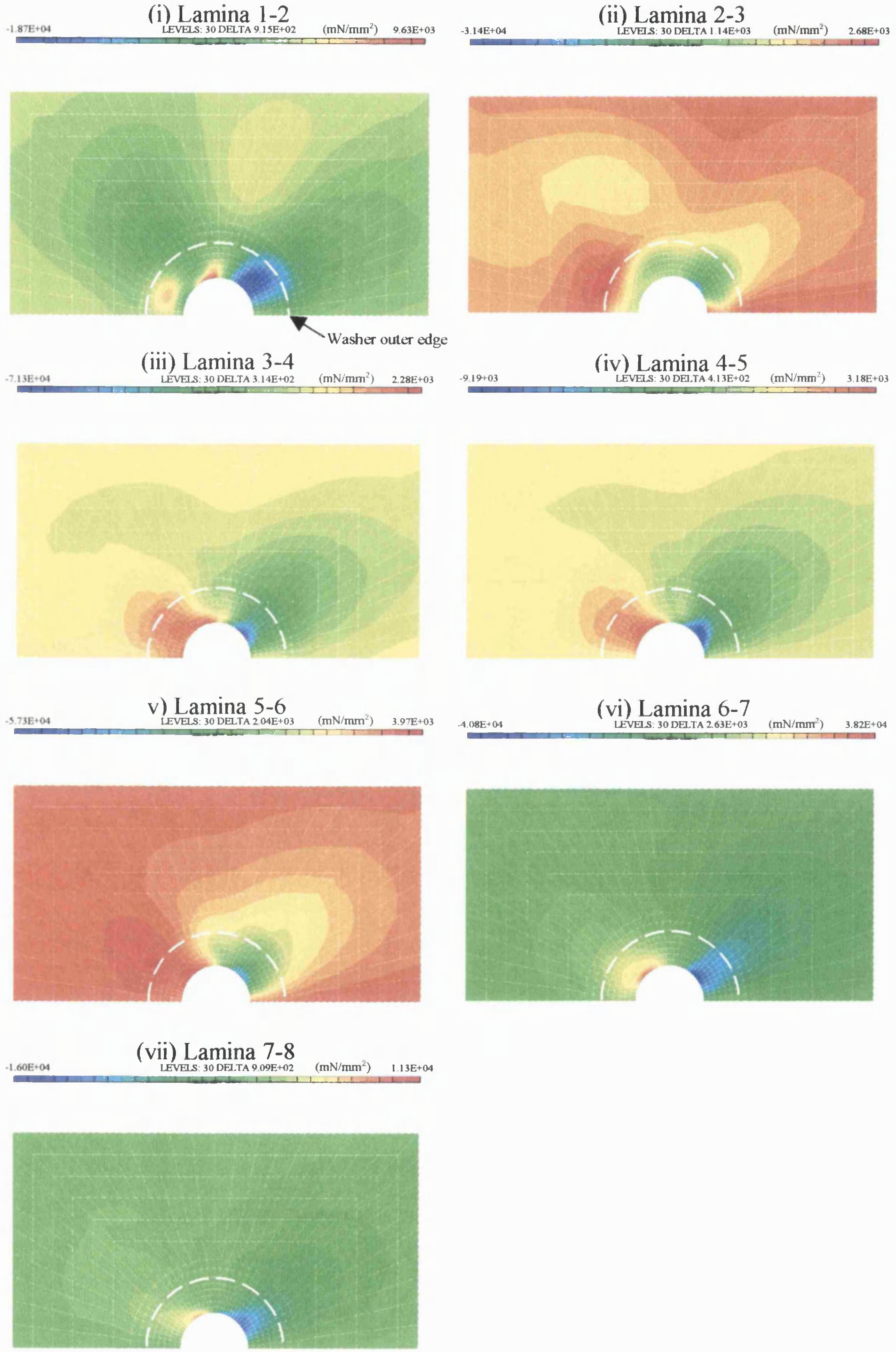

Figure 5.15 – Interlaminar shear stress between plies – outer lap – 6Nm clamping

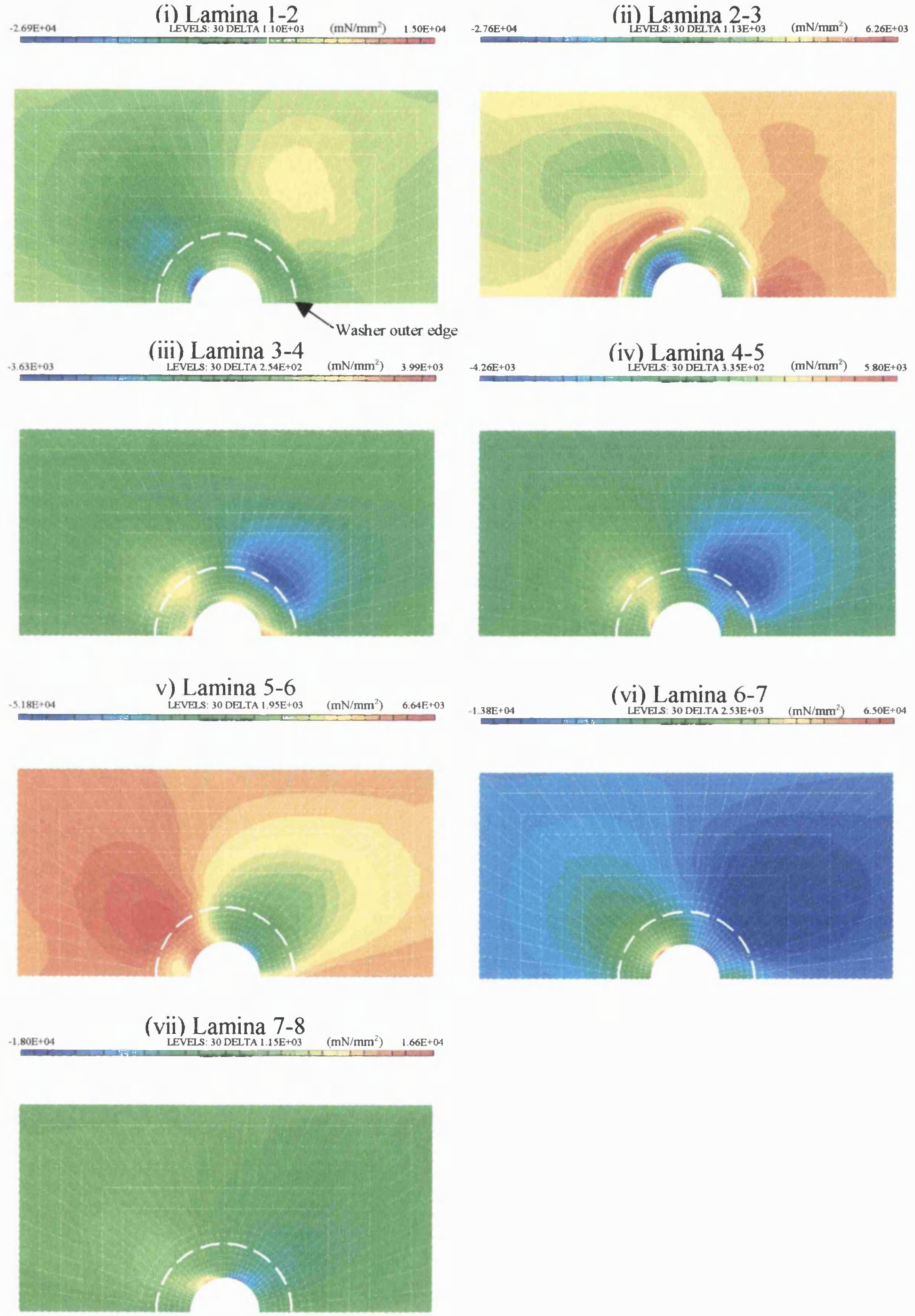

Figure 5.16 – Interlaminar shear stress between plies – outer lap – 16Nm clamping

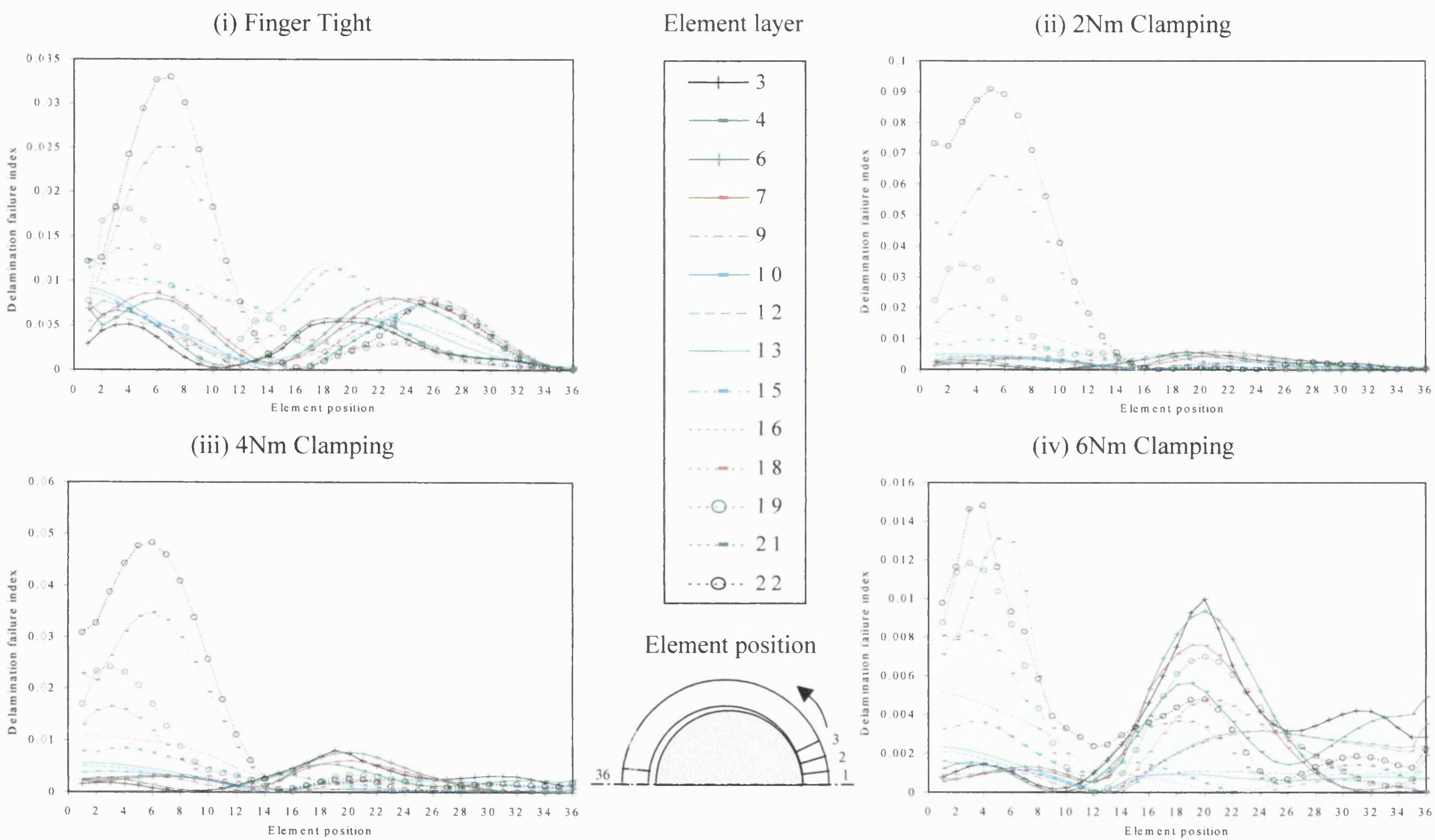

Figure 5.17a – Delamination failure index plots for the outer lap – aluminium bolt and washer assembly 0Nm, 2Nm, 4Nm and 6Nm clamping

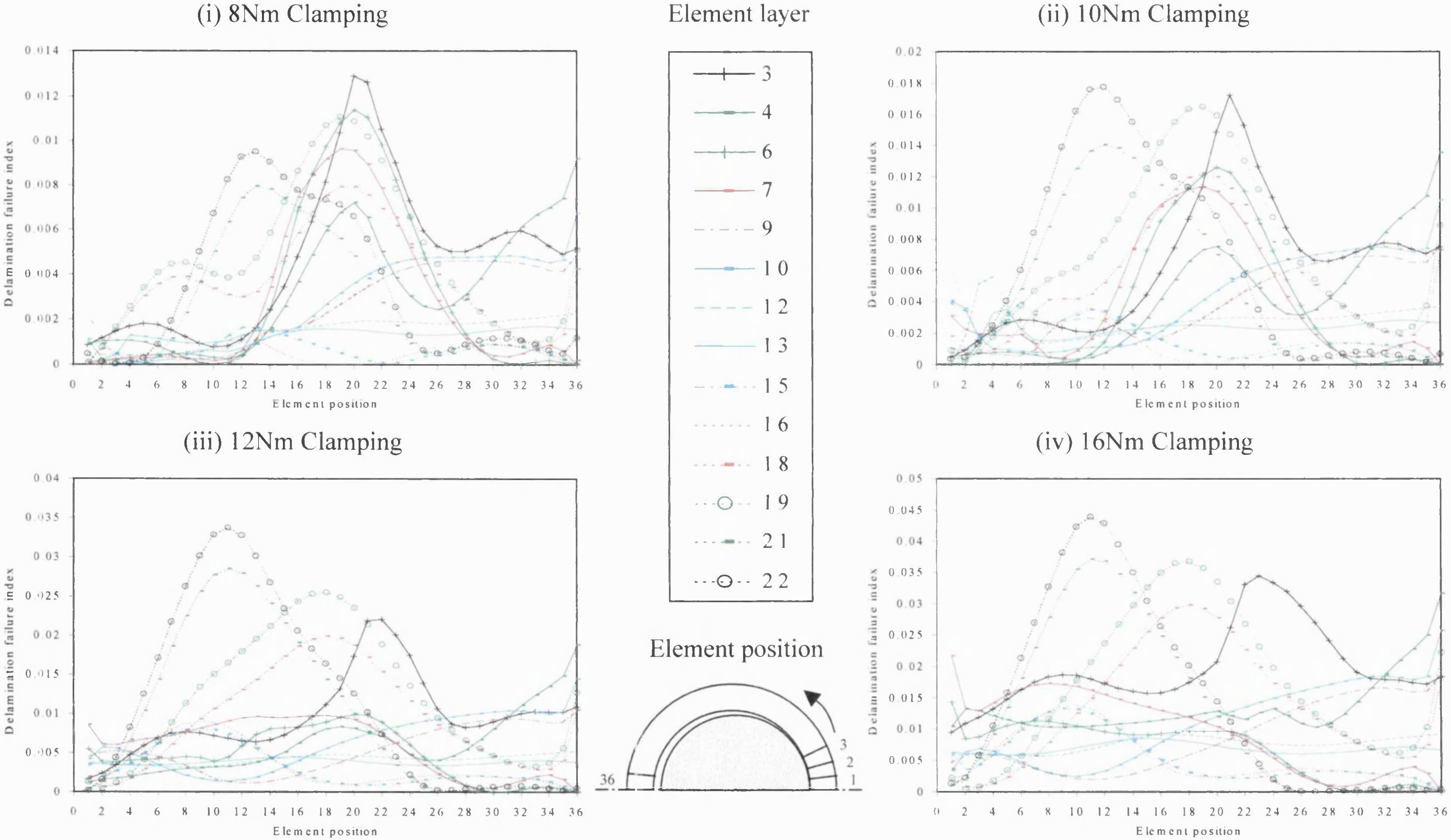

Figure 5.17b – Delamination failure index plots for the outer lap – aluminium bolt and washer assembly 8Nm, 10Nm, 12Nm and 16Nm clamping

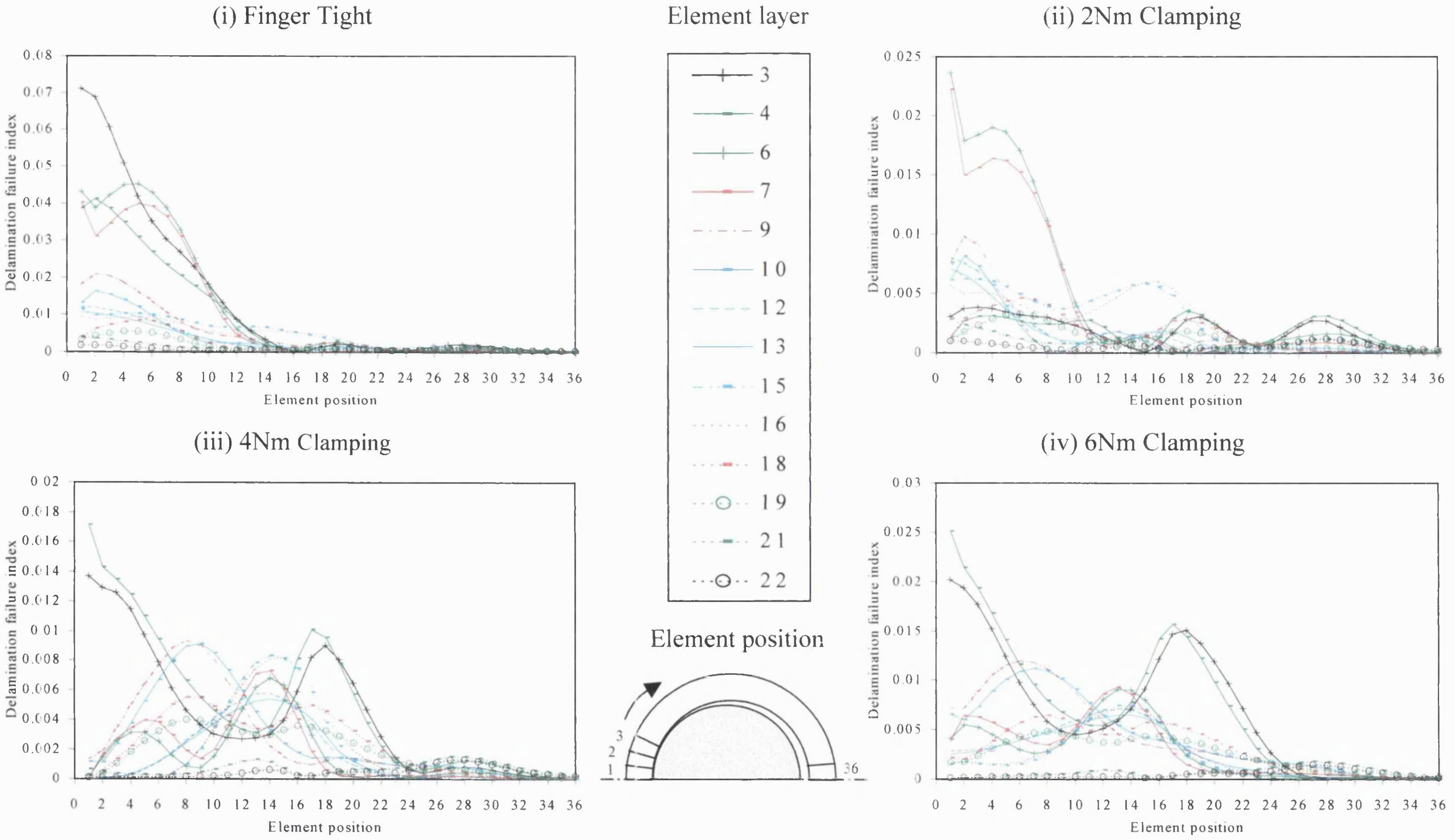

Figure 5.18a – Delamination failure index plots for the inner lap – aluminium bolt and washer assembly 0Nm, 2Nm, 4Nm and 6Nm clamping

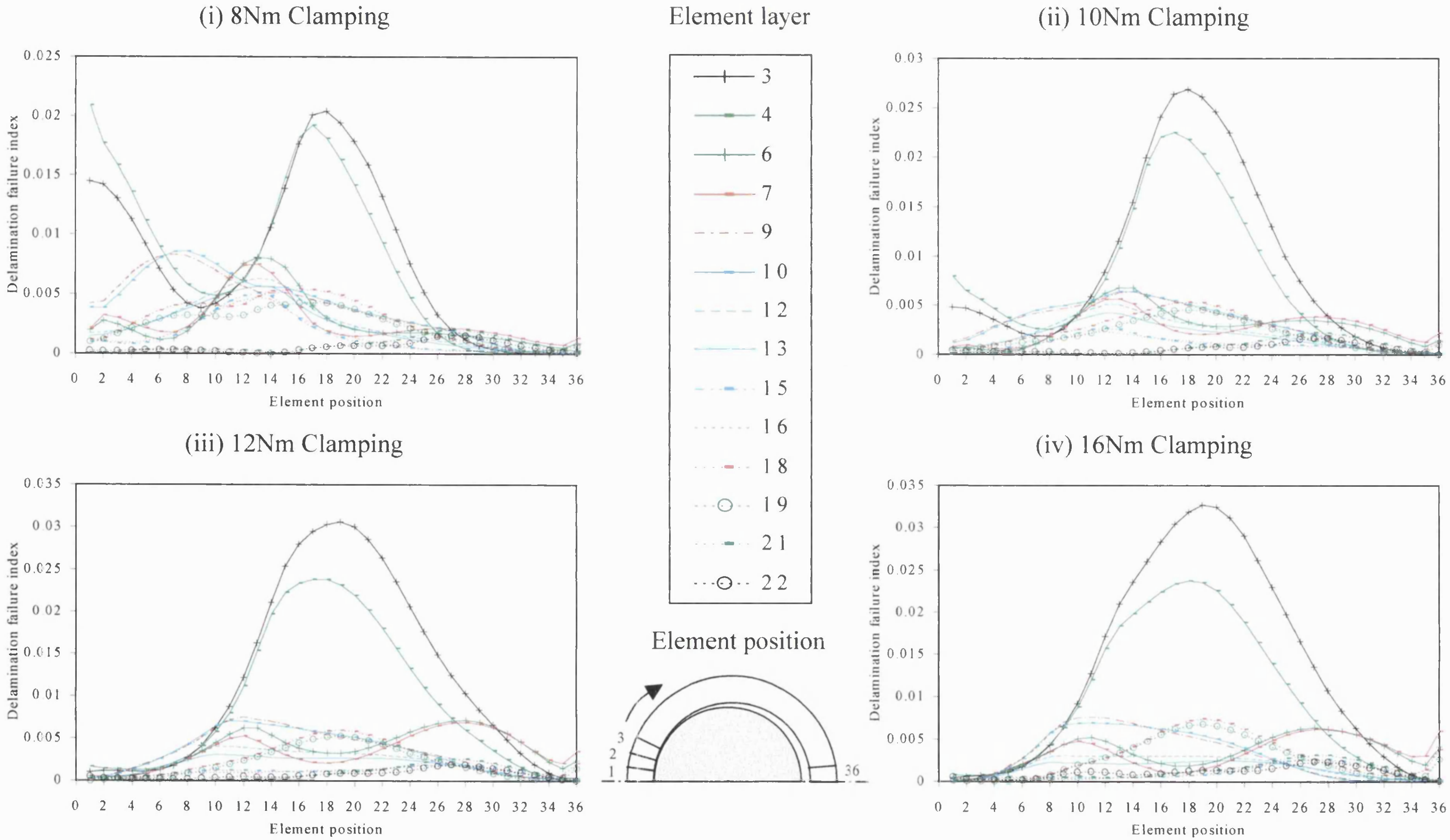

Figure 5.18b – Delamination failure index plots for the inner lap – aluminium bolt and washer assembly 8Nm, 10Nm, 12Nm and 16Nm clamping

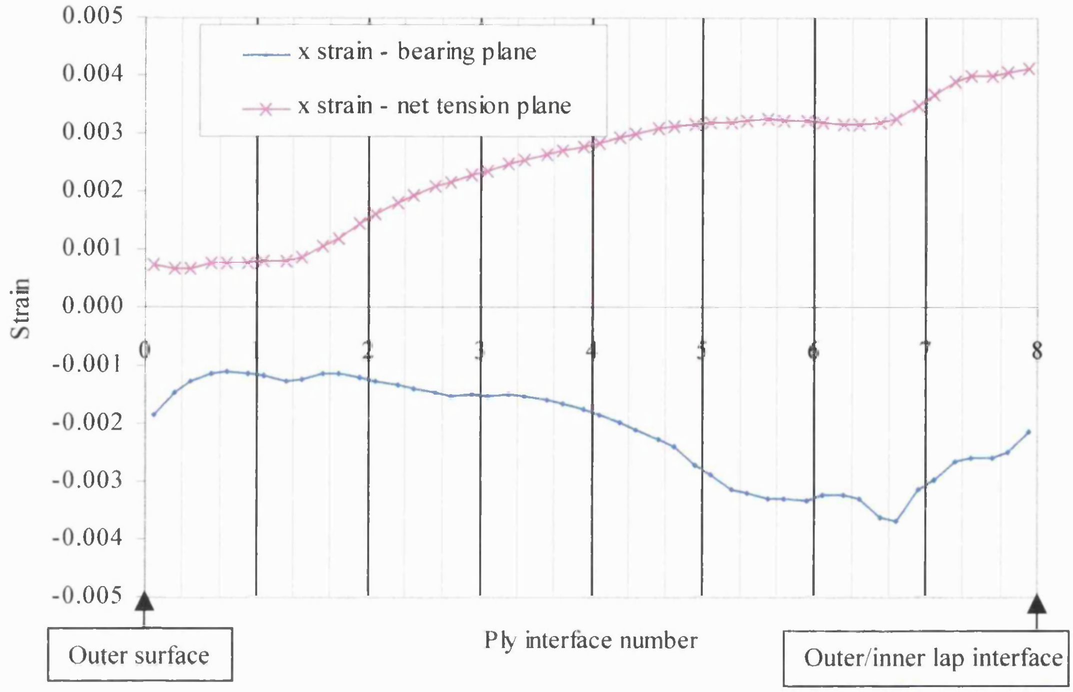

Figure 5.19 – Longitudinal strain distribution through the thickness of the outer lap aluminium bolt and washer assembly – 6Nm torque

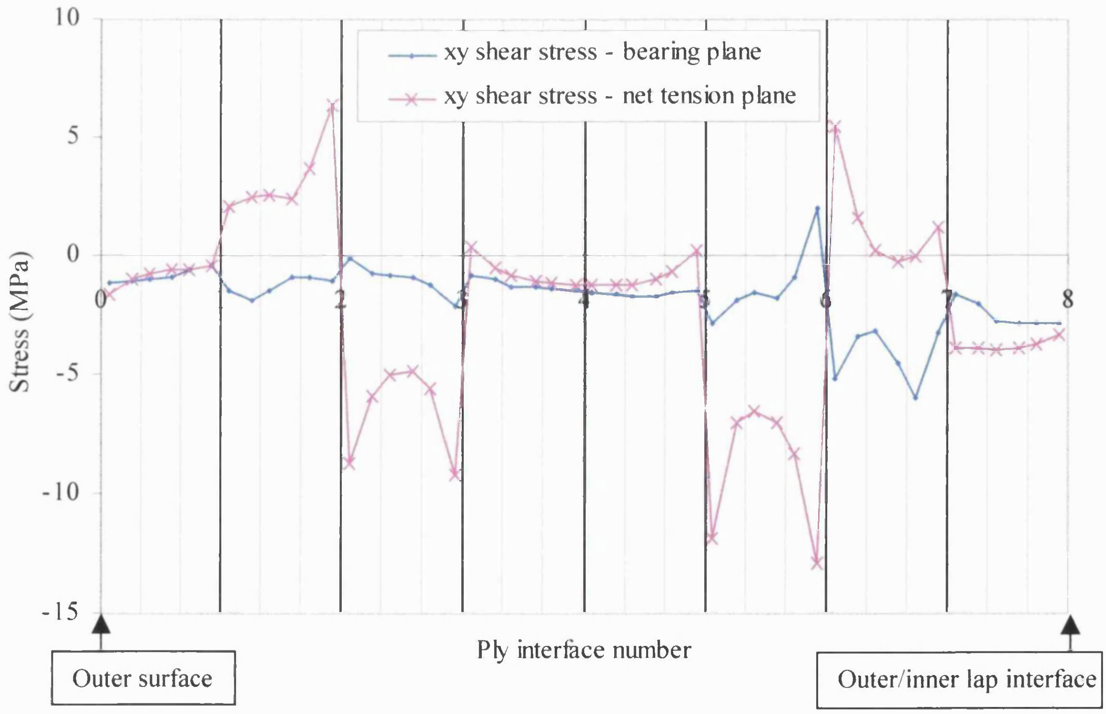

Figure 5.20 – Shear stress distribution through the thickness of the outer lap aluminium bolt and washer assembly – 6Nm torque

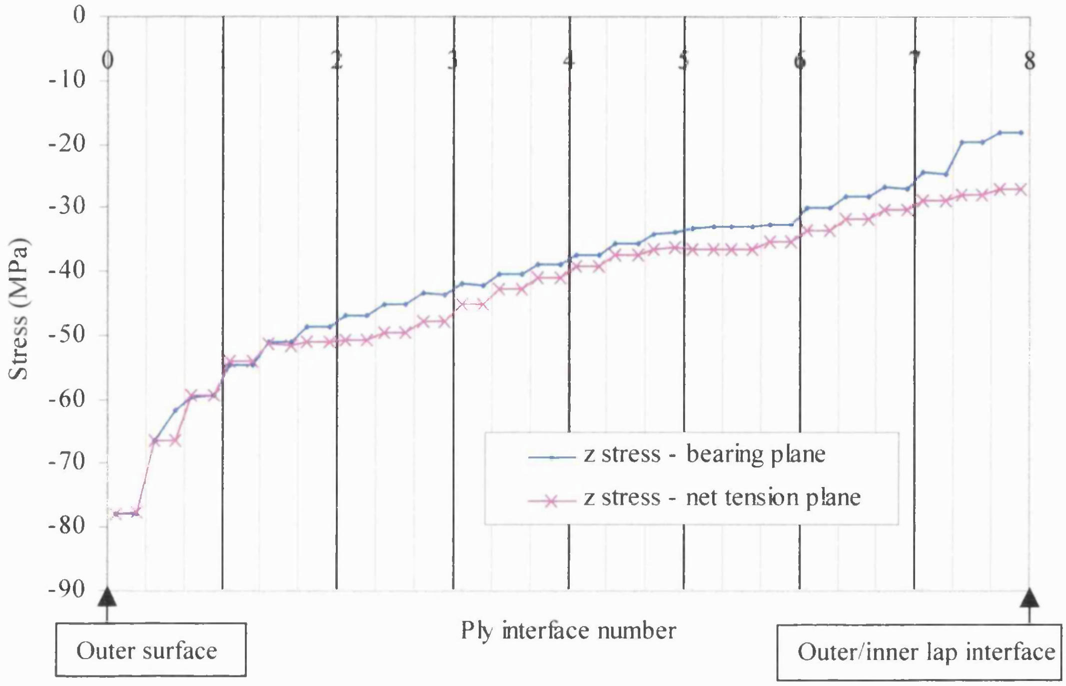

Figure 5.21 – z- direction stress distribution through the thickness of the outer lap aluminium bolt and washer assembly – 6Nm torque

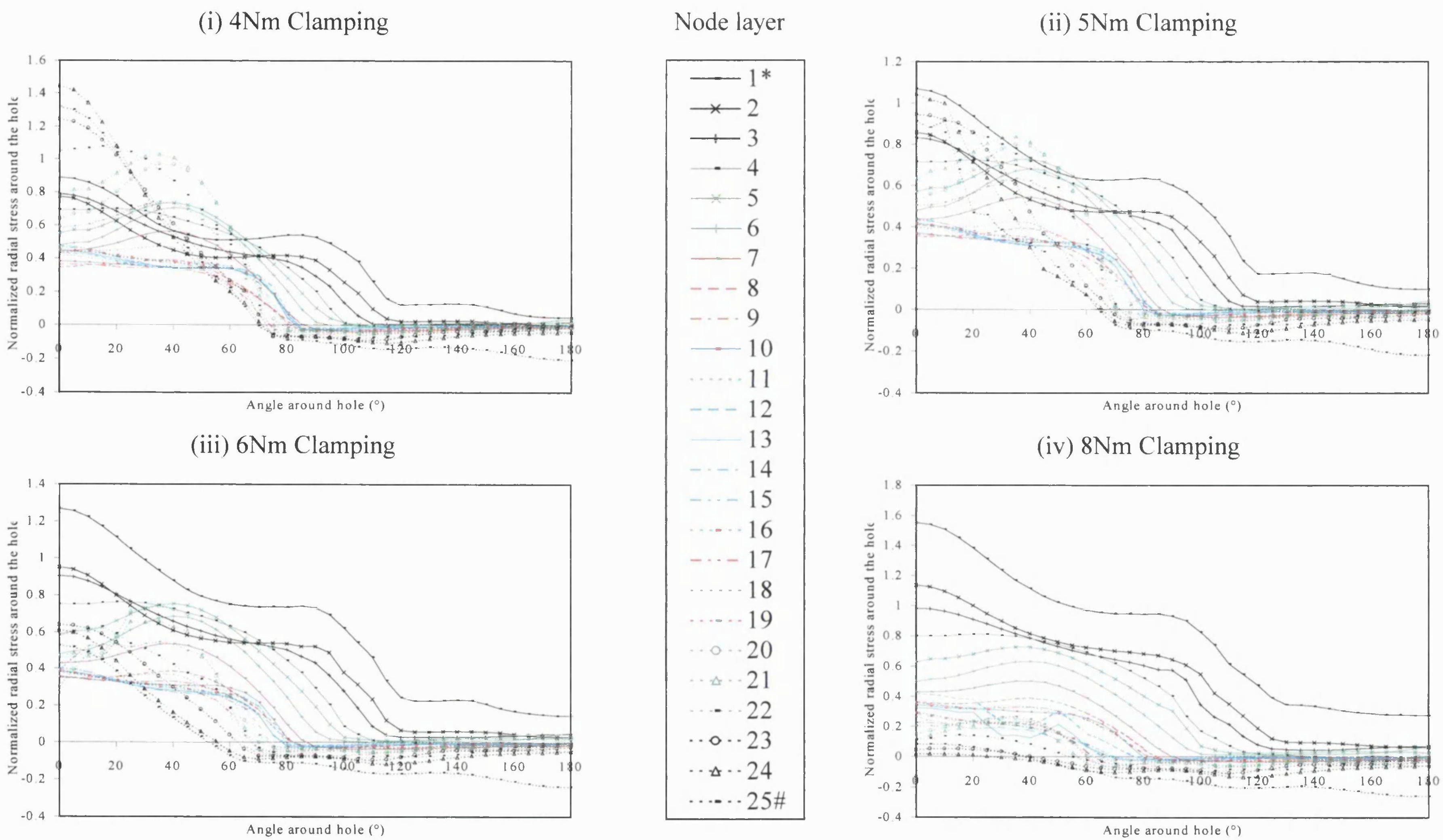

Figure 5.22 – Normalized radial stress around the hole boundary of the outer lap – steel bolt and washer assembly 4Nm, 5Nm, 6Nm and 8Nm clamping - * = Outer surface, # = Laminate interface

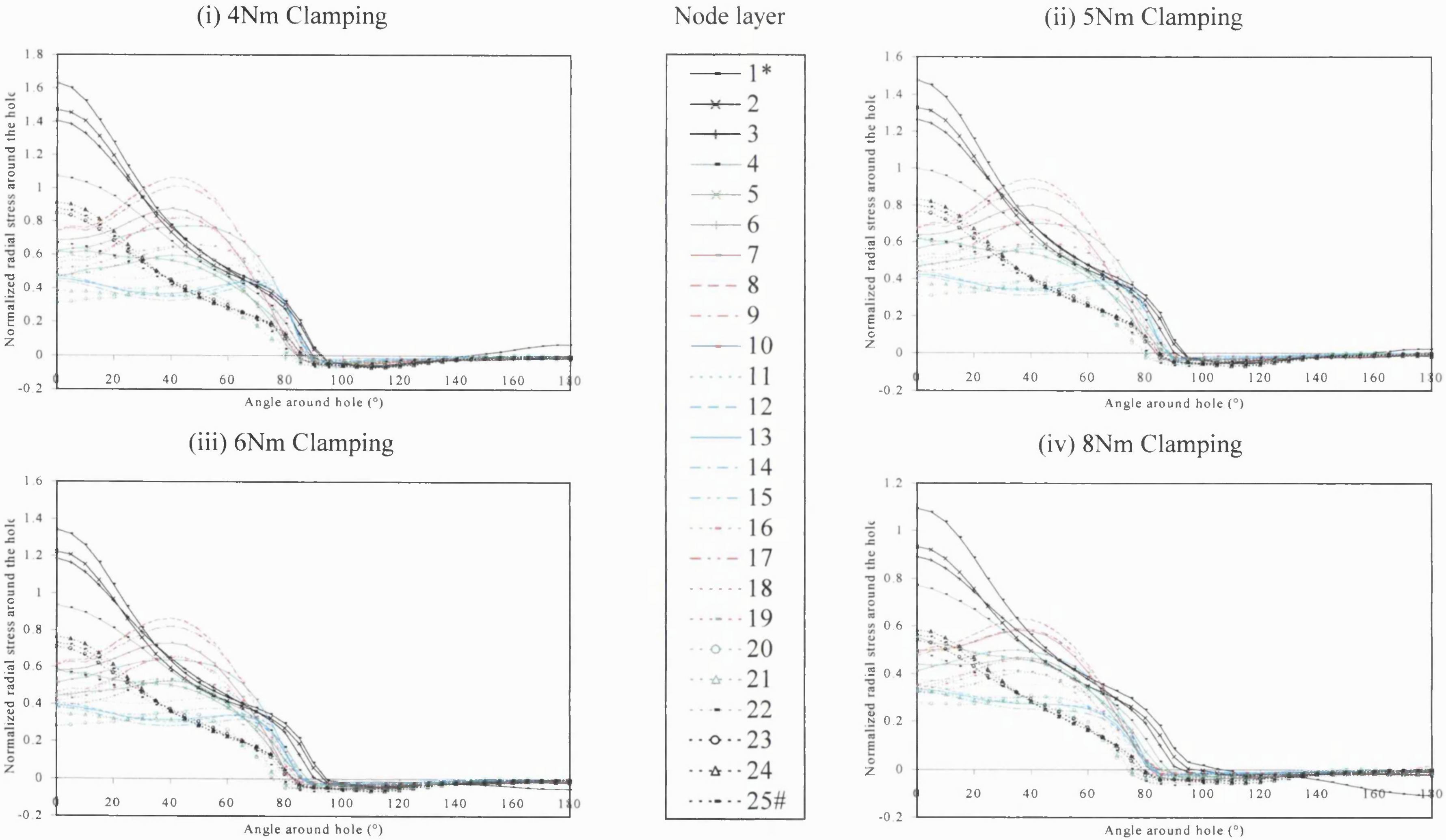

Figure 5.23 – Normalized radial stress around the hole boundary of the inner lap – steel bolt and washer assembly
4Nm, 5Nm, 6Nm and 8Nm clamping - * = Laminate interface, # = Laminate mid-plane

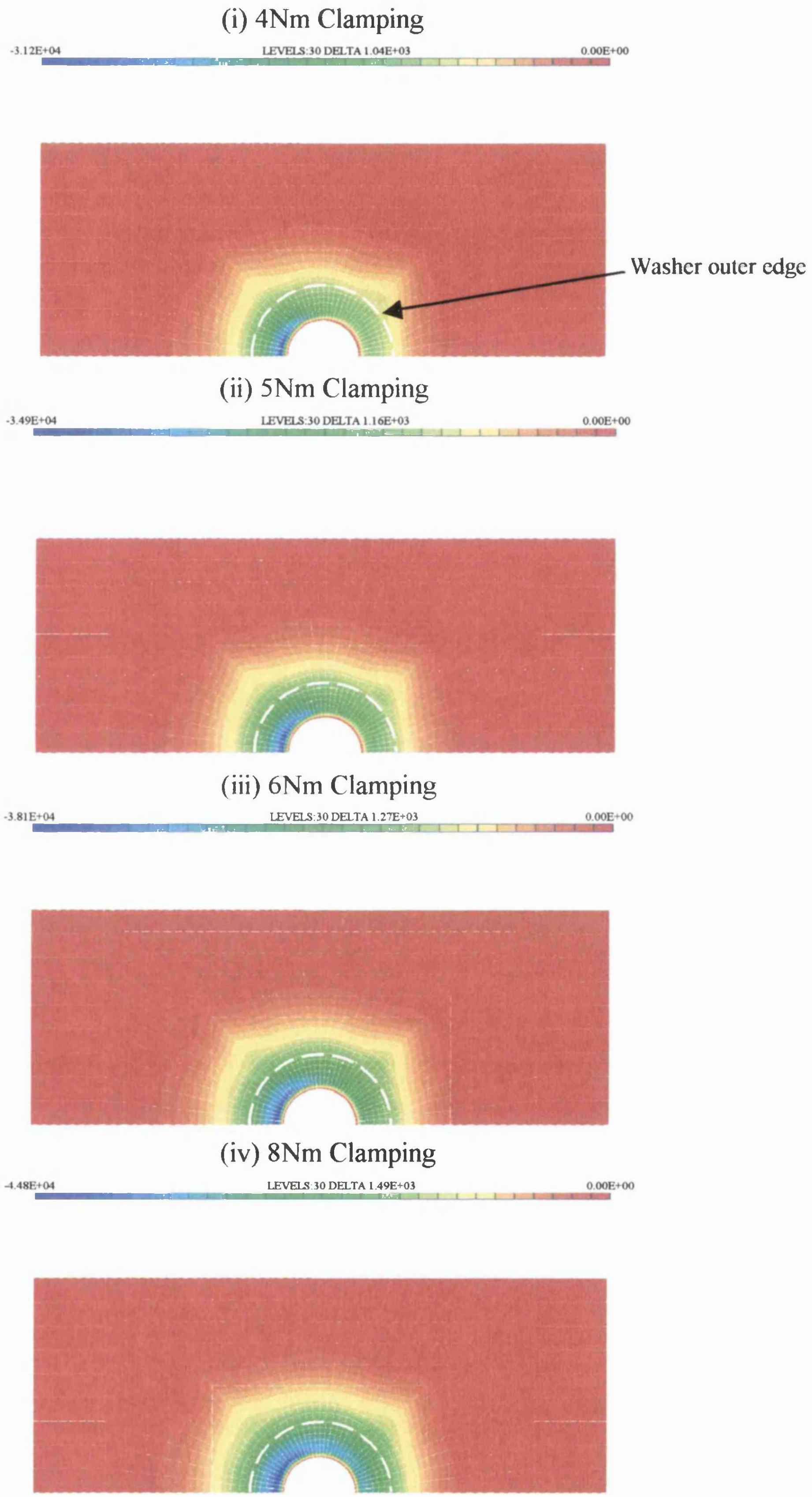

Figure 5.24 – Through thickness contact stress on the inner lap at the laminate interface steel bolt and washer assembly – 4Nm, 5Nm, 6Nm and 8Nm clamping

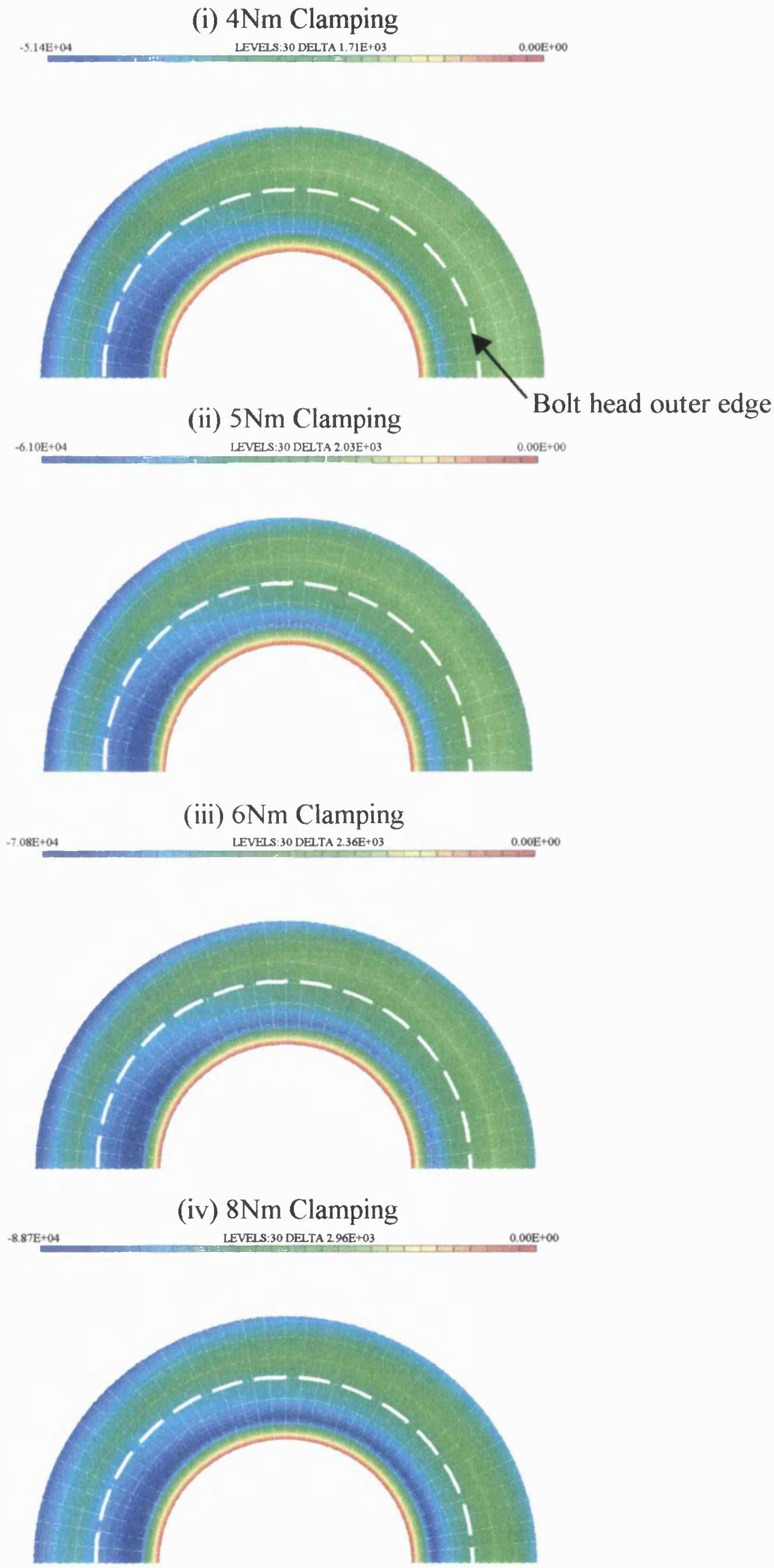

Figure 5.25 – Through thickness contact stress under the washer on the outer lap steel bolt and washer assembly – 4Nm, 5Nm, 6Nm and 8Nm clamping

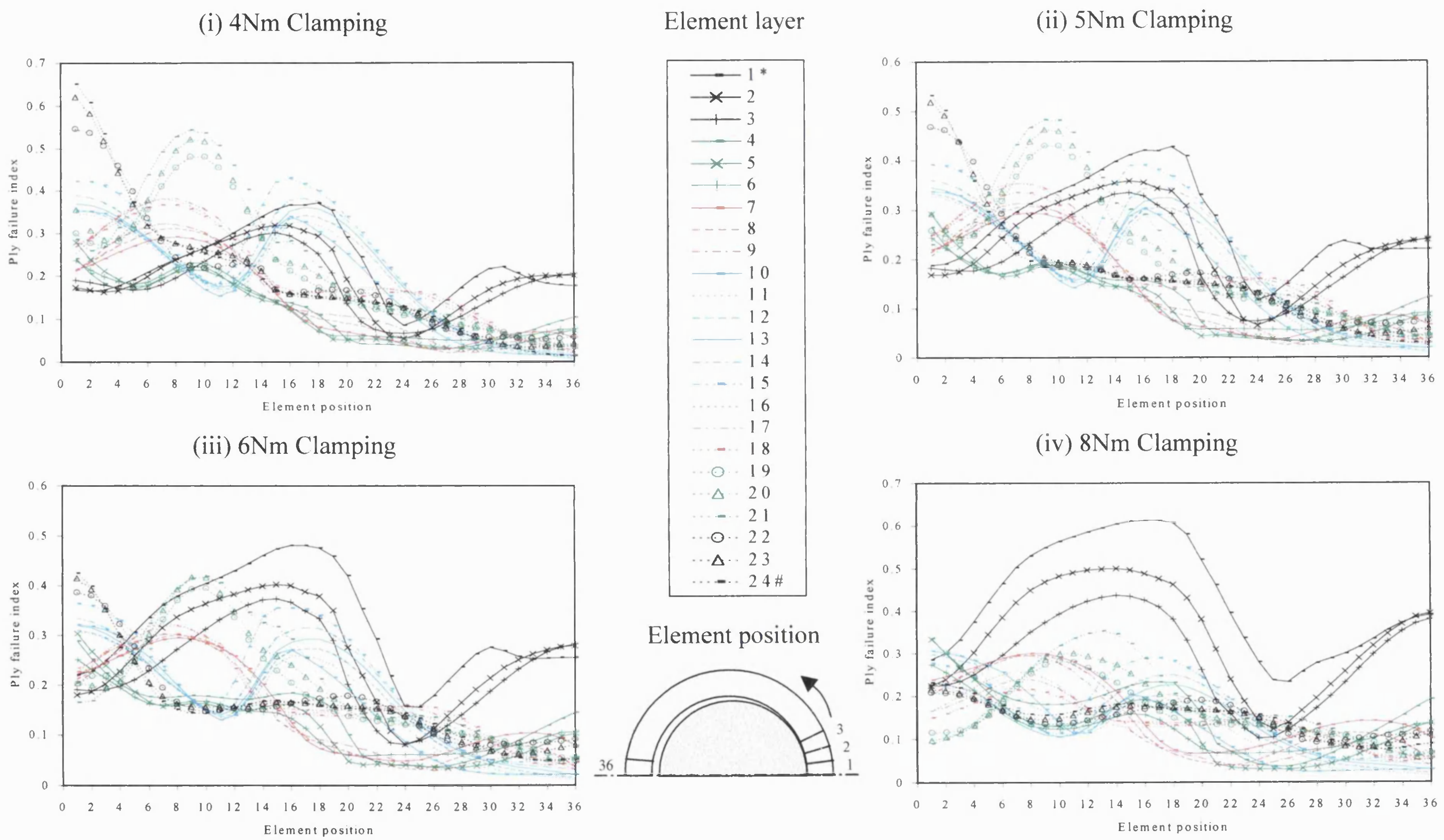

Figure 5.26 – Ply failure index plots for the outer lap – steel bolt and washer assembly
4Nm, 5Nm, 6Nm and 8Nm clamping - * = Outer surface, # = Laminate interface

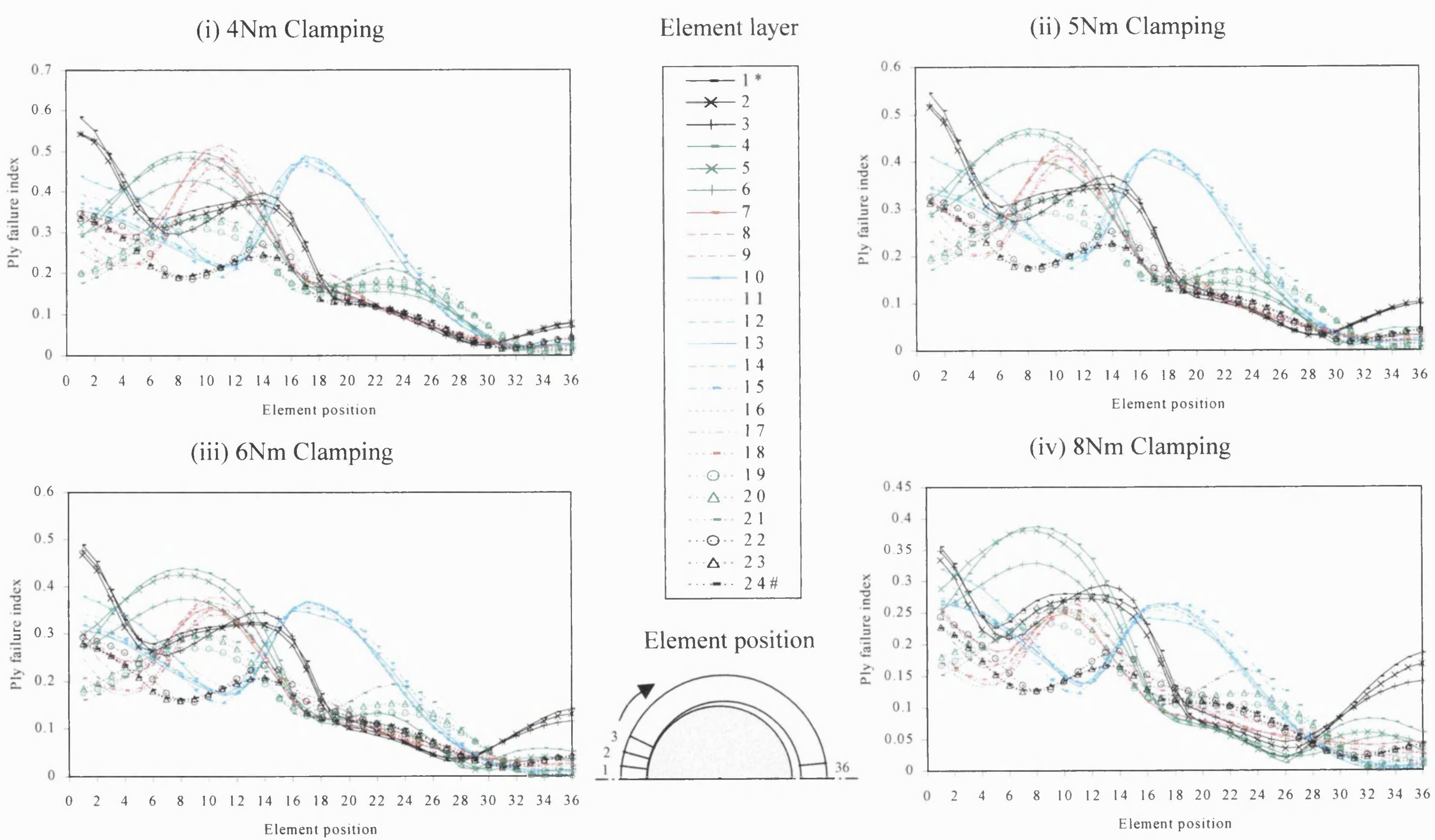

Figure 5.27 – Ply failure index plots for the inner lap – steel bolt and washer assembly 4Nm, 5Nm, 6Nm and 8Nm clamping - * = Laminate interface, # = Laminate mid-plane

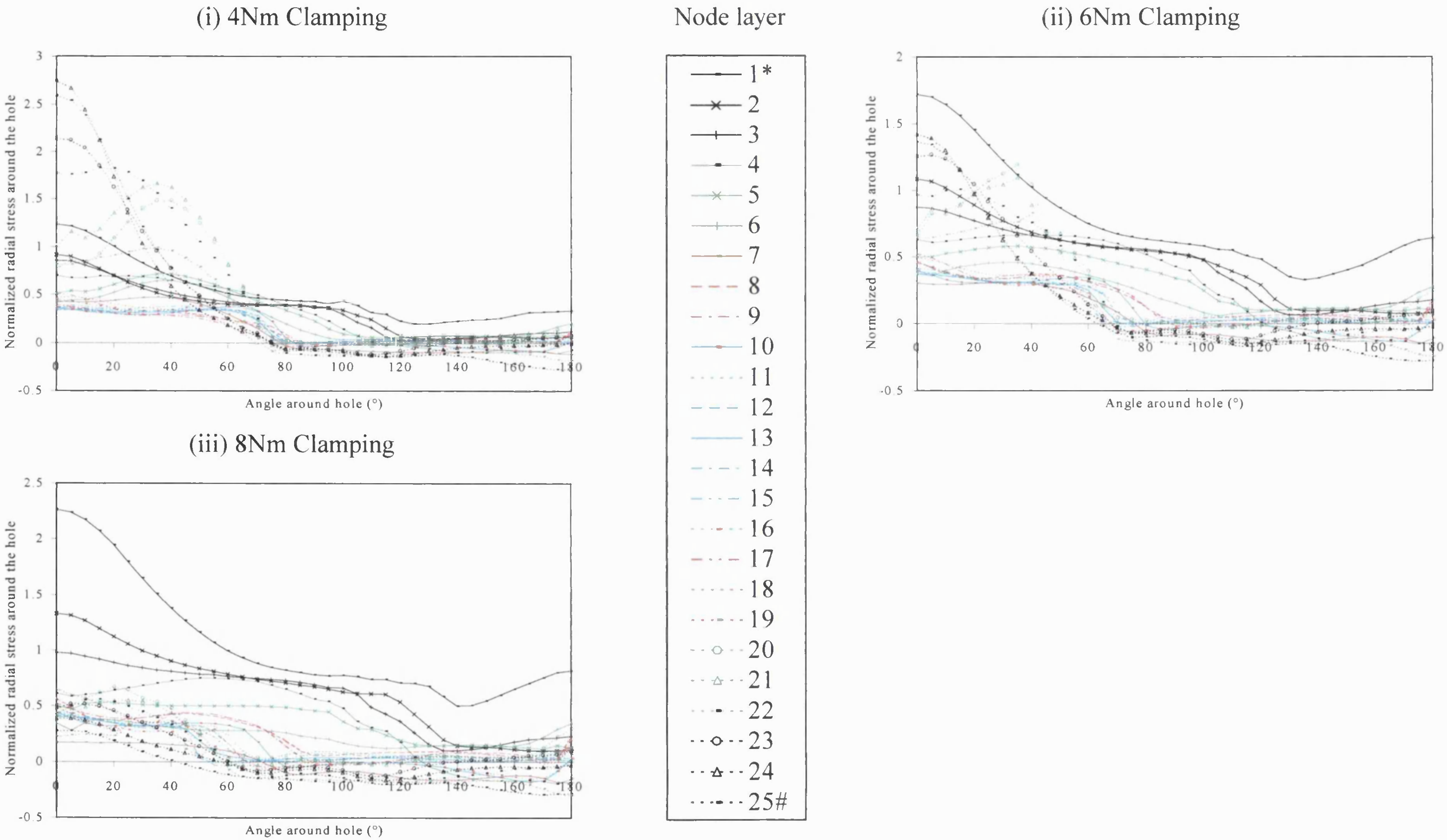

Figure 5.28 – Normalized radial stress around the hole boundary of the outer lap – CFRP laminates with steel bolt assembly 4Nm, 6Nm and 8Nm clamping - * = Outer surface, # = Laminate interface

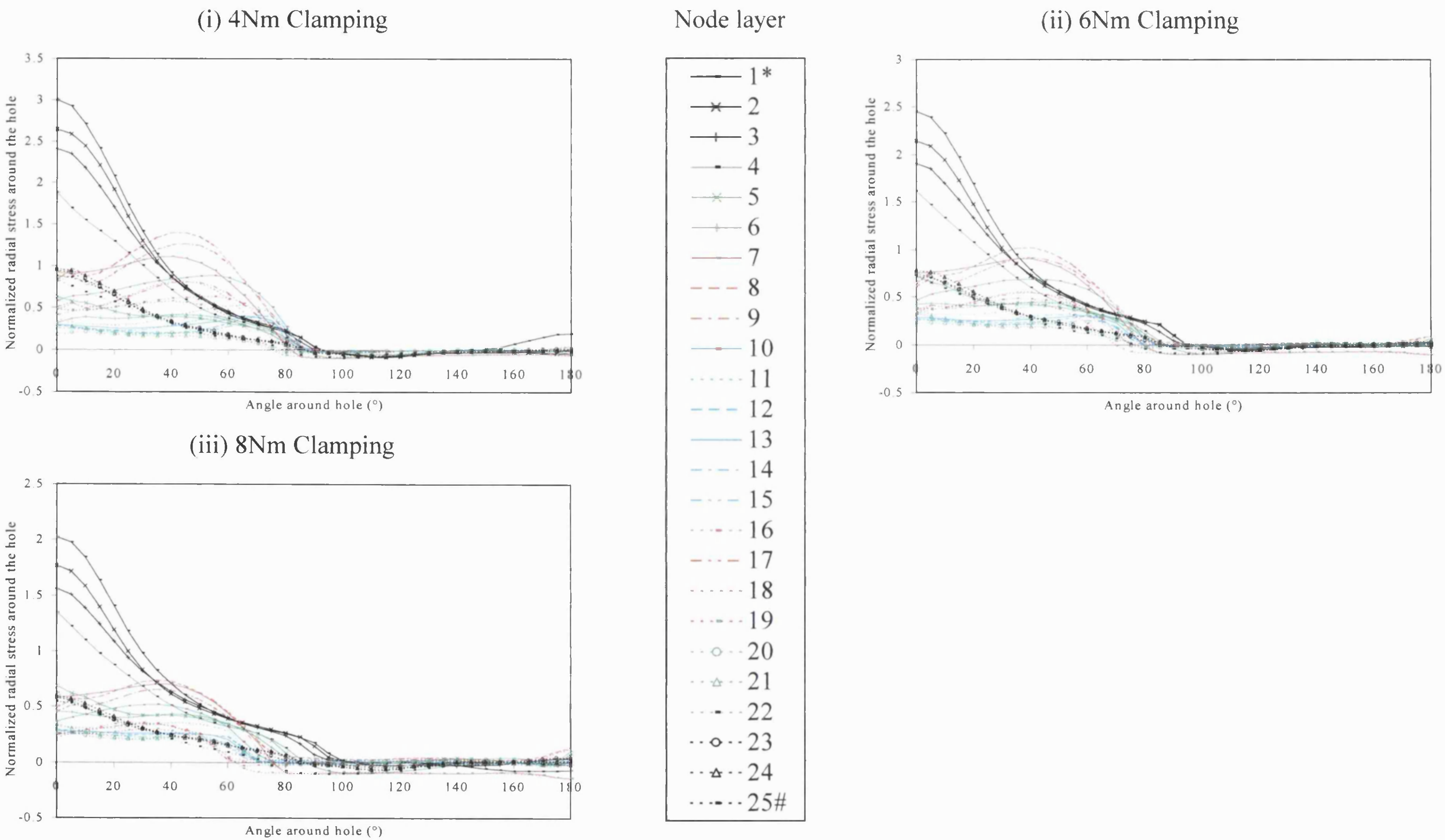

Figure 5.29 – Normalized radial stress around the hole boundary of the inner lap – CFRP laminates with steel bolt assembly 4Nm, 6Nm and 8Nm clamping - * = Laminate interface, # = Laminate mid-plane

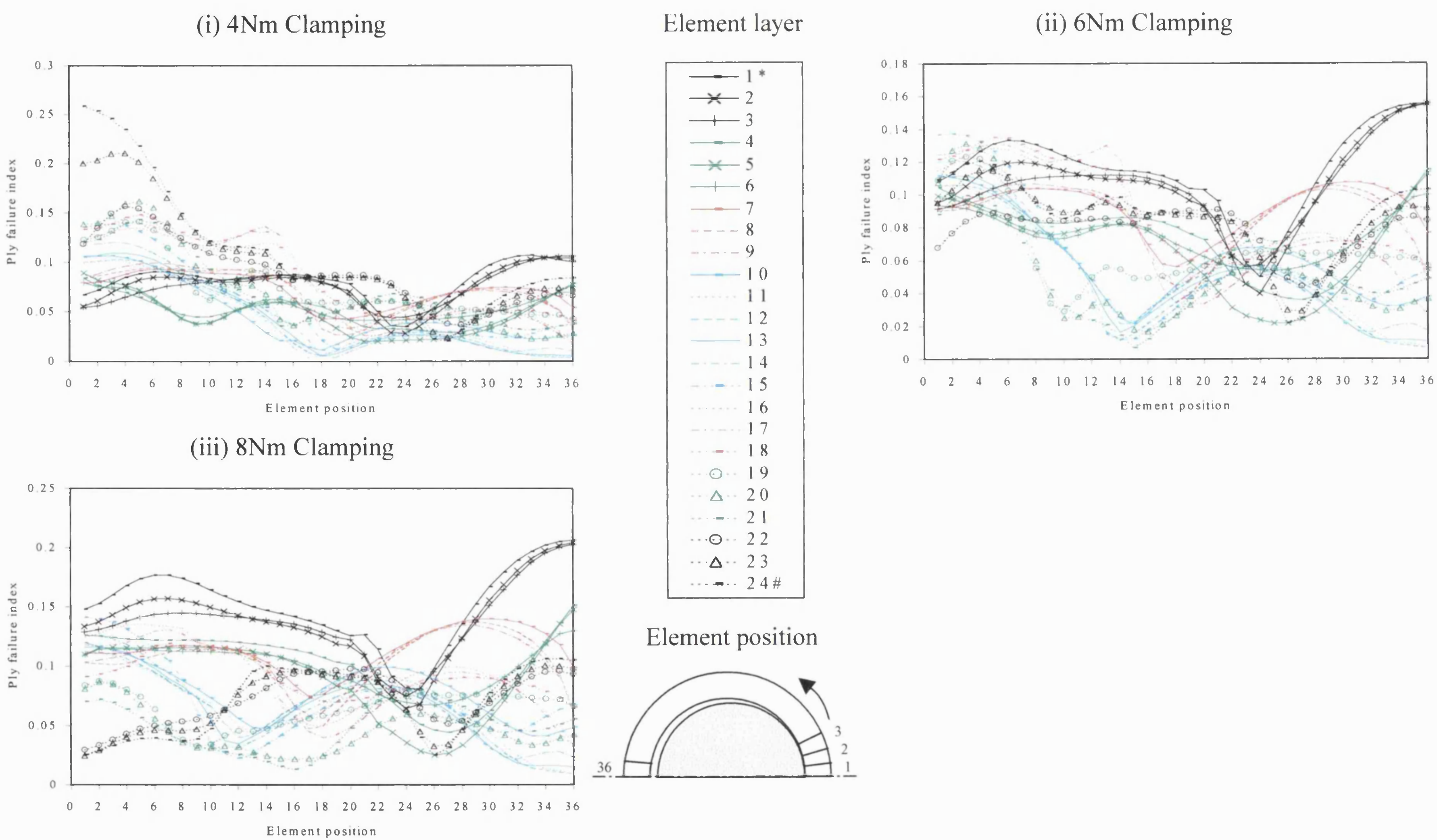

Figure 5.30 – Ply failure index plots for the outer lap – CFRP laminates with steel bolt assembly 4Nm, 6Nm and 8Nm clamping - * = Outer surface, # = Laminate interface

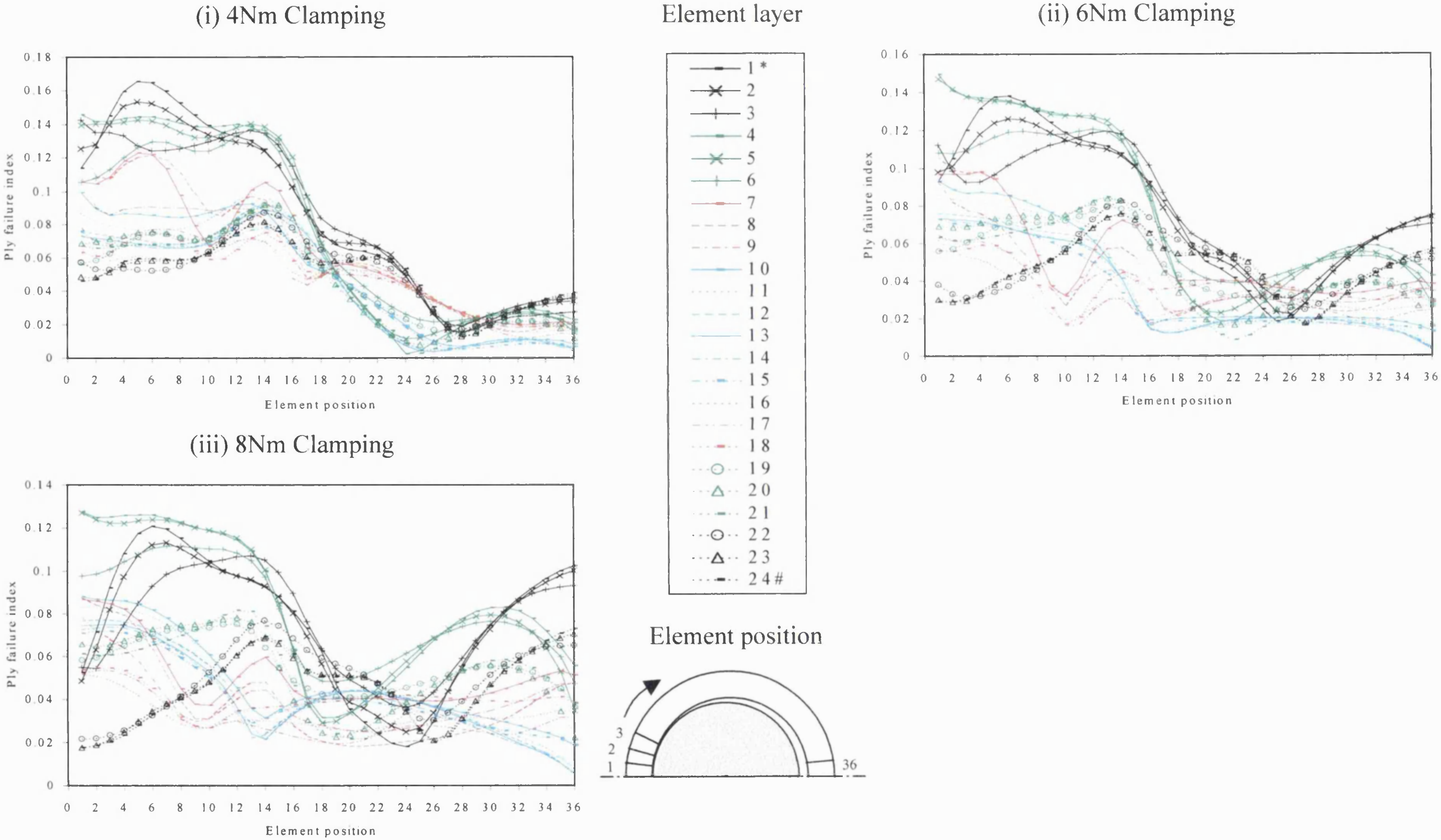

Figure 5.31 – Ply failure index plots for the inner lap – CFRP laminate with steel bolt assembly
4Nm, 6Nm and 8Nm clamping - * = Laminate interface, # = Laminate mid-plane

(i) 4Nm Clamping

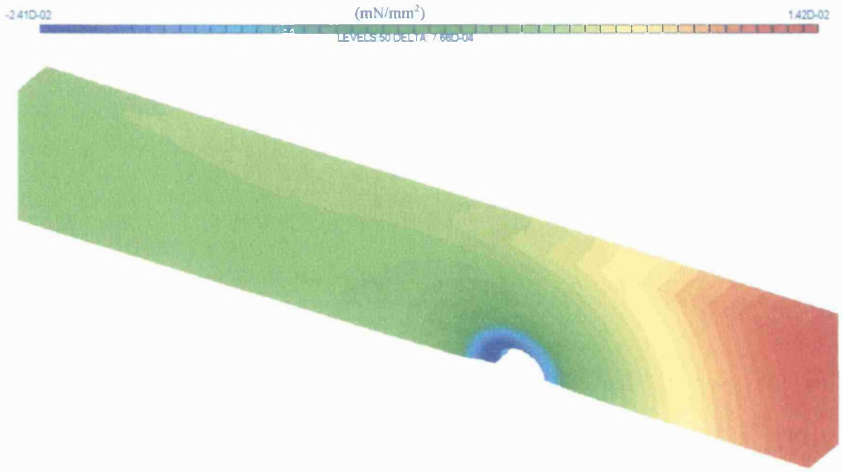

(ii) 6Nm Clamping

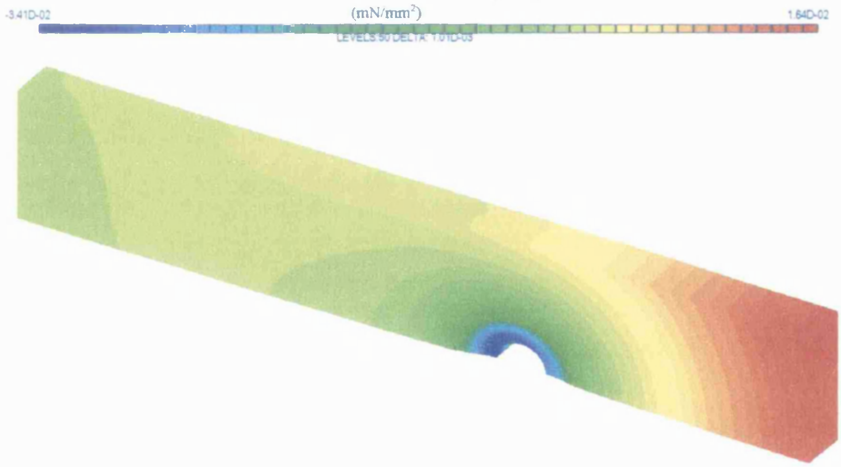

(iii) 8Nm Clamping

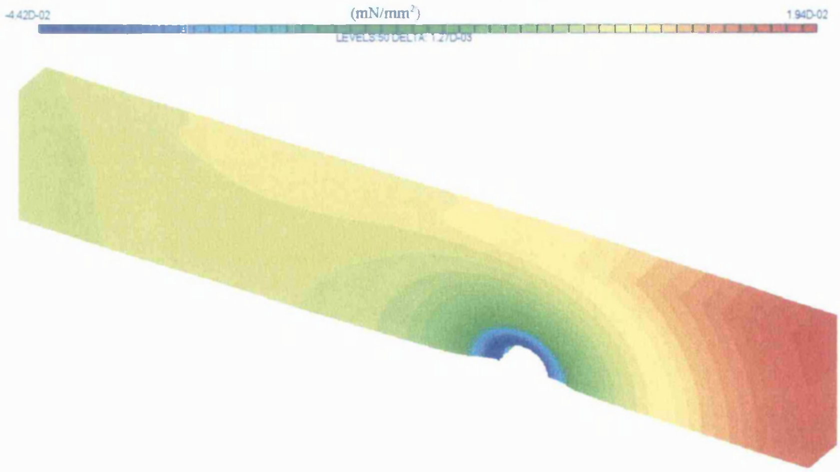

Figure 5.32 – Through thickness displacement of the outer lap – CFRP laminates with steel bolt assembly – 4Nm, 6Nm and 8Nm clamping

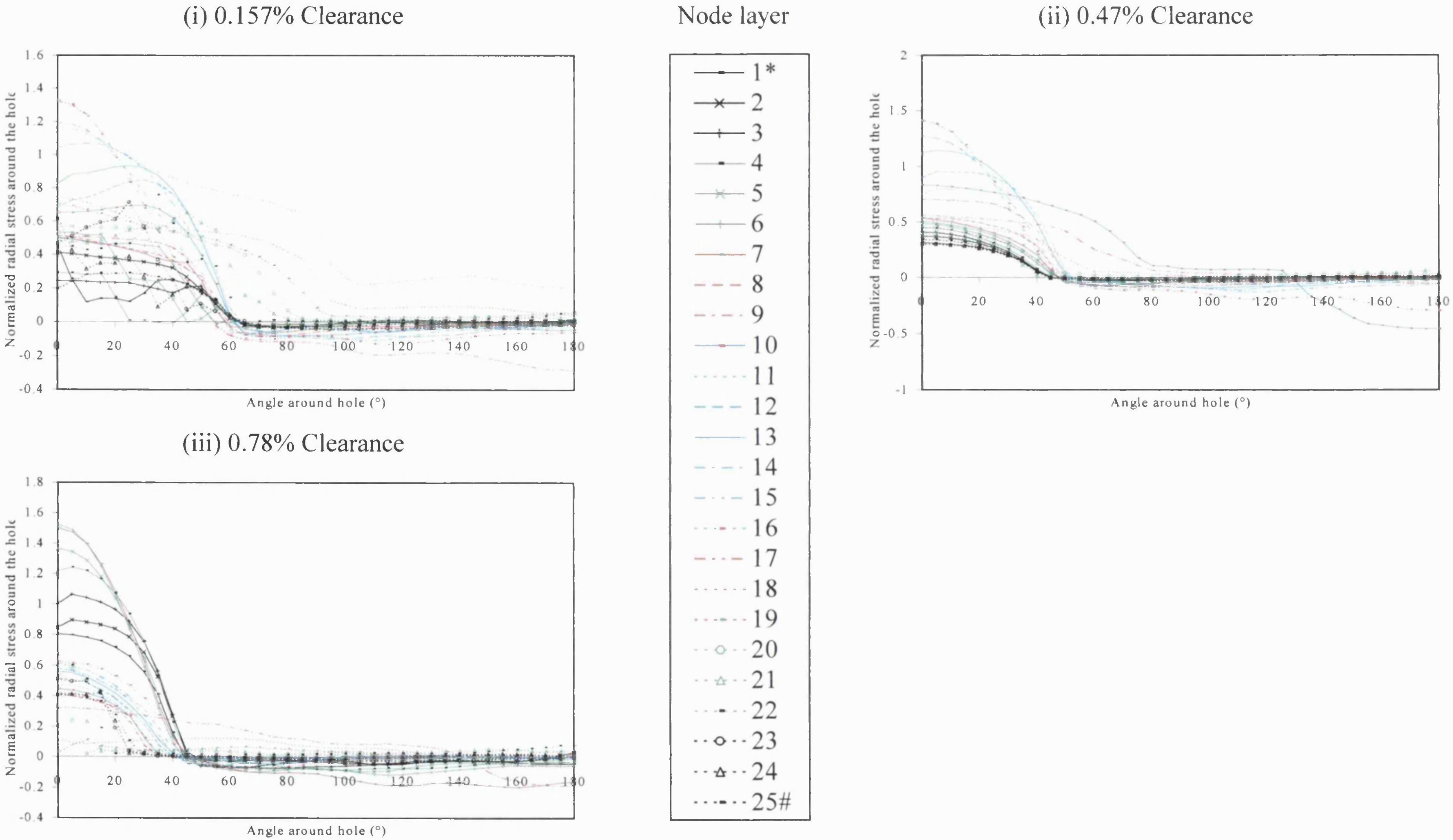

Figure 5.33 – Normalized radial stress around the hole boundary of the outer lap – aluminium bolt and washer assembly 6Nm clamping – 0.157%, 0.47% and 0.78% clearance - * = Outer surface, # = Laminate interface

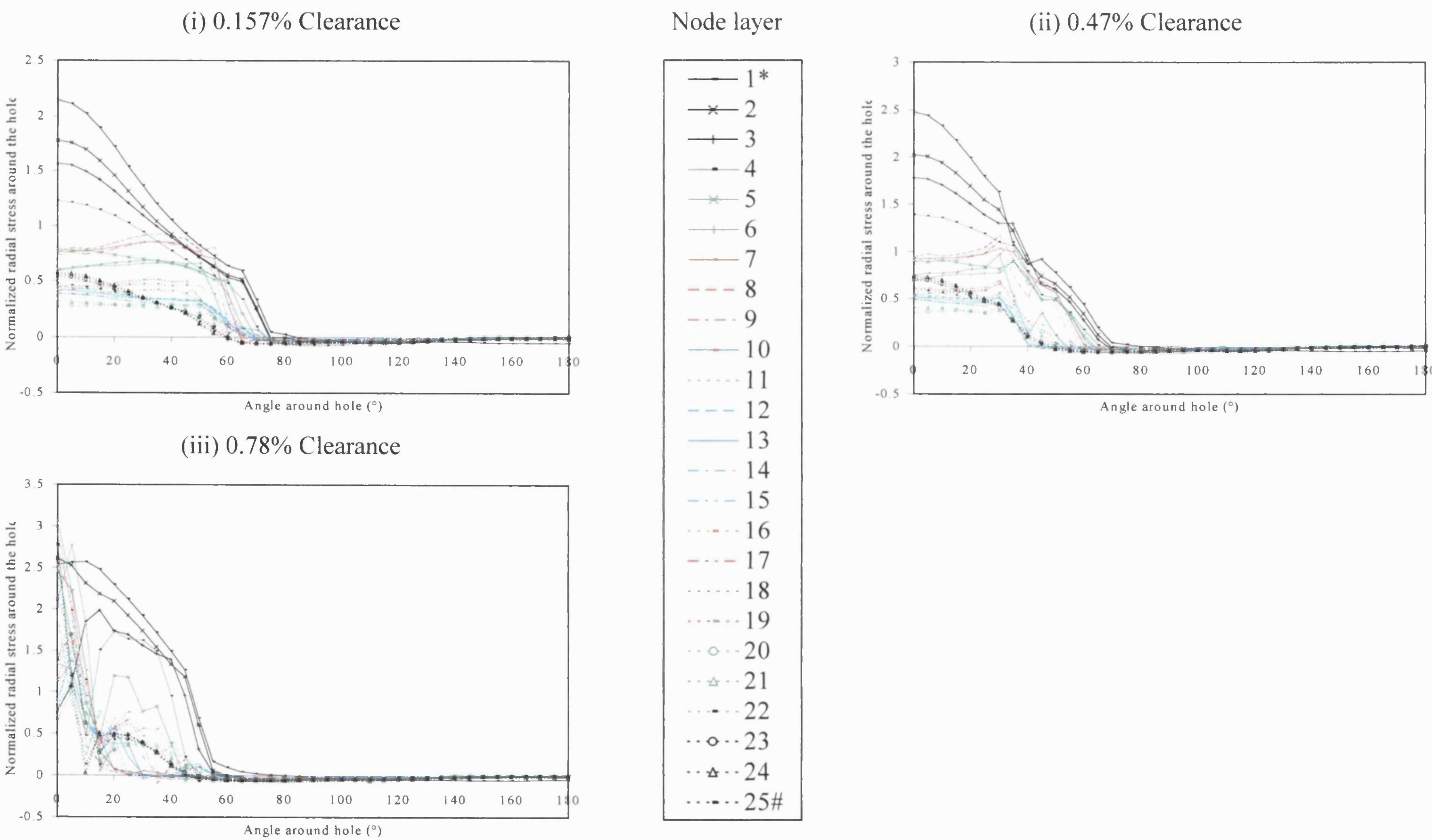

Figure 5.34 – Normalized radial stress around the hole boundary of the inner lap – aluminium bolt and washer assembly 6Nm clamping – 0.157%, 0.47% and 0.78% clearance - * = Laminate interface, # = Laminate mid-plane

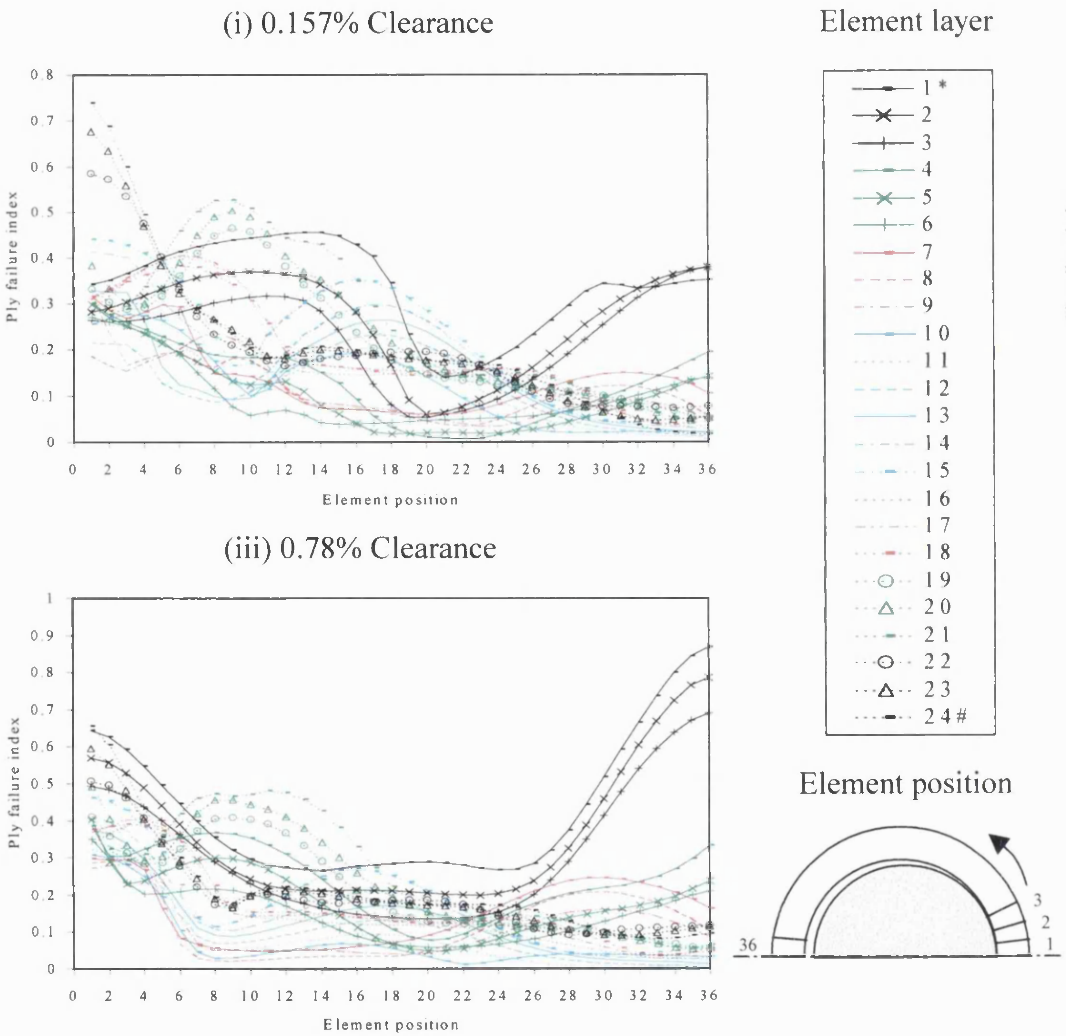

Figure 5.35 – Ply failure index plots for the outer lap – aluminium bolt and washer assembly 6Nm clamping - 0.157%, 0.47% and 0.78% clearance - * = Outer surface, # = Laminate interface

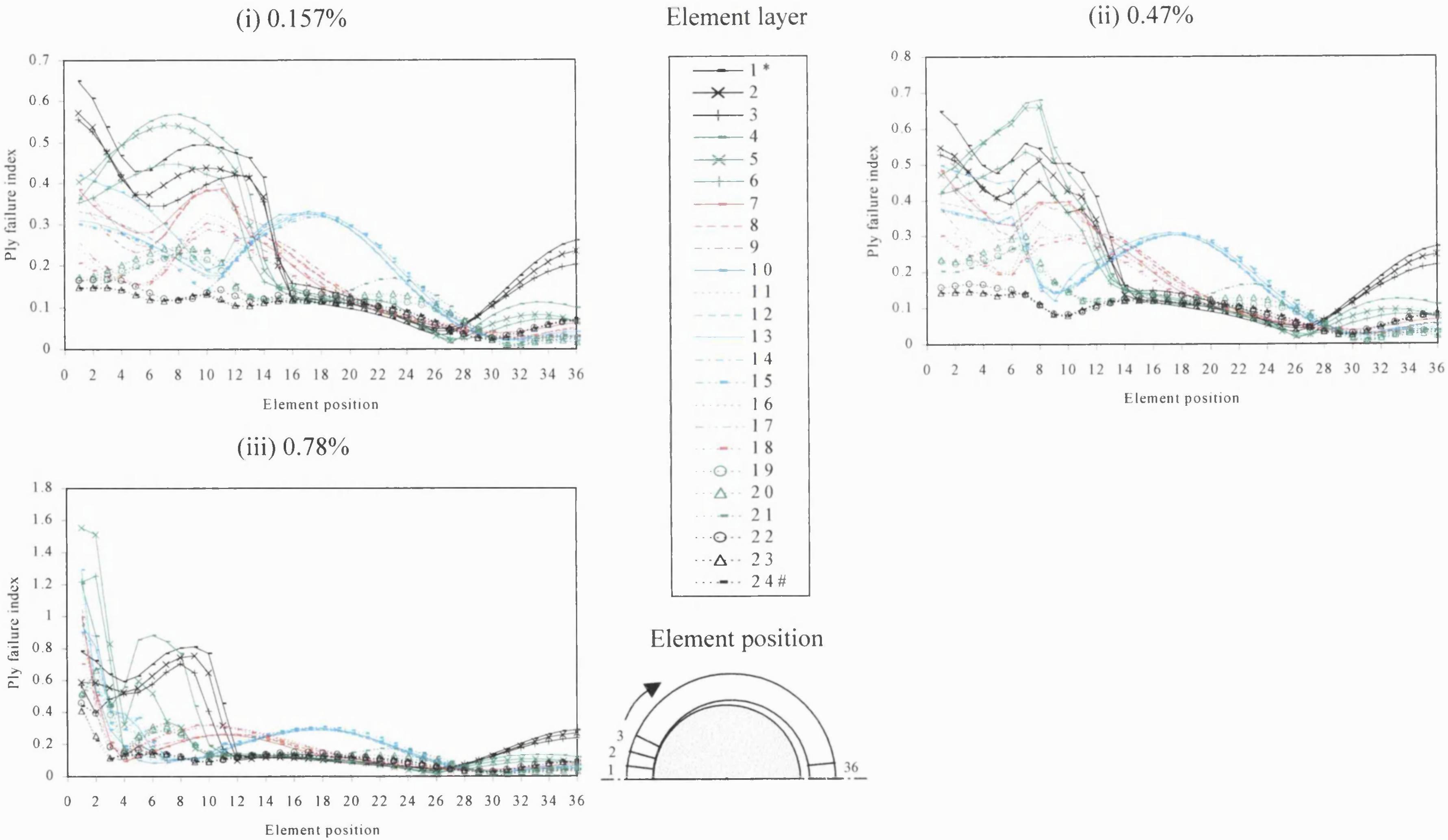

Figure 5.36 – Ply failure index plots for the inner lap – aluminium bolt and washer assembly
6Nm clamping - 0.157%, 0.47% and 0.78% clearance - * = Laminate interface, # = Laminate mid-plane

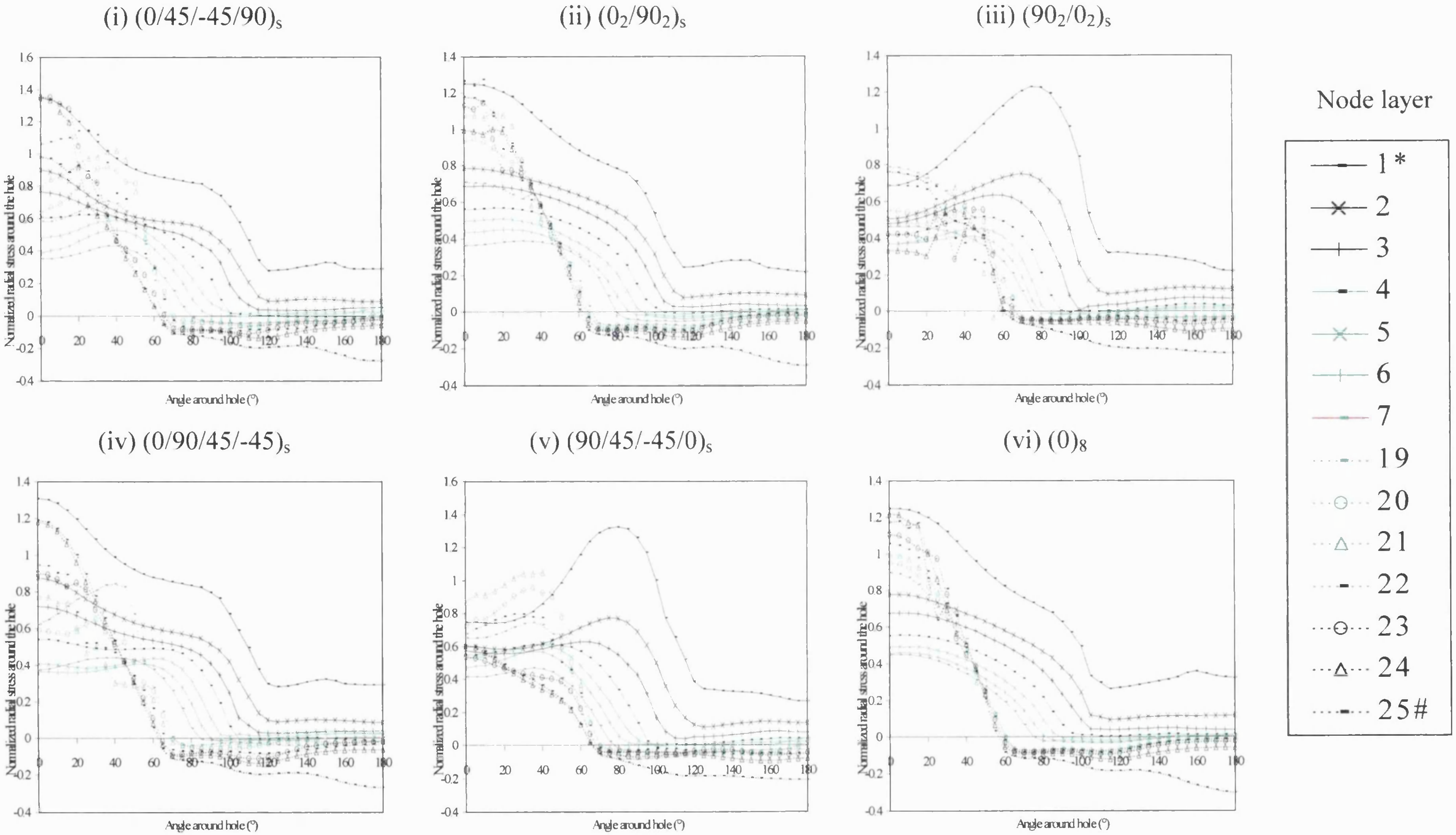

Figure 5.37 – Normalized radial stress around the hole boundary of the outer lap – aluminium bolt and washer assembly 6Nm clamping - stacking sequence A to F - * = Outer surface, # = Laminate interface

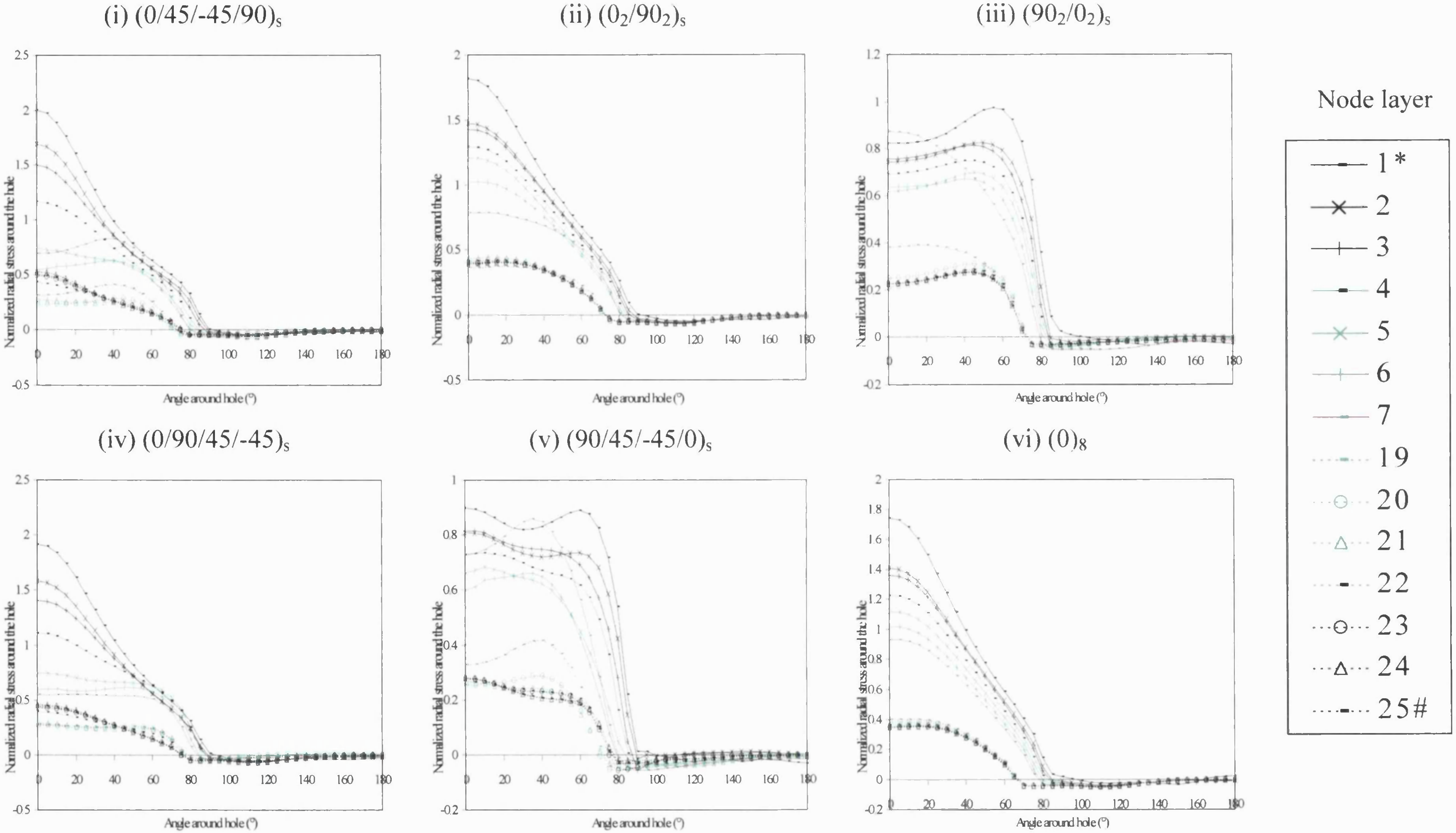

Figure 5.38 – Normalized radial stress around the hole boundary of the inner lap – aluminium bolt and washer assembly 6Nm clamping - stacking sequence A to F - * = Laminate interface, # = Laminate mid-plane

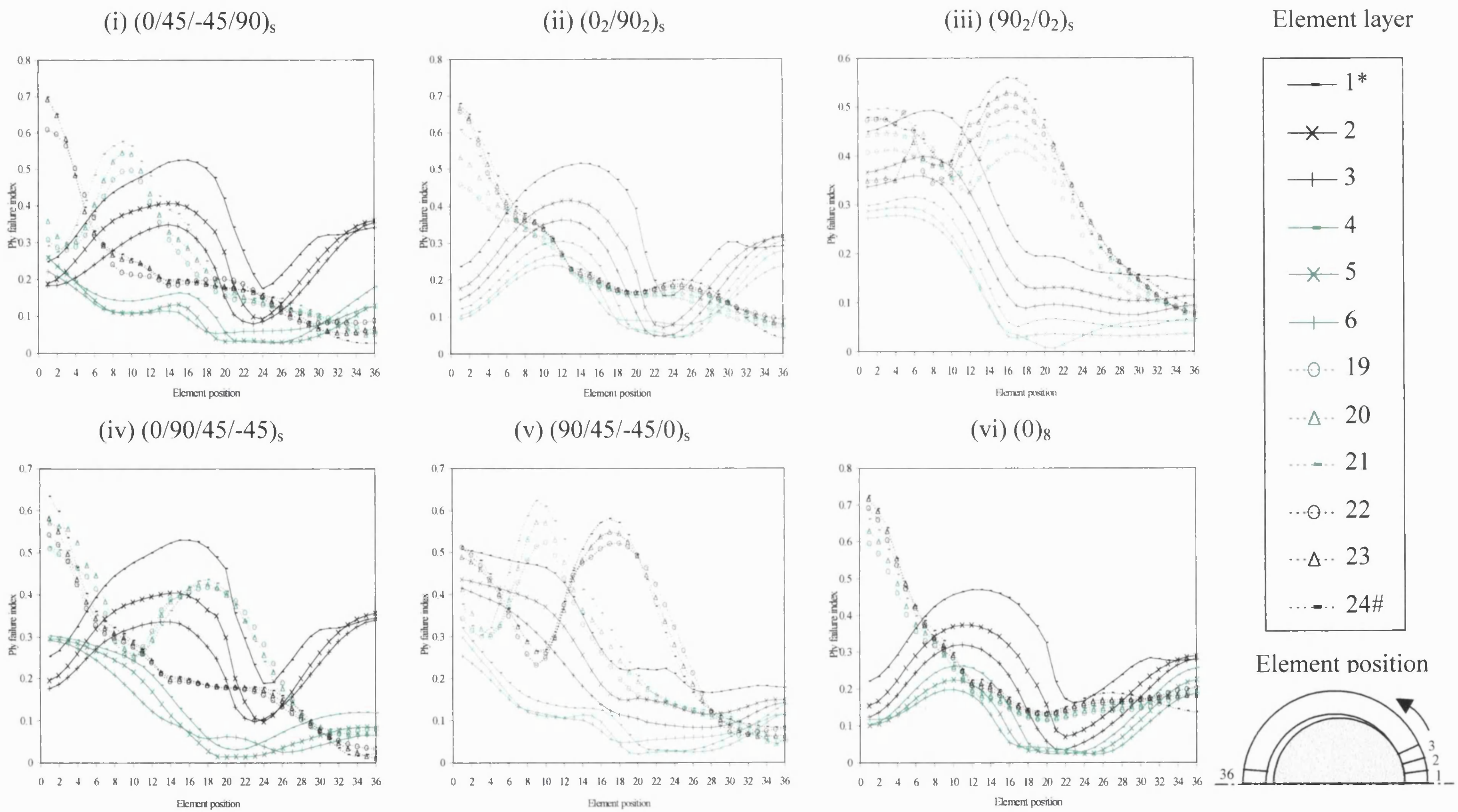

Figure 5.39 – Ply failure index plots for the outer lap – aluminium bolt and washer assembly 6Nm clamping - stacking sequence A to F - * = Outer surface, # = Laminate interface

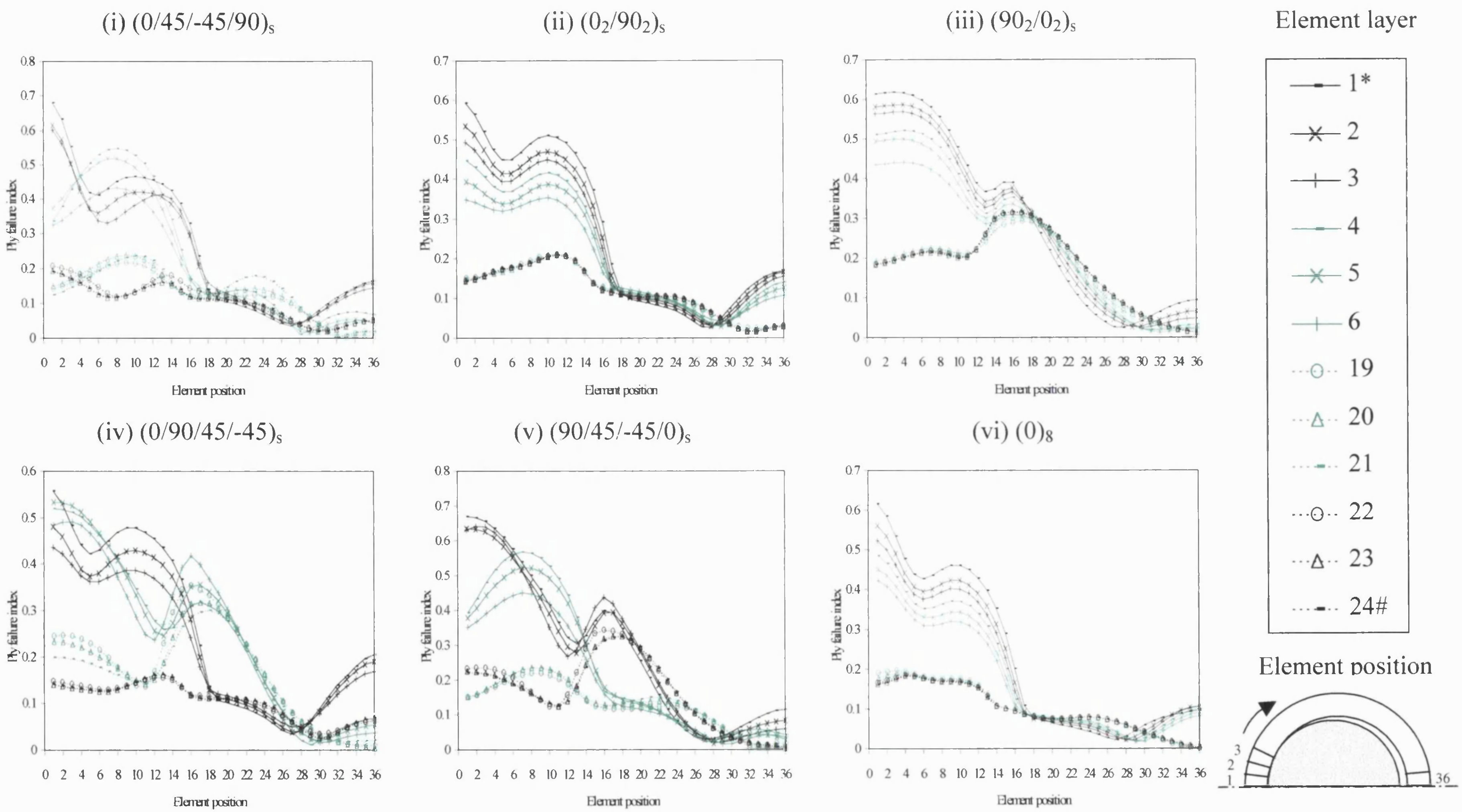

Figure 5.40 – Ply failure index plots for the inner lap – aluminium bolt and washer assembly 6Nm clamping - stacking sequence A to F - * = Laminate interface, # = Laminate mid-plane

CHAPTER SIX

THE EFFECTS OF CHANGING WASHER PARAMETERS

6.1 – INTRODUCTION

Using the same model as described in Chapter 5, the effects of washer size and stiffness on the stress distribution in the laminate and the location of failure were investigated and the results obtained from this study are presented in this chapter. The washer outside diameter was varied between $2.0d_{bo}$ and $4.5d_{bo}$, and the stiffness was varied by changing the washer material and thickness.

Ply failure indices were calculated using the equation given by Tsai and Wu (1971) to provide details as to the location of ply failure. Also, the onset of delamination was determined using the criterion proposed by Ye (1988).

6.2 – METHOD

Each lap was constructed from GRP having the quasi-isotropic stacking sequence $(0/45/-45/90)_s$. The inner lap was made to be twice as thick as the outer lap and the end furthest from the bolt was restrained from movement in all directions. A 2kN tensile load was applied to the end of each outer lap and the laps were joined using an aluminium bolt, with either an aluminium or a steel washer. The washer outside diameter and thickness were varied throughout the investigation. The physical representation of the joint is shown in Figure 6.1. The material properties used are given in Table 5.1 with the corresponding material strengths given in Table 5.2.

In the simulation a quarter of the joint was modelled by applying the appropriate nodal restraints along the symmetry planes as detailed in Chapter 5. At the end of the inner lap furthest from the bolt the nodes were restrained in all directions to simulate clamped conditions, while at the end of the outer lap furthest from the bolt, the nodes were loaded in the negative x- direction to simulate the 4kN tensile load on the joint.

Three elements in the through thickness direction were used to represent each ply, giving the mesh a total of 30240 eight-node solid linear brick elements for the laminates. The clamping torque was obtained by applying a temperature drop along the axis of a short beam element, which connected the 1764 six-node solid linear wedge elements of the bolt shank to the 108 six-node wedge and 324 eight-node brick elements of the bolt head. The washer consisted of 216 eight-node solid linear brick elements for the initial analysis, which was then increased as the outside diameter and thickness of the washer increased throughout the investigation. A typical finite element mesh used in this study can be seen in Figure 6.2.

Contact was modelled using the global search facility available in the I-DEAS software, which placed a contact element between each element face likely to come into contact. A friction coefficient of μ=0.2 was used at all contacting surfaces and the bolt was designed to be a tight fit within the hole.

The temperature drop applied to the beam element of the bolt assembly was determined by using Equation 5.1. From the results in Chapter 5 it was determined that for a washer having an outside diameter of $2.0d_{bo}$, a clamping torque of 6Nm (50MPa equivalent clamping pressure) should be used. In this particular investigation the washer size was varied as a constant clamping pressure of 50MPa was maintained. The analysis was then pursued by varying the washer size while maintaining a constant bolt torque of 6Nm.

Initially the clamping pressure was maintained at 50MPa while the washer size and stiffness was varied. The washer types investigated were: (i) an aluminium washer, 1mm in thickness, (ii) a steel washer, 2mm in thickness and (iii) a steel washer, 4mm in thickness. For the first two washer types the outside diameter was varied between $2.0d_{bo}$ and $3.5d_{bo}$, whereas, for the latter washer type the outside diameter was varied between $2.0d_{bo}$ and $4.5d_{bo}$.

In the subsequent analysis the bolt torque was maintained at 6Nm, while the outside diameter of the 4mm thick steel washer was varied between $2.0d_{bo}$ and $4.5d_{bo}$. Finally, a 3mm thick ceramic washer with outside diameter of $3.5d_{bo}$ was modelled with a clamping load equivalent to 50MPa pressure, as an alternative to the heavier 4mm thick steel washer.

6.3 – RESULTS AND DISCUSSION

For each investigation the radial stress results on nodes around the hole boundary as well as the average element stresses around the hole boundary and washer edge were extracted. The relevant normalized radial stress results as well as the ply failure and delamination failure indices at these locations are presented in this section. Stress contour plots have also been provided where necessary.

The method by which the nodal stress results were extracted and normalized has been described previously in Chapter 5. The ply failure and the delamination failure indices were calculated using the equations given by Tsai and Wu (1971) and Ye (1988) respectively. Average element stresses were used in both equations as also detailed in Chapter 5.

6.3.1 - Aluminium bolt with 1mm washer assembly

Figures 6.3 and 6.4 shows the variation in the normalized radial stress around the hole boundary for the outer and inner laps, respectively, of the models constructed having washer outside diameters between $2.0d_{bo}$ and $3.5d_{bo}$. Figure 6.3 shows that the magnitude of maximum normalized radial stress in the outer lap increases from approximately 1.35 to approximately 4.7 as the washer size is increased. This increase in radial stress may be attributed to the friction between the washer and the outer lap, as well as higher through thickness stress close to the hole boundary due to the clamping. This deforms the outer surface of the outer lap resulting in higher contact force between the bolt shank and the hole. As the washer size is increased, the corresponding increase in bolt load to maintain the washer pressure at 50MPa should be spread over a larger portion of the outer lap surface, which would result in a reduction in the load carried through bearing around the hole boundary and in the magnitude of the radial stress.

However, this does not seem to be the case for this joint configuration due to the compliance of the 1mm thick aluminium washer.

Figure 6.4 shows that the radial stresses are higher in the inner lap than the outer lap for a washer size of $2.0d_{bo}$, however, these decrease rapidly as the washer outside diameter is increased and are lower than in the outer lap for values of $d_w = 2.5d_{bo}$ and greater.

The ply failure plots of the outer lap are shown in Figure 6.5. This figure demonstrates a similar variation to that observed for the radial stress, whereby the surface of the outer lap carries a higher proportion of the load as the washer size increases. The indices of the outer lap increase from approximately 0.7 at the bearing plane, close to the interface with the inner lap, for a washer diameter of $2.0d_{bo}$ to approximately 1.7 on the outer surface of the laminate for a washer diameter of $3.5d_{bo}$. Hence failure is likely to occur for washer diameters of $3.0d_{bo}$ and above. This increase in failure index is similar to the behaviour observed from the clamping investigation reported in Chapter 5.

Figure 6.6 shows the effects of varying the aluminium washer diameter on the ply failure indices around the hole boundary of the inner lap. From this figure, it can be seen that the indices are lower than those provided by the outer lap, and reduce from a magnitude of approximately 0.68 for the smallest diameter washer, to approximately 0.28 for $d_w = 3.0d_{bo}$. The index then rises very slightly to approximately 0.31 for the largest washer diameter tested. The position of maximum failure index is also shown to move from the elements at the interface with the outer lap to the elements in the adjacent ply as the washer size is increased above $2.0d_{bo}$.

The contour plots showing the through thickness contact stress under the washer on the surface of the outer lap are shown in Figure 6.7 and demonstrate that the 1mm thick aluminium washer does not distribute the clamping load evenly. The increased load applied to the bolt in order to maintain the washer pressure at 50MPa, does not spread over the entire washer area as the washer diameter is increased but concentrates on an area of the laminate similar in size to the bolt head. Hence, the through thickness load increases in the area close to the hole boundary and ply failure is likely to occur for the larger diameter washers.

Figure 6.8 shows the delamination index plots obtained for elements either side of each ply interface around the hole boundary of the outer lap. The indices calculated using the Ye (1988) delamination criterion are much lower then those produced by the ply failure criterion, indicating that ply failure would be the more likely mode of failure. However, the low values may arise from using the average element stresses in the delamination equations, as discussed in Chapter 5, and therefore the indices should be used only for comparative purposes rather than an indication of potential failure. From Figure 6.8 it is clear that the magnitude of delamination index increases as the washer outside diameter increases from $2.0d_{bo}$ to $3.5d_{bo}$, in a similar way to the ply failure index and normalized radial stress plots. The position of the maximum index is shown to change from the interface of the –45° and +45° plies and the 45° and 0° plies (close to the inner lap interface) on the bearing plane, to the interface between the 0° and +45° plies, which is a position nearer the outer surface of the outer lap.

The delamination index plots for the inner lap have not been included for this joint configuration as the magnitude of the indices continue to decrease with increased washer diameter, and as a result are less significant than the results obtained for the outer lap.

6.3.2 - Aluminium bolt with a 2mm thick steel washer

Figures 6.9 and 6.10 show the normalized radial stress plots for the outer and inner laps respectively. As can be seen in Figure 6.9 the variation in radial stress shows a similar trend to that observed with the aluminium washer, whereby the stresses increase as the washer size increases. However, the magnitude of maximum stress is not as high in this case, ranging from approximately 1.52 for a washer diameter of $2.0d_{bo}$, to approximately 2.35 for a $3.5d_{bo}$ diameter, indicating that the stress is being distributed more evenly than with the thinner washer. Figure 6.10 shows that the magnitude of normalized radial stress on the inner lap decreases as the washer outside diameter increases from $2.0d_{bo}$ to $3.0d_{bo}$, however, a further increase in diameter raises the radial stress. The stresses are higher on the inner lap than the outer lap for $d_w = 2.0d_{bo}$, as observed for the aluminium washer, however, for $d_w = 2.5d_{bo}$ and above, the outer lap exhibits the highest stresses due to localized washer loading close to the hole boundary.

The contour plots showing the through thickness contact stress on the outer lap under the washer are given in Figure 6.11, and demonstrate that as the washer outside diameter increases, the clamping force is distributed more evenly and over a larger area. Thus, the peak contact stress is reduced compared to the aluminium washer. It can clearly be seen, however, that the pressure exerted on the surface of the outer lap is by no means constant and uniformly distributed as many investigators have assumed, such as Lessard et al. (1993) and Benchekchou and White (1993).

The ply failure index plots for the outer lap at the hole boundary are shown in Figure 6.12. Again, as the radial stress plots have demonstrated the stresses do not increase to the same extent as observed with an aluminium washer, and as a result the ply failure indices are also lower and only exceed unity when the outside diameter of $3.5d_{bo}$ is used. However, the magnitude of the index only just exceeds the failure criterion, with a value of approximately 1.03.

Although not presented here, the ply failure index plots for the inner lap were found to be lower than the outer lap and exhibit a similar variation as encountered with the analysis of the aluminium washer, hence are considered insignificant.

The variation in delamination index for the outer lap as the washer diameter increases is shown in Figure 6.13. Again, the delamination indices are much lower than the ply failure indices and the trend observed from the previous investigation is repeated, whereby the index increases with increasing washer diameter and changes position, moving towards the outer surface of the laminate. However, the magnitude is slightly larger at approximately 0.017 for the washer diameter of $2.0d_{bo}$, than that obtained from the aluminium washer investigation, although the highest index obtained at the washer diameter of $3.5d_{bo}$ is lower at a magnitude of approximately 0.075.

The delamination indices have not been included for the inner lap as they are lower than for the outer lap and continually reduce with increasing washer diameter and hence are considered less significant.

6.3.3 - Aluminium bolt with a 4mm thick steel washer

Figures 6.14 and 6.15 show the variation in the normalized radial stress at the hole boundary for the outer lap and inner lap, respectively. Figure 6.14 shows that for a washer outside diameter of $2.0d_{bo}$ the stresses close to the interface with the inner lap are higher than those close to the outer surface, indicating that 50MPa may not be the optimum clamping pressure for this type of washer, as is the case for a 1mm thick aluminium washer. As the washer size is increased the normalized radial stress on the outer lap falls to approximately 0.29 for a washer outside diameter of $3.0d_{bo}$, and then rises gradually for diameters of $3.5d_{bo}$ and greater. The magnitude of maximum normalized radial stress is much lower than for the two other types of washers examined with outside diameters greater than $2.0d_{bo}$. This indicates that due to the extra stiffness imposed by the increased cross section of the 4mm thick steel washer the bolt clamp-up pressure is distributed more evenly on the surface of the outer lap, over an area similar in size to the washer rather than the bolt head.

The inner lap radial stresses are slightly higher than those recorded for the outer lap with washer outside diameters of $2.0d_{bo}$ and $2.5d_{bo}$, however, as the washer size increases the stresses on the inner lap close to the interface continue to fall, indicating that failure may be more likely to occur on the outer lap rather than the inner lap for larger washer sizes at this clamping pressure.

Figure 6.16 demonstrates that a more uniform through thickness contact stress distribution is obtained for all washer sizes when a 4mm thick steel washer is used, and thus a larger washer will carry a high proportion of the load through friction. Also, the peak stress has decreased compared to the equivalent washer sizes constructed using aluminium and 2mm thick steel. A high stress concentration is also shown to exist at the outside edge of the smaller washers due to out of plane laminate deformation and bolt bending. It is also interesting to note from this figure that for the smaller washer diameters the laminate material is disturbed due to higher bearing load, hence the contact is less uniform radially between the hole boundary and the washer outside edge than for the joints with larger washer diameters.

From an analysis of the effect of the previous washer types it may be predicted that the plots of the variation in the ply failure index would follow the same pattern as the normalized radial stress plots, however, for the model having a stiffer washer, it may also be necessary to look at the failure indices further away from the hole boundary. Figures 6.18, 6.19 and 6.20 show the outer lap ply failure indices for elements around the hole boundary, inside the washer edge and outside the washer edge respectively, while Figure 6.17 shows the elements used to provide the failure indices for these figures.

Figure 6.18 shows that the ply failure index at the hole boundary follows the same pattern as the radial stress distribution, whereby the maximum failure index reduces as the washer diameter increases from $2.0d_{bo}$ to $3.0d_{bo}$, and then increases again as the washer size is increased beyond $3.0d_{bo}$. The position of maximum failure index also changes position from the bearing plane close to the interface with the inner lap, to the outer surface of the outer lap. All the indices indicate that the ply failure is unlikely to occur on the hole boundary, as even the maximum index, with a washer diameter of $2.0d_{bo}$, does not exceed 0.7.

Figure 6.19 demonstrates that the ply failure indices are higher on the area inside the washer edge than on the hole boundary for these models having washer outside diameters between $2.0d_{bo}$ and $3.5d_{bo}$. The maximum index occurs on the outside surface of the outer lap for the model having a washer outside diameter of $2.0d_{bo}$, with an index of approximately 0.74. The maximum indices in each case seem to occur on a portion of the laminate between angles of approximately 60° and 130°, with respect to the bearing plane, indicating that a tensile failure mode may result for higher tensile loading. It can also be observed that the magnitude of maximum failure index decreases as the washer size increases.

Figure 6.20 demonstrates that the index outside the washer edge continues to fall as the washer diameter is increased from $2.0d_{bo}$ to $4.5d_{bo}$, however the values are smaller than inside the washer edge, as the maximum index in this figure does not exceed 0.43.

Although the ply failure indices of the inner lap are only slightly lower than the outer lap for elements around the hole boundary, for each of the washer diameters tested the magnitude of the index decreases radially from the hole boundary and with increasing washer diameter. Thus the results are insignificant compared to those provided by the outer lap and are therefore not included here.

The variation in the delamination index for the outer lap can be seen in Figures 6.21, 6.22 and 6.23, for elements around the hole boundary, inside the washer edge and outside the washer edge, respectively.

Figure 6.21 demonstrates that the delamination indices for the hole boundary are very low, with the maximum obtained for the $4.5d_{bo}$ washer diameter, having a value of approximately 0.029 between the 0° and 45° plies, close to the outer surface of the outer lap. For all the other washer sizes the peak delamination indices occur between the plies close to the laminate interface.

Figure 6.22 shows that the likelihood of delamination is higher inside the washer edge than at the hole boundary, although the indices are still relatively low when compared to the ply failure results. All washer sizes show a similar pattern, with the lowest index provided by the model with a $2.5d_{bo}$ washer. The highest index of approximately 0.047 occurs near the outer surface of the outer lap for the model having a $2.0d_{bo}$ washer.

Figure 6.23 shows that outside the washer edge the delamination failure index is higher than under the washer, with the highest value obtained for the $2.0d_{bo}$ washer, with an index of approximately 0.125, at a position close to the outer surface of the outer lap. This value then continues to decrease as the washer size is increased.

Considering the maximum delamination and Tsai-Wu failure indices the joint configuration having a washer diameter of $2.0d_{bo}$ would be most likely to fail, although none of the indices exceed unity. It is clear that the joints having larger washer diameters result in stronger joints.

6.3.4 - Aluminium bolt with a 4mm thick steel washer (6Nm bolt torque)

This model was constructed to examine the effects of changing the washer size, whilst keeping the bolt preload/torque constant, on the stress distribution around the fastener.

As the bolt torque was maintained at 6Nm the clamping pressure provided over the washer area was reduced with increased washer diameter, according to Equation 5.1.

As can be seen in Figure 6.24, the magnitude of maximum normalized radial stress at the hole boundary for the outer lap increases very slightly, from approximately 1.45 to 1.72, as the washer diameter is increased from $2.0d_{bo}$ to $4.5d_{bo}$. This effect can be explained by the fact that as the clamping pressure reduces the radial stress should increase, as demonstrated by the clamping pressure investigation discussed in Chapter 5. This increase in stress should be quite large as the clamping pressure reduces from 50MPa to approximately 8MPa, which is equivalent to a bolt torque of less than 1Nm for the models previously investigated. However, as the washer is larger, inducing more friction between the washer and laminate and reducing out of plane deformation of the outer lap, the increase in stress through bearing loading is kept to a minimum. The angle of contact between the bolt shank and the hole is also shown to reduce slightly from about 90° to 70°, with respect to the bearing plane, as the washer size is increased.

The variation in radial stress for the inner lap as the washer diameter is increased is shown in Figure 6.25. The figure demonstrates that the radial stress distribution is higher than that obtained for the outer lap, with a magnitude of approximately 1.8, and reduces very slightly as the washer size is increased.

Figure 6.26 demonstrates that the ply failure indices for elements around the hole boundary remain at approximately 0.7 and follow the same pattern as the radial stress distribution, whereby they increase slightly with increasing washer size. Figures 6.27 and 6.28 demonstrate that the ply failure indices for elements inside and outside the washer edge respectively, follow the same pattern as in the previous investigation discussed in section 6.3.3, whereby they reduce as the washer size increases. This is due in part to the increased distance from the point of maximum stress as well as the reduction in clamping pressure, as the indices are smaller than those provided using a constant clamping pressure of 50MPa.

Although not presented here, the delamination indices for the outer lap for elements around the hole boundary are approximately the same as in Figure 6.21(i) for the range of washer diameters tested, and the indices for the inside and outside of the washer edge are the same as in Figures 6.22(i) and 6.23(i) respectively, for a washer diameter of $2.0d_{bo}$. These values decrease more rapidly than the constant pressure joint as the washer size is increased. The delamination and Tsai-Wu failure indices for the inner lap are also not presented here as they follow a similar trend to results provided by the outer lap, only with smaller magnitude and hence are less significant.

6.3.5 – An alternative to the 4mm thick steel washer

Although a good clamping condition is provided by the 4mm thick steel washer, the increased weight compared to an aluminium washer for example, could dramatically increase the weight of the structure, especially if a multiple fastener configuration is adopted. An alternative washer could be manufactured from aluminium oxide ceramic having the material properties E = 371GPa, G = 143.8GPa and $\nu = 0.29$. A test was conducted on a joint consisting of an aluminium bolt with a 3mm thick ceramic washer, having an outside diameter of $3.5d_{bo}$. A torque equivalent to 50MPa clamping pressure was applied to the bolt and the resultant contact stress on the outer lap under the washer can be seen in Figure 6.29. This figure can be compared to the contact stress contour for the equivalent joint configuration having a 4mm thick steel washer, shown in Figure 6.16. This comparison shows that the contact stress distribution for each washer type is very similar, however the saving in weight is quite considerable. Typical values for the mass density of steel and Al_2O_3 are 7.82×10^{-6}kg/mm^3 and 3.9×10^{-6}kg/mm^3. Therefore, for this particular single bolt joint configuration, the weight of the 3mm thick ceramic washer is 4.2×10^{-3}kg compared to 11×10^{-3}kg for the 4mm thick steel washer.

6.4 – CONCLUDING REMARKS

For a double lap quasi-isotropic GRP laminate joint constructed using a 1mm thick aluminium washer, the bolt clamping load is not uniformly distributed on the laminate surface. The washer is too compliant and hence as the washer size is increased the contact area of the outer lap is not shown to increase.

A slightly more uniform contact stress distribution is exhibited with a 2mm thick steel washer, however, the pressure on the surface of the laminate is still by no means uniform as assumed in previous investigations such as Lessard et al. (1993) and Benchekchou and White (1993).

As a result of the compliance of both of these washer types, the increased force applied to the bolt in order to provide a washer pressure of 50MPa as the washer diameter increases, results in a higher compressive force close to the hole boundary, hence failure results in this area at high bolt loads.

The 4mm thick steel washer provides the most uniform contact stress distribution and comes closer to a constant pressure over the entire washer area, however the weight is significantly increased and hence the weight savings from using composites within a structure are reduced.

As the diameter of this type of washer is increased and the pressure maintained at 50MPa, the ply failure indices reduce and hence the joint is less likely to fail as the washer diameter increases from $2.0d_{bo}$ to $3.5d_{bo}$. However, tensile failure may result with increased tensile load due to the indices being maximum around the tensile area of the laminate close to the washer edge. For washer sizes of $4.0d_{bo}$ and $4.5d_{bo}$, the higher indices are obtained on both sides of the hole boundary on the bearing plane due to compression of the washer.

For a washer diameter of $2.0d_{bo}$ the increased stiffness of the thicker steel washers does not reduce the likelihood of failure compared to the 1mm thick aluminium washer. Therefore it is apparent that the stiffness of the washer is not so important for small diameter washers as the bolt head is of comparable size to a standard washer, however, increasing the washer diameter is only beneficial when using the stiffer washers.

If the bolt torque is maintained at 6Nm as the diameter is increased, the joint does not fail, however, the indices at the hole boundary on the bearing plane increase very slightly indicating that bearing failure may result with higher loading for larger washer sizes. Although the smallest washer diameter is more likely to fail in the tensile region at the washer edge. This indicates that for a double lap joint with a 6Nm clamping torque, a slightly higher bearing strength may be obtained with a larger washer diameter.

The 3mm thick Al_2O_3 ceramic washer was shown to give an equivalent contact stress on the outer lap as the 4mm thick steel washer and results in a weight reduction of more than 60%. This type of washer will therefore be used in further investigations.

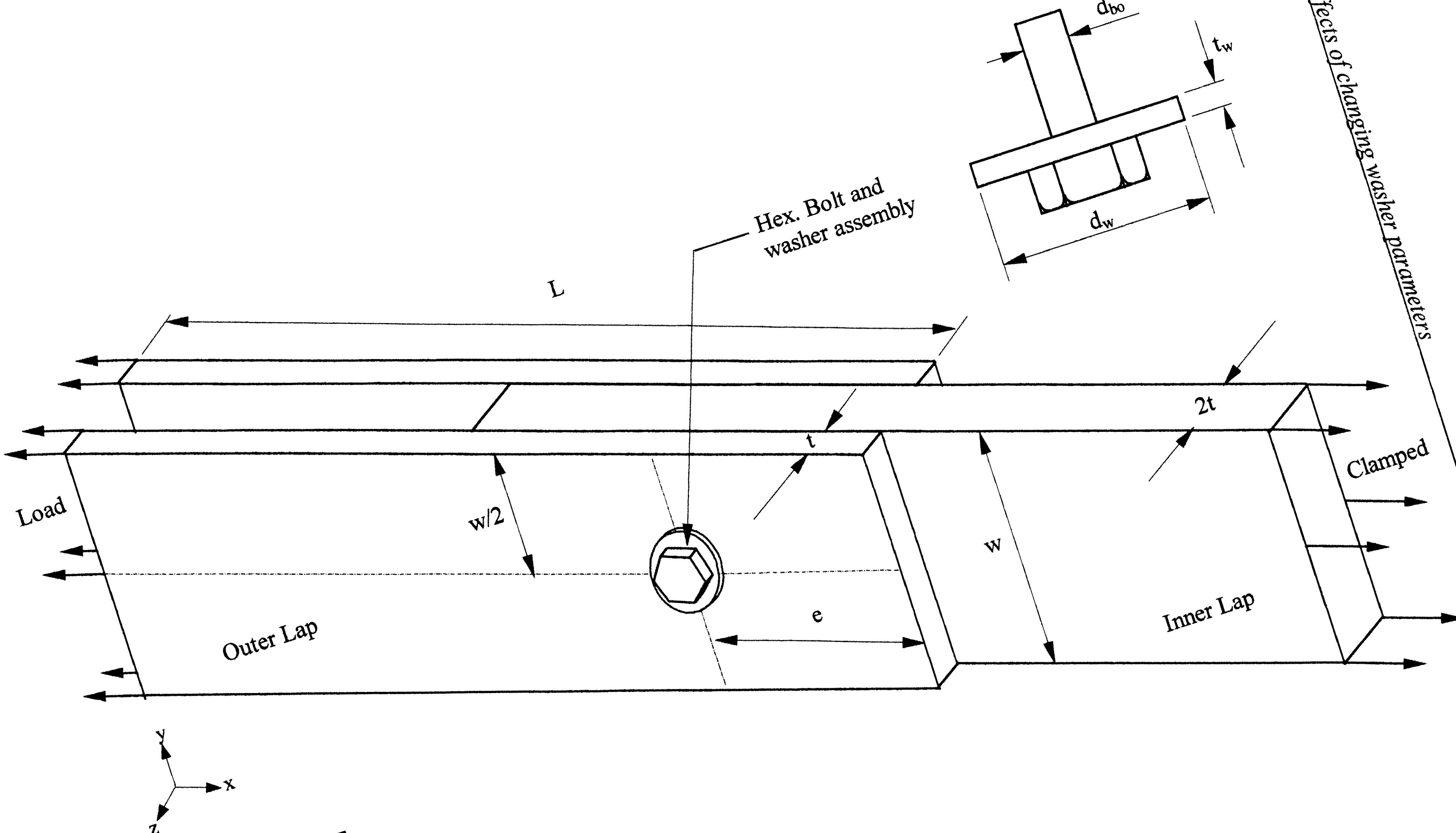

$d_{bo} = 6.35mm$
$d_w = 2d_{bo}$ to $4.5d_{bo}$
$e = 38.1$ ($\equiv 6d$)
$L = 101.6mm$
$t = 6mm$
$t_w = 1mm$ to $4mm$
$w = 38.1mm$ ($\equiv 6d$)

Figure 6.1 – Physical model of the double shear joint

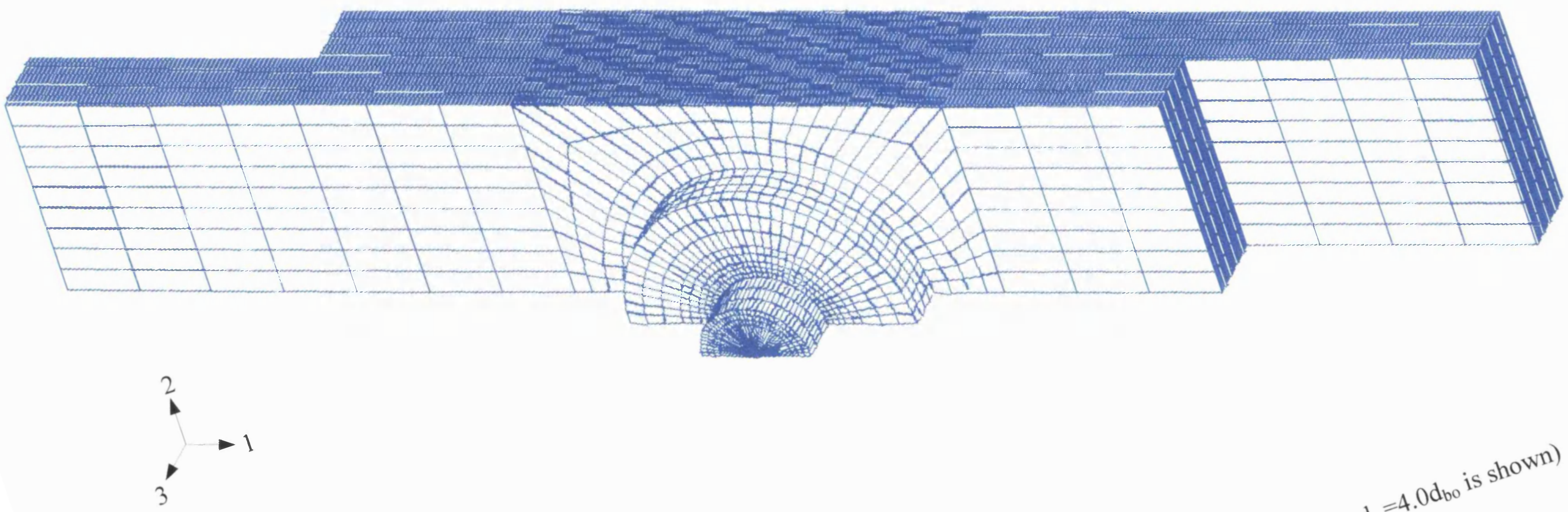

Figure 6.2 – Typical finite element mesh (mesh having 4mm thick steel washer with outside diameter d_w=4.0d_{bo} is shown)

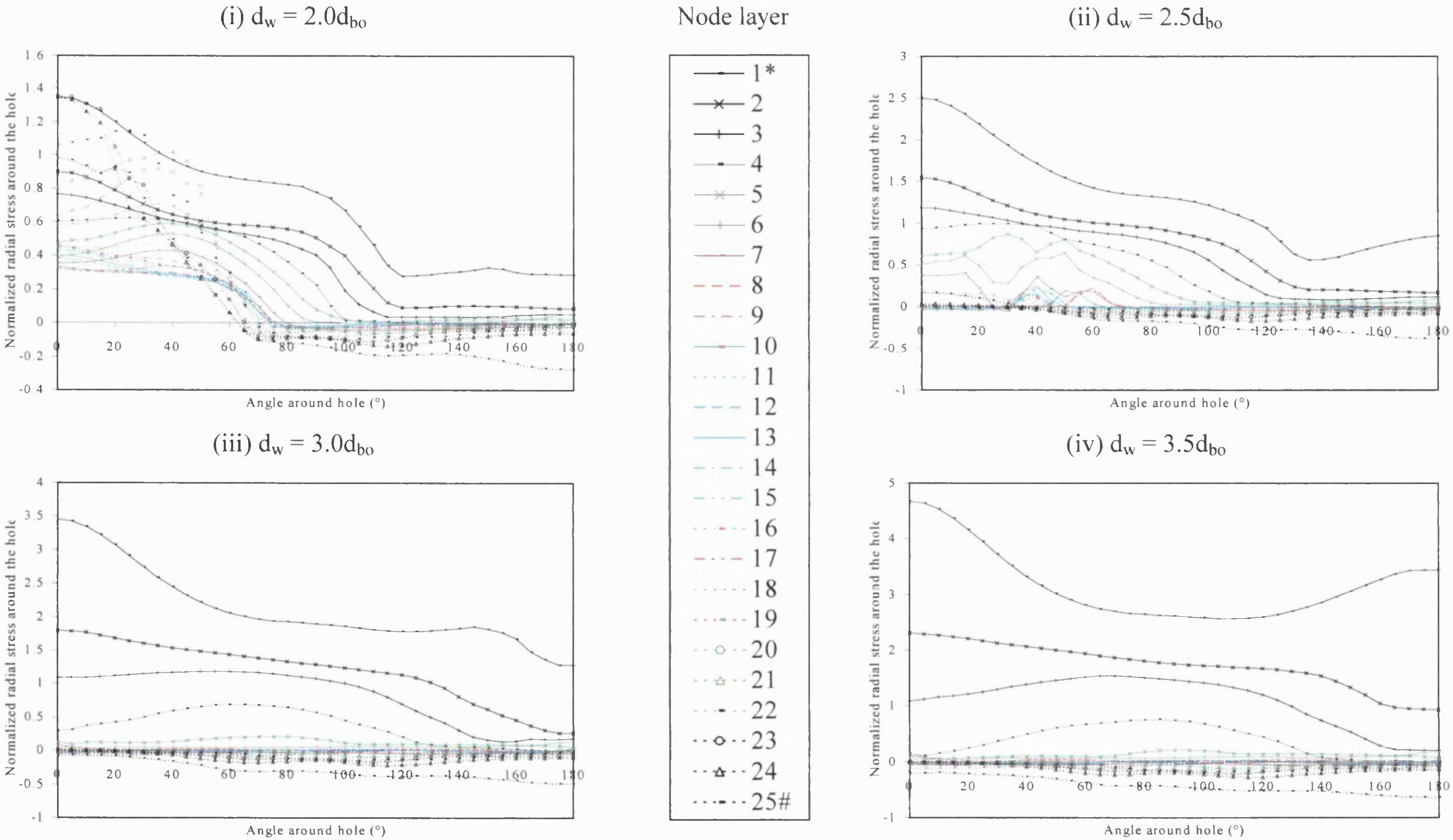

Figure 6.3 – Normalized radial stress around the hole boundary of the outer lap – aluminium bolt with 1mm washer assembly $d_w = 2.0d_{bo}$ to $3.5d_{bo}$ - * = Outer surface, # = Laminate interface

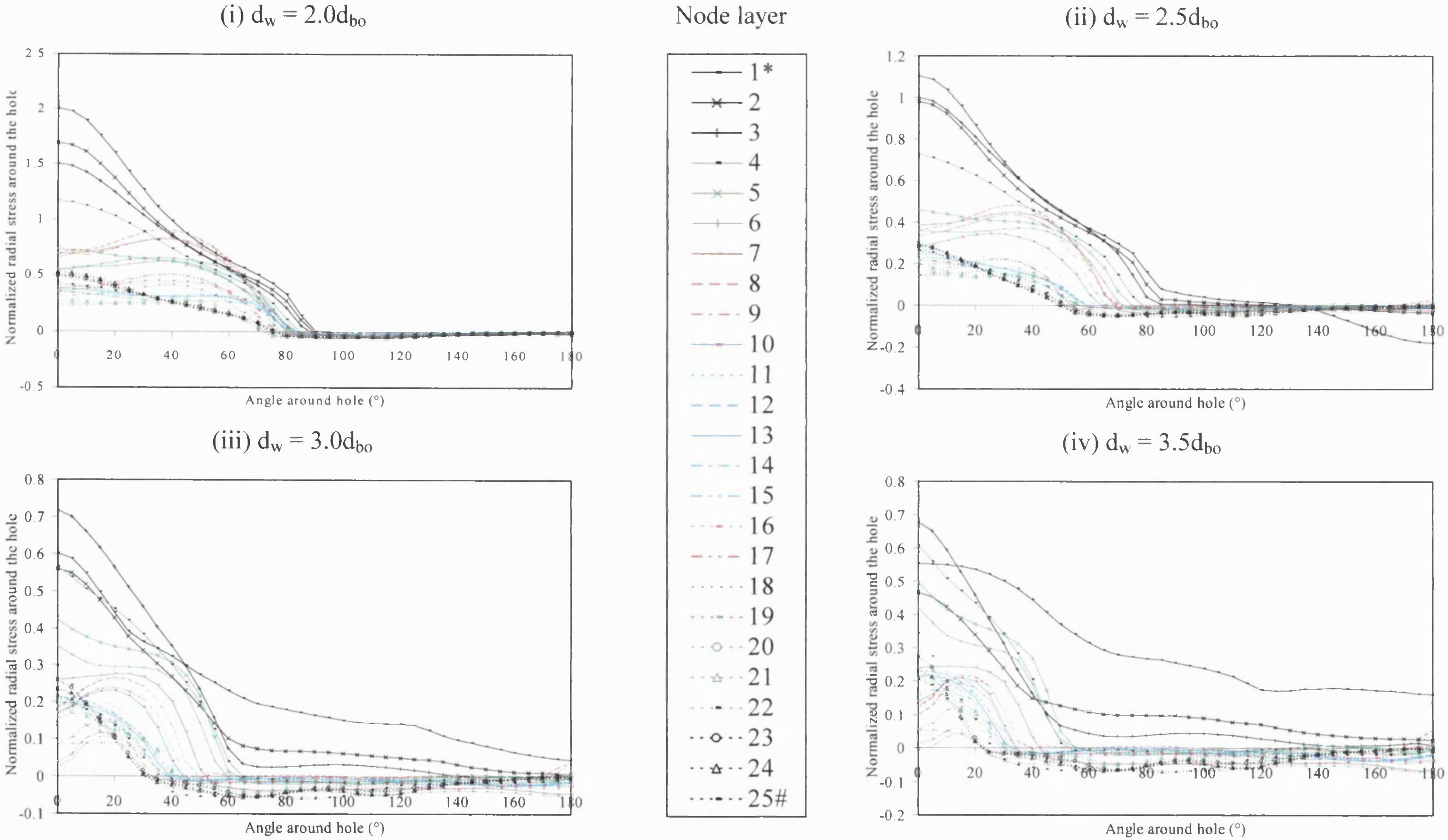

Figure 6.4 – Normalized radial stress around the hole boundary of the inner lap – aluminium bolt with 1mm washer assembly $d_w = 2.0d_{bo}$ to $3.5d_{bo}$ - * = Laminate interface, # = Laminate mid-plane

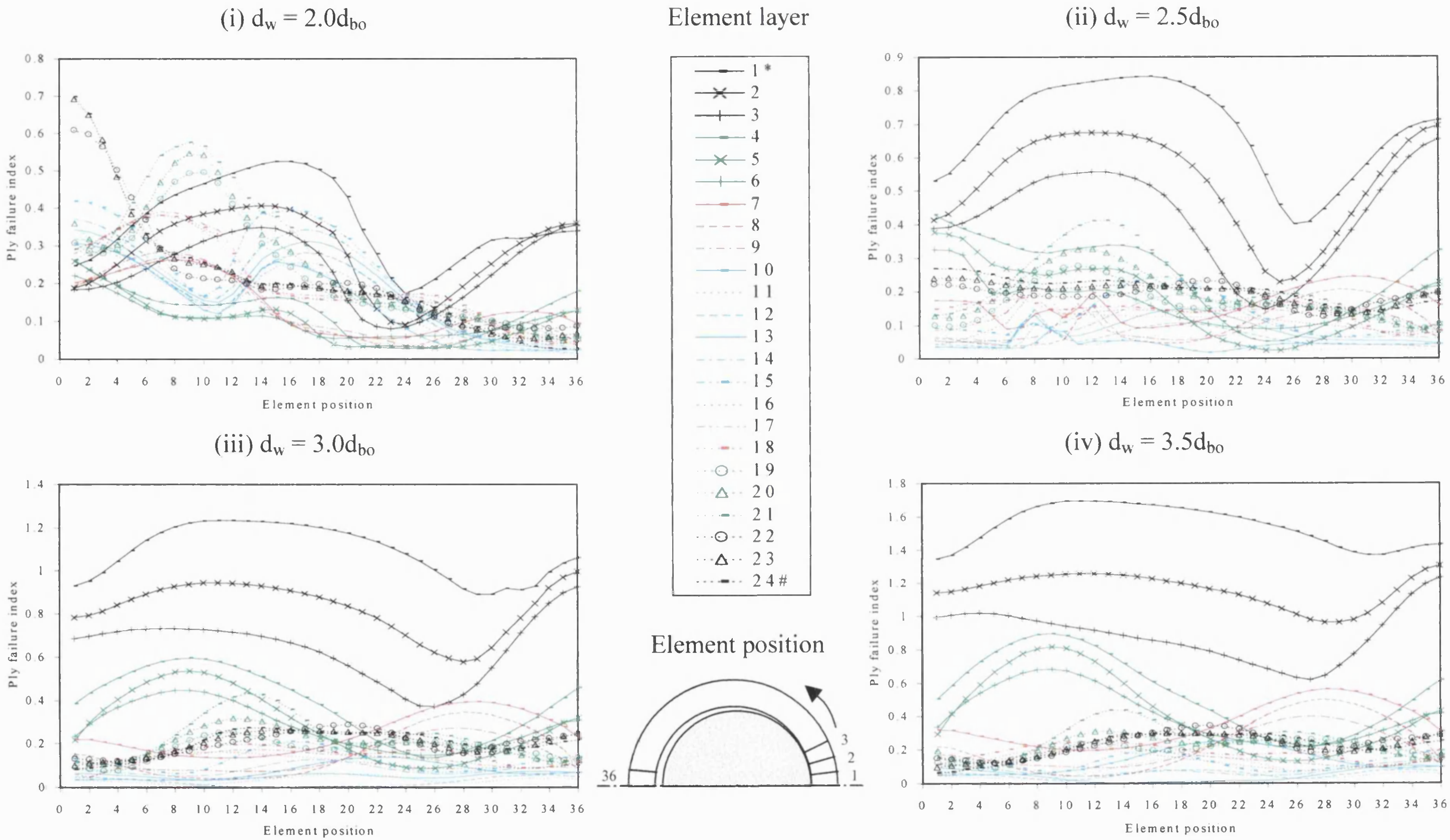

Figure 6.5 – Ply failure index plots for the outer lap – Aluminium bolt with 1mm washer assembly $d_w = 2.0d_{bo}$ to $3.5d_{bo}$ - * = Outer surface, # = Laminate interface

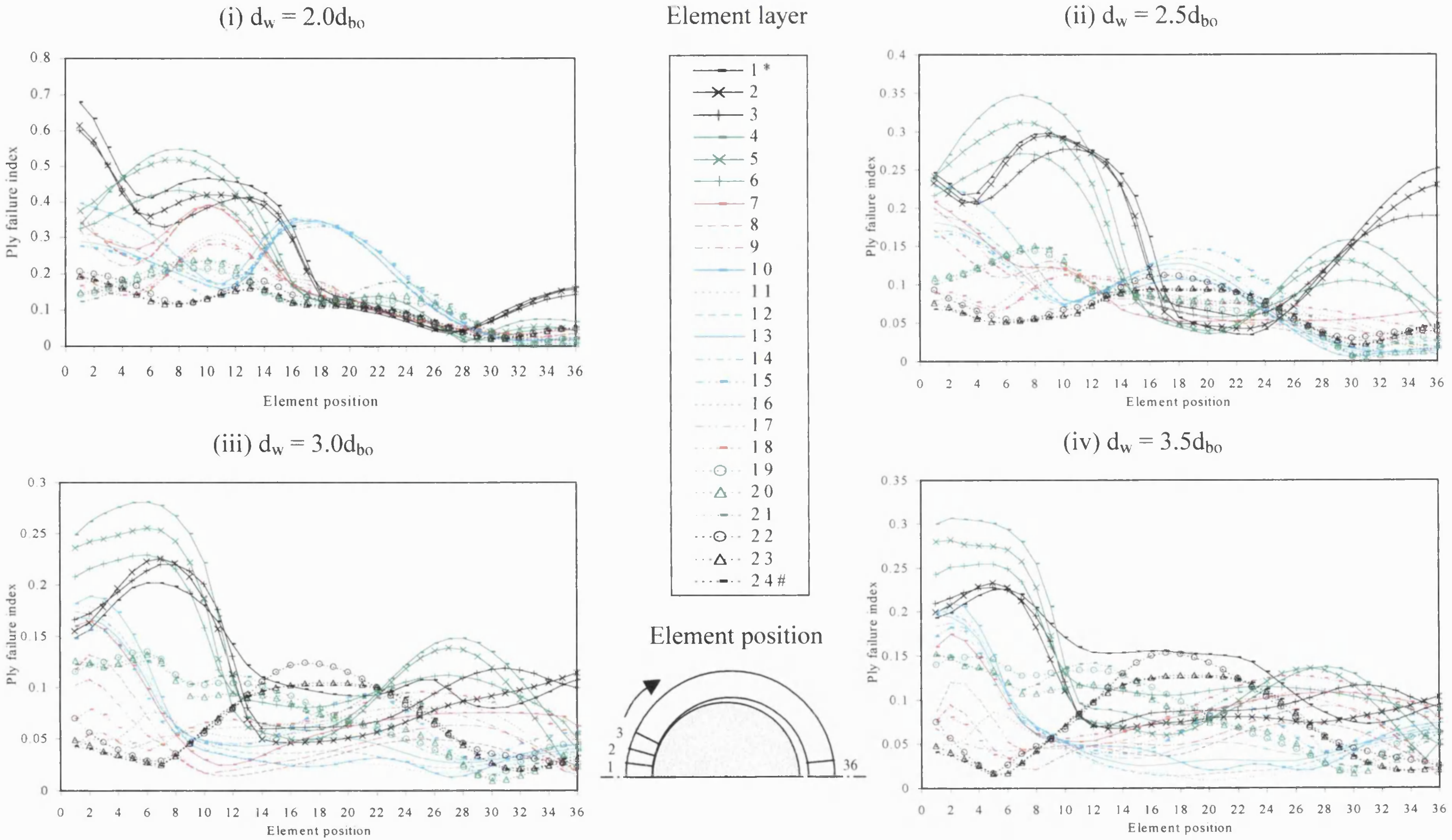

Figure 6.6 – Ply failure index plots for the inner lap – aluminium bolt with 1mm washer assembly $d_w = 2.0d_{bo}$ to $3.5d_{bo}$ - * = Laminate interface, # = Laminate mid-plane

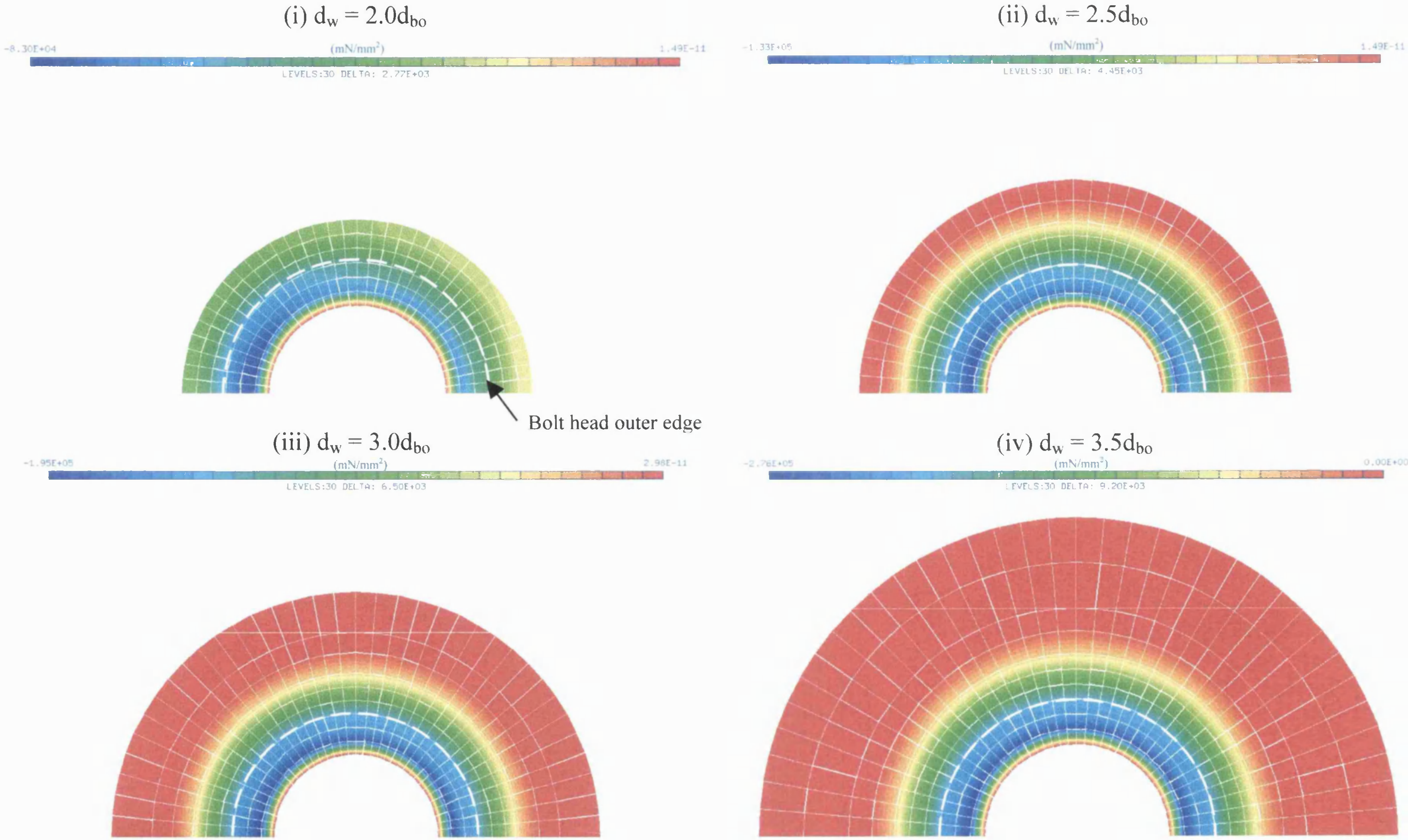

Figure 6.7 – Through thickness contact stress on the outer lap under the washer – aluminium bolt with 1mm washer assembly $d_w = 2d_{bo}$ to $3.5d_{bo}$

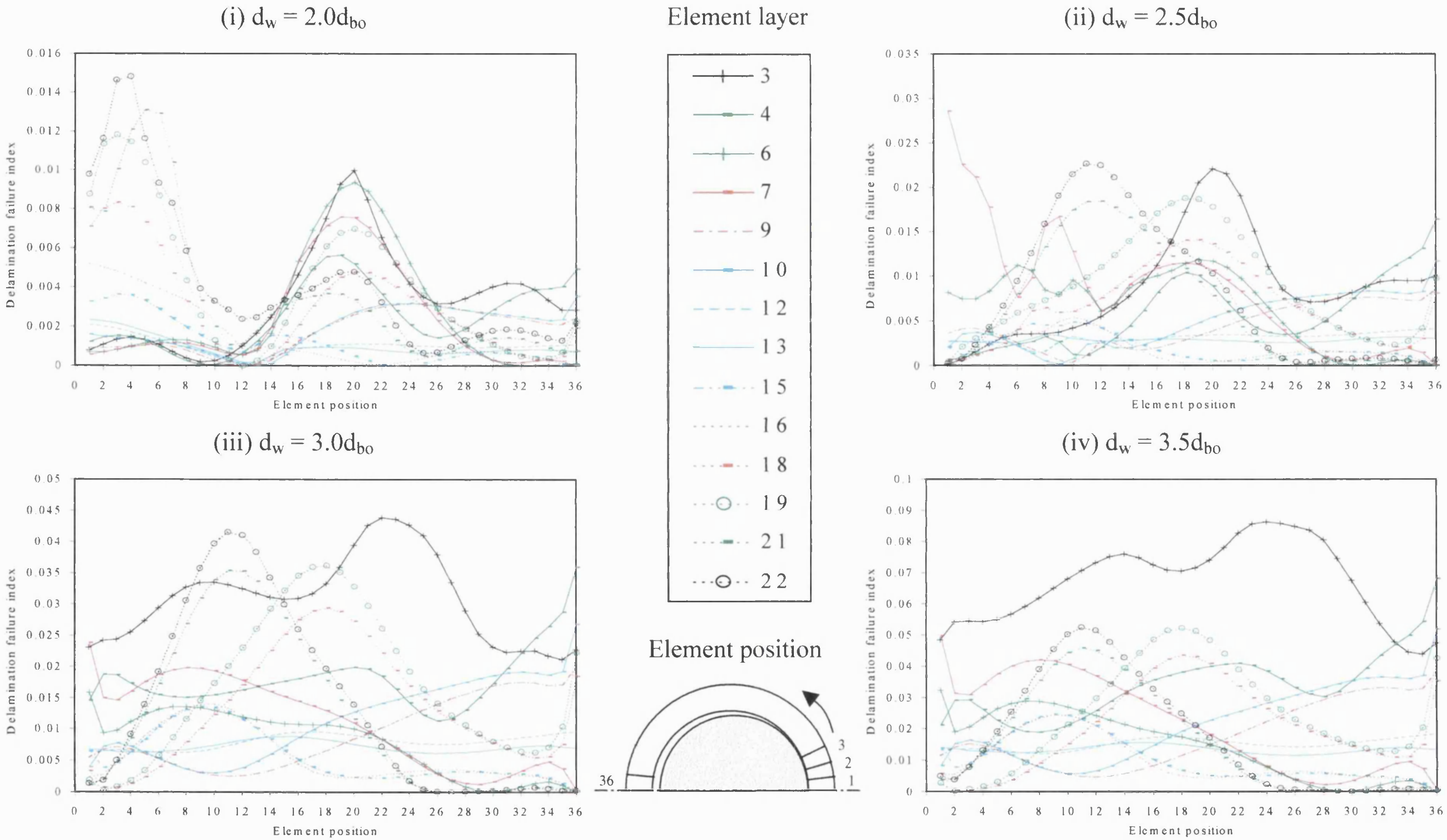

Figure 6.8 – Delamination failure index plots for the outer lap – aluminium bolt with 1mm washer assembly $d_w = 2.0d_{bo}$ to $3.5d_{bo}$

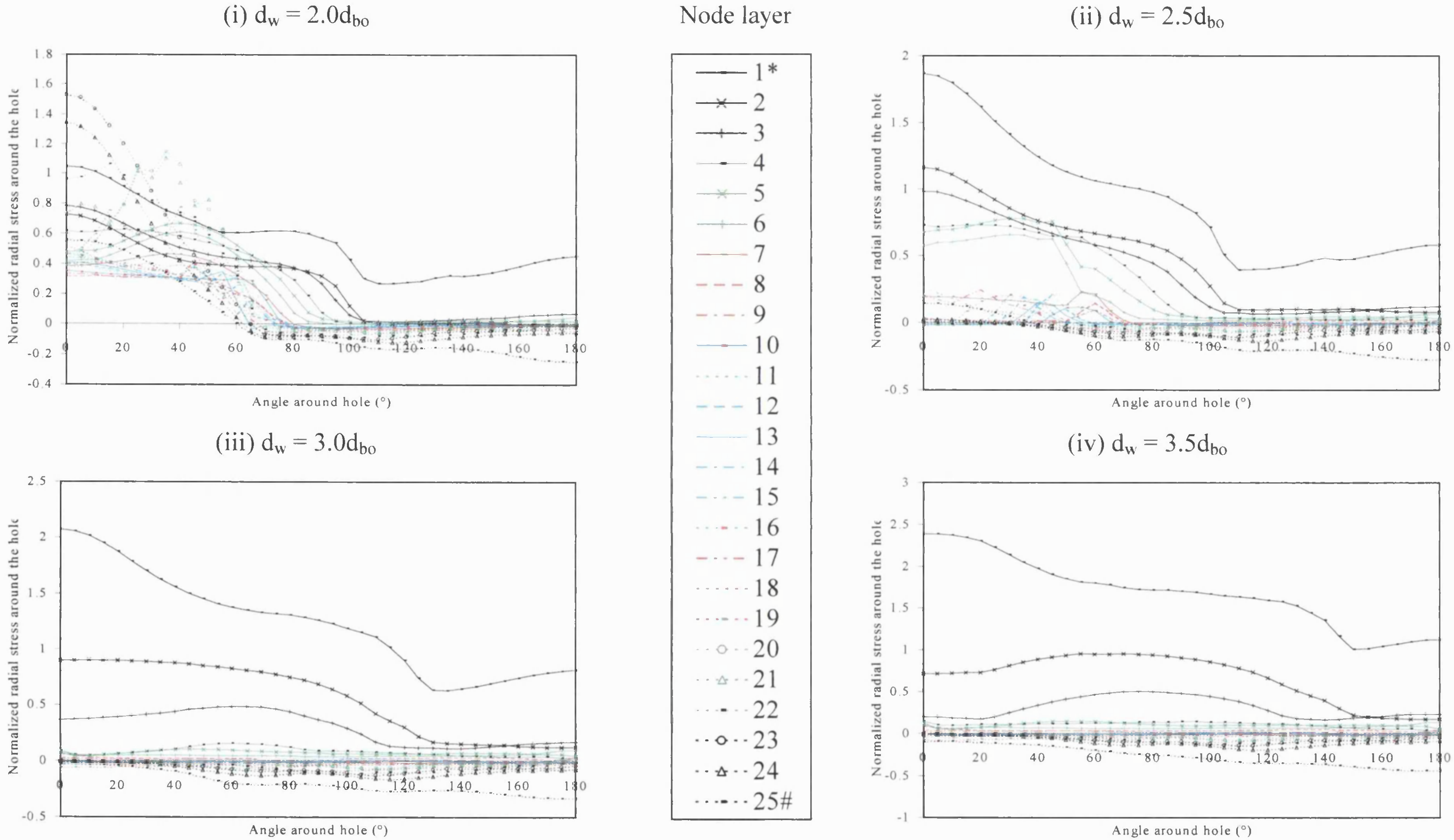

Figure 6.9 – Normalized radial stress around the hole boundary of the outer lap – aluminium bolt with 2mm steel washer $d_w = 2.0d_{bo}$ to $3.5d_{bo}$ - * = Outer surface, # = Laminate interface

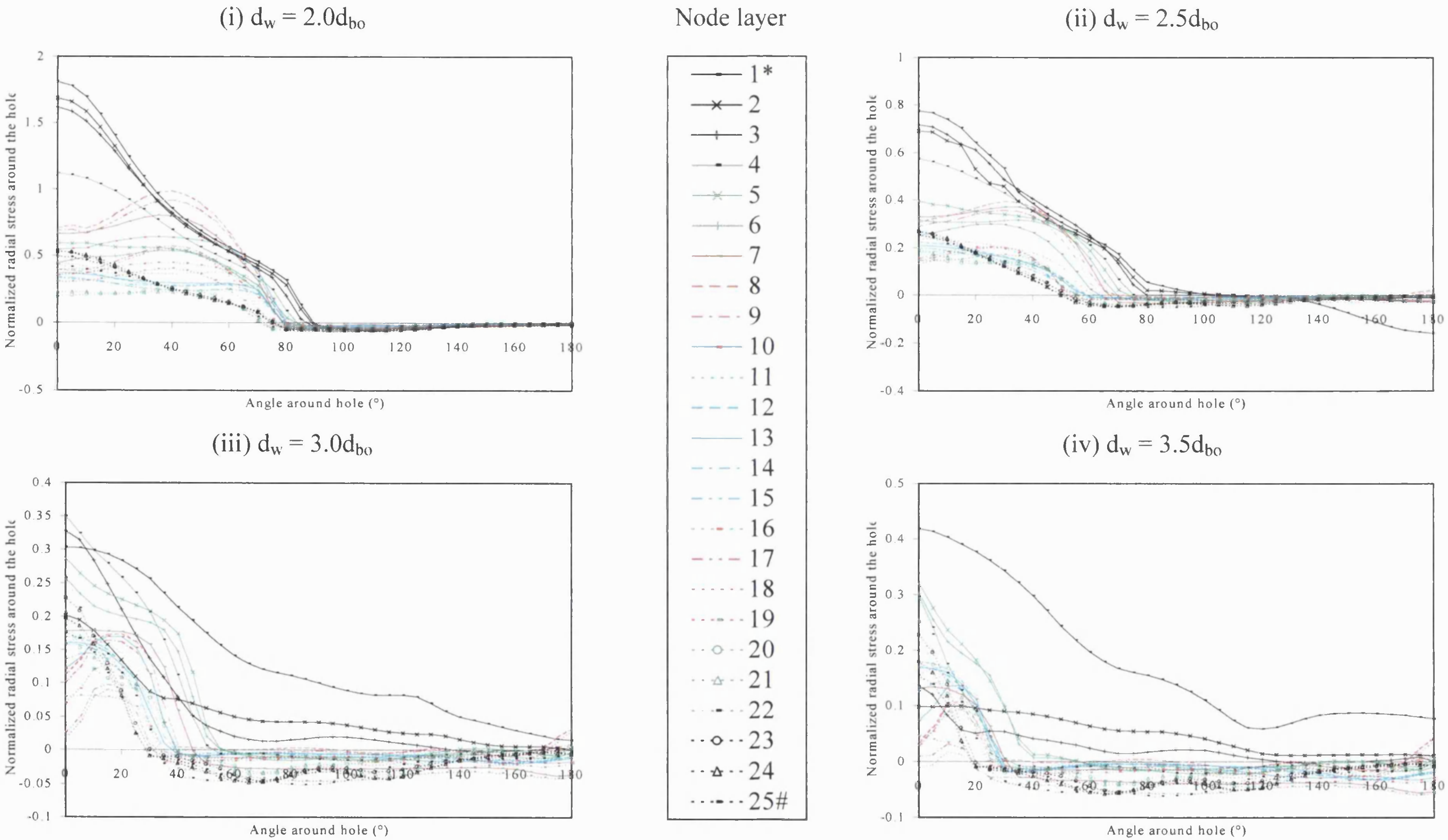

Figure 6.10 – Normalized radial stress around the hole boundary of the inner lap – aluminium bolt with 2mm steel washer $d_w = 2.0d_{bo}$ to $3.5d_{bo}$ - * = Laminate interface, # = Laminate mid-plane

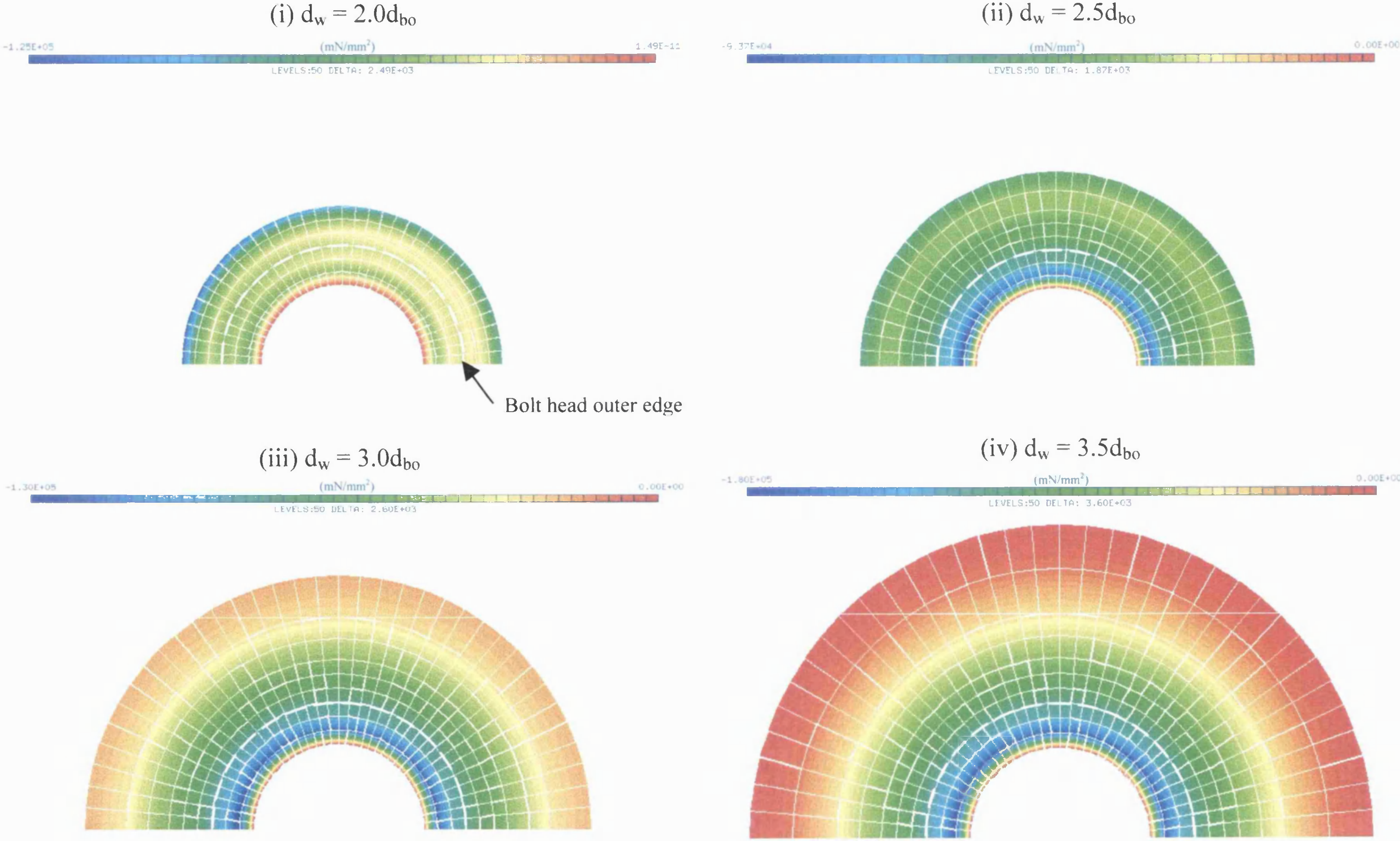

Figure 6.11 – Through thickness contact stress on the outer lap under the washer – aluminium bolt with 2mm thick steel washer $d_w = 2.0d_{bo}$ to $3.5d_{bo}$

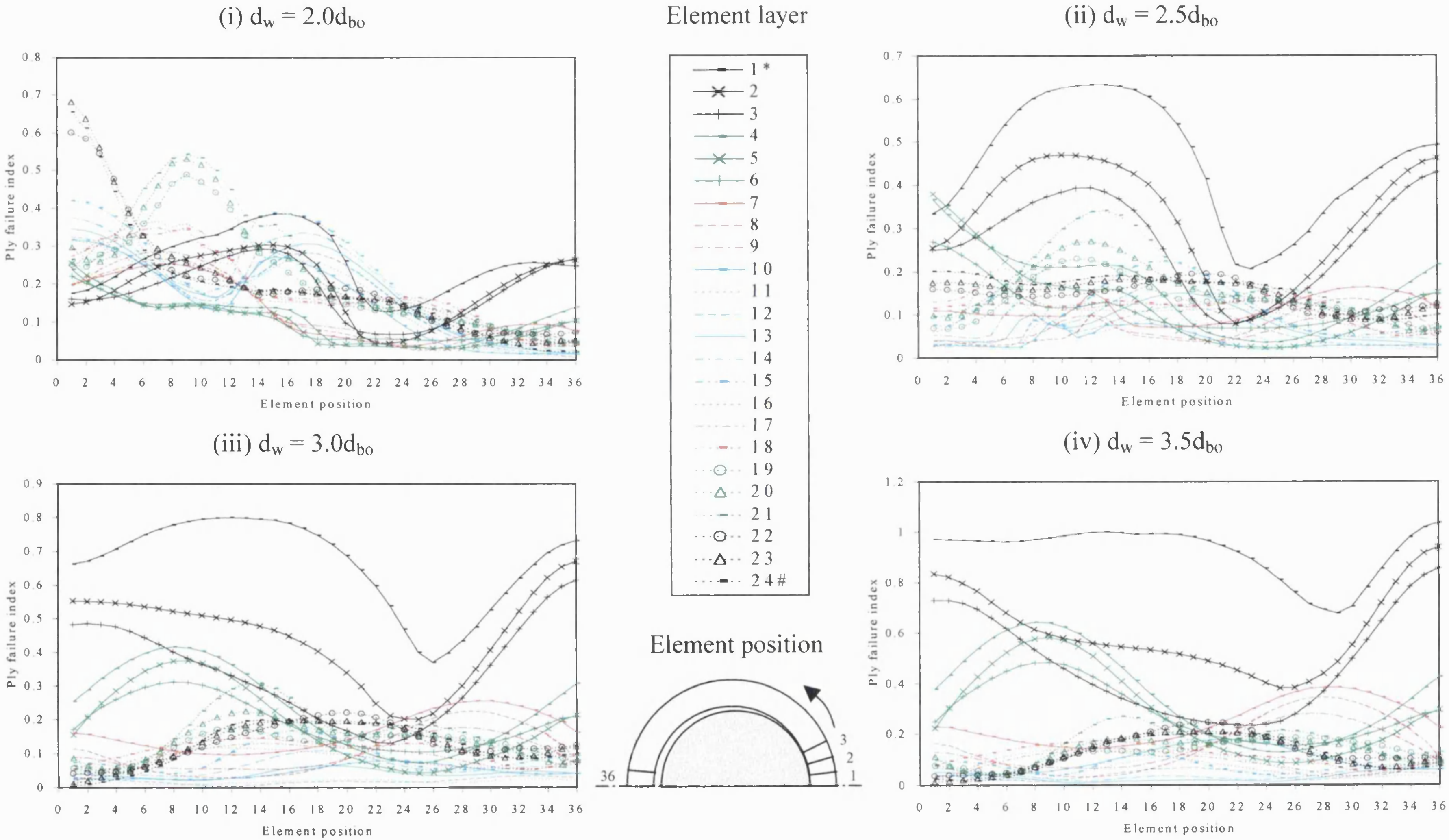

Figure 6.12 – Ply failure index plots for the outer lap – aluminium bolt with 2mm thick steel washer $d_w = 2.0d_{bo}$ to $3.5d_{bo}$ - * = Outer surface, # = Laminate interface

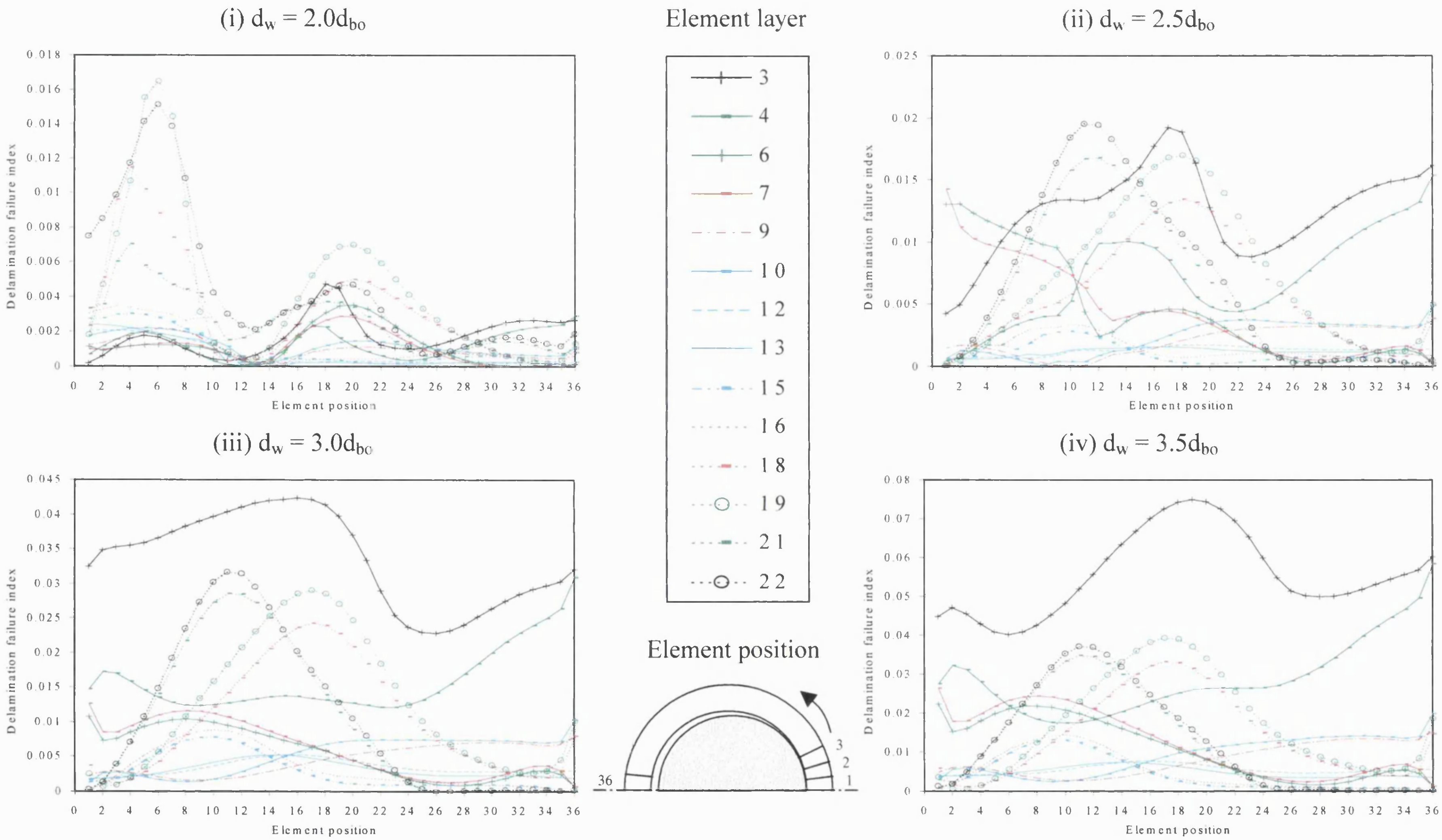

Figure 6.13 – Delamination failure index plots for the outer lap – aluminium bolt with 2mm thick steel washer $d_w = 2.0d_{bo}$ to $3.5d_{bo}$

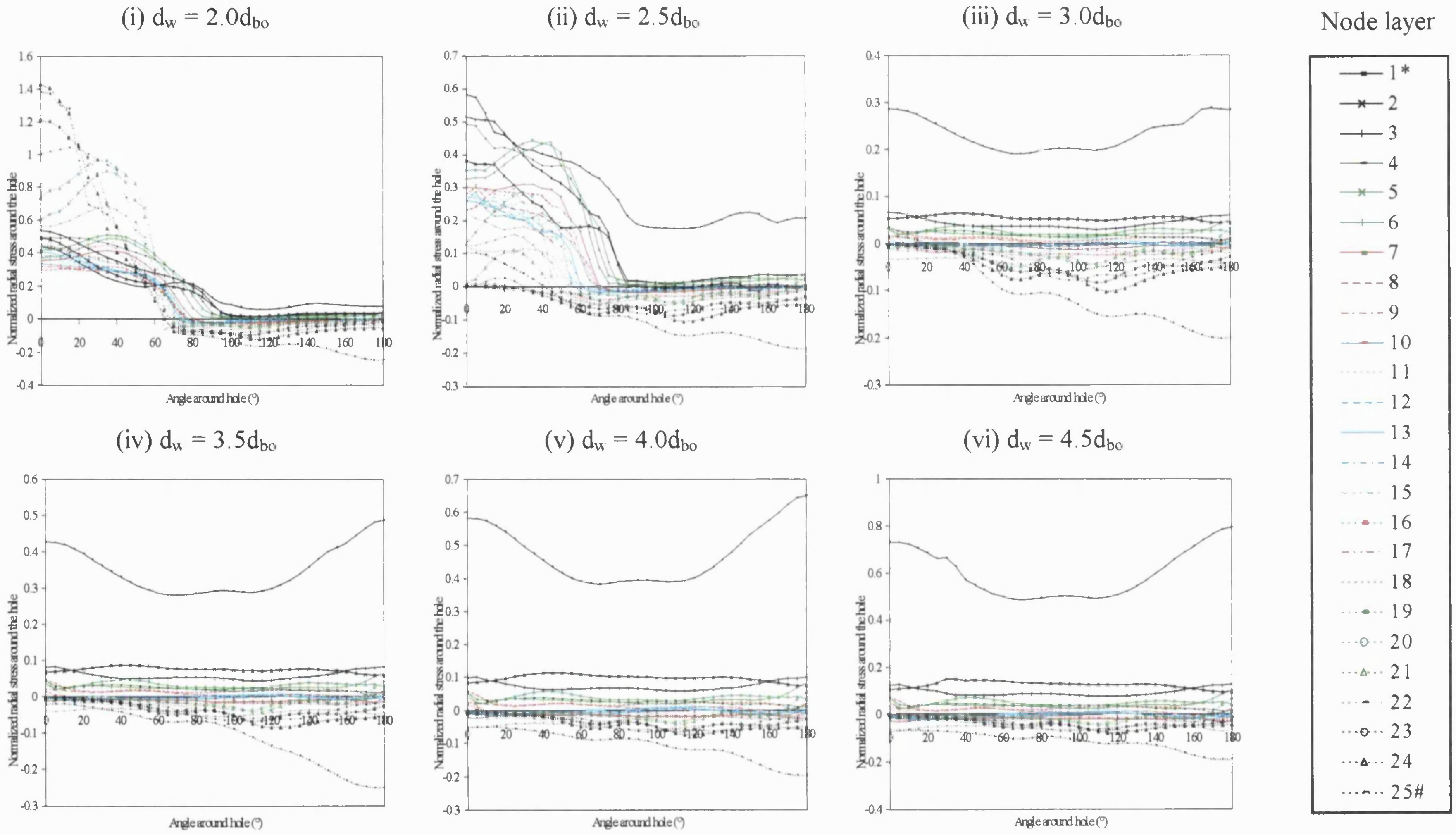

Figure 6.14 – Normalized radial stress around the hole boundary of the outer lap – aluminium bolt with 4mm thick steel washer d_w=2.0d_{bo} to 4.5d_{bo} - * = Outer surface, # = Laminate interface

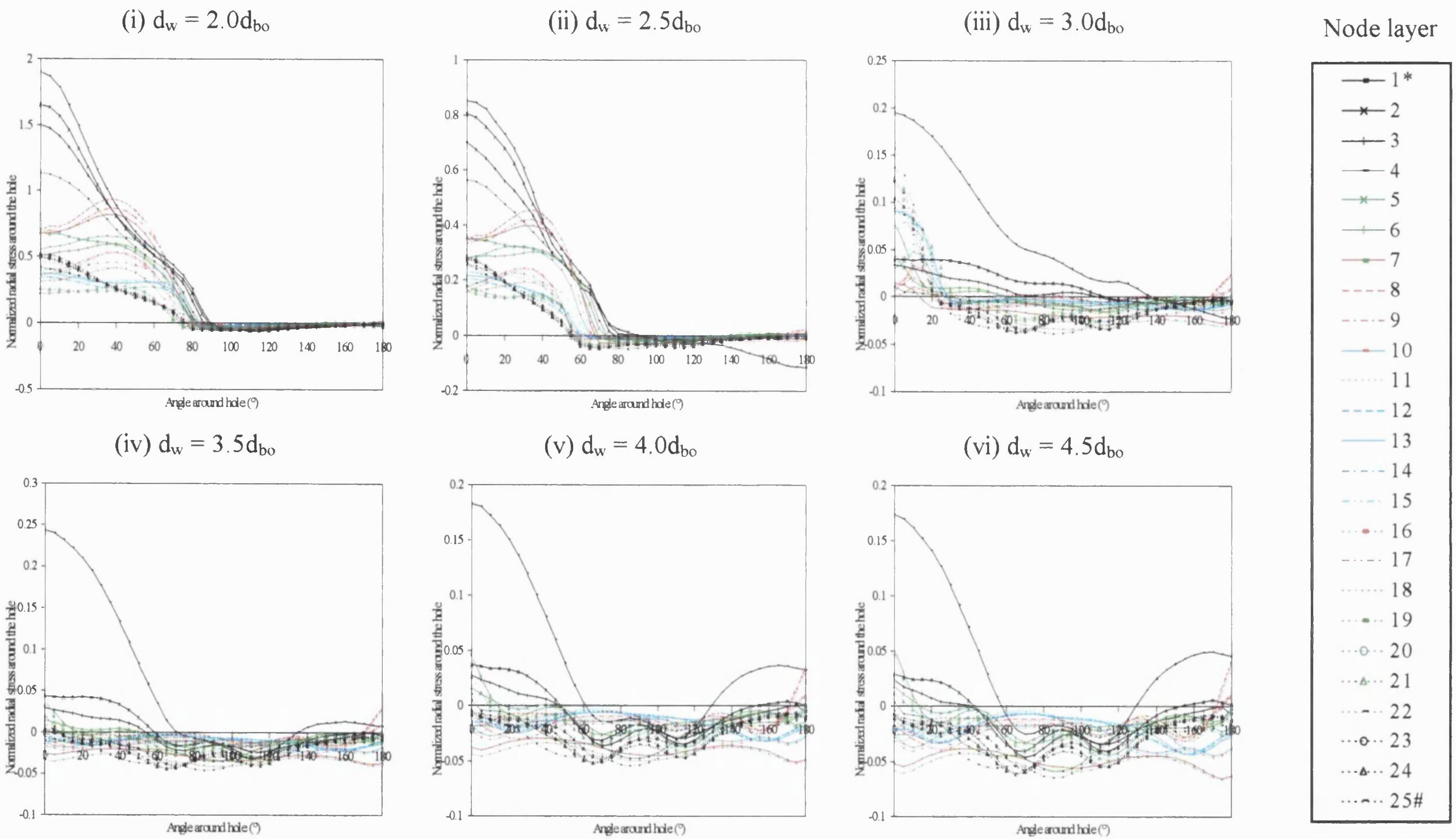

Figure 6.15 – Normalized radial stress around the hole boundary of the inner lap – aluminium bolt with 4mm thick steel washer d_w=2.0d_{bo} to 4.5d_{bo} - * = Laminate interface, # = Laminate mid-plane

(i) $d_w = 2.0d_{bo}$

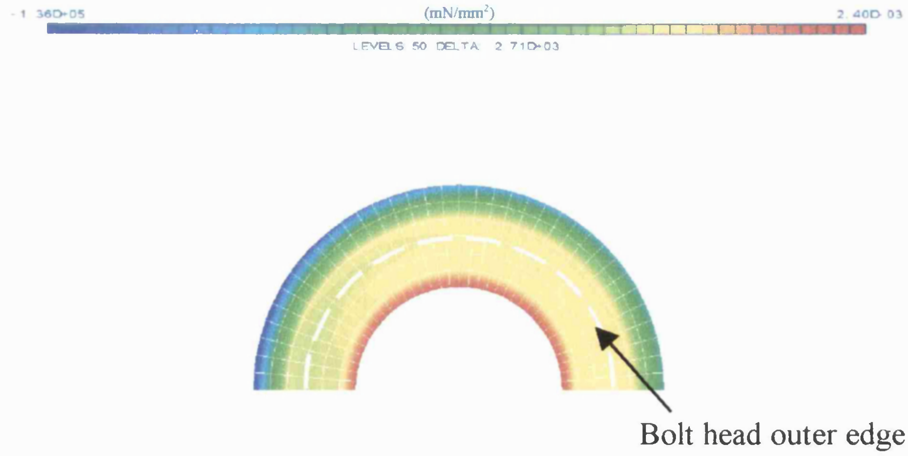

(ii) $d_w = 2.5d_{bo}$

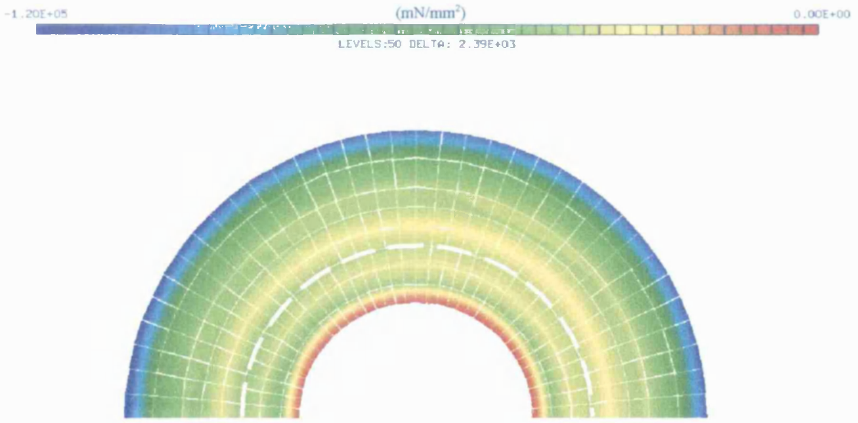

(iii) $d_w = 3.0d_{bo}$

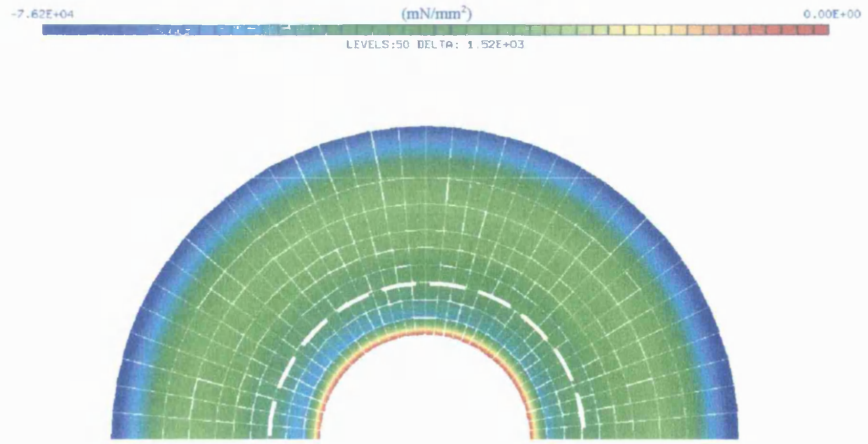

Figure 6.16a – Through thickness contact stress on the outer lap under the washer aluminium bolt with 4mm thick steel washer – $d_w = 2.0d_{bo}$ to $3.0d_{bo}$

(i) $d_w = 3.5d_{bo}$

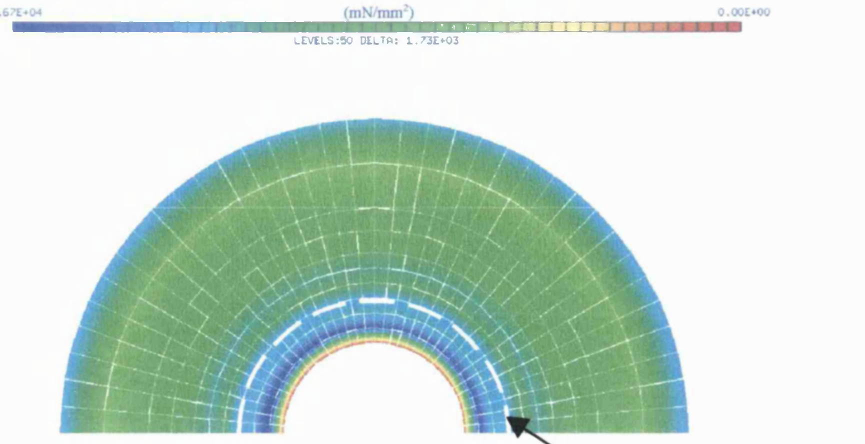

(ii) $d_w = 4.0d_{bo}$

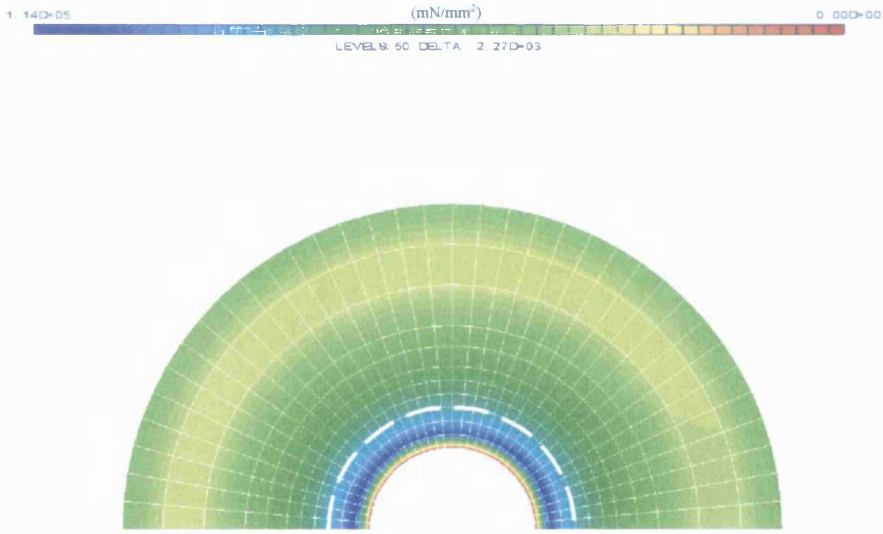

(iii) $d_w = 4.5d_{bo}$

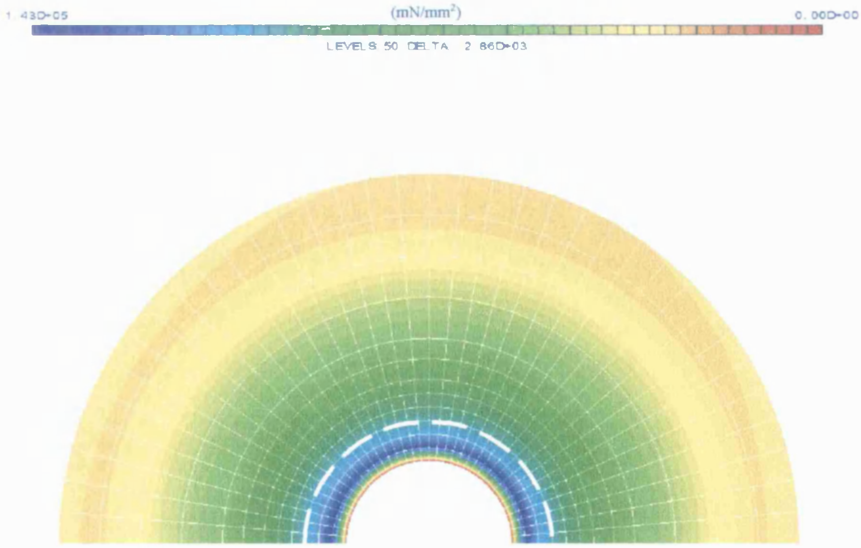

Figure 6.16b – Through thickness contact stress on the outer lap under the washer aluminium bolt with 4mm thick steel washer – $d_w = 3.5d_{bo}$ to $4.5d_{bo}$

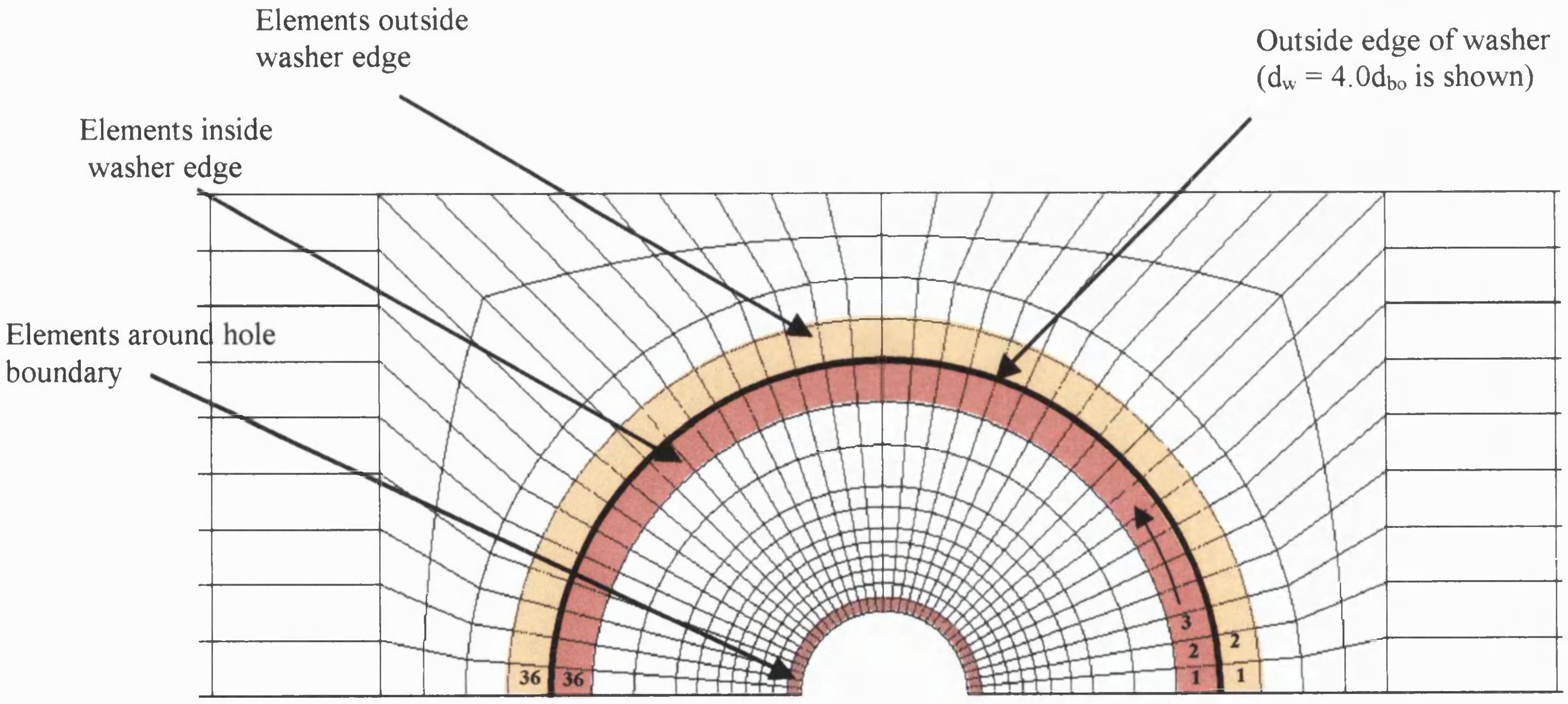

Figure 6.17 – Figure showing areas of elements used for ply failure and delamination index plots (portion of outer lap and bolt shank mesh is shown)

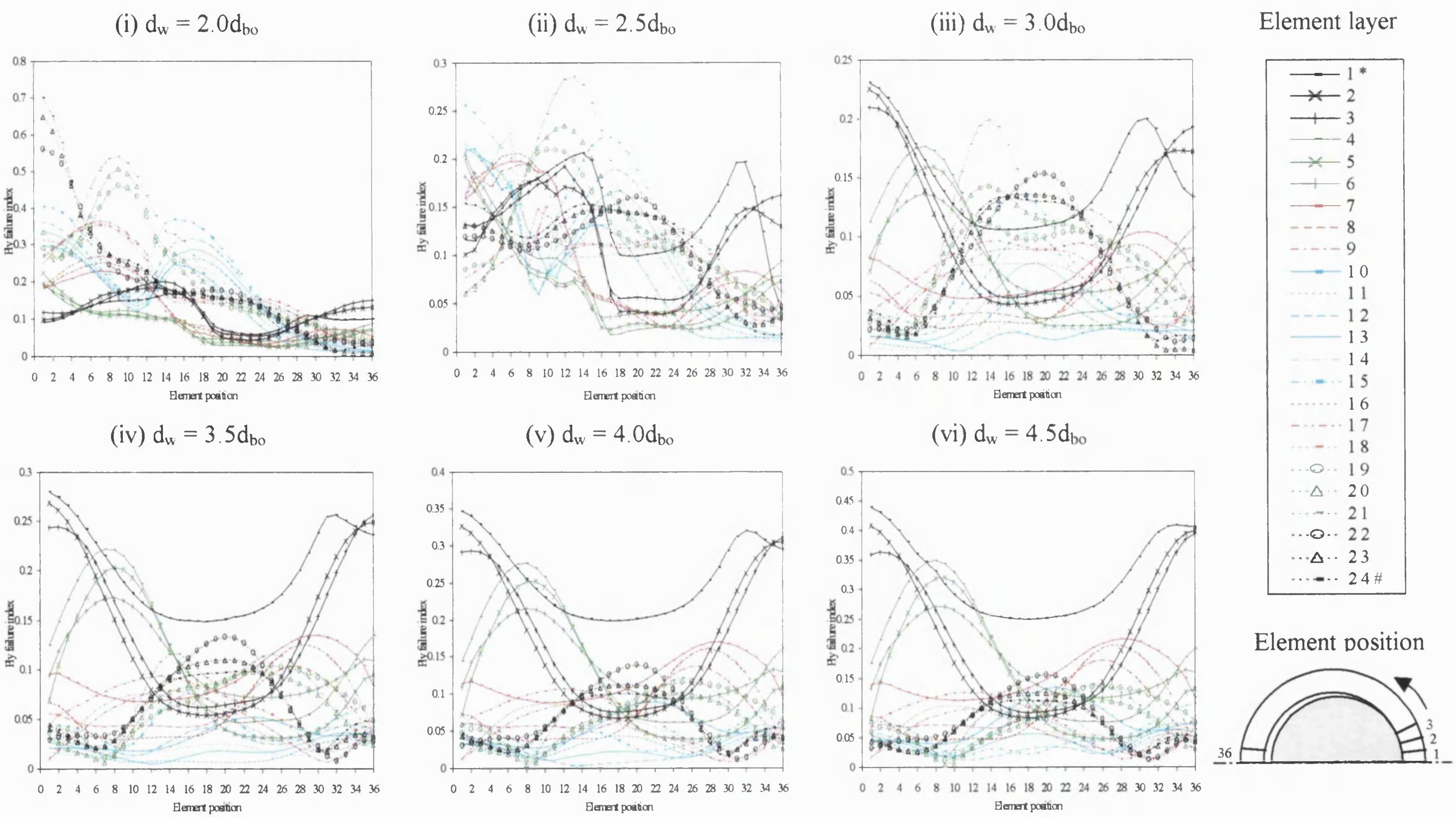

Figure 6.18 – Ply failure index plots for the outer lap – aluminium bolt with 4mm thick steel washer d_w=2.0d_{bo} to 4.5d_{bo} – Elements around the hole boundary * = Outer surface, # = Laminate interface

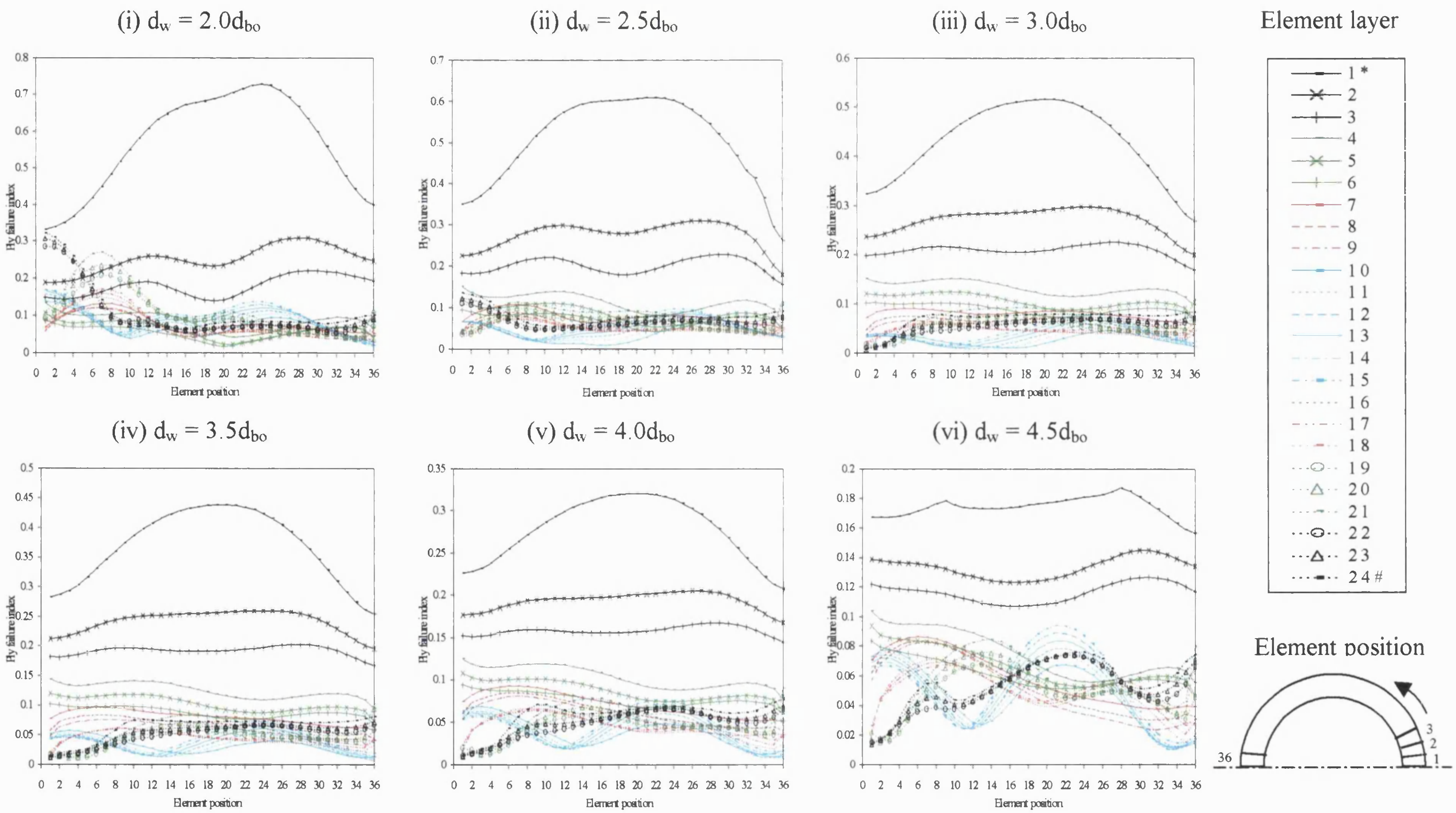

Figure 6.19 – Ply failure index plots for the outer lap – aluminium bolt with 4mm thick steel washer d_w=2.0d_{bo} to 4.5d_{bo} – Elements inside the washer edge - * = Outer surface, # = Laminate interface

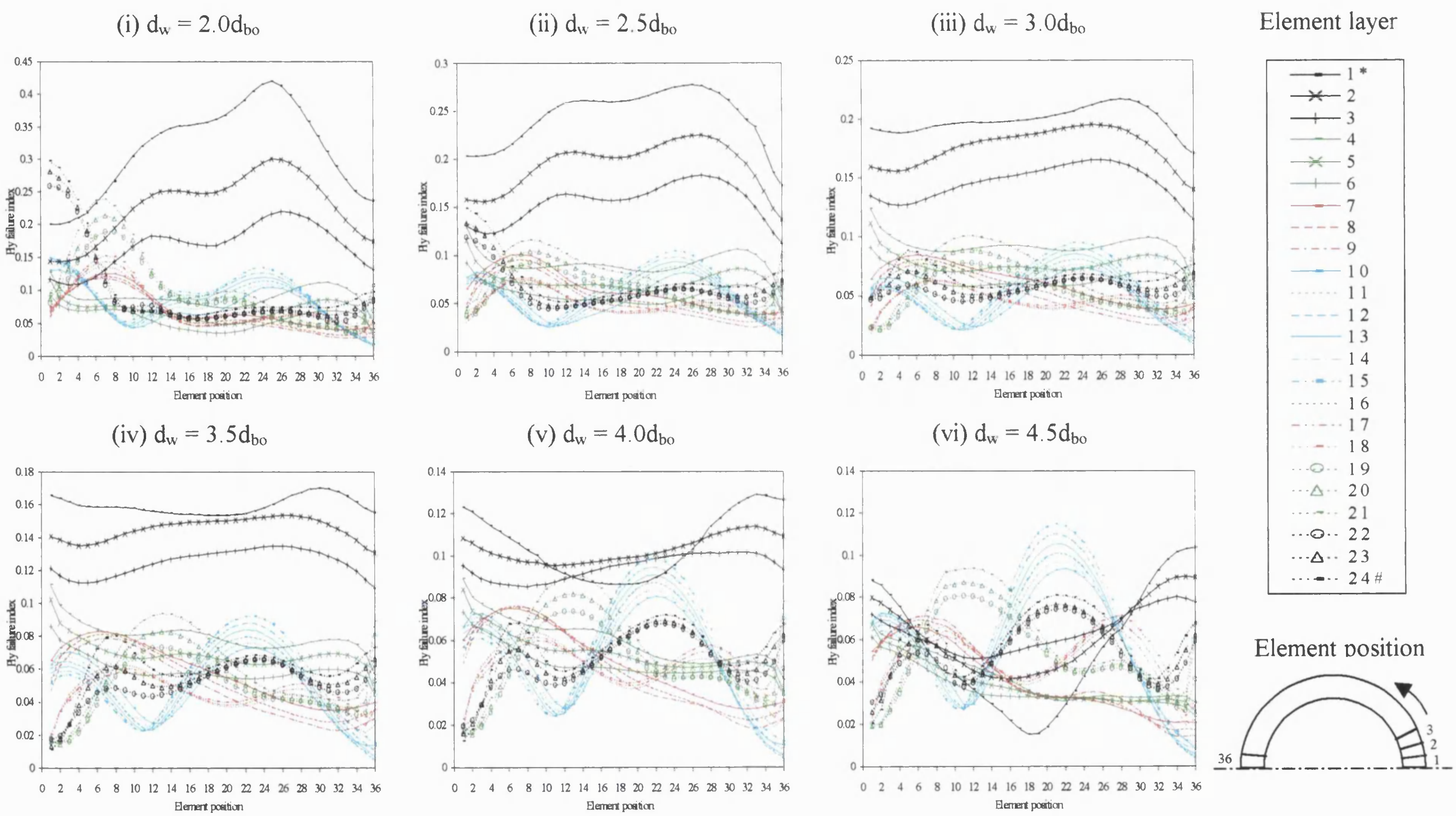

Figure 6.20 – Ply failure index plots for the outer lap – aluminium bolt with 4mm thick steel washer d_w=2.0d_{bo} to 4.5d_{bo} – Elements outside the washer edge - * = Outer surface, # = Laminate interface

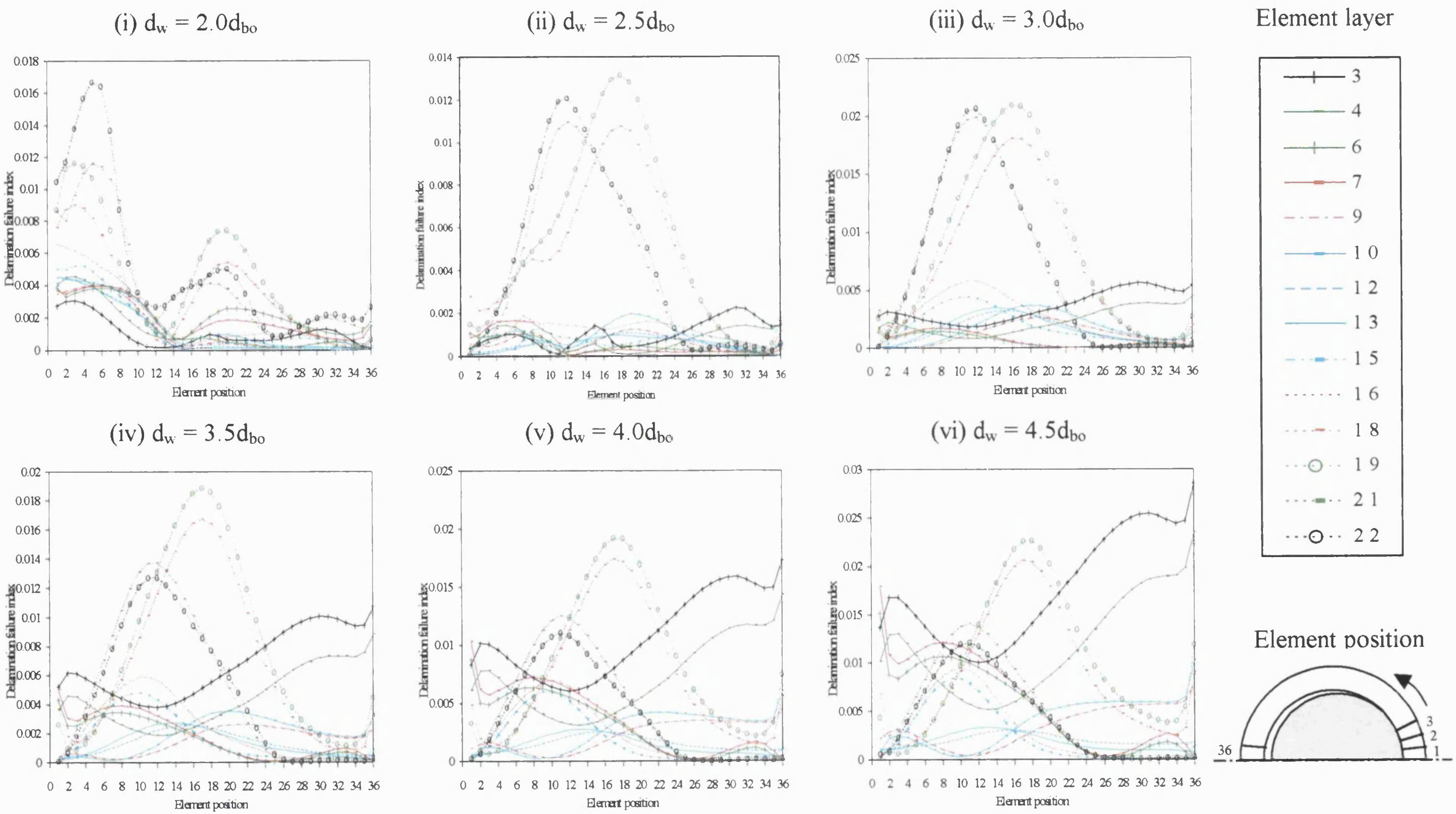

Figure 6.21 – Delamination failure index plots for the outer lap – aluminium bolt with 4mm thick steel washer d_w=2.0d_{bo} to 4.5d_{bo} – Elements around the hole boundary

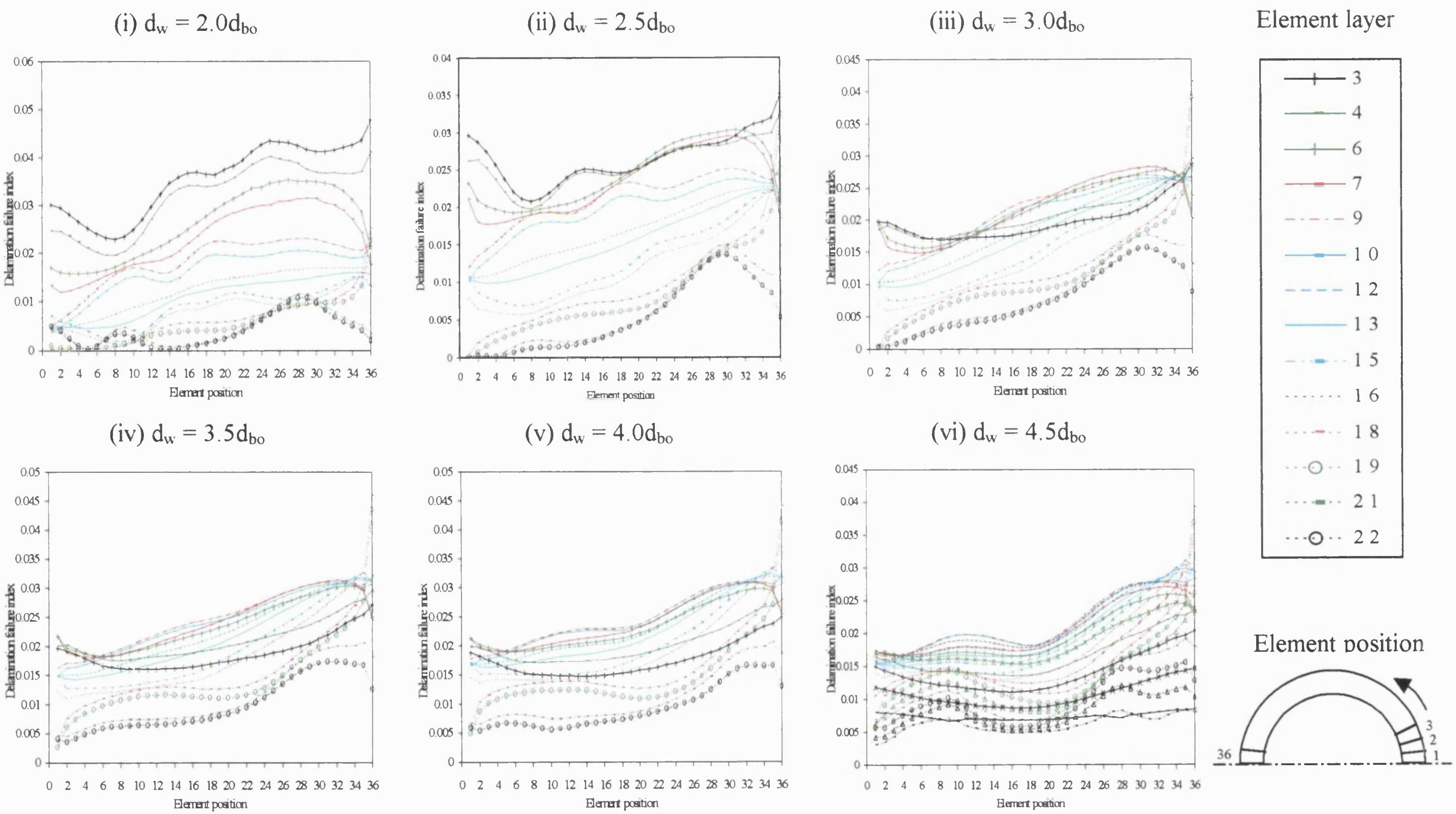

Figure 6.22 – Delamination failure index plots for the outer lap – aluminium bolt with 4mm thick steel washer d_w=2.0d_{bo} to 4.5d_{bo} – Elements inside the washer edge

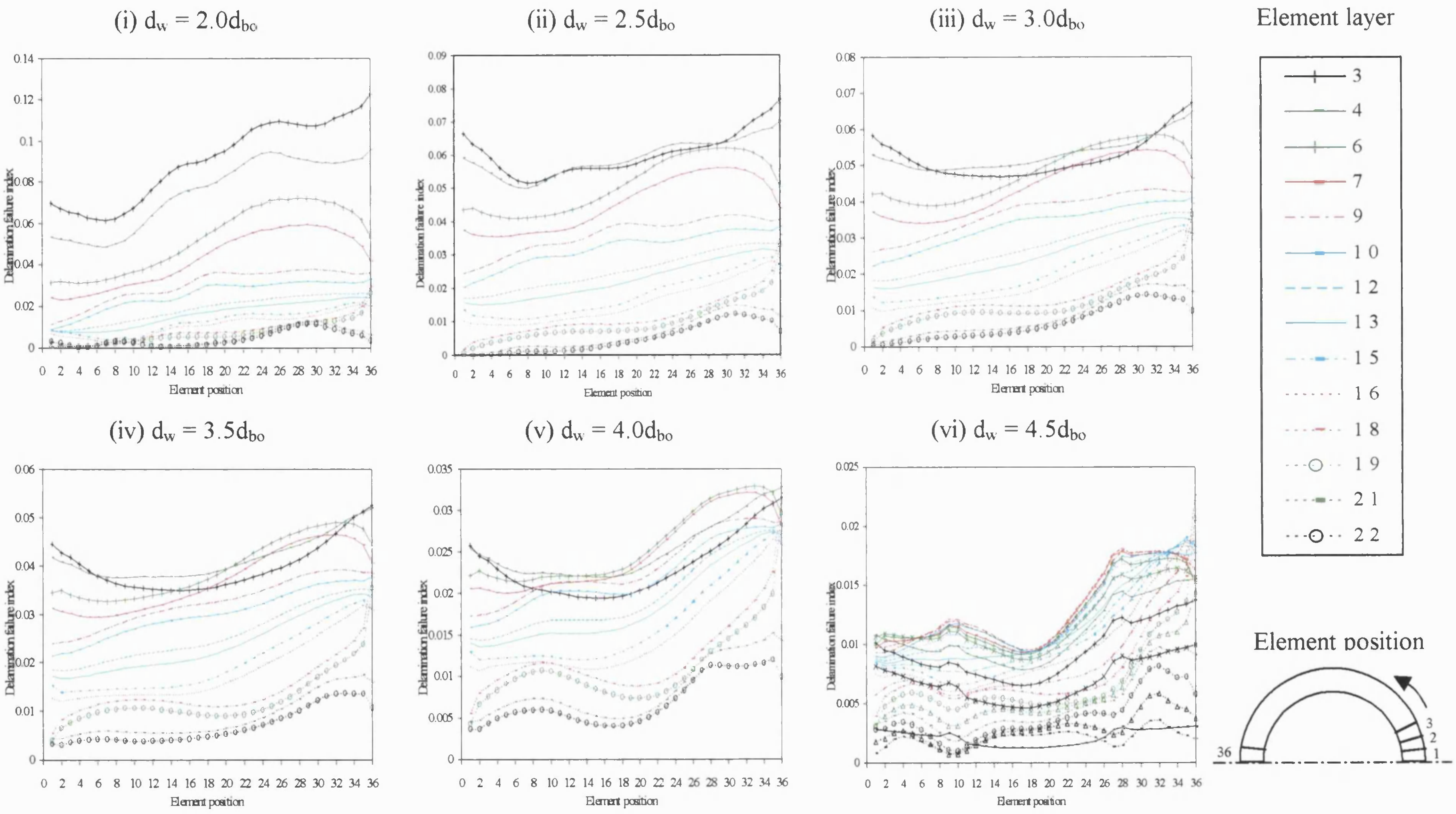

Figure 6.23 – Delamination failure index plots for the outer lap – aluminium bolt with 4mm thick steel washer d_w=2.0d_{bo} to 4.5d_{bo} – Elements outside the washer edge

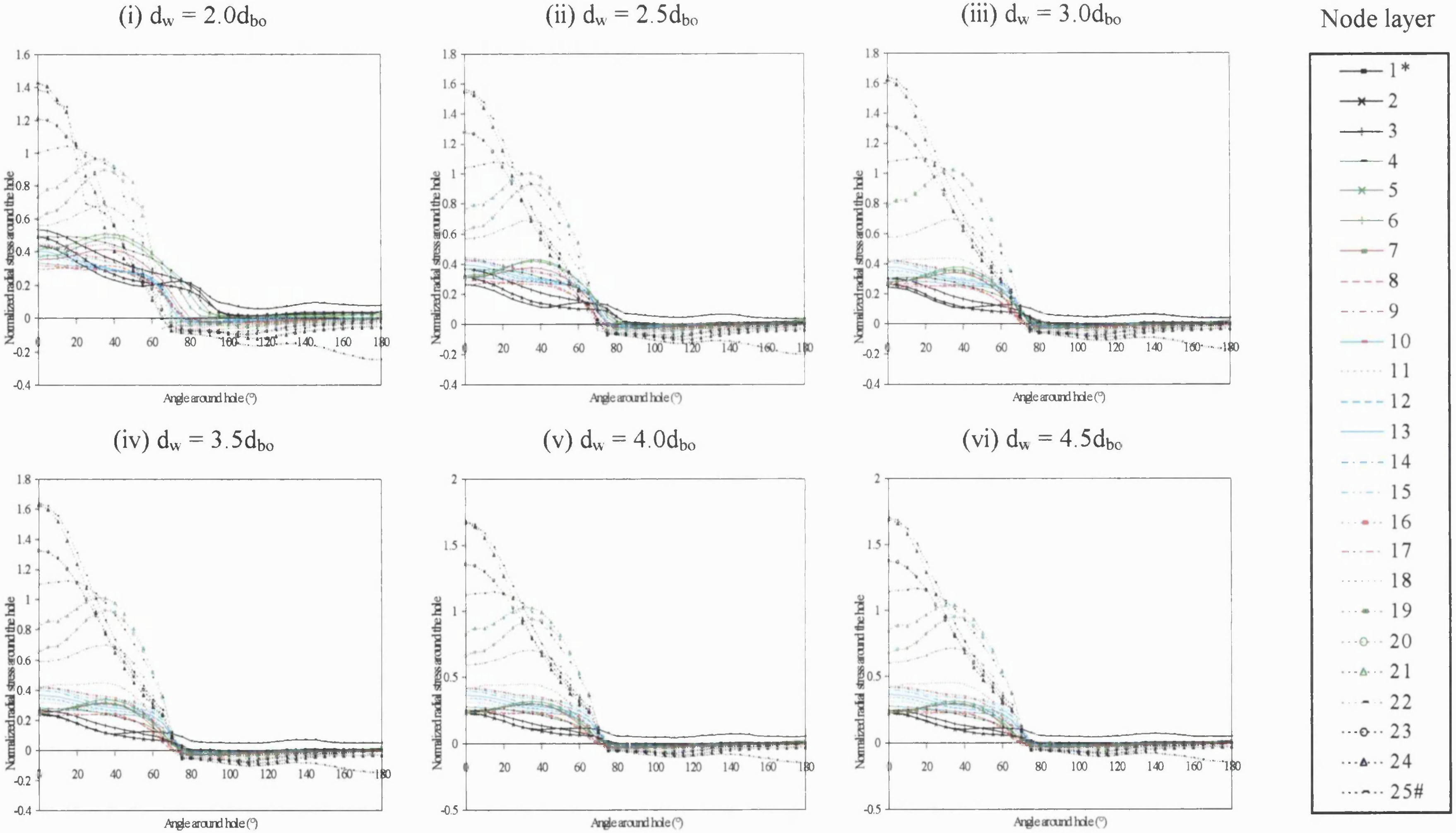

Figure 6.24 – Normalized radial stress around the hole boundary of the outer lap – aluminium bolt with 4mm thick steel washer d_w=2.0d_{bo} to 4.5d_{bo} – 6Nm Clamping - * = Outer surface, # = Laminate interface

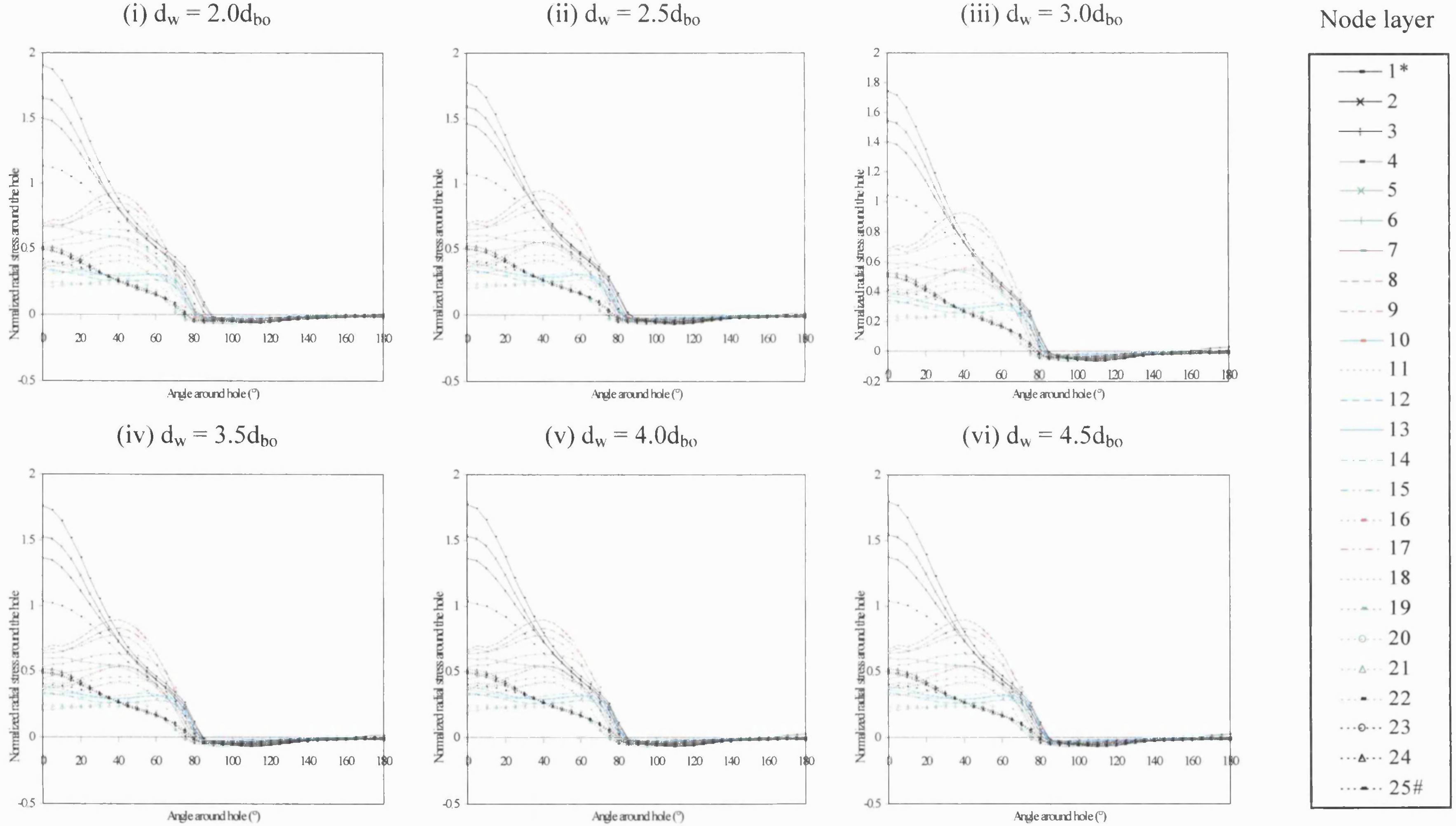

Figure 6.25 – Normalized radial stress around the hole boundary of the inner lap – aluminium bolt with 4mm thick steel washer d_w=2.0d_{bo} to 4.5d_{bo} – 6Nm clamping - * = Laminate interface, # = Laminate mid-plane

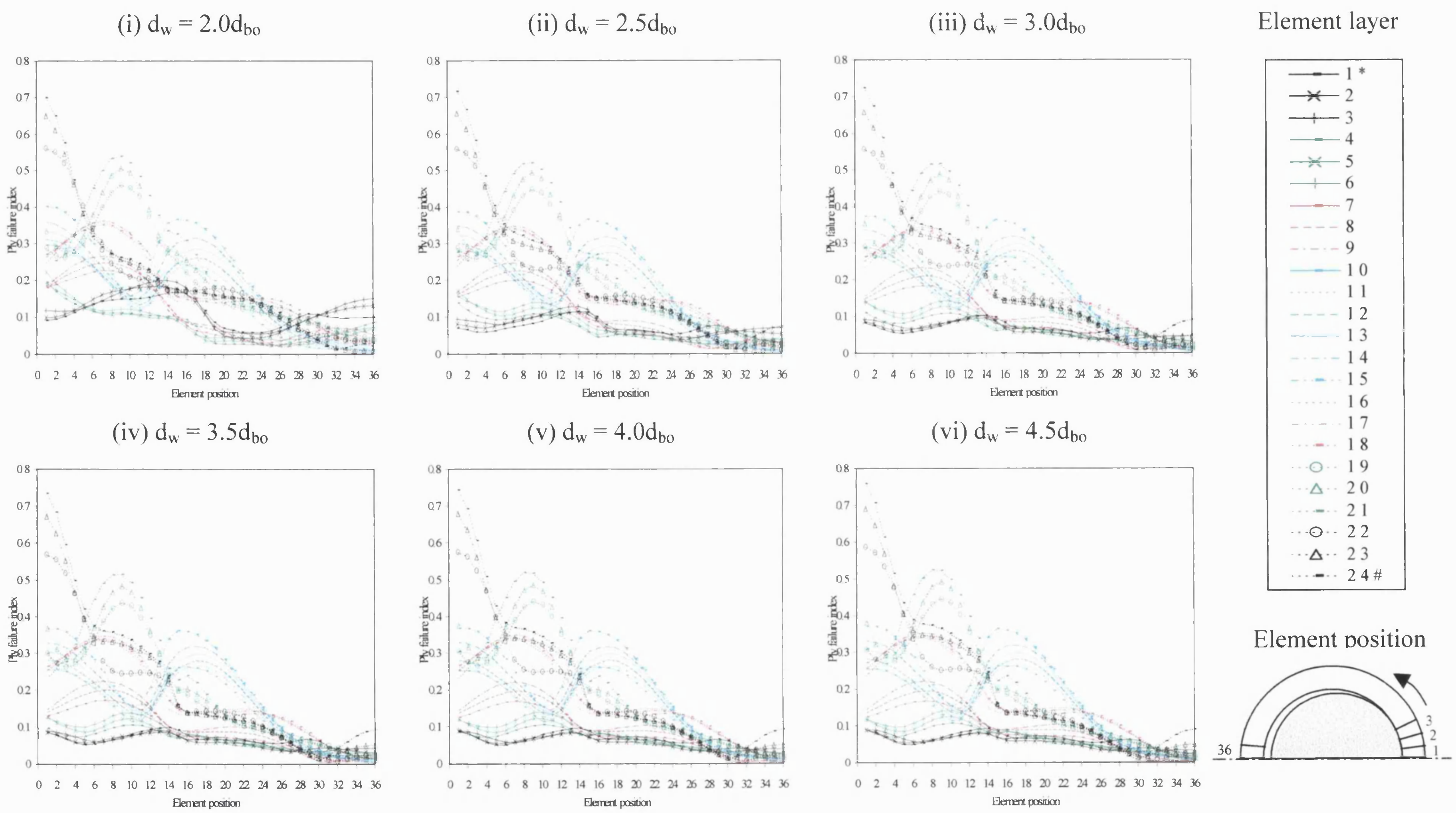

Figure 6.26 – Ply failure index plots for the outer lap – aluminium bolt with 4mm thick steel washer d_w=2.0d_{bo} to 4.5d_{bo} – Elements around the hole boundary – 6Nm Clamping - * = Outer surface, # = Laminate interface

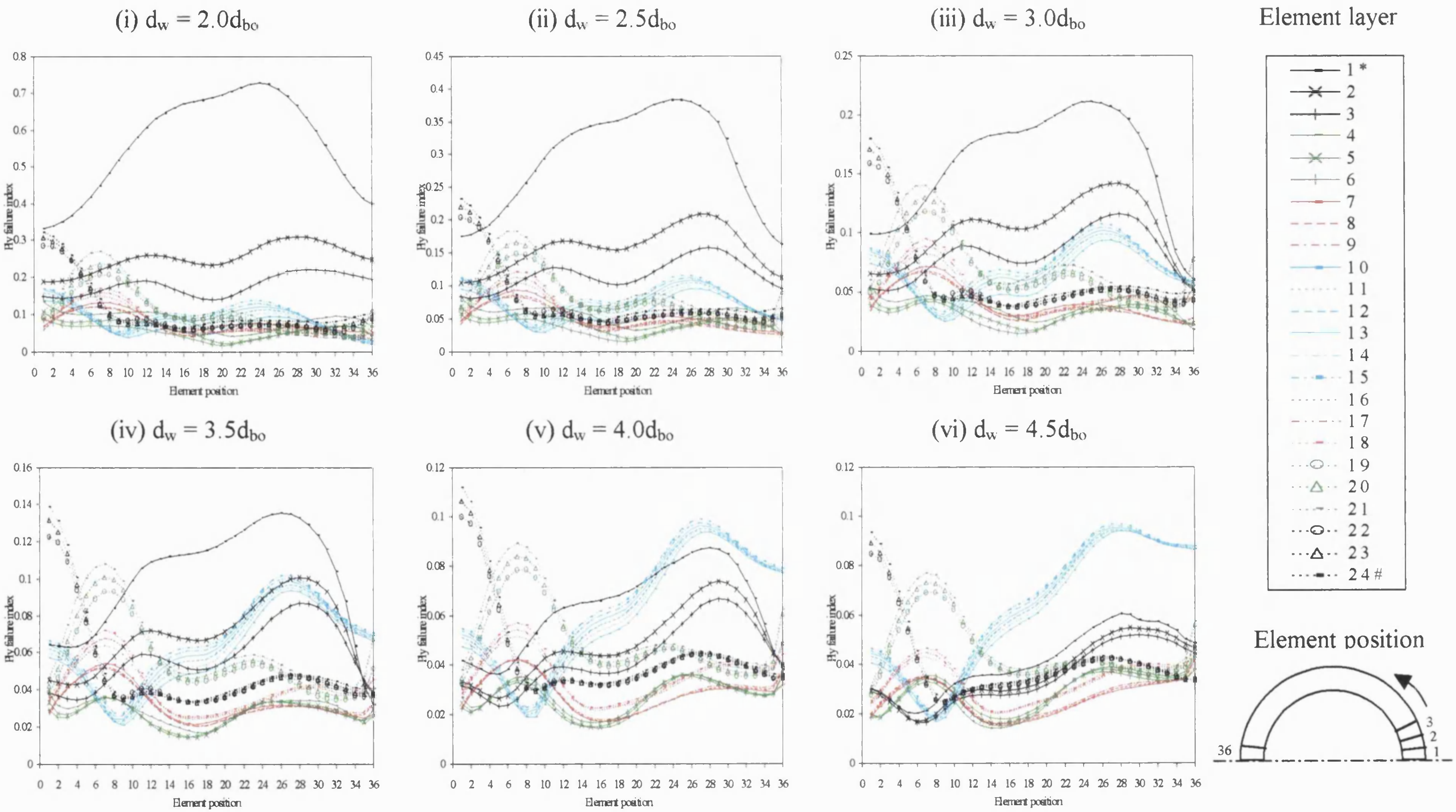

Figure 6.27 – Ply failure index plots for the outer lap – aluminium bolt with 4mm thick steel washer $d_w=2.0d_{bo}$ to $4.5d_{bo}$ – Elements inside the washer edge – 6Nm Clamping - * = Outer surface, # = Laminate interface

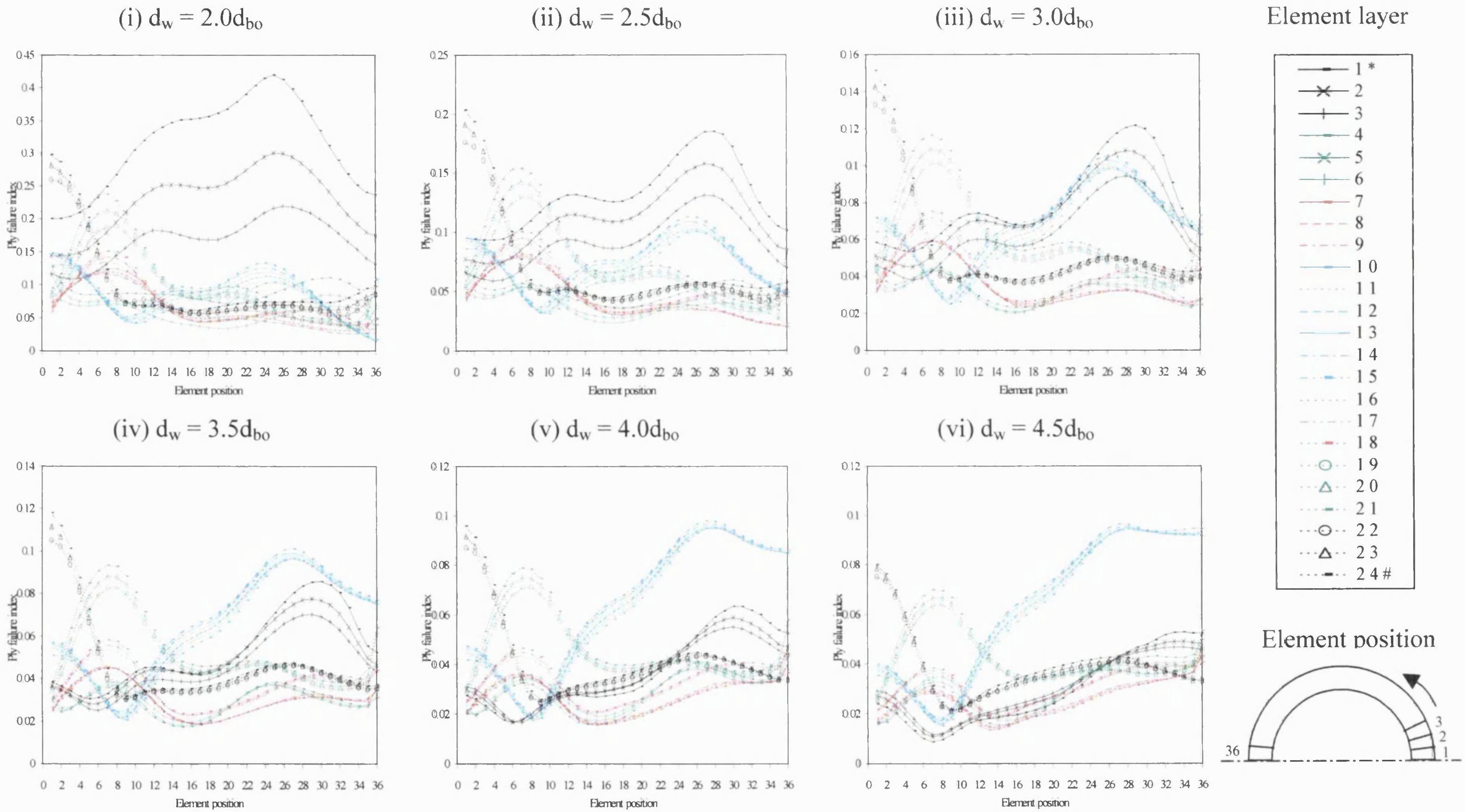

Figure 6.28 – Ply failure index plots for the outer lap – aluminium bolt with 4mm thick steel washer d_w=2.0d_{bo} to 4.5d_{bo} – Elements outside the washer edge – 6Nm Clamping - * = Outer surface, # = Laminate interface

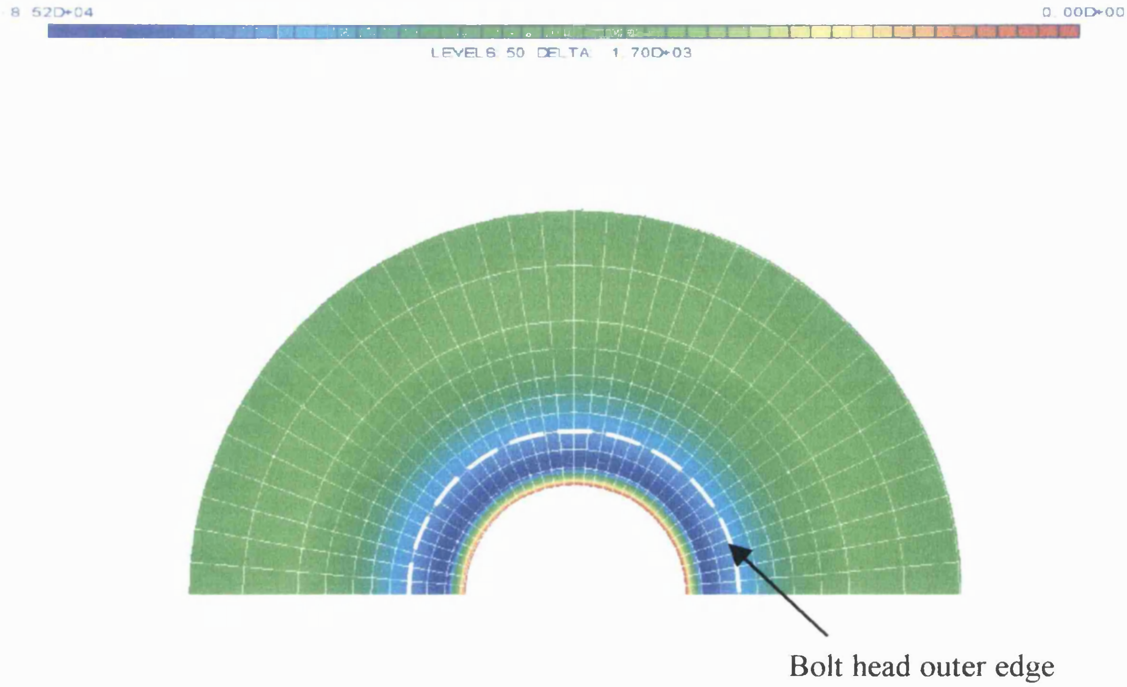

Figure 6.29 – Through thickness contact stress on outer lap under the washer
3mm thick ceramic (Al_2O_3) washer – $d_w = 3.5d_{bo}$

CHAPTER SEVEN

MULTIPLE FASTENER JOINTS

7.1 - INTRODUCTION

Many engineering applications require joints containing multiple fasteners, however a number of investigations carried out on such joints have assumed that the spacing between each fastener is large enough so that interaction does not occur. The aim of the investigation reported in this chapter is to assess the possible interaction of the stresses in such multiple fastener joints.

Using a typical double lap staggered bolt joint configuration, with quasi-isotropic GRP laminates, the effects of washer diameter and row spacing on the stress distribution within the laminate, and the location of failure were investigated. The washer diameter was varied between $2.0d_{bo}$ and $3.5d_{bo}$ for a joint configuration having a row spacing of 3.0d, a pitch distance of 6.0d and an end distance of 5.0d. The row spacing was then varied between 2.0d and 5.0d for washer diameters of $2.0d_{bo}$ and $3.5d_{bo}$.

Ply failure indices were calculated using the equation given by Tsai and Wu (1971) to provide details as to the location of ply failure, and the onset of delamination was determined using the criterion proposed by Ye (1988).

7.2 – METHOD

A double lap joint consisting of multiple bolts in a staggered arrangement was used in this investigation. Each lap was constructed from GRP with the quasi-isotropic stacking sequence $(0/45/\text{-}45/90)_s$, and the inner lap was made twice as thick as the outer lap. The inner lap was restrained from movement in any direction at the end furthest from the fastener and a tensile load equivalent to 2kN per bolt was applied to the outer lap, at the end furthest from the fastener. The laps were joined using an aluminium bolt and a ceramic washer assembly, with a bolt preload equivalent to a 50MPa clamping pressure. The washer outside diameter and the bolt row spacing were varied throughout the investigation. The physical representation of the joint can be seen in Figure 7.1, which also identifies the so-called outboard and inboard rows of the joint (for the outer lap the outboard row of bolts are those nearest the free edge of the laminate; conversely the inboard row is furthest from the free edge). The material properties used in this study are given in Table 7.1 with the corresponding strengths given in Table 7.2.

Table 7.1 – Material properties for each unidirectional lamina and each component of the fastener assembly

Material	E_{11} (GPa)	E_{22} (GPa)	E_{33} (GPa)	G_{12} (GPa)	G_{23} (GPa)	G_{31} (GPa)	ν_{12}	ν_{23}	ν_{31}
GRP[1]	31.8	10.2	7.14	2.14	2.14	2.14	0.328	0.199	0.045
Aluminium[1] T6061-T6	68.3	68.3	68.3	25.7	25.7	25.7	0.33	0.33	0.33
Ceramic (Al_2O_3)	371	371	371	143.8	143.8	143.8	0.29	0.29	0.29

Table 7.2 – Material strengths for each unidirectional lamina

Material	X_t (MPa)	X_c (MPa)	Y_t (MPa)	Y_c (MPa)	Z (MPa)	R (MPa)	S (MPa)
GRP	514[2]	240[2]	60[1]	70[2]	60[1]	60[1]	60[1]

[1] – Chutima (1996), [2] – Estimated from Hancox and Mayer (1994)

In the simulation the shaded portion shown in Figures 7.1a and 7.1b was modelled by applying appropriate nodal restraints along the planes of symmetry, as detailed in the previous chapters. It is therefore assumed that each bolt within a row carries the same load, which is representative of the centre of a large multiple fastener joint rather than a laminate of finite width. On the inner lap at the end furthest from the hole the nodes were restrained in all directions to simulate the clamped conditions, and on the outer lap at the end furthest from the hole, the nodes were loaded in the negative x- direction to simulate a load of 2kN on that portion of the laminate.

A replica technique of modelling was adopted, whereby the material axis for each element within a ply was oriented to provide the quasi-isotropic stacking sequence $(0/45/-45/90)_s$ for the laminate, as detailed in previous chapters. Suitable mesh refinement was applied by using three elements to represent the thickness of each ply and elements around the boundary of each hole subtended an angle of 9°.

The bolt was constructed as detailed in Chapter 5, whereby a short beam element connects the six-node solid linear wedge elements of the bolt shank, to the six-node wedge and eight-node solid linear brick elements of the bolt head. The temperature drop applied to the beam element of the bolt assembly was determined by using Equation 5.1 so that a bolt preload equivalent to a clamping pressure of 50MPa could be applied. This clamping pressure was maintained throughout the investigation.

From the work contained in Chapter 6 a good clamping condition was provided by the 4mm thick steel washer, however, the increased weight of the joint would be significant in commonly used multiple fastener configurations. An alternative material was considered and the contact stress between the washer and the laminate for a 3mm thick ceramic washer was found to be very similar to that provided by the 4mm thick steel washer. An aluminium oxide ceramic washer was therefore used throughout the subsequent investigation.

Contact was modelled using the global search facility available in the I-DEAS software, which placed a contact element between each pair of element faces likely to make contact during loading. A friction coefficient of $\mu=0.2$ was used at all contacting surfaces and the bolt was designed to be tight fitting within the hole.

Initially, the row spacing, pitch distance and end distance were maintained at 3.0d, 6.0d and 5.0d, respectively, while the washer diameter was varied between $2.0d_{bo}$ and $3.5d_{bo}$. In a subsequent analysis the pitch and end distance were maintained at the same level as in the previous investigation, while the row spacing was varied between 2.0d and 5.0d for washer diameters of $2.0d_{bo}$ and $3.5d_{bo}$.

The numbers of each type of element used for the components in this investigation are shown in Table 7.3, and a typical finite element mesh used in the investigation is shown in Figure 7.2.

Table 7.3 – Number of each type of element used throughout the investigation

Joint configuration	Laminates	Bolts			Washers	Total no. of elements including contact
	8-node solid linear brick element	6-node wedge element	8-node brick element	2-node beam element	8-node solid linear brick element	
s=2.0d $d_w=2.0d_{bo}$	26208	2040	360	2	600	32012
s=2.0d $d_w=3.5d_{bo}$	26208	2040	360	2	1080	32662
s=3.0d $d_w=2.0d_{bo}$	25152	2040	360	2	600	30900
s=3.0d $d_w=2.5d_{bo}$	25152	2040	360	2	840	31220
s=3.0d $d_w=3.0d_{bo}$	25152	2040	360	2	960	31380
s=3.0d $d_w=3.5d_{bo}$	25152	2040	360	2	1080	31540
s=4.0d $d_w=2.0d_{bo}$	28224	2040	360	2	600	34070
s=4.0d $d_w=3.5d_{bo}$	28224	2040	360	2	1080	34710
s=5.0d $d_w=2.0d_{bo}$	27408	2040	360	2	600	33240
s=5.0d $d_w=3.5d_{bo}$	27408	2040	360	2	1080	33880

7.3 – RESULTS AND DISCUSSION

For each investigation the radial and contact stress results on nodes around the hole boundary were extracted. Using these results relevant normalized radial stress graphs as well as bar charts showing the percentage of load transferred through each bolt were produced and are given in this section. Average element stresses around the hole boundary and washer edge were also extracted to provide ply and delamination failure index graphs at these locations. Also, stress contour plots have been provided where necessary. The method by which the nodal stress results were extracted and normalized has been described previously in Chapter 5.

7.3.1 – Investigation of varying the washer size

Throughout this investigation, the row spacing was maintained at 3.0d while the washer outside diameter was varied between $2.0d_{bo}$ and $3.5d_{bo}$. The normalized radial stress graphs as well as the ply failure and delamination index plots have been provided for the joint having a washer diameter of $2.0d_{bo}$. The maximum magnitudes of the failure indices and radial stress results obtained for the inner and outer laps, for the range of washer sizes used throughout this investigation, are summarized in Table 7.4.

Figure 7.3 presents the distribution of normalized radial stress around the hole boundary for the inboard and outboard hole of the outer lap for this joint configuration. Figure 7.3(i) shows that the normalized radial stress for the inboard hole is a maximum close to the interface with the inner lap, having a magnitude of 1.54. In contrast the maximum stress on the outboard hole, as shown in Figure 7.3(ii), is lower with a magnitude of 1.3. However, away from the laminate interface higher radial stress is encountered at the outboard hole rather than the inboard hole indicating slightly different contact conditions.

The distribution of normalized radial stress around the hole boundary for the inboard and outboard hole of the inner lap is presented in Figure 7.4. This figure shows that the maximum normalized radial stresses are approximately the same for both the inboard and outboard hole, having magnitudes of 1.88 and 1.84, respectively. These occur at the interface with the outer lap and are shown to be greater than the stresses recorded in the outer lap. The stresses at positions further away from the interface with the outer lap are shown to be slightly lower for the outboard hole than for the inboard hole, arising from different contact between each of the bolts and their respective holes.

The results in Table 7.4 demonstrate that the normalized radial stresses for the outer lap reduce to approximately 0.3 for a washer diameter of $3.0d_{bo}$ but then increase to approximately 0.5 for the largest diameter tested. This effect was observed for the single joint reported in Chapter 6 and is considered to arise from more significant bending in the larger diameter washers combined with higher bolt loads for constant clamping pressure.

The Tsai-Wu failure indices for both the inboard and outboard hole for elements around the hole boundary as well as the washer inside and outside edge for the outer lap are shown in Figure 7.5 for the washer diameter $2.0d_{bo}$. Clearly, the highest indices were recorded at elements around the hole boundary for both the inboard and outboard holes. Failure at the inboard hole seems to be more likely than at the outboard hole, possibly due to reduced bolt and laminate bending around this area, and hence high contact stresses are concentrated on the bearing plane between the bolt and laminate interface, although both indices are less than unity. However, away from the hole boundary the indices are approximately the same for each hole and reduce with increased distance from the hole boundary.

The results in Table 7.4 show that the highest Tsai-Wu failure indices are obtained on the inboard hole rather than the outboard hole for all the washer diameters tested except the largest ($d_w = 3.5d_{bo}$), however, the difference in magnitude is small for this washer size. The failure indices also seem to reduce with increased washer size except for the largest diameter tested. It is also apparent that for washer diameters of $2.5d_{bo}$ and $3.0d_{bo}$, the indices obtained for elements inside the washer edge are higher than at the hole boundary, as concluded for single bolt configuration reported in Chapter 6. As the graphs for this area of the laminate show maximum indices around the net tension plane, this suggests a catastrophic failure mode would result for either bolt if the loading is increased for these joint configurations.

The failure indices for the smallest washer diameter on the inner lap, shown in Figure 7.6, indicate that the highest value was also obtained at the hole boundary for this joint configuration, with the magnitude of the indices reducing with increased distance from the hole boundary. The maximum index for the inboard hole is slightly lower for the inner lap than for the outer lap, with a magnitude of 0.62 compared to 0.8. However, the maximum index for the outboard hole is slightly larger for the inner lap than the outer lap, with a magnitude of 0.7 compared to 0.66.

The magnitude of the maximum failure indices and radial stress results for the inner lap given in Table 7.4, show that as the washer diameter is increased the indices reduce to an insignificant level, however, a slight increase occurs as the diameter is increased from $3.0d_{bo}$ and $3.5d_{bo}$ on the outboard hole. The highest indices on the inner lap are obtained on the outboard hole rather than the inboard irrespective of the washer diameter.

The delamination indices for the outer lap are shown in Figure 7.7. It can clearly be seen that the magnitudes are very small for reasons discussed in the previous chapters, however, the elements outside the washer edge are an order of magnitude greater than at the hole boundary close to the outer surface of the outer lap. The results in Table 7.4 indicate that the delamination indices outside the washer edge reduce with increasing washer size until they are at approximately the same level as those obtained inside the washer edge, for a washer diameter of $3.5d_{bo}$. The highest magnitude of average delamination index was obtained for a washer diameter of $2.0d_{bo}$, and the lowest was obtained for the largest washer size tested, indicating that the larger washers reduce the likelihood of delamination as clamping is spread over a larger area.

The delamination indices obtained for the inner lap are shown in Figure 7.8. The maximum index is shown to be slightly lower for the outboard hole than the inboard hole for elements around the hole boundary due to different contact conditions. Also, for the washer size used in this investigation the indices inside the washer edge are higher than on the hole boundary or outside the washer edge. It is observed that for elements either side of the washer edge, the outboard hole has the higher indices. The indices obtained for the inner lap are shown to be higher than the outer lap for elements around the hole boundary but smaller for elements inside and outside the washer edge. Results in Table 7.4 indicate that the delamination index for the inner lap reduces with increasing washer diameter to insignificant magnitudes.

These results indicate that delamination is more likely to occur in the outer lap for a joint configuration with a standard washer size, and specifically at the outer edge of the washer around the outboard hole.

The bar chart shown in Figure 7.9 presents the results for the load transferred from the outer lap to each bolt and shows clearly for washer sizes greater than $2.5d_{bo}$, that there is no load transferred through the bolt shank. This is not the case for smaller washer diameters where approximately 53.5% of the total load for a washer diameter of $2.0d_{bo}$, and approximately 13.8% for a washer diameter of $2.5d_{bo}$ is transferred by the bolt. As there is likely to be better contact between the laminates around the inboard hole, due to less out of plane deformation, the load carried through frictional clamping is higher in this region and hence the percentage of load transferred through bearing is lower than for the outboard bolt.

The contour plots shown in Figure 7.10 demonstrate the effects of changing the washer size on the through thickness contact stress at the laminate interface for multiple fastener joints having a constant row spacing of 3.0d. From Figure 7.10(i) it can be seen that a washer diameter of $2.0d_{bo}$ gives the smallest area of contact at the laminate interface, however, a slightly larger area of contact is shown for the inboard hole compared to the outboard hole. This latter observation also applies as the washer size is increased, although naturally the area of contact also increases. As the washer size exceeds $3.0d_{bo}$ the contact area increases significantly, so that contact between the laminates is increased in the region between the fasteners.

7.3.2 – Investigation of varying the row spacing with a washer diameter of $2.0d_{bo}$

In this investigation the washer diameter was maintained at $2.0d_{bo}$, and the row spacing was increased between 2.0d and 5.0d. Figures showing the normalized radial stress as well as the Tsai-Wu and delamination failure indices have been included for the most important results. The maximum stress and failure index results obtained for each analysis in this investigation have also been included in Table 7.5.

Figure 7.11 shows the variation of normalized radial stress around the hole boundary of the inboard hole in the outer lap for the range of row spacings tested. This figure demonstrates that the radial stress, equivalent to approximately 1.55, remains virtually unaffected as the row spacing is increased except for the largest row spacing tested where the stress reduces to 1.31. The results in Table 7.5 show a similar effect for the outboard hole, whereby a slightly reduced stress is obtained for the largest row spacing tested, however, the stresses are lower than the inboard row.

The variation in normalized radial stress at the inboard hole of the inner lap, affected by changing the row spacing, is shown in Figure 7.12. This figure shows that the maximum radial stress remains virtually constant with a magnitude of approximately 1.85 at the interface with the outer lap. Further, the results presented in Table 7.5 indicate that apart from the hole boundary of the inner lap for s = 2.0d, the stresses are higher for the inboard hole than the outboard hole, for both the inner and outer laps, although this is only marginal in the former. This may arise from small out of plane deformation at the end of the outer lap as the load is applied, hence the radial stress is lower but spreads more uniformly as the bolt bends. The area of the laminate around the inboard hole does not deform in the same manner due to the presence of the outboard fastener, and hence a high stress exists at the laminate interface due to bearing.

Figure 7.13 shows the variation in Tsai-Wu ply failure index as the row spacing is increased for the elements around the inboard hole boundary of the outer lap. From this figure it can be seen that the maximum index occurs at the interface with the inner lap and increases marginally for the joint geometries having s = 3.0d and s = 4.0d. A further increase in row spacing leads to a reduction in the index to approximately 0.75. Figure 7.14 shows that a similar effect also occurs for elements in the same row of the inner lap, although the magnitudes are slightly smaller.

The failure indices for the outboard hole, shown in Table 7.5, demonstrate that the magnitudes are lower than the inboard hole for the outer lap, however, the reverse is observed for the holes in the inner lap. The indices around the outboard hole in the outer lap increase when s is changed from 3.0d to 4.0d, and then decrease for the largest row spacing tested, exhibiting a similar response as observed with the inboard hole. For the outboard hole in the inner lap the index remains constant, only reducing slightly for the largest row spacing tested. In summary the maximum index occurs in elements around the inboard hole boundary of the outer lap, adjacent to the laminate interface, for row spacings of 3.0d and 4.0d. This is considered to arise since the laminate does not bend with the inboard fastener due to constraints imposed by the outboard fastener.

Further, the results in Table 7.5 indicate that the indices for elements inside and outside the washer edge for the inner lap are much lower than at the hole boundary and remain constant as the row spacing is increased. However, the outer lap exhibits a different response, whereby, for a row spacing of 2.0d, the indices for elements inside the washer edge are much lower than at the hole boundary but for larger row spacings the indices in this region increase. In particular for s = 3.0d to 5.0d the indices for elements inside the washer edge are very similar to those around the hole boundary, hence failure may result in modes other than bearing as the maximum indices were recorded near the net-tension plane. The lower indices inside the washer edge for the smaller row spacing may arise from the relatively larger contact area created by the interaction between the fastener assemblies. The indices outside the washer also continue to rise with increasing row spacing, however the magnitude is not as large as inside the washer edge for the range of joint geometries tested.

Figure 7.15 shows the delamination indices obtained for elements inside the washer edge for the inboard hole in the outer lap. A row spacing of 2.0d shows the maximum index at an angle of approximately 126° from the bearing plane, having a value of 0.11. As the row spacing is increased the delamination indices reduce significantly, with the position of maximum index changing to the bearing plane, close to the application of the tensile load. From the results shown in Table 7.5 it can be seen that with a row spacing greater than 2.0d the delamination index obtained outside the washer edge is similar to the value obtained inside the washer edge for a geometry of s = 2.0d. This value increases slightly as the row spacing increases, possibly due to the reduced laminate contact between the fasteners. The highest index of 0.122 was obtained for elements outside the washer edge of the outboard hole for the largest row spacing investigated. The indices calculated for the inner lap are smaller than the values recorded for the outer lap, except for elements around the hole boundary, however, the magnitudes at this position are very small.

As the highest index for the row spacing 2.0d was obtained for elements inside the washer edge, failure in this joint configuration may be more difficult to detect, however, this joint configuration seems to be the least likely to fail.

A bar chart showing the percentage of the load transferred from the outer lap to each fastener is given in Figure 7.16. The highest load transferred through bearing, considering both bolts in the joint, is for a row spacing of 2.0d and 3.0d, although the difference for the other geometries is very small. As discussed in the previous section, the greatest proportion of the bearing load is carried by the outboard hole rather than the inboard hole, regardless of the row spacing used, due to the fastener and plate bending together resulting in contact over a greater area.

The contact stress contour plots of the inner lap, shown in Figure 7.17, demonstrates the influence of row spacing on the contact between the laminates. The joint configurations with smaller row spacings show a higher contact area due to fastener interaction. As the row spacing is increased the area of contact resembles that developed by single fastener joints suggesting that the strength of these configurations may be predicted from analysis of such joint types.

Figure 7.18 demonstrates that by using the smallest row spacing clamping exerts a through thickness stress to the whole area between the bolts of the inner lap. With the largest row spacing it can be seen that there is a 'flat spot' where the clamping stress is not transferred to a section of the inner lap between the outboard and inboard bolts. In this case there is no fastener interaction and no load transferred through friction between the plates.

7.3.3 – Investigation of row spacing with a washer diameter of $3.5d_{bo}$

In this investigation the washer diameter was maintained at $3.5d_{bo}$, and the row spacing was increased between 2.0d and 5.0d. Figures showing the normalized radial stress as well as Tsai-Wu and delamination failure indices have been included for the most relevant results. The maximum stress and failure index values obtained from each analysis in this investigation have been included in Table 7.6.

The distribution of normalized radial stress around the inboard hole boundary of the outer lap can be seen in Figure 7.19. By comparing the results from this figure with those presented in the previous section, it can be seen that the larger washer moves the position of maximum stress from the laminate interface to the outer surface of the outer lap, as concluded for the single bolt joint configuration reported in Chapter 6, whereby the stress at this position is largely determined by the clamping and frictional effects from the washer. As the row spacing is increased the normalized radial stress increases marginally and then reduces for row spacing geometries greater than 3.0d.

Table 7.6 shows that the outboard hole has a higher stress than the inboard hole for s = 2.0d, s = 4.0d and s = 5.0d. The highest stress was obtained for the outboard hole with the largest row spacing tested. The difference between values obtained by the inboard hole and outboard hole is also greatest for this row spacing, with the value obtained at the outboard hole of 0.86 compared to 0.324 for the inboard hole. This effect is very different to that observed for the joint having a $2.0d_{bo}$ washer diameter, whereby the maximum stress is obtained on the inboard hole.

Figure 7.20 shows the normalized radial stress distribution around the hole in the same row but for the inner lap. These results are lower than the outer lap, as expected from the single bolt joint configuration. From Table 7.6, it can be seen that the outboard hole has lower stresses than the inboard for the joint geometries tested and there is little change in magnitude as the row spacing is varied. It may also be observed that the stresses are higher on the outer lap than the inner lap as the stresses arise from the friction and clamping under the washer area.

The Tsai-Wu ply failure indices for elements around the inboard hole boundary of the outer lap are shown in Figure 7.21. This figure shows similar curves for the range of row geometries tested, however, the magnitude of the indices on the bearing plane at the outer surface of the outer lap increase on both sides of the hole, resulting in a maximum index of 0.37 as the row spacing is increased to 5.0d. The results in Table 7.6 show that the highest failure index obtained by these joint configurations was 0.467, which occurred on the outboard hole boundary of the outer lap for the largest row spacing tested.

Figure 7.22 shows the ply failure indices around the inboard hole boundary in the inner lap. The highest indices were obtained at an angle of 90° around the hole boundary and as the row spacing increased, the value was reduced from 0.19 to 0.11, approximately. So that for the largest row spacing tested the index at this angular position is approximately the same as that on the bearing plane, indicating that the possibility of tensile failure is reduced as the row spacing is increased.

From Table 7.6 it can be seen for both the inner and outer laps the highest failure indices were obtained on the outboard fastener hole, and for each geometry the index is higher on the outer lap than the inner lap. Further, it can be seen that the indices obtained inside the washer edge are similar to those obtained at the hole boundary, except for the largest row spacing tested, where the indices obtained on the outer lap inside the washer edge are lower than at the hole boundary.

Figure 7.23 shows the delamination indices for elements inside the washer edge of the inboard bolt for the outer lap. The highest index for each joint configuration is shown to be close to the interface with the inner lap at an angle of 180° around the hole. The magnitude of maximum index remains approximately constant as the row spacing is increased. However, for a row spacing of 2.0d the indices for elements between an angle of approximately 25° and 90° are lower than for the remainder of the elements, possibly due to interference from the clamping on the outboard hole. Although not shown here the delamination indices for the outboard hole are also lower for elements between 90° and 140° around the washer edge. This shows that the higher clamping area developed through fastener interaction may be beneficial for this type of joint.

The results shown in Table 7.6 indicate that the indices obtained for elements around the inboard hole boundary of the outer lap are lower (approximately half) than those obtained inside the washer edge. The indices obtained for the inner lap are much smaller and around the hole boundary the magnitudes are approximately equal to those obtained inside the washer edge.

Figure 7.24 shows the contact stress between the outer lap and the inner lap for each of the joint geometries tested in this investigation. Each of the contour plots shows that good clamping is transferred to the inner lap. For the largest row spacing there does not seem to be any interaction between the clamping of each fastener, whereas for the smaller row spacing a larger contact area exists between the laminates. It can also be seen that less contact occurs around the outboard hole compared to the inboard hole due to fastener and outer lap deformation at this location.

This investigation shows that the row spacing does not seem to affect the radial stress and ply failure indices of the joint very significantly. The magnitudes of the results are lower than those provided by the joint configurations with a smaller washer, and due to the increased clamping area, there does not seem to be any load transferred through bearing between the bolts and their respective holes.

7.4 – CONCLUDING REMARKS

From the results reported in the previous section, the following conclusions can be drawn from the geometric parameters investigated.

7.4.1 - Investigation of varying the washer size

For a multiple bolt double lap GRP joint with a clamping preload equivalent to a pressure of 50MPa and a row spacing of 3.0d, an increase in washer diameter was shown to increase the joint strength as with a single bolt joint. It is also evident that the load is not evenly distributed between the fastener assemblies in a multiple fastener joint, and in this investigation it was concluded that less load is transferred through bearing on the inboard hole compared to the outboard hole, due to better clamping conditions from fastener interaction and deformation of the outer lap with the outboard fastener. Further, it is apparent that for washer sizes greater than $2.5d_{bo}$, there is no load carried through bearing at either hole boundary, hence the entire load is carried through frictional clamping which can affect the failure mode.

7.4.2 – Investigation of varying the row spacing with a washer diameter of $2.0d_{bo}$

For a multiple bolt GRP laminate double lap joint with a clamping preload equivalent to a pressure of 50MPa applied to a $2.0d_{bo}$ diameter washer, varying the row spacing does not have a significant effect on the radial stress distribution and hence joint strength. This is thought to be due to a high proportion of the load being carried through clamping by the stiff washer, thus the position of the hole is less important. However, a slightly improved joint strength was observed for row spacing geometries of 2.0d and 5.0d compared to 3.0d and 4.0d. The smallest row spacing would provide the most appropriate joint configuration when using a standard washer size of $2.0d_{bo}$ if a reduction in the likelihood of net-tensile failure is sought.

7.4.3 – Investigation of varying the row spacing with a washer diameter of $3.5d_{bo}$

For a multiple bolt GRP laminate double lap joint, with a clamping preload equivalent to 50MPa pressure applied to a $3.5d_{bo}$ diameter washer, varying the row spacing affects the joint strength even less than for the joint with a smaller diameter washer. This arises as none of the load is carried through bearing and hence the strength is not as dependent upon the position of the holes. However, with a larger washer the strength is improved, irrespective of the row spacing, and the likelihood of tensile failure mode is reduced if a larger row spacing is adopted.

The results presented in this chapter indicate that the joint strength may be marginally improved by having a small row spacing (s = 2.0d) for a standard washer size ($2.0d_{bo}$). Alternatively, the joint strength may be affected to a greater extent by utilizing a large washer with any row spacing up to 5.0d. However, in this case failure may occur around the tension plane for joints having minimum row spacing.

JOINT CONFIGURATION		RADIAL STRESS		TSAI-WU FAILURE INDEX						DELAMINATION FAILURE INDEX					
				Outer Lap			Inner Lap			Outer Lap			Inner Lap		
Washer diameter	Bolt row	Outer Lap	Inner Lap	Hole boundary	Inside washer edge	Outside washer edge	Hole boundary	Inside washer edge	Outside washer edge	Hole boundary	Inside washer edge	Outside washer edge	Hole boundary	Inside washer edge	Outside Washer edge
$2.0d_{bo}$	inboard	1.54	1.88	0.8	0.63	0.35	0.62	0.3	0.25	0.01	0.039	0.105	0.021	0.025	0.022
	outboard	1.30	1.84	0.66	0.65	0.384	0.7	0.303	0.25	0.013	0.0355	0.116	0.018	0.029	0.026
$2.5d_{bo}$	inboard	0.25	0.86	0.36	0.6	0.23	0.246	0.155	0.114	0.019	0.0435	0.065	0.012	0.013	0.01
	outboard	0.52	0.74	0.273	0.6	0.224	0.366	0.157	0.157	0.014	0.0425	0.07	0.0176	0.015	0.0067
$3.0d_{bo}$	inboard	0.265	0.22	0.34	0.42	0.182	0.134	0.14	0.1	0.031	0.0436	0.065	0.01	0.0084	0.0069
	outboard	0.33	0.21	0.264	0.43	0.185	0.267	0.14	0.15	0.026	0.0417	0.064	0.0177	0.011	0.008
3.5_{bo}	inboard	0.56	0.28	0.3	0.323	0.17	0.129	0.146	0.11	0.023	0.045	0.05	0.01	0.01	0.0087
	outboard	0.48	0.14	0.352	0.334	0.143	0.297	0.16	0.16	0.0227	0.045	0.047	0.0176	0.012	0.0079

Table 7.4 – Maximum normalized radial stress and failure index values – multiple bolt model
row spacing = 3.0d – washer diameter = $2.0d_{bo}$ to $3.5d_{bo}$

JOINT CONFIGURATION		RADIAL STRESS		TSAI-WU FAILURE INDEX						DELAMINATION FAILURE INDEX					
				Outer Lap			Inner Lap			Outer Lap			Inner Lap		
Row spacing	Bolt row	Outer Lap	Inner Lap	Hole boundary	Inside washer edge	Outside washer edge	Hole boundary	Inside washer edge	Outside washer edge	Hole boundary	Inside washer edge	Outside washer edge	Hole boundary	Inside washer edge	Outside Washer edge
2.0d	inboard	1.56	1.83	0.78	0.376	0.243	0.6	0.245	0.2	0.011	0.11	0.0437	0.019	0.022	0.0184
	outboard	1.24	1.86	0.625	0.384	0.241	0.7	0.26	0.21	0.012	0.116	0.043	0.015	0.0256	0.02
3.0d	inboard	1.54	1.88	0.8	0.63	0.35	0.62	0.3	0.25	0.01	0.039	0.105	0.021	0.025	0.022
	outboard	1.30	1.84	0.66	0.65	0.384	0.7	0.303	0.25	0.013	0.0355	0.116	0.018	0.029	0.026
4.0d	inboard	1.54	1.89	0.806	0.63	0.373	0.63	0.3	0.256	0.01	0.0383	0.108	0.0211	0.0251	0.0226
	outboard	1.36	1.81	0.682	0.65	0.4	0.7	0.3	0.24	0.013	0.0332	0.119	0.0161	0.0296	0.026
5.0d	inboard	1.31	1.84	0.75	0.619	0.416	0.626	0.29	0.25	0.01	0.034	0.116	0.024	0.023	0.021
	outboard	1.2	1.69	0.64	0.624	0.415	0.677	0.282	0.23	0.014	0.028	0.122	0.026	0.027	0.024

Table 7.5 – Maximum normalized radial stress and failure index values – multiple bolt model
row spacing = 2.0d to 5.0d – washer diameter = $2.0d_{bo}$

JOINT CONFIGURATION		RADIAL STRESS		TSAI-WU FAILURE INDEX						DELAMINATION FAILURE INDEX					
				Outer Lap			Inner Lap			Outer Lap			Inner Lap		
Row spacing	Bolt row	Outer Lap	Inner Lap	Hole boundary	Inside washer edge	Outside washer edge	Hole boundary	Inside washer edge	Outside washer edge	Hole boundary	Inside washer edge	Outside washer edge	Hole boundary	Inside washer edge	Outside Washer edge
2.0d	inboard	0.554	0.283	0.296	0.3	-	0.187	0.13	-	0.029	0.044	-	0.014	0.01	-
	outboard	0.578	0.144	0.39	0.34	-	0.32	0.15	-	0.023	0.05	-	0.022	0.013	-
3.0d	inboard	0.56	0.277	0.3	0.323	0.17	0.129	0.146	0.11	0.023	0.045	0.05	0.011	0.01	0.009
	outboard	0.48	0.14	0.352	0.334	0.143	0.297	0.16	0.16	0.023	0.045	0.047	0.018	0.012	0.008
4.0d	inboard	0.465	0.274	0.284	0.32	-	0.11	0.149	-	0.02	0.049	-	0.01	0.01	-
	outboard	0.491	0.15	0.338	0.337	-	0.29	0.157	-	0.023	0.045	-	0.016	0.012	-
5.0d	inboard	0.324	0.276	0.37	0.26	-	0.11	0.146	-	0.022	0.04	-	0.011	0.01	-
	outboard	0.86	0.195	0.467	0.275	-	0.29	0.175	-	0.026	0.043	-	0.018	0.012	-

Table 7.6 – Maximum normalized radial stress and failure index values – multiple bolt model row spacing = 2.0d to 5.0d – washer diameter = $3.5d_{bo}$

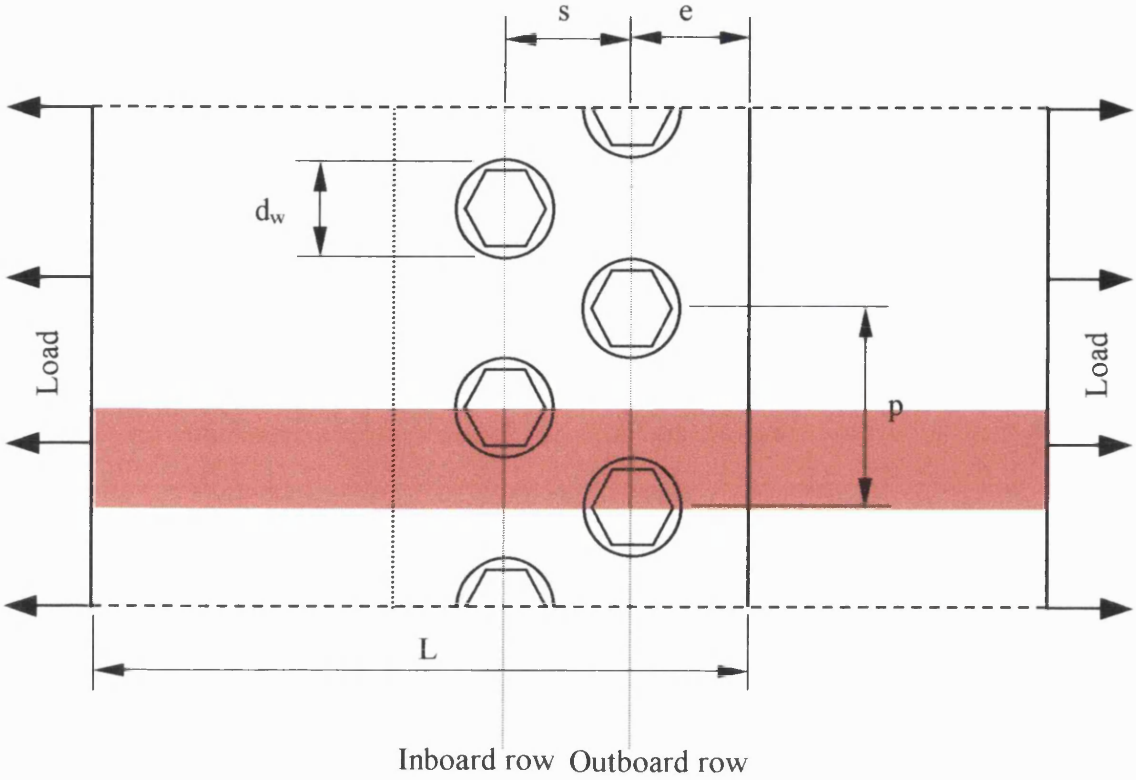

Figure 7.1a – Physical representation of the multiple fastener joint (front view)

d_{bo} = 6.35mm (≡d)	p = 38.1mm (≡6.0d)	L = 95.25mm (for s=2.0d)
d_w = 2.0d_{bo} to 3.5d_{bo}	s = 2.0d to 5.0d	L = 101.6mm (for s=3.0d)
e = 31.75mm (≡5.0d)	t = 6mm	L = 107.95mm (for s=4.0d)
= area modelled in simulation	t_w = 3mm	L = 114.3mm (for s=5.0d)

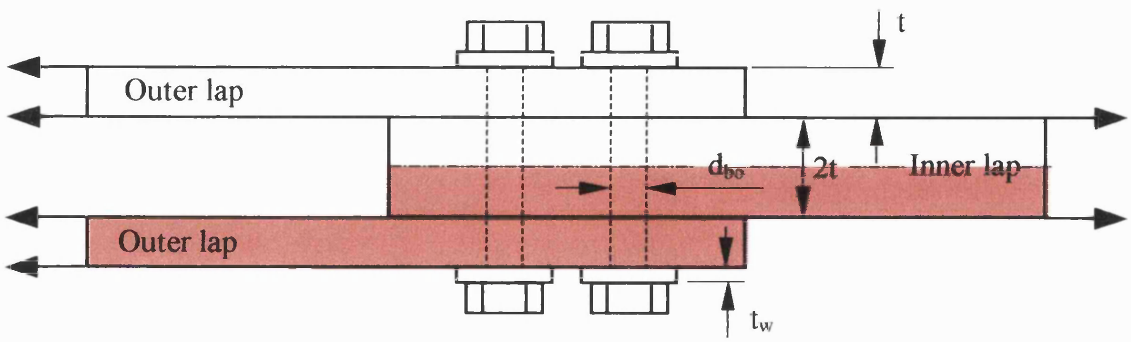

Figure 7.1b – Physical representation of the multiple fastener joint (plan view)

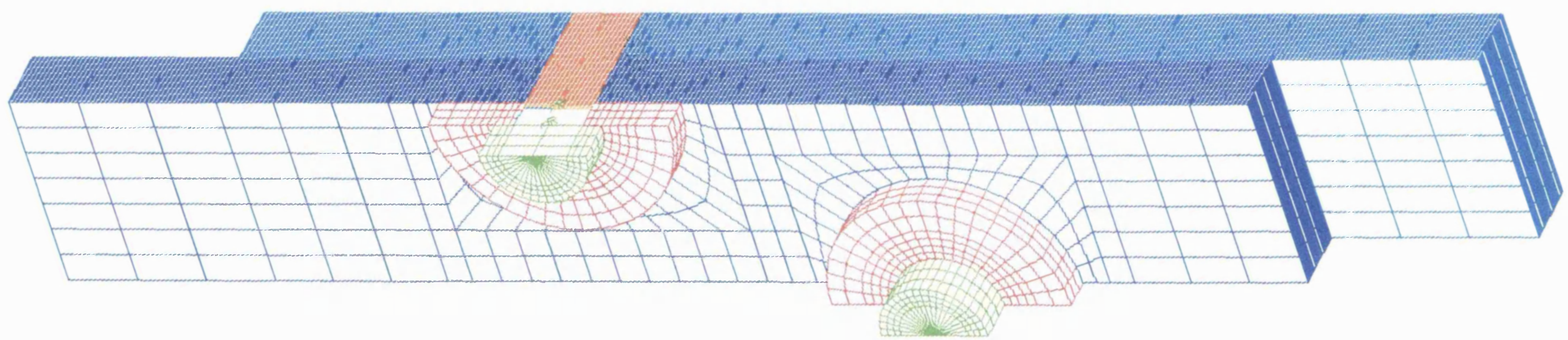

Figure 7.2 – Typical finite element mesh (mesh having a row spacing of 5.0d and a washer diameter d_w=3.5d_{bo} is shown)

(i) Inboard bolt hole

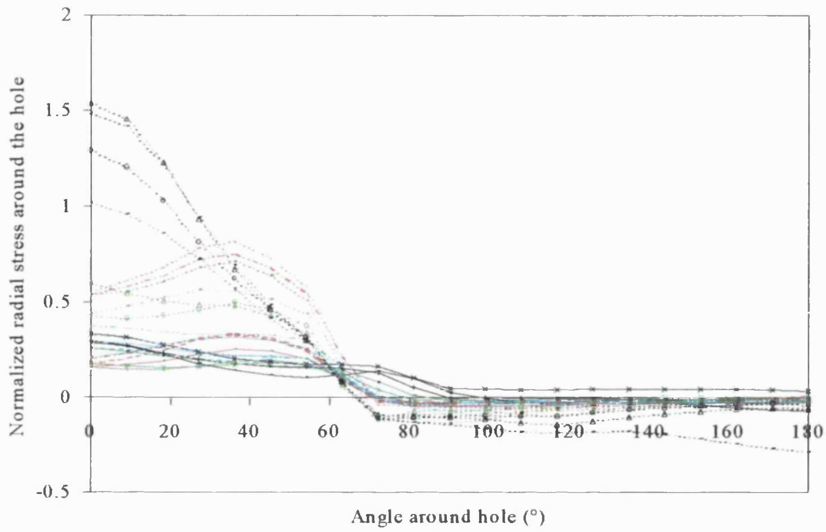

(ii) Outboard bolt hole

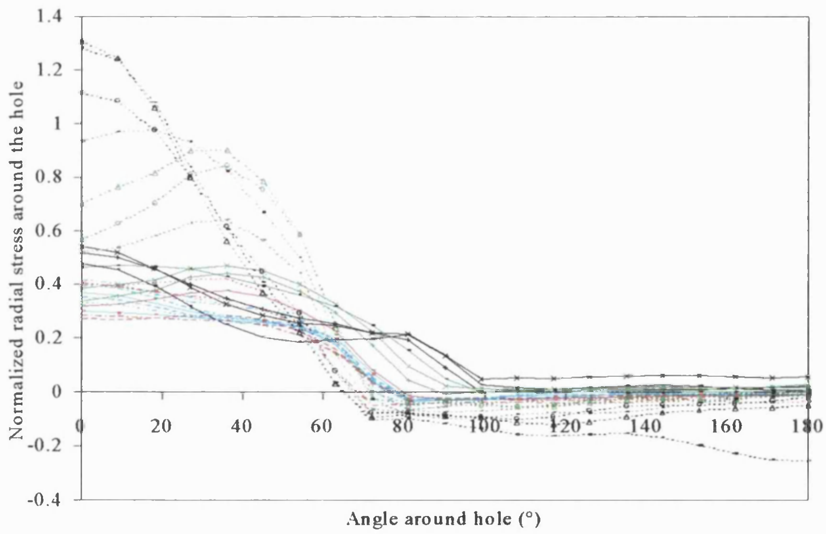

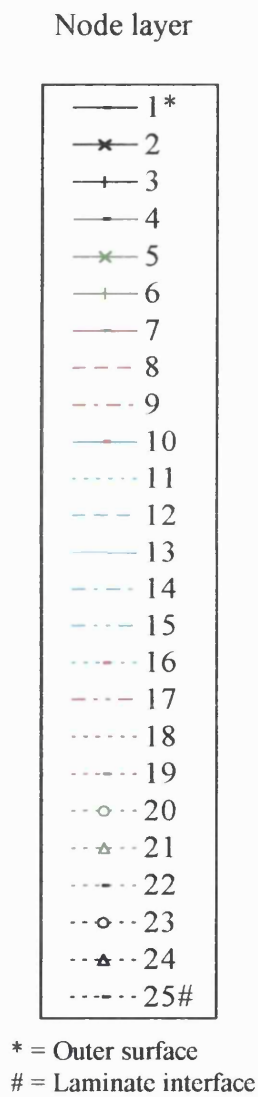

Figure 7.3 – Normalized radial stress around the hole boundary of the outer lap – multiple bolt model – row spacing = 3.0d – washer diameter = $2.0d_{bo}$

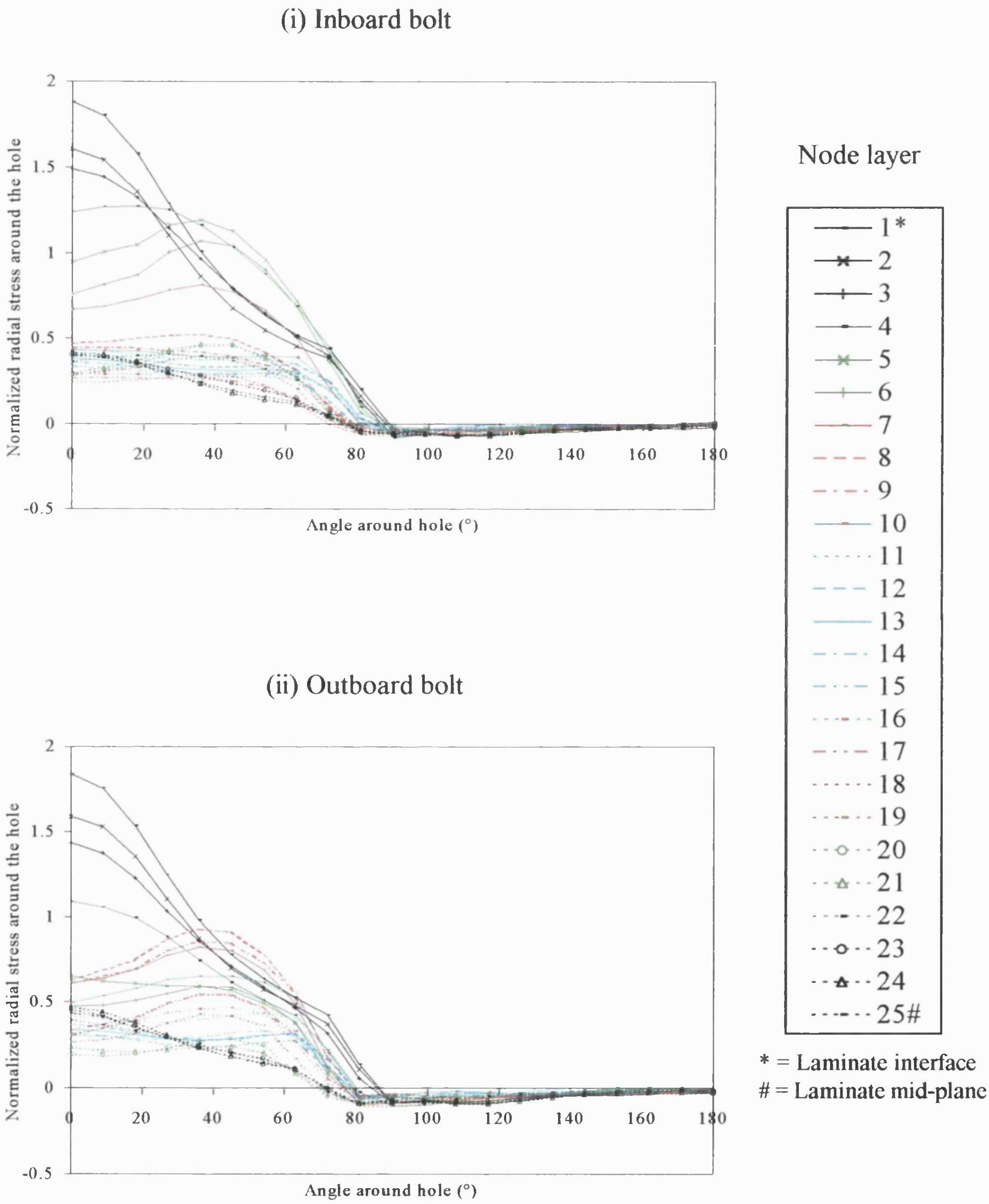

Figure 7.4 – Normalized radial stress around the hole boundary of the inner lap – multiple bolt model – row spacing = 3.0d – washer diameter = $2.0d_{bo}$

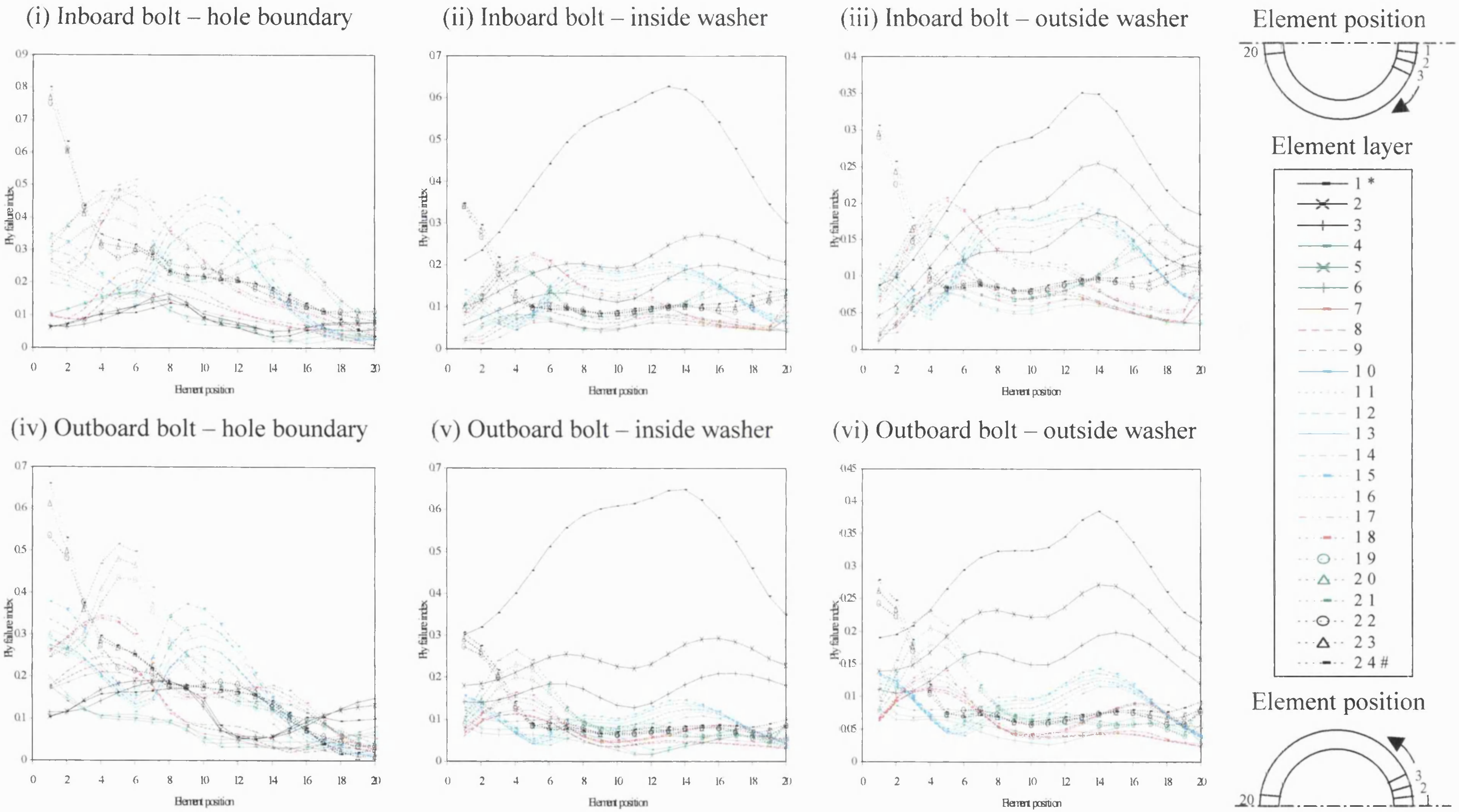

Figure 7.5 – Ply failure index plots for the outer lap – multiple-bolt model
row spacing = 3.0d – washer diameter = $2.0d_{bo}$ - * = Outer surface, # = Laminate interface

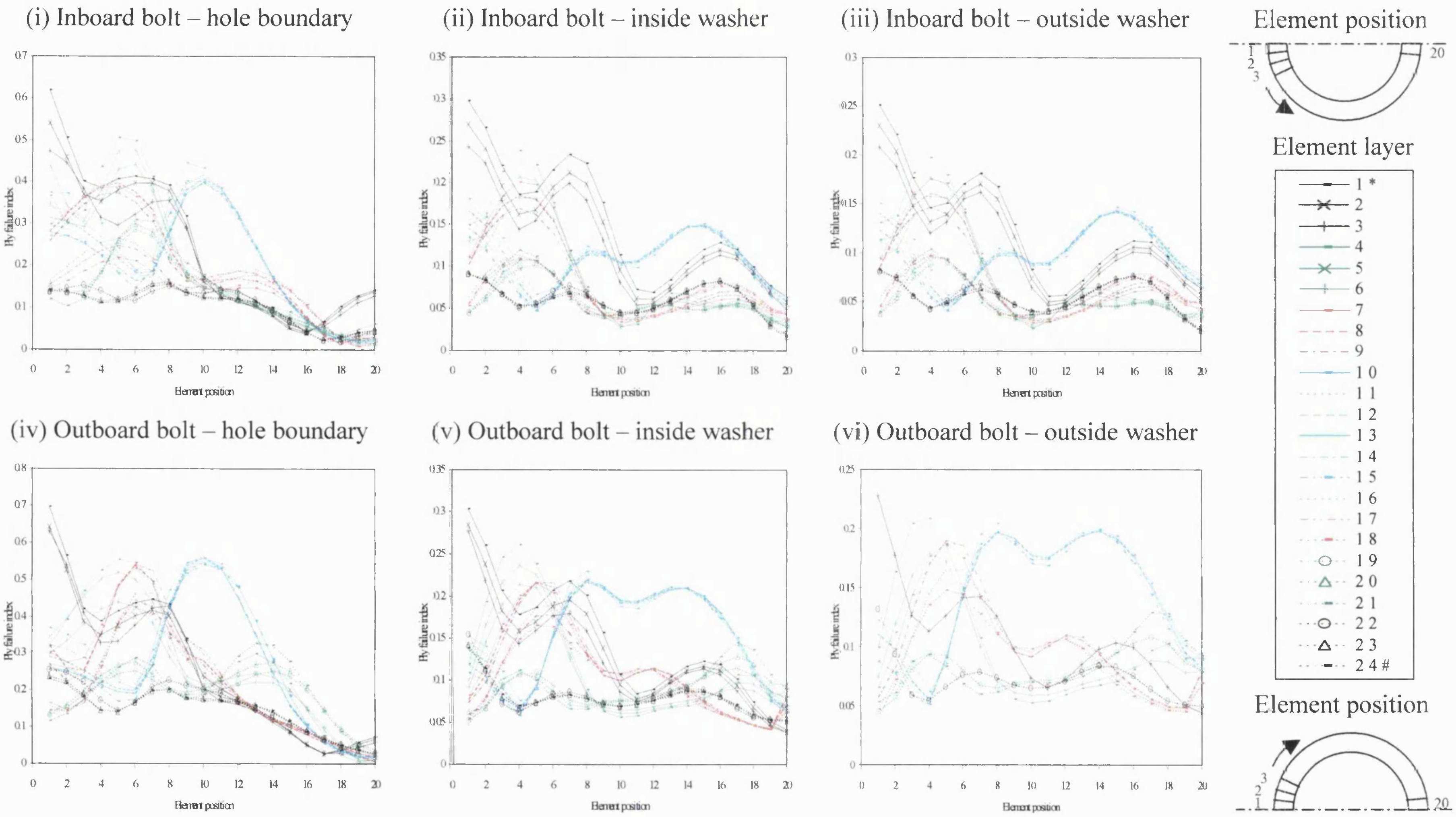

Figure 7.6 – Ply failure index plots for the inner lap – multiple-bolt model
row spacing = 3.0d – washer diameter = $2.0d_{bo}$ - * = Laminate interface, # = Laminate mid-plane

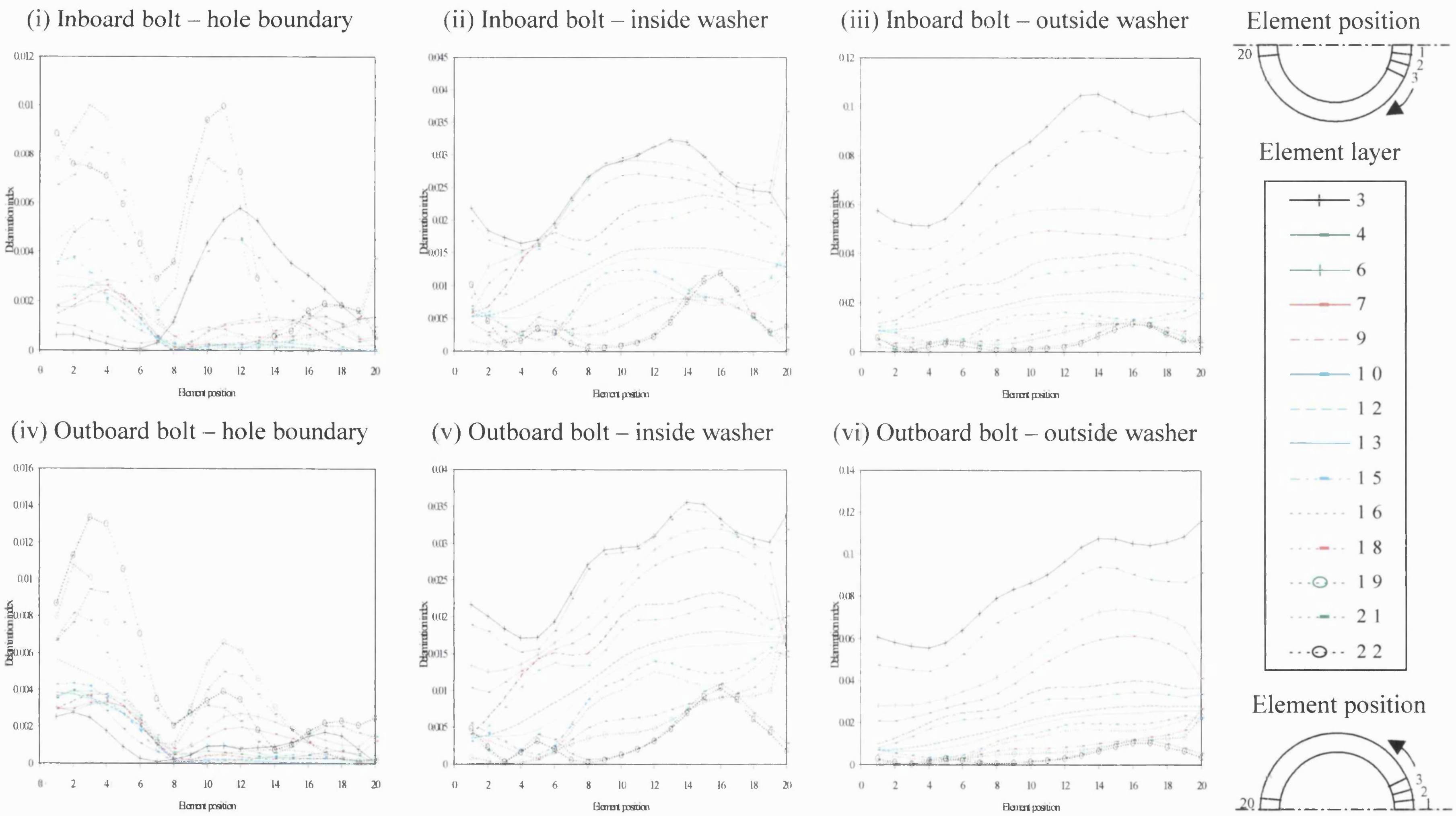

Figure 7.7 – Delamination failure index plots for the outer lap – multiple-bolt model
row spacing = 3.0d – washer diameter =2.0d_{bo}

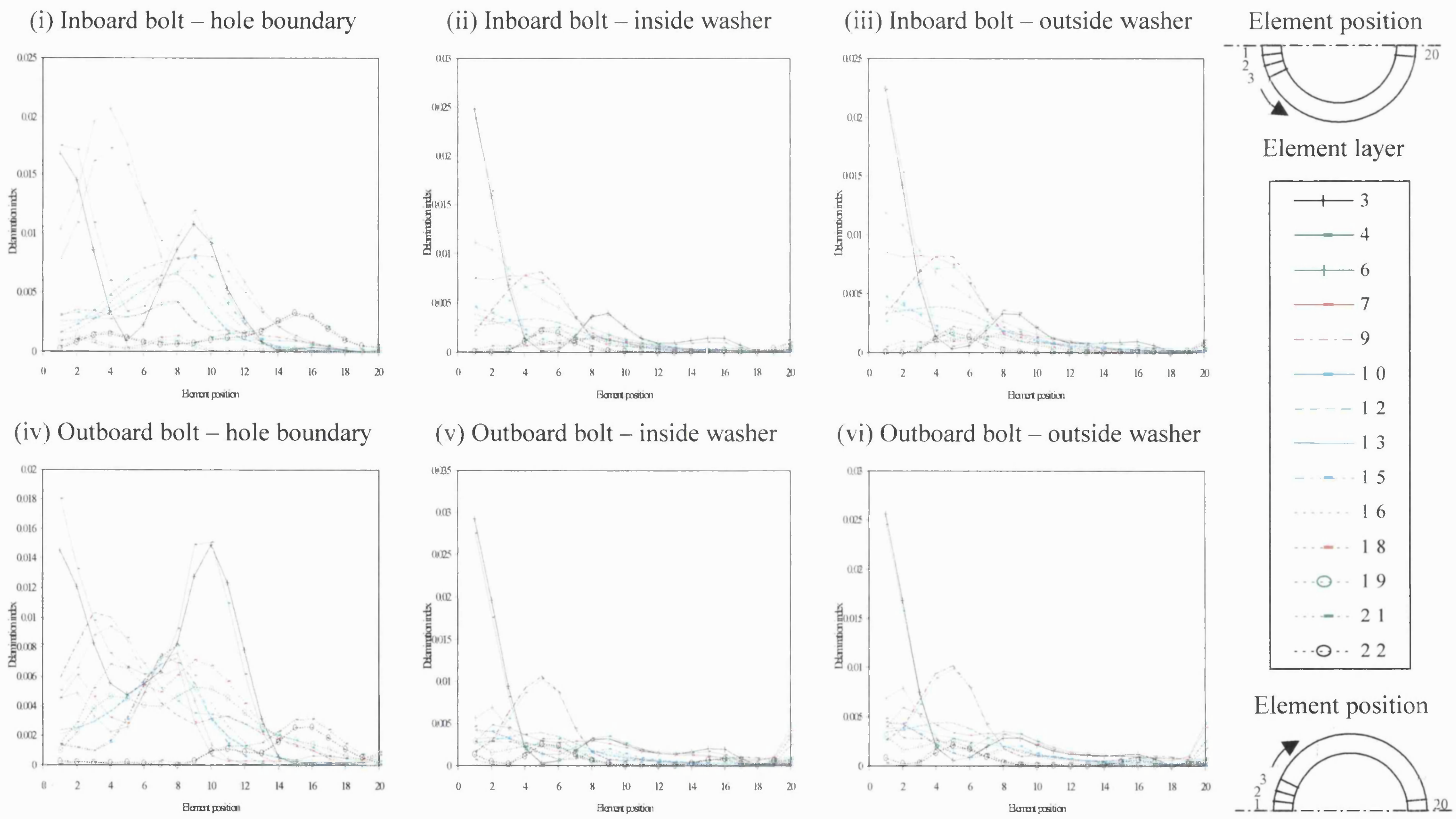

Figure 7.8 – Delamination failure index plots for the inner lap – multiple-bolt model
row spacing = 3.0d – washer diameter = $2.0d_{bo}$

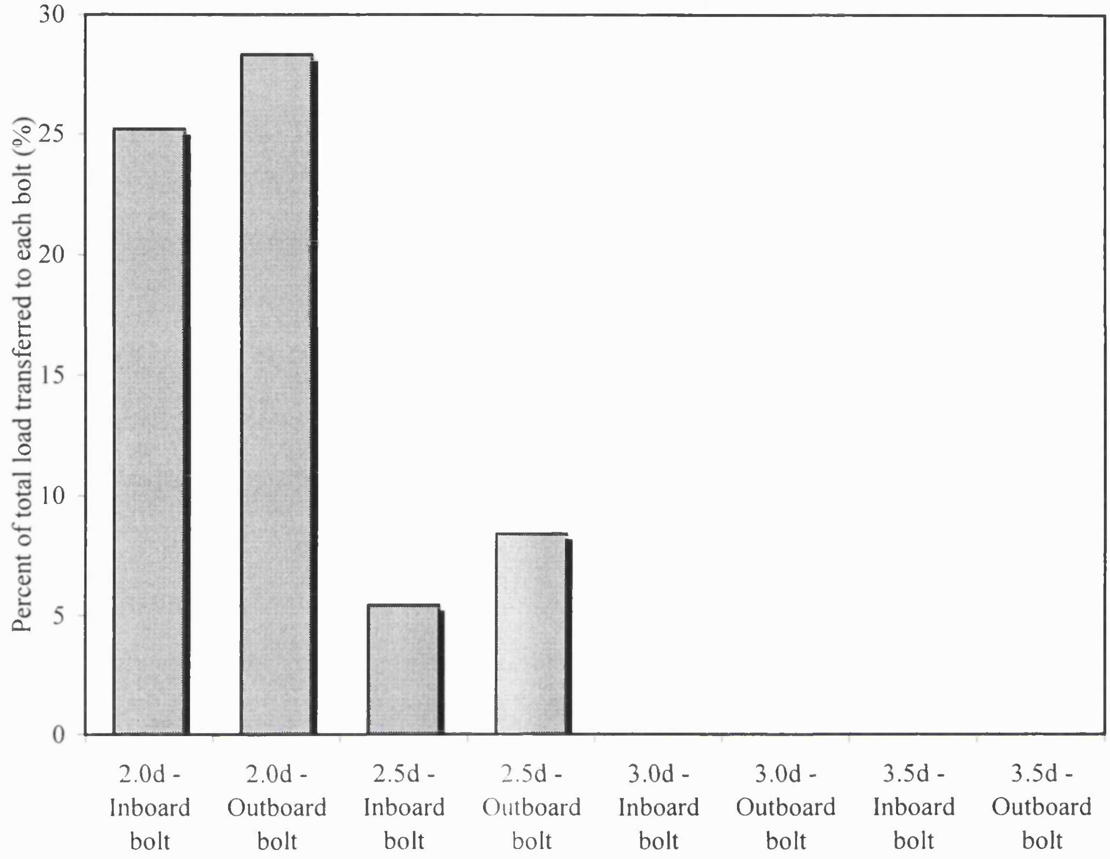

Figure 7.9 – Percent of the total load transferred from the outer lap to each bolt – multiple bolt model – row spacing = 3.0d – washer diameter = $2.0d_{bo}$ – $3.5d_{bo}$

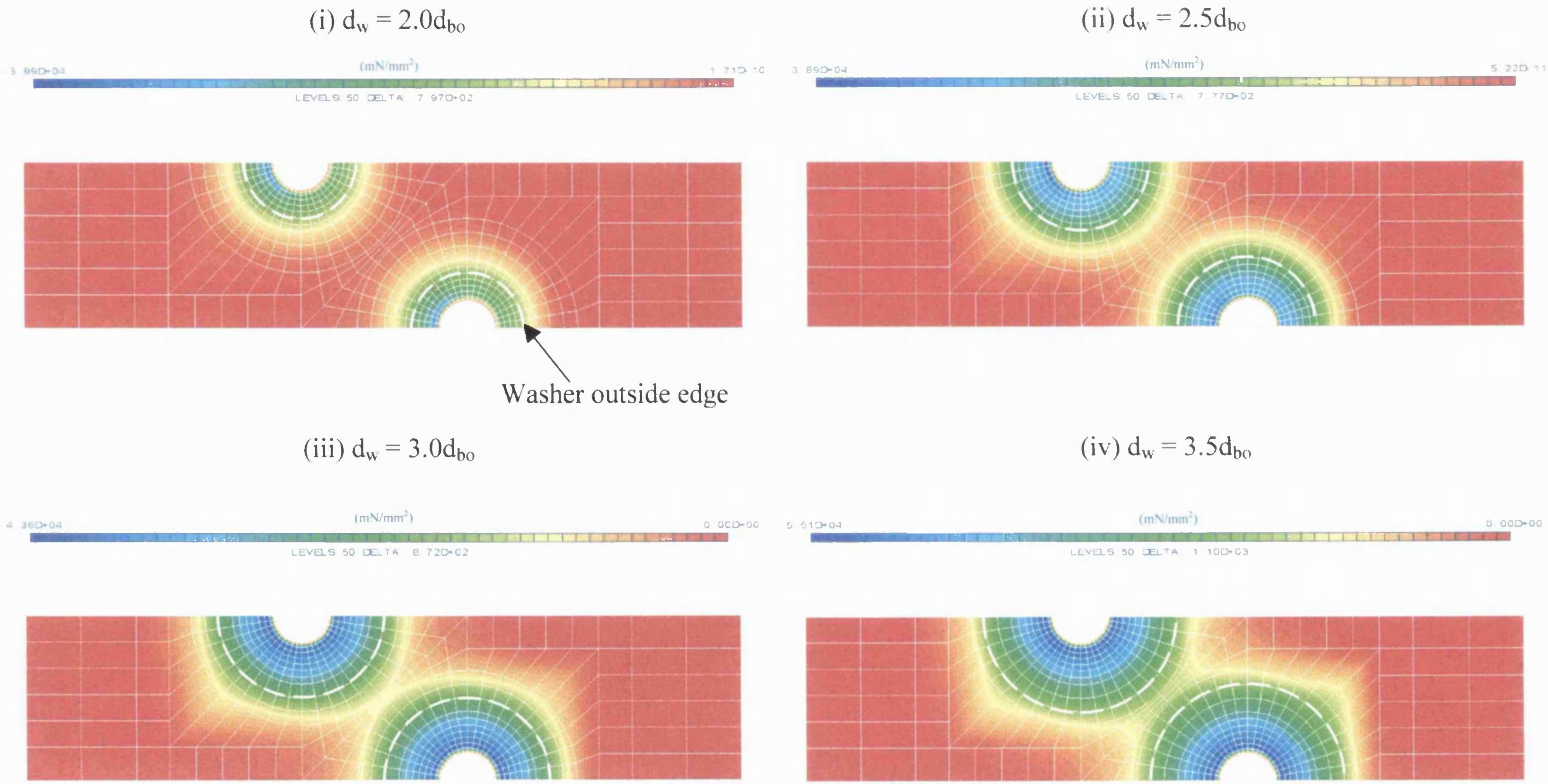

Figure 7.10 – Through thickness contact stress on the inner lap at the laminate interface – multiple bolt model row spacing = 3.0d – washer diameter = $2.0d_{bo}$ to $3.5d_{bo}$

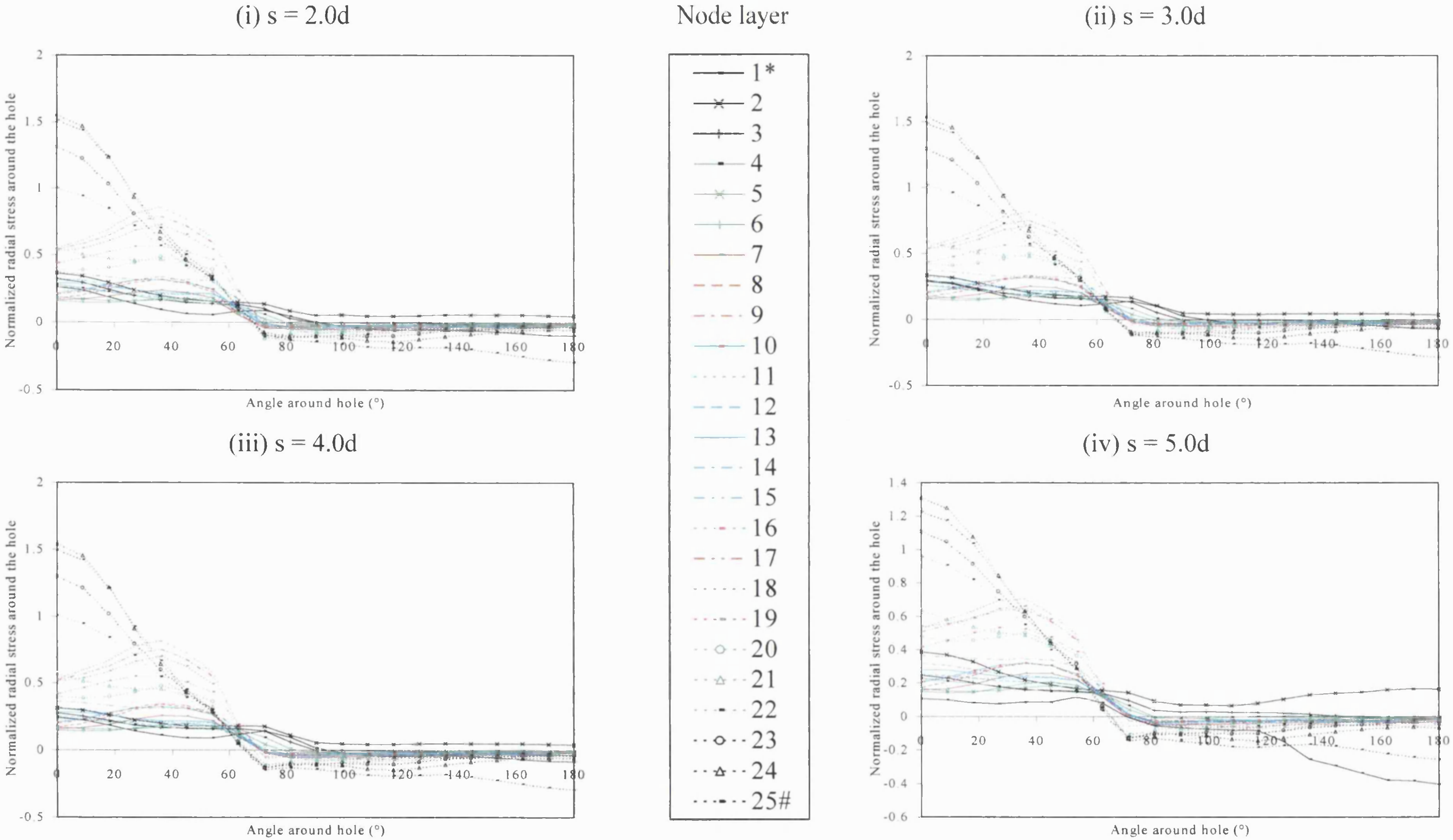

Figure 7.11 – Normalized radial stress around the hole boundary of the outer lap – multiple bolt model – inboard bolt washer diameter = 2.0d_{bo} – row spacing = 2.0d to 5.0d - * = Outer surface, # = Laminate interface

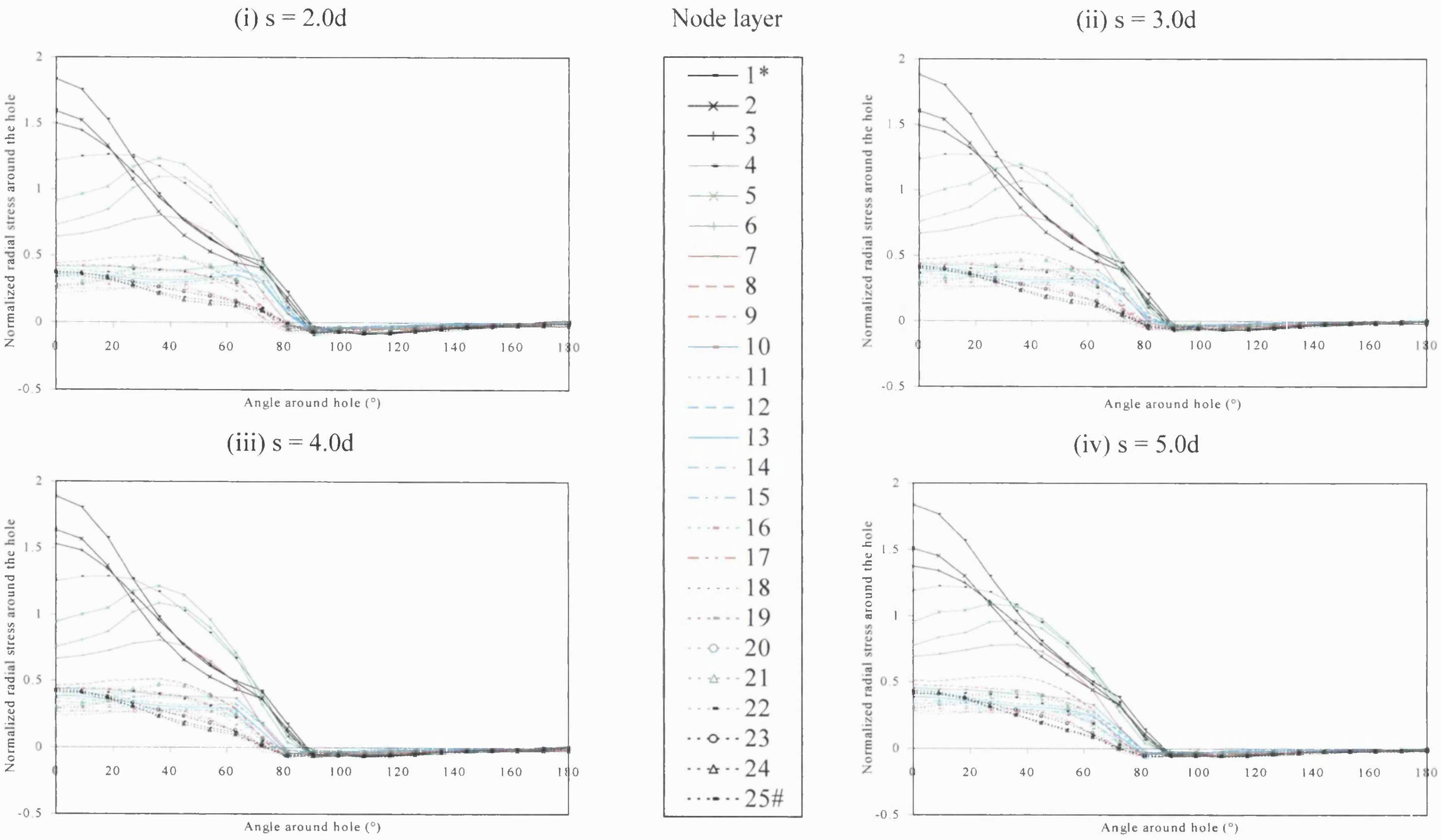

Figure 7.12 – Normalized radial stress around the hole boundary of the inner lap – multiple bolt model – inboard bolt washer diameter = 2.0d$_{bo}$ – row spacing = 2.0d to 5.0d - * = Laminate interface, # = Laminate mid-plane

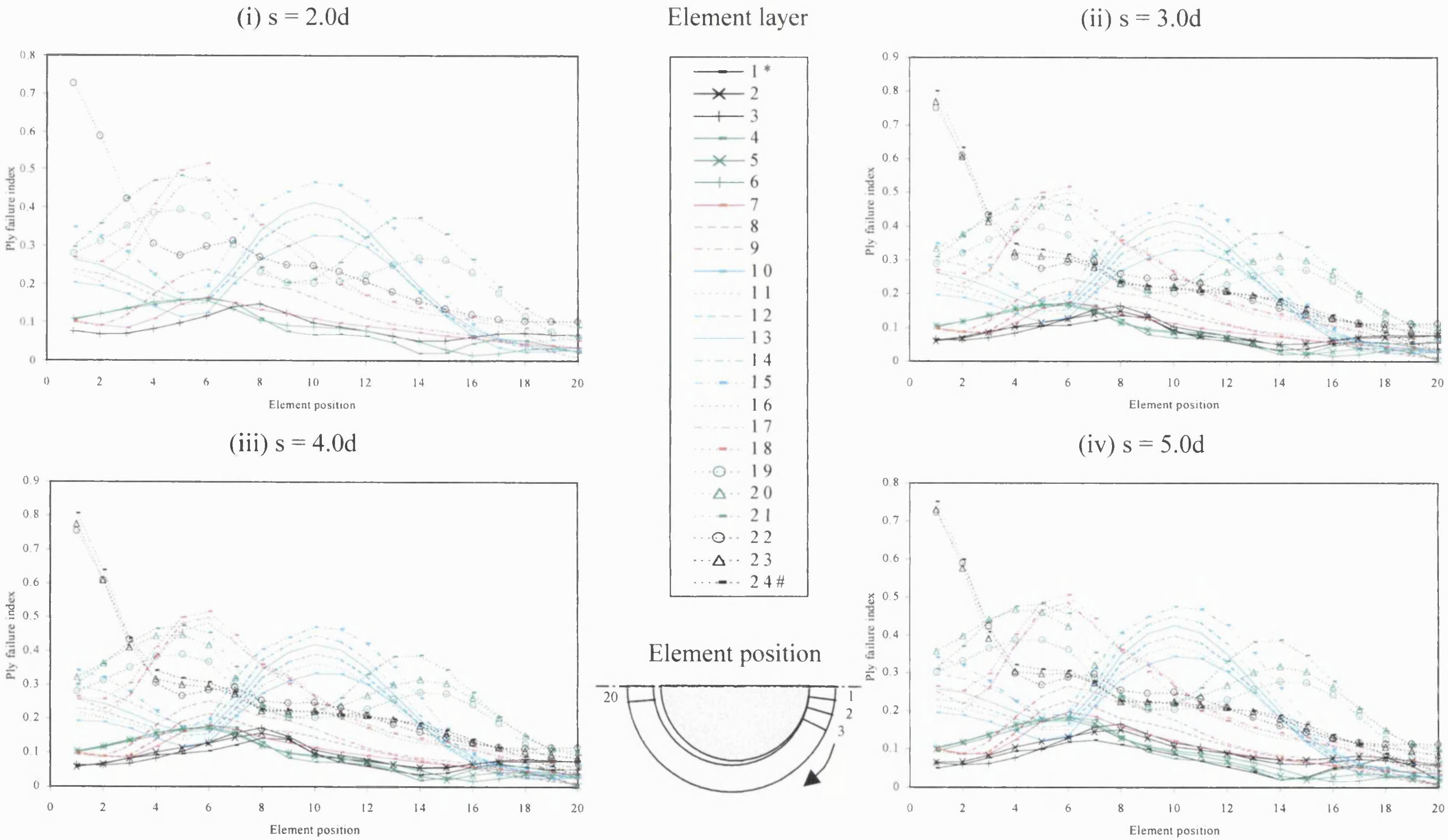

Figure 7.13 – Ply failure index plots for elements around the hole boundary of the outer lap –multiple bolt model – inboard bolt washer diameter = 2.0d$_{bo}$ – row spacing = 2.0d to 5.0d - * = Outer surface, # = Laminate interface

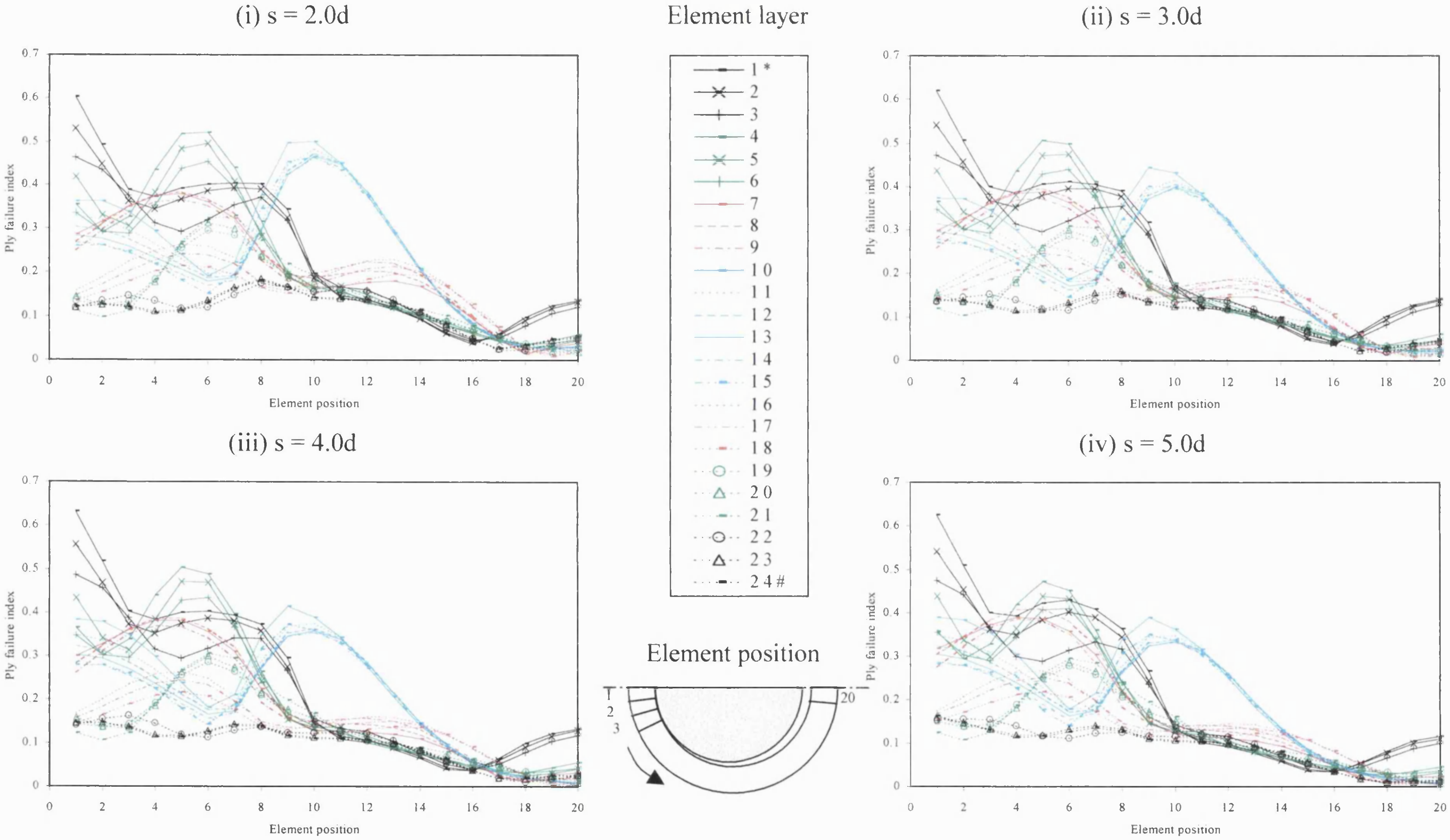

Figure 7.14 – Ply failure index plots for elements around the hole boundary of the inner lap – multiple bolt model – inboard bolt washer diameter = 2.0d_{bo} – row spacing = 2.0d to 5.0d - * = Laminate interface, # = Laminate mid-plane

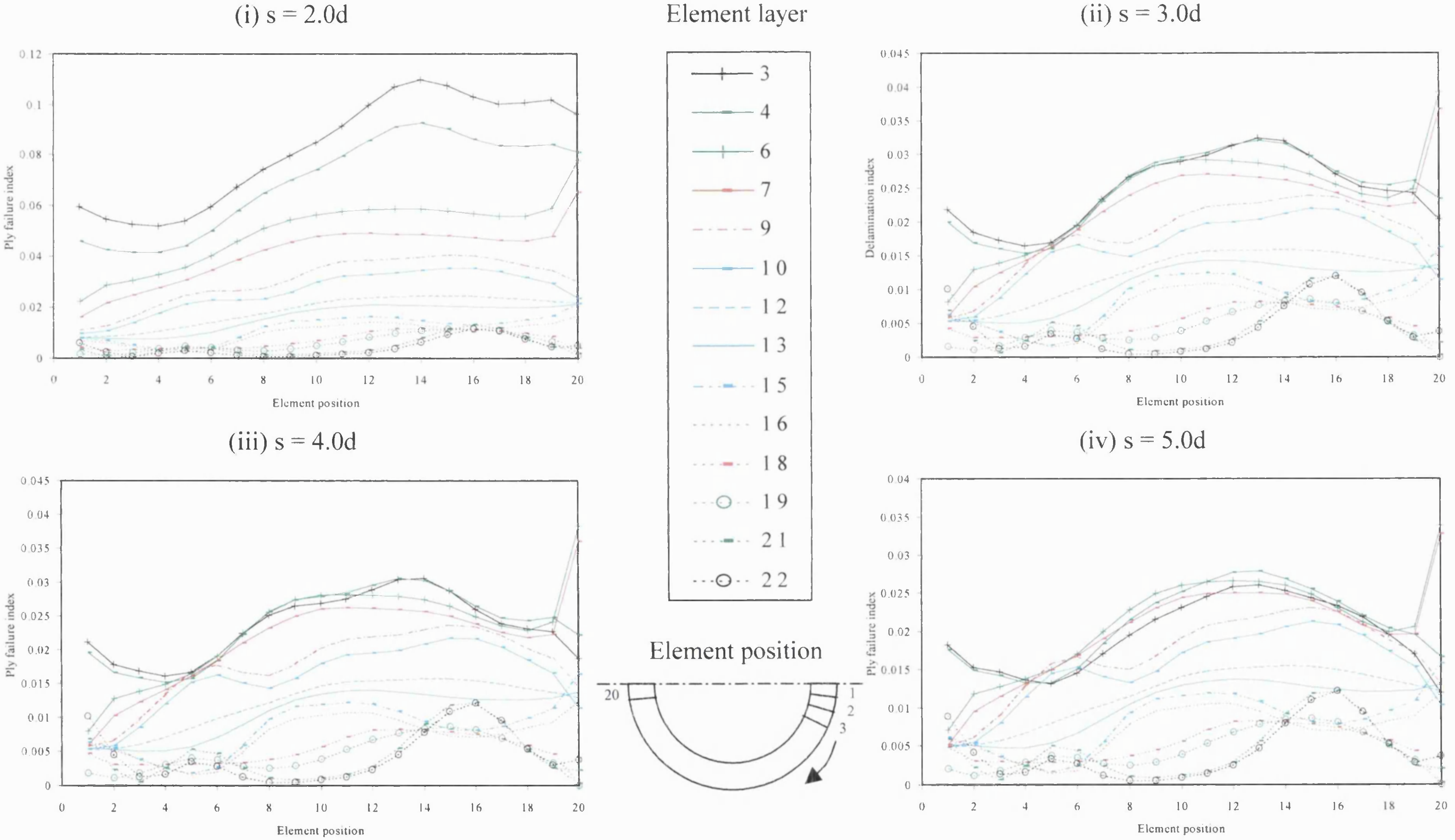

Figure 7.15 – Delamination index plots for elements inside the washer edge of the outer lap –multiple bolt model – inboard bolt washer diameter = 2.0d$_{bo}$ – row spacing = 2.0d to 5.0d

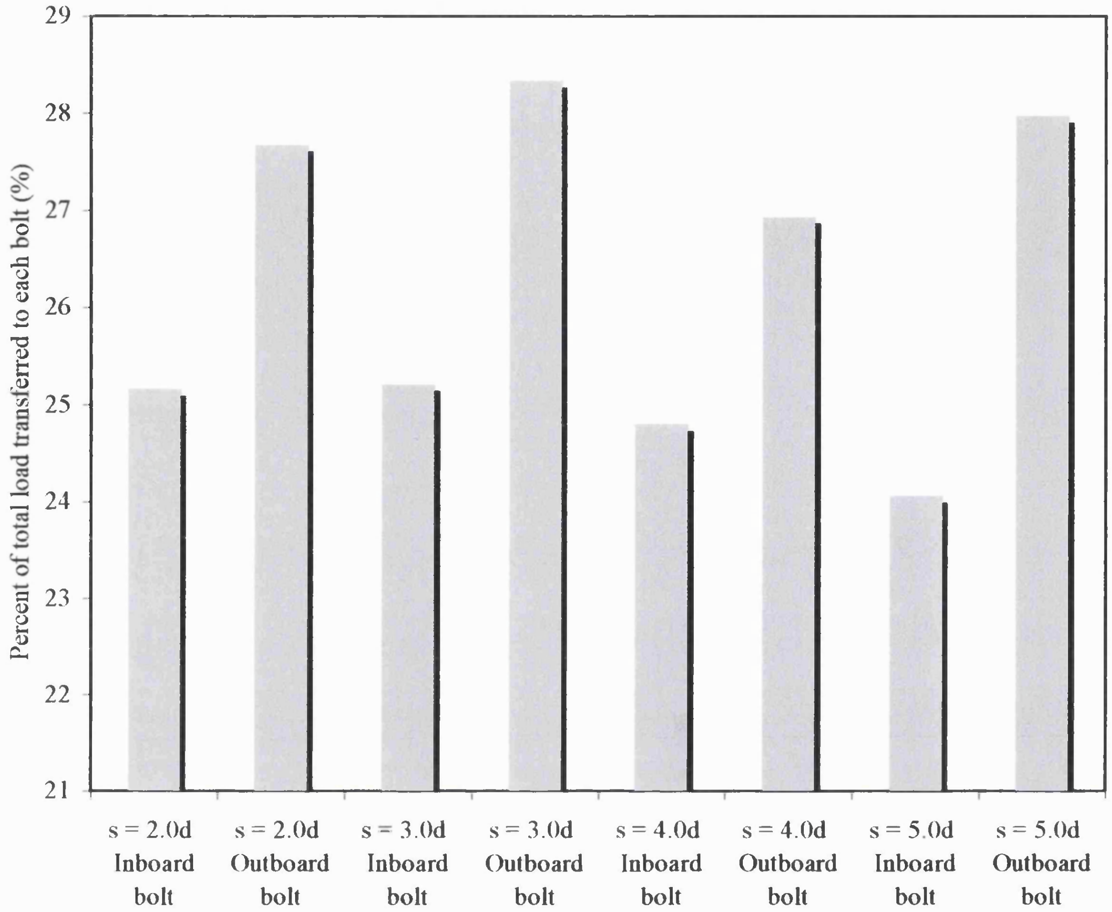

Figure 7.16 – Percent of the total load transferred by each bolt – multiple bolt model – row spacing = 2.0d to 5.0d – washer diameter = $2.0d_{bo}$

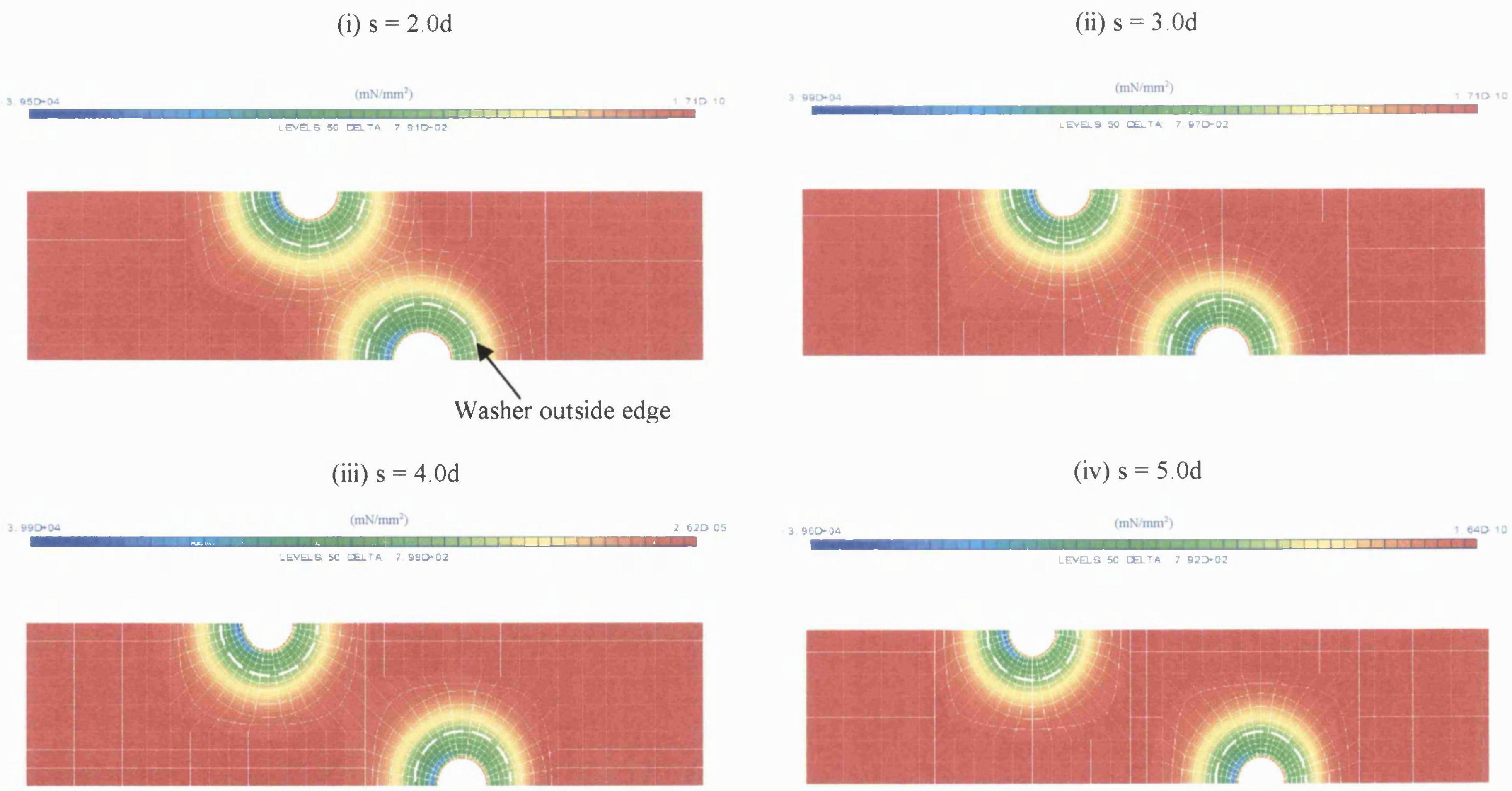

Figure 7.17 – Through thickness contact stress on the inner lap at the laminate interface – multiple bolt model row spacing = 2.0d to 5.0d – washer diameter = $2.0d_{bo}$

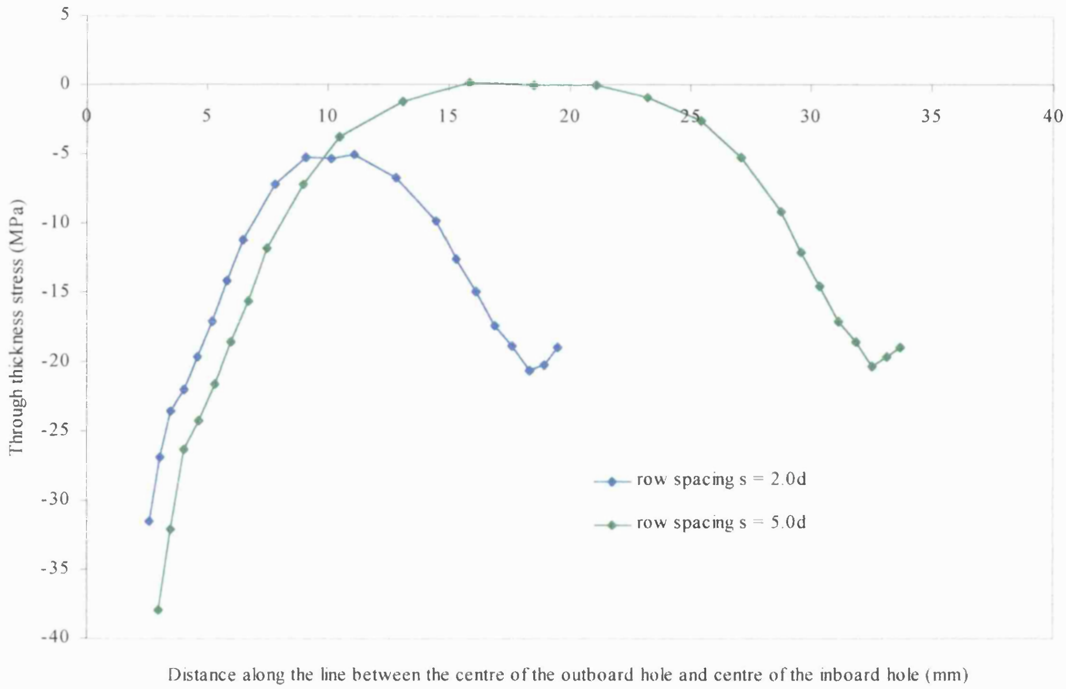

Figure 7.18– Through thickness stress distribution between the centre of the outboard hole and the inboard hole on the surface of the inner lap

$d_w = 2.0d_{bo}$ (s=2.0d and s=5.0d)

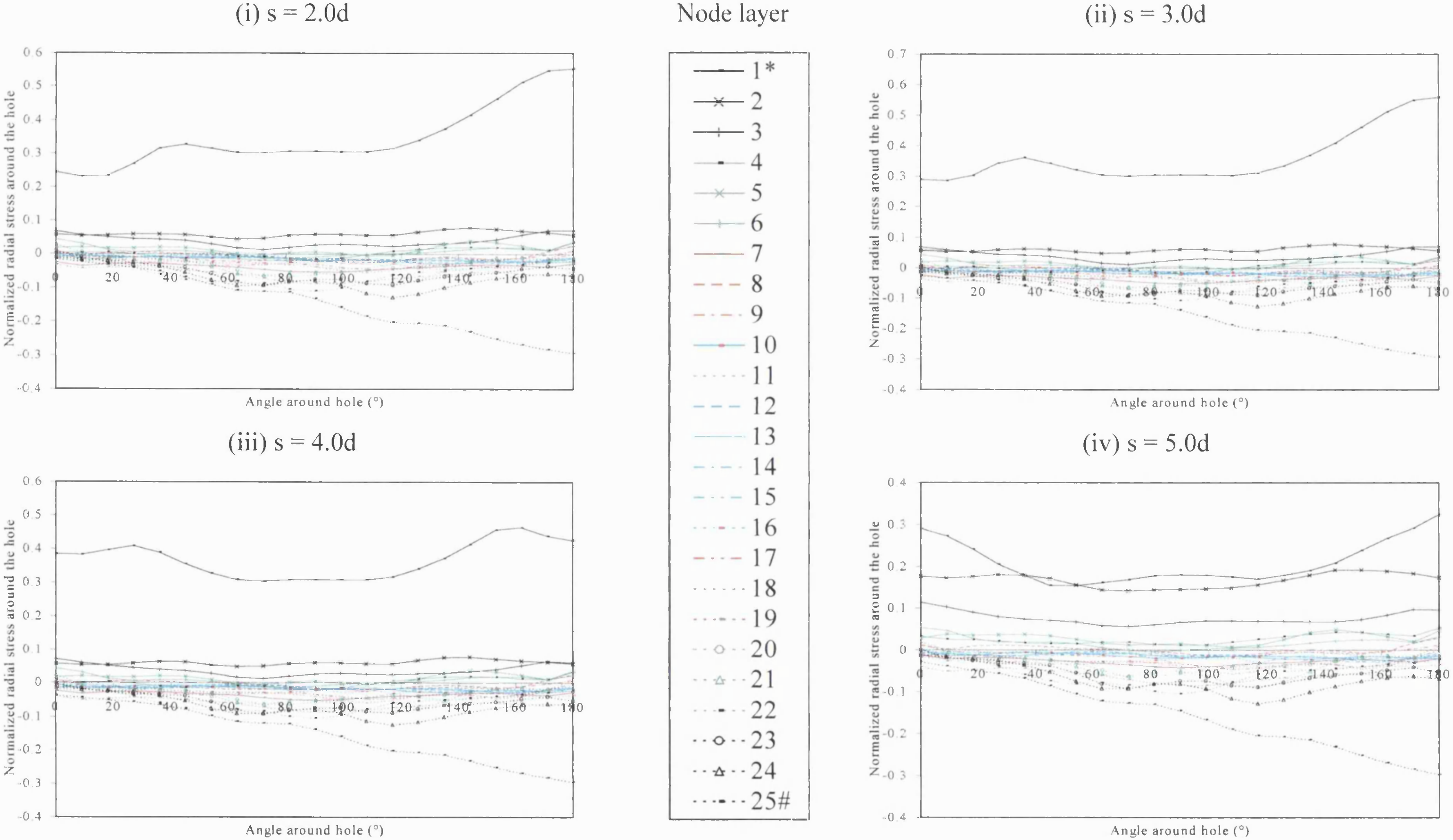

Figure 7.19 – Normalized radial stress around the hole boundary of the outer lap – multiple bolt model – inboard bolt washer diameter = $3.5d_{bo}$ – row spacing = 2.0d to 5.0d - * = Outer surface, # = Laminate interface

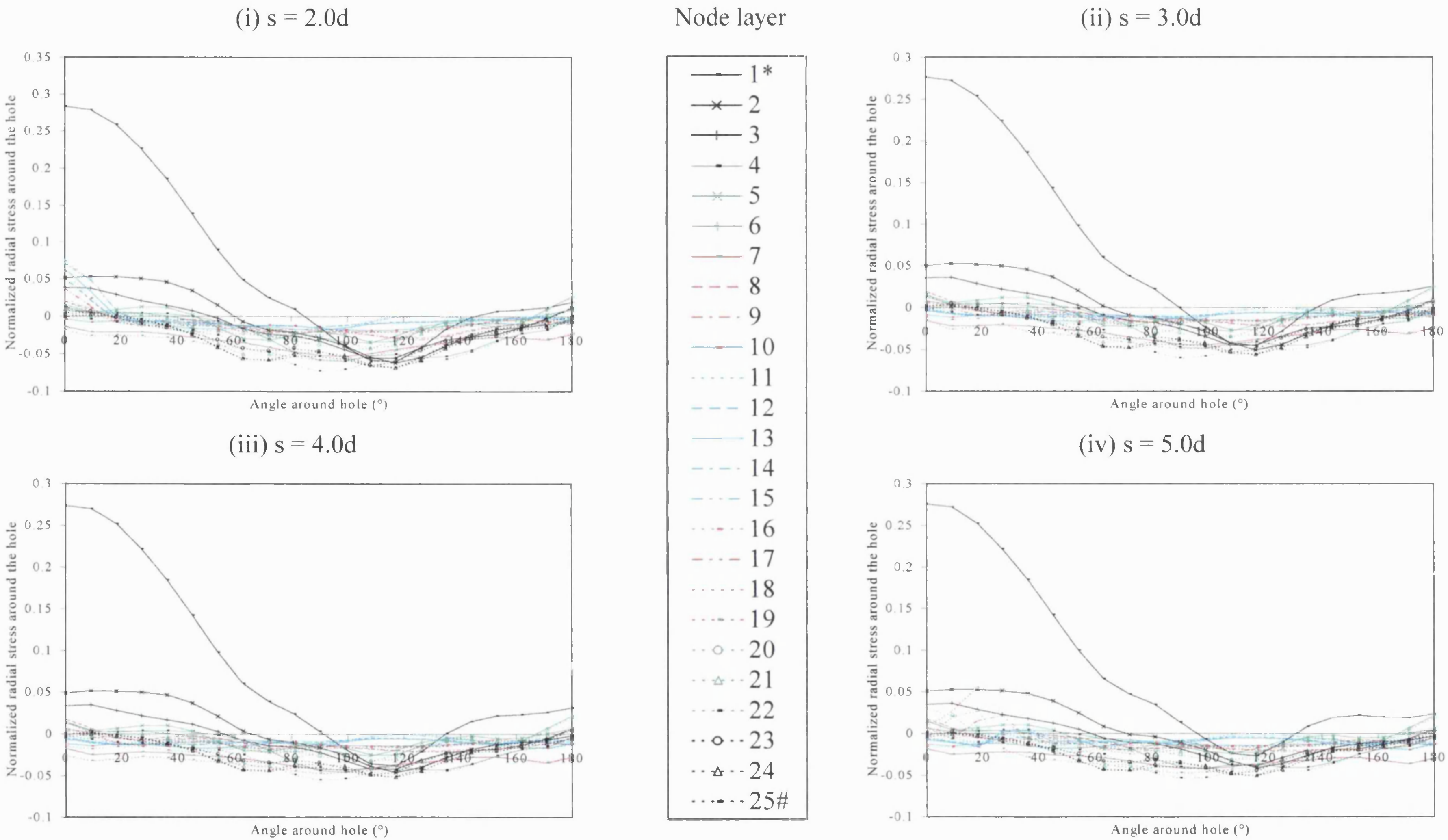

Figure 7.20 – Normalized radial stress around the hole boundary of the inner lap – multiple bolt model – inboard bolt washer diameter = $3.5d_{bo}$ – row spacing = 2.0d to 5.0d - * = Laminate interface, # = Laminate mid-plane

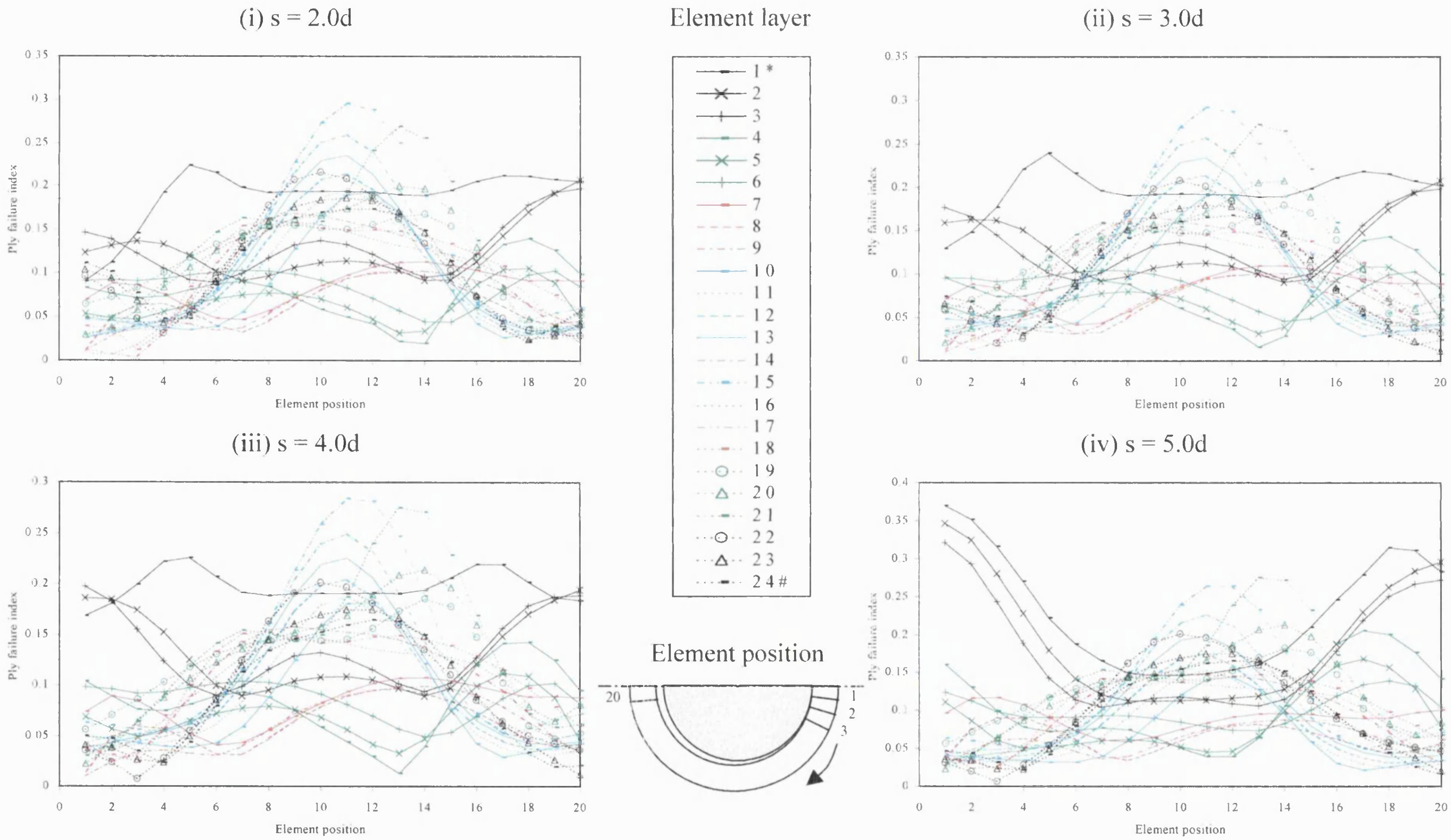

Figure 7.21 – Ply failure index plots for elements around the hole boundary of the outer lap –multiple bolt model – inboard bolt washer diameter = $3.5d_{bo}$ – row spacing = 2.0d to 5.0d - * = Outer surface, # = Laminate interface

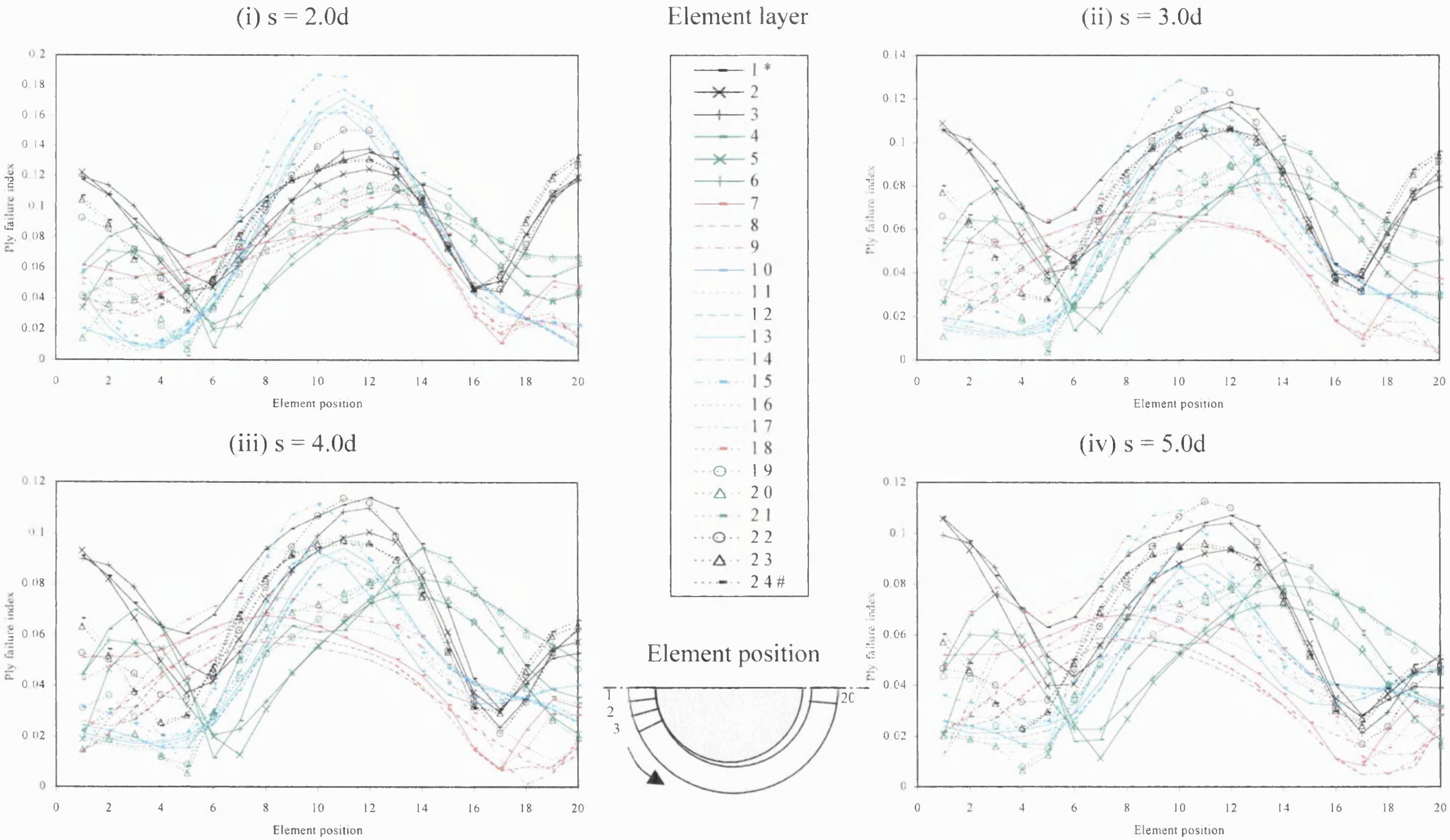

Figure 7.22 – Ply failure index plots for elements around the hole boundary of the inner lap – multiple bolt model – inboard bolt washer diameter = $3.5d_{bo}$ – row spacing = 2.0d to 5.0d - * = Laminate interface, # = Laminate mid-plane

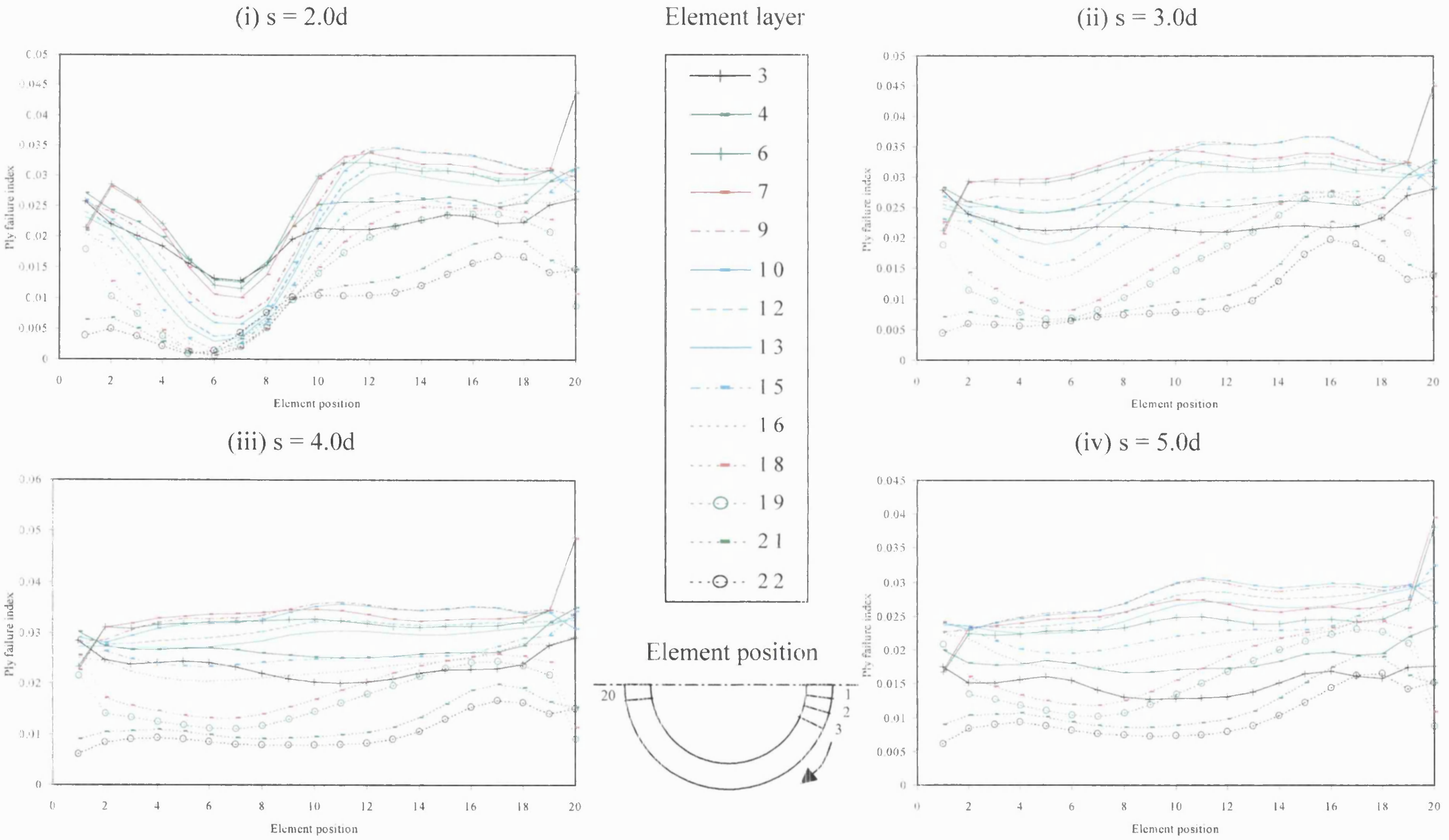

Figure 7.23 – Delamination index plots for elements inside the washer edge of the outer lap –multiple bolt model – inboard bolt washer diameter = $3.5d_{bo}$ – row spacing = 2.0d to 5.0d

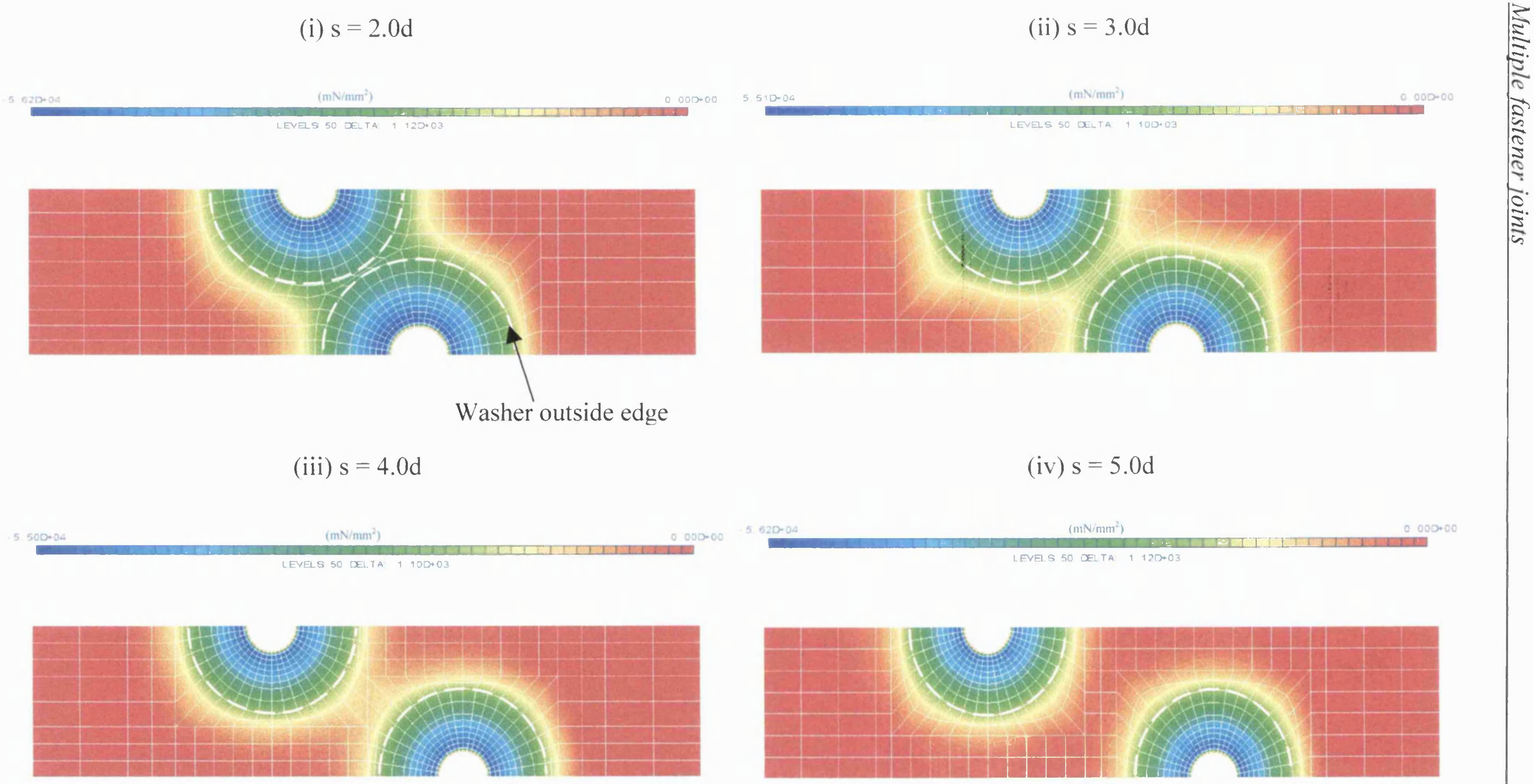

Figure 7.24 – Through thickness contact stress on the inner lap at the laminate interface – multiple bolt model row spacing = 2.0d to 5.0d – washer diameter = $3.5d_{bo}$

CHAPTER EIGHT

CONCLUSIONS AND SUGGESTIONS FOR FURTHER RESEARCH

8.1 - INTRODUCTION

In this chapter further discussion and an overview of the conclusions drawn from each investigation, as well as an indication of the relevance of this study to the current understanding of mechanically fastened composites, are provided. Suggestions for extending this research have also been included.

8.2 – FURTHER DISCUSSION AND CONCLUSIONS

This section provides further discussion and the main conclusions drawn from each chapter.

8.2.1 – Chapter two

This chapter presented a literature review of recent experimental and analytical work conducted on mechanically fastened composite joints. Conclusions concerning geometric parameters were reported for the experimental investigations and details of modelling technique were presented for the analytical studies.

It is clear that experimental evaluations are an expensive method for testing joint geometries, hence there is a requirement for accurate analytical studies. The finite element method has been used by many investigators and providing the bolt to hole contact is iteratively modelled rather than assumed, three dimensional finite element analysis has been shown to provide accurate stress and strain predictions for these types of joint. In particular the replica method for modelling the laminate has shown to be most appropriate, as interlaminar stresses can also be obtained.

With appropriate failure criteria the joint strength can be predicted, however, the accuracy of the results can be highly dependent upon the assumptions adopted when constructing the models.

8.2.2 – Chapter four

This chapter presented details of the modelling technique adopted for this study and comparisons were made with previously published work. The stress distributions around the hole boundary of both laps of the joint were found to be in excellent agreement. It was also considered appropriate to use three elements per ply thickness for modelling the laminates, as this presents a level of resolution in the determination of the stresses that was not observed when using a coarse mesh and does not adversely affect the processing time.

8.2.3 – Chapter five

This chapter presented results from an investigation of material and geometric parameters of a single bolt double lap joint. The effect of clamping on the stress distribution around the hole was investigated by modelling the bolt and washer as separate elastic entities and applying a temperature drop to effect a bolt preload. Bolt elasticity, laminate elasticity and stacking sequence were also investigated as well as a small degree of clearance between the bolt shank and hole.

Bolt preload was found to significantly affect the joint strength. Small clamping preloads were found to be beneficial, however, large preloads were shown to raise the likelihood of joint failure through tensile failure mechanisms. For good joint strength with a more uniform load transfer between the bolt and hole, an optimum bolt preload equivalent to a 6Nm bolt torque has been suggested for a double lap joint with a standard size washer ($2.0d_{bo}$ diameter). This induces a bolt axial force of 4.72kN and for both aluminium and steel fasteners improved the strength of the laminate joint. For a 6.35mm diameter bolt this axial force results in a bolt stress of 149MPa which is well within the allowable stress for aluminium alloy and steel having yield strengths of 490MPa and 1480MPa, respectively (Sun, 1998).

In this study an optimum bolt torque of 6Nm was recommended based on assessment of the stress distribution and failure analysis. In practice bolt torque will be affected by the surface condition of the bolt, nut and washer assembly, hence the optimum bolt preload may not be achieved in other than new fasteners. The results contained in this study indicate that over tightening by 30% only raised the failure index marginally, whereas higher clamping torques might lead to a catastrophic failure mode and therefore should be avoided. The effect on the failure index of under tightening to the same degree is similar but in this case bearing failure results.

Another practical aspect to consider in using these joints is that bolt preload may reduce slightly with time, depending upon the materials used in construction of the laminate matrix and their respective creep resistance. E-glass polyester has been shown to withstand 50% of its ultimate stress for 100,000 hours at 30°C (Hancox and Mayer, 1994), and CFRP laminates are also regarded as having very low creep rates (Phillips, 1989). However, more often creep rates are measured with respect to the fibre orientation, whereas, with friction grip bolted connections clamping is resisted more by the matrix than the fibres. Hence, when using higher clamping loads as well as high modulus washers some consideration must be given in the design process to the long term effects of in-service loading.

It has also been shown in this study that the washer and fastener elasticity are important parameters to consider in joint design. Many investigators have applied a uniform clamping pressure to a laminate to represent bolt clamping, however, this is an unrealistic approximation when considering traditional aluminium or steel washer types. In the case of bolt stiffness this work has shown that steel bolts provide higher strength joints compared with aluminium bolts when using GRP laminates, as a direct consequence of the reduced fastener bending contributing to a more uniformly distributed load. Clearly, increasing the diameter of the fastener shank may also induce this effect. However, to provide the same bending stiffness as the steel bolt the aluminium bolt shank diameter would have to be increased by approximately 2mm, which would lead to a significant increase in the end distance and width of the laminate. While this increase in bolt diameter imposes a weight penalty in design the mass of the aluminium bolt would still be lower than that of the steel bolt having an equivalent stiffness, however, the increase in the overall weight is likely to be considerable given the increased dimensions of the laminate.

In comparing the response of the GRP and CFRP laminates it is clear that the contact area on the hole boundary as well as the out of plane deformation for the former are greater in magnitude, which gives rise to a lower peak stress on the bearing plane. However, owing to the higher failure stress of the CFRP the derived failure indices for this material are invariably lower than those encountered for the GRP laminate.

The through thickness compressive strengths of the GRP and CFRP utilised in this study were estimated as 140MPa (Barbero, 1998) and 321MPa (Camanho, 1999), respectively. For the purposes of this study clamping torques up to and including 16Nm were investigated. However, for the bolts studied, this upper limit is unrealistic as it exerts a through thickness stress which exceeds the CFRP compressive strength, using a conventional washer design. This was simply employed to establish the trend in the stress data as a consequence of increasing torque. For intermediate values of torque, i.e. 6Nm, these have been shown to provide optimum clamping conditions and result in compressive stresses well within the ultimate stress requirement of the lowest strength laminate considered.

For this joint configuration with a 6Nm bolt torque, varying the stacking sequence does not affect the joint strength nor the stress distribution significantly. The strength of the outer lap of a double lap joint may be improved slightly by placing 90° plies on the outer surfaces of quasi-isotropic and cross ply laminates. Although laminates constructed with 0° plies on the outer surfaces are weaker by comparison, their strength may be improved by including 90° plies adjacent to the outer surface plies. However, the clamping load that is applied during assembly of the joint moderates the difference in the strength of these laminates.

Introducing bolt clearance was found to reduce joint strength owing to a decrease in bolt to hole contact area and should therefore be minimised. However, for a more precise assessment of this parameter it is proposed that a non-linear analysis would be more appropriate since the contact analysis of clearance fit bolts involves large changes in contact area as the load is applied.

8.2.4 – Chapter six

The washer diameter and stiffness were varied to investigate their effects on the stress distribution and joint strength. Increasing the stiffness of the washer did not significantly affect the strength of joints constructed with standard size washers since the bolt head contact area and washer surface area are comparable. However, as the washer size is increased there is a corresponding increase in the joint strength provided the washer can maintain a sufficiently high pressure. This objective may lead to a change in failure mode from bearing to tensile failure as higher washer pressures restrict bearing contact. An examination of the failure indices derived in this study indicates that the moderate joint strengths can be achieved by using a washer diameter in the range of $3.5d_{bo}$ to $4.0d_{bo}$, whilst maintaining a washer contact pressure in the order of 50MPa.

For double lap joints having a standard washer with a 6Nm clamping torque failure analysis indicated maximum indices in the order of 0.7. Increasing the washer diameter with the same bolt torque had negligible effect on the failure indices, indicating that adequate joint strength may be achieved without resorting to high through thickness stresses and excessive clamping loads. This represents a better design strategy since the anticipated failure mode is through bearing.

For the larger washer diameters, such as $3.5d_{bo}$, a 4mm thick steel washer was considered as the optimum in transferring a more uniform clamping pressure to the laminate. However, the increase in weight arising from adopting this washer would be significant. An alternative washer material with a lower density and comparable or improved stiffness would be more suitable. A 3mm thick aluminium oxide ceramic washer, having an elastic modulus of 371GPa (ν = 0.29) was estimated to exert a similar clamping pressure to the joint, thereby contributing to an improvement in joint strength with a considerable weight saving. Alternative washer geometries and materials to provide equivalent clamping pressures, as recommended in this study, may be evaluated by utilising the equations given in Appendix B.

8.2.5 – Chapter seven

The results obtained from the analysis of a multiple bolt GRP double lap joint, with a clamping preload equivalent to 50MPa pressure, were reported in this chapter. The effects of washer diameter and row spacing on the stress distribution and joint strength were evaluated for a staggered bolt arrangement.

By increasing the washer diameter the joint strength was found to improve, however, the percentage of load transferred through bolt bearing reduced, such that for washer diameters greater than $2.5d_{bo}$, the load was entirely supported through the clamping mechanism. It was also noted from this investigation that the radial stress was not uniformly distributed between each of the holes. A higher stress and hence failure index was obtained in the vicinity of the inboard hole compared to the outboard hole. This was attributed to lower out of plane deformation in this locality as a consequence of improved interfacial contact that arises from more effective fastener interaction. Hence, as the outer lap is loaded the hole boundary at the laminate interface carries a high concentrated load through bolt bearing. The end of the laminate close to the outboard hole is less restrained, as there is no fastener interaction, and hence can deform in the through thickness direction as the bolt bends under load, thus maintaining a more uniform bearing stress. This indicates that using a higher stiffness fastener would provide an improvement in the stress distribution within the laminate and increase joint strength.

For joints constructed using stiff washers, with a clamping pressure of 50MPa, changing the row spacing was shown to have only a marginal influence on the joint strength. For a standard washer diameter ($2.0d_{bo}$) selecting a small row spacing resulted in a slight improvement in joint performance, as the lowest failure indices were recorded and the likelihood of failure in the net-tension plane was reduced.

For joints constructed using a large washer diameter ($3.5d_{bo}$), the joint strength was improved compared to those containing a standard sized washer, however, the strength was not significantly affected by altering the row spacing. This was considered to arise as the load in this case is carried entirely by the clamping mechanism, hence the fastener location appears less influential. The failure indices were higher around the tension plane than at the bearing plane due to the washer clamping, indicating that tensile failure may result from using a larger diameter washer. However, the likelihood of failure occurring through this mechanism is reduced as the row spacing is increased. This is in contrast to the observation made previously for joint configurations containing a standard size washer.

Comparing the results obtained in the failure analysis for single and multiple bolt joints, it can be seen that the single bolt joint, having a 4mm thick steel washer, has smaller failure indices around the hole boundary than the multiple bolt joint (with a 3mm thick ceramic washer). This is due to a slight difference in the bending stiffness between the two washer types. However, the multiple bolt joints have lower indices inside and outside the washer edge than the single bolt joints, which may also be attributed to the difference in bending stiffness as well as fastener interaction. These conclusions indicate that different failure modes would prevail for each type of joint under comparable loading conditions.

8.3 –ACHIEVEMENTS OF THIS WORK

An original three dimensional model was developed which enabled simulation of each entity within a mechanically fastened double lap joint. This resulted in a more realistic simulation than has previously been reported, as the elasticity of each component as well as the contact interaction could be modelled.

Clamping parameters such as the bolt preload and washer size were shown to influence the joint strength. Optimum values were suggested for these parameters in order to obtain a more even load transfer and good joint strength in design. Laminate and bolt elasticity also affect the bolt to hole contact area and hence stress distribution and strength, thereby highlighting the importance of including these parameters within a simulation for this type of mechanically fastened joint.

This model was extended to assess a more commonly used multiple bolt joint configuration and is the first investigation to use a realistic simulation to examine joint performance in relation to the geometric parameters of the joint. The study has shown the effects attributable to fastener interaction and clamping preload on the stress distribution in critical regions within the laminates. With optimum clamping conditions variations in row spacing were shown to exert only a marginal effect on the joint strength, although contact conditions between the laminates may be affected with smaller row spacings.

8.4 – SUGGESTIONS FOR FURTHER WORK

This section provides suggestions for improving the joint configuration and strength prediction techniques to extend the work reported here.

8.4.1 – Joint configuration

In this study out of plane deformation at the end of the outer lap has been shown to occur for single and multiple bolt joints. By applying a clamping preload to a sufficiently stiff washer the out of plane deformation of the laminate is reduced but not eliminated. The joint is more efficient but may be improved if the contact area can be extended across the entire joint interface. Recent advances in adhesives technology have meant that a hot-melt epoxy, which can be re-melted for disassembly, may be applied to a mechanically fastened joint and thereby improve interfacial contact between the laps. This is likely to reduce out of plane deformation and improve strength and the joint may still be disassembled for inspection or renewal.

The multiple bolt joint analysed in this work has a staggered fastener arrangement. Further studies should be conducted on other multiple joint configurations and an investigation into the effect of pitch distance on the joint strength should be addressed, as fastener interaction has shown to influence the stress distribution and failure indices. This would be a useful topic to address since it is unlikely, based on the results contained in this study, that failure analysis of single fastener joints can be used in predicting the strength of multiple bolt joints, particularly if a sufficiently high clamping load is neglected, (excepting cases with very little bolt interaction).

In this study it was assumed that the same load was applied to each bolt within a single row of a multi-fastened joint and as a consequence of the symmetry conditions applied to the model an area of an infinitely wide plate is considered in the analysis. Hence, as a comparison it would be interesting to assess the stress distribution and failure index results for different joint geometries in finite width laminates. The effects of bolt/hole tolerance on the distribution of load between each of the fasteners should also be investigated using a statistical approach, since in practice it would be very difficult to ensure a perfect fit between each fastener and hole.

The effects of various geometric and material parameters on the joint strength of statically loaded tensile joints have been investigated in this study. It may also be necessary to investigate these parameters under multiple load conditions, depending upon the typical application of the joint. Further analysis should be carried out with the single or multiple fastener joints subjected to bending and/or dynamic loading.

8.4.2 – Method of analysis

The failure indices reported for each investigation provide an insight into the approximate first ply failure strength. This work should be extended so that the final failure strength of the joint can be predicted by undertaking a progressive damage model. In such analyses the properties of an element are reduced if the failure index exceeds unity and the load is increased until failure of a sufficient number of elements has occurred. However, a non-linear analysis would have to be used, resulting in a significant increase in the computational resource.

The delamination indices provided in the graphs throughout this study are shown to be very low. This could be due to the fact that average element stresses were used in the failure criterion, and hence the indices could only be used for a comparative assessment of joint parameters, rather than an indication of joint strength. Although previous work has reported that the stresses should be averaged over a small distance from the hole boundary to avoid singularities, the distance should be determined by comparing a range of derived strengths with experimentally obtained values. Experimental testing should be carried out to determine this distance and also to compare results obtained from this study.

Mesh refinement should also be considered in further work, as out-of-plane stresses may be evaluated with greater accuracy than reported in this study, providing an appropriate element aspect ratio is maintained. This would also improve the delamination and ply failure index results. With the advent of more powerful computers significant mesh refinement in the vicinity of the hole boundary and at each ply interface would be desirable; this is unlikely to significantly increase the processing time. Higher order parabolic elements could also be employed, however, care must be taken when using contact elements in this case as in some contact algorithms negative contact forces can exist at the corner nodes (Camanho, 1999).

The delamination and ply failure strength predictions may also be improved if a resin rich layer is incorporated between each lamina of the laminate. However, as this layer would be very thin in comparison to a lamina, the mesh would have to be much more refined to provide an adequate aspect ratio, and a non-linear material analysis may also be necessary, which would therefore greatly increase the computational costs.

Clearly semi-empirical approaches to failure prediction have provided excellent correlation with experimental work and are considered very useful for the design of mechanically fastened composite joints. Even simplified two-dimensional finite element analysis can be used to provide accurate ultimate failure prediction, once correlation with experimental strengths has been carried out. The three-dimensional finite element analysis as used in this study could be incorporated into a semi-empirical design procedure, which uses characteristic distances at various angles around the hole boundary, as proposed by Arnold et al. (1990), or a characteristic curve as adopted by Chang et al. (1982). With three-dimensional analysis it would be possible to predict all possible failure modes and could be used to provide first ply failure and ultimate failure strengths for various joint geometries. However, this procedure would require complicated experimental studies such as the acoustic emission techniques to determine the onset of first ply failure, so that a relationship between the three-dimensional stress distribution and failure strength may be established.

Analytical equations currently used to calculate the strength and number of bolts required in joints constructed from isotropic materials, such as steel, may be adapted and applied to composite laminate joints and then compared with the work reported here. The stiffness of the bolt can be easily determined from simple calculations, while the laminate stiffness may be determined using the pressure cone angle, as described by Shigley (1986) with an appropriate modification to account for the anisotropic material properties. The resultant load on the bolt and the plate could then be predicted for a given size of washer. Using this method it may also be possible to determine an optimum preload from an assessment of the load transferred by each bolt.

REFERENCES

Abd-El-Naby, S. F. M., and Hollaway, L. (1993a): "The experimental behaviour of bolted joints in pultruded glass/polyester material. Part 1: Single-bolt joints", Composites, Vol. 24, No. 7, pp. 531-538

Abd-El-Naby, S. F. M., and Hollaway, L. (1993b): "The experimental behaviour of bolted joints in pultruded glass/polyester material. Part 2: Two-bolt joints", Composites, Vol. 24, No. 7, pp. 539-546

Agarwal, B. L. (1980): "Static strength prediction of bolted joints in composite materials", AIAA, Vol. 18, pp. 1371-1375

Akay, M., and Kong-Ah-Mun, S. (1995): "Bearing strength of autoclave and oven cured Kevlar/epoxy laminates under static and dynamic loading", Composites Vol. 26, No. 6, pp. 451-456

Andreasson, N., Mackinlay, C. P., and Soutis, C. (1998): "Experimental and numerical failure analysis of bolted joints in CFRP woven laminates", The Aeronautical Journal, December 1998, pp. 445-450

Ankara, A. O. and Dara, G. (1994): "Computer modeling of mechanical joints in advanced composites", PD-Vol. 64-2, Engineering Systems Design and Analysis, Vol. 2, ASME

Arnold, W. S., Marshall, I. H. and Wood, J. (1989): "Effects of biaxial loading in pin jointed CFRP plates" Composite Structures 5, Elsevier, 24-26 July

Arnold, W. S., Marshall, I. H. and Wood, J. (1990): "Optimum design considerations for mechanically fastened composite joints" Composite Structures, Vol. 16, pp. 85-101

Azzi, V. D. and Tsai, S. W. (1965): "Anisotropic strength of composites", Experimental Mechanics, pp. 283-289

Bailie, J. A., Fisher, L. M., Howard, S. A., and Perry, K. G. (1981): "Some environmental and geometric effects on the static strength of graphite cloth epoxy bolted joints" Composite Structures, Marshall, I. H. (ed.), Applied Science publishers Ltd.

Barbero, E. J. (1988): "Introduction to composite materials design" Taylor & Francis Ltd.

Barboni, R., Carbonaro, R. and Gaudenzi, P. (1995): "On the use of a multilayer higher-order theory for the stress analysis around a circular hole of laminates in tension", Composite Structures, Vol. 32, pp. 649-658

Barrois, W. (1978): "Stresses and displacements due to load transfer by fasteners in structural assemblies", Engineering Fracture Mechanics, Vol. 10, pp. 115-176

Benchekchou, B. and White, R. G. (1993): "Stresses around fasteners in composite materials", AIAA

Benchekchou, B. and White, R. G. (1995a): "Stresses around fasteners in composite structures in flexure and effects on fatigue damage initiation part 1: cheese-head bolts", Composites Structures, Vol. 33, pp. 95-108

Benchekchou, B. and White, R. G. (1995b): "Stresses around fasteners in composite structures in flexure and effects on fatigue damage initiation part 2: countersunk bolts", Composite Structures, Vol. 33, pp. 109-119

Brewer, J. C. and Lagace, P. A. (1988): "Quadratic stress criterion for initiation of delamination", Journal of Composite Materials, Vol. 22, pp. 1141-1155

Camanho, P. M. P. R. D. C. (1999): "Application of numerical methods to the strength prediction of mechanically fastened joints in composite laminates", PhD. Thesis, University of London, 1999

Chang, F. K., Scott, R. A. and Springer, G. S. (1982): "Strength of mechanically fastened composite joints" Journal of Composite materials, Vol. 16, pp. 470-494

Chang, F. K., Scott, R. A. and Springer, G. S. (1984a): "Failure of composite laminates containing pin loaded holes – method of solution" Journal of Composite Materials, Vol. 18, pp. 255-278

Chang, F. K., Scott, R. A. and Springer, G. S. (1984b): "Design of composite laminates containing pin loaded holes" Journal of Composite Materials, Vol. 18, pp. 279-289

Chang, F. K. and Chang, K. Y. (1987a): "A progressive damage model for laminated composites containing stress concentrations" Journal of Composite Materials, Vol. 21, pp. 834-855

Chang, F. K. and Chang, K. Y. (1987b): "Post-failure analysis of bolted composite joints in tension or shear-out mode failure" Journal of Composite Materials, Vol. 21, pp. 809-833

Chen, W. H. and Lee, S. S. (1995): "Numerical and experimental failure analysis of composite laminates with bolted joints under bending loads", Journal of Composite Materials, Vol. 29, No. 1, pp. 15-36

Chen, W. H, Lee, S. S. and Yeh, J. T. (1995): "Three dimensional contact stress analysis of a composite laminate with bolted joint", Composite Structures, Vol. 30, pp. 287-297

Chutima, S., and Blackie, A. P. (1996): "Effect of pitch distance, row spacing, end distance and bolt diameter on multi-fastened composite joints", Composites, Part A, Vol. 27A, pp. 105-110

Chutima, S. (1996): "Computer aided analysis of mechanically fastened composite laminates", Ph.D. Thesis, University of London, May 1996

Cohen, D., Hyer, M. W., Shuart, M. J., Griffin, O. H., Prasad, C., and Yalamanchili, S. R. (1995): "Failure criterion for thick multifastener graphite epoxy composite joints", Journal of Composites Technology & Research, pp. 237-248

Collings, T. A. (1977): "The strength of bolted joints in multi-directional CFRP laminates", Composites, January 1977, pp. 43-55

Collings, T. A. (1982): "On the bearing strengths of CFRP laminates", Composites, July 1982, pp. 241-252

Conti, P. (1986): "Influence of geometric parameters on the stress distribution around a pin-loaded hole in a composite laminate", Composites Science and Technology, Vol. 25, pp. 83-101

Cook, R. D. (1995): "Finite element modelling for stress analysis", John Wiley & Sons, New York

Cooper, C., and Turvey, G. J. (1995): "Effects of joint geometry and bolt torque on the structural performance of single bolt tension joints in pultruded GRP sheet material", Composite Structures, Vol. 32, pp. 217-226

Dano, M. L., Gendron, G. and Picard, A. (2000): "Stress and failure analysis of mechanically fastened joints in composite laminates", Composite Structures, Vol. 50, pp. 287-296

De Jong, T. (1977): "Stresses around pin-loaded holes in elastically orthotropic or isotropic plates", Journal of Composite Materials, Vol. 11, pp. 313-331

Eriksson, L. I. (1986): "Contact stresses in bolted joints of composite laminates", Composite Structures, Vol. 6, pp. 57-75

Eriksson, I. (1990): "On the bearing strength of bolted graphite/epoxy laminates", Journal of Composite Materials, Vol. 24, pp. 1246-1269

Eriksson, I., Backlund, J., and Moller, P. (1995): "Design of multiple-row bolted composite joints under general in-plane loading", Composites Engineering, Vol. 5, No. 8, pp. 1051-1068

Erki, M. A. (1995): "Bolted glass-fibre-reinforced plastic joints", Canadian Journal of Civil Engineering, Vol. 22, pp. 736-744

Fracchia, C. A., and Bohlmann, R. E. (1994): "The effects of assembly induced delaminations at fastener holes on the mechanical behavior of advanced composite materials", 39th International SAMPE Symposium, April 11-14, pp. 2665-2678

Gamble, K., Pilling, M. and Wilson, A. (1995): "An automated finite element analysis of the initiation and growth of damage in carbon fibre composite materials", Composite Structures, Vol. 32, pp. 265-274

Ger, G. S., Kawala, K., and Itabashi, M. (1996): "Dynamic tensile strength of composite laminate joints fastened mechanically", Theoretical and Applied Fracture Mechanics, Vol. 24, pp. 147-155

Godwin, E. W., Matthews, F. L., and Kilty, P. F. (1982): "Strength of multi-bolt joints in GRP", Composites, Vol. 13, pp. 268-272

Graham, U., Wisnom, M. R., and Webber, J. P. H. (1994): "A novel finite element investigation of the effects of washer friction in composite plates with bolt filled holes", Composite Structures, Vol. 29, pp. 329-339

Hamada, H., Haruna, K., and Maekawa, Z. I. (1995): "Effects of stacking sequences on mechanically fastened joint strength in quasi-isotropic carbon-epoxy laminates", Journal of Composites Technology & Research, Vol. 17, No. 3, pp. 249-259

Hanauska, J., Kradinov, V., and Madenci, E. (2001): "A composite double-lap joint with staggered bolts: an experimental and analytical investigation", Composite Structures, Vol. 54, pp. 3-15

Hancox, N. L. and Mayer, R. M. (1994): "Design data for reinforced plastics", First Edition, Chapman & Hall, London

Hart-Smith, L. J. (1978): "Mechanically-fastened joints for advanced composites – phenomenological considerations and simple analysis", Douglas Paper 6748, pp. 1-32

Hashin, Z. (1980): "Failure criteria for unidirectional fiber composites", Journal of Applied Mechanics, Vol. 47, pp. 329-334

Hassan, N. K., Mohamedien, M. A. and Rizkalla, S. H. (1996): "Finite element analysis of bolted connections for PFRP composites", Composites, part B, Vol. 27B, pp. 339-349

Hill, R. (1950): "The mathematical theory of plasticity" Oxford Press, 1950

Hodgkinson, J. M., De Beer, D. L., and Matthews, F. L. (1986): "The strength of bolted joints in 'Kevlar' RP", Proceedings of Workshop: 'Composites design for Space Applications', ESTEC, Noordwijk, 15-18 October 1985, pp. 53-61

Hollmann, K. (1996): "Failure analysis of bolted composite joints exhibiting in-plane failure modes", Journal of Composite Materials, Vol. 30, No. 3, pp. 358-384

Hu, F. Z., Soutis, C. and Edge, E. C. (1997): "Interlaminar stresses in composite laminates with a circular hole", Composite Structures, Vol. 37, pp. 223-232

Hung, C. L., and Chang, F. K. (1996): "Bearing failure of bolted composite joints. Part II: Model and Verification", Journal of Composite Materials, Vol. 30, No. 12, pp.1359-1401

Hyer, M. W., and Chastain, P. A. (1988): "Effect of bolt load proportioning on the capacity of multiple bolt composite joints", Journal of Aircraft, Vol. 25, No. 2, pp. 184-189

Hyer, M. W., Klang, E. C. and Cooper, D. E. (1987): "The effects of pin elasticity, clearance, and friction on the stresses in a pin-loaded orthotropic plate

Iarve, E. (1995): "Three dimensional stress analysis of fastener hole composites", MD-Vol. 69-1, 1995 IMECE, Proceedings of the ASME Materials Division

Iarve, E. (1997): "Three-dimensional stress analysis in laminated composites with fasteners based on the B-spline approximation", Composites, part A, Vol. 28A, pp. 559-571

I-DEAS Master Series 1.3c/7.0 (1993/1999), 2000 Eastman Drive, Milford, OH 45150, USA

Ireman, T. (1998): "Three-dimensional stress analysis of bolted single-lap composite joints", Composite Structures, Vol. 43, pp. 195-216

Ireman, T., Nyman, T., and Hellbom, K. (1993): "On design methods for bolted joints in composite aircraft structures", Composite Structures, Vol. 25, pp. 567-578

Jurf, R. A. and Vinson, J. R. (1990): "Failure analysis of bolted joints in composite laminates", Composite Materials, Vol. 9, pp. 165-190

Kallmeyer, A. R., and Stevens, R. I. (1997): "Creep elongation of bolt holes subjected to bearing loads in a polymer matrix composite laminate", Composite Materials: Fatigue and Fracture, pp. 452-467

Kang, T. J., and Lee, K. W. (1997): "Strength prediction for mechanical joints in laminated composite plate using progressive failure analysis", Polymers & Polymer Composites, Vol. 5, No. 5, pp. 343-351

Kim, J. Y. and Hong, C. S (1991): "Three-dimensional finite element analysis of interlaminar stresses in thick composite laminates", Computers & Structures, Vol. 40, No. 6, pp.1395-1404

Kim, S. J. and Kim, J. H. (1995): "Finite element analysis of laminated composite plates with multi-pin joints considering friction", Computers & Structures, Vol. 55, No. 3, pp. 507-514

Ko, H. Y., Kwak, B. M. and Im, S. (1996): "Contact stress and failure analysis on bolted joints in composite plates by considering material nonlinearity", Computer Aided Design in Composite Material Technology V, Ch. 35, pp. 31-40

Kretsis, G., and Matthews, F. L. (1985): "The strength of bolted joints in glass fibre/epoxy laminates", Composites, Vol. 16, pp. 92-102

Lekhnitskii, S. G. (1968): "Anisotropic plates", Translated by Tsai, S. W. and Cheron, T., Gordon and Breach Science Publishing, New York

Lessard, L. B., and Shokrieh, M. M. (1995): "Two-dimensional modeling of composite pinned joint failure", Journal of Composite Materials, Vol. 29, No. 5, pp. 671-697

Lessard, L. B., Shokrieh, M. M. and Esbensen, J. H. (1993): "Analysis of stress singularities in laminated composite pinned/bolted joints". 38th International SAMPE Symposium, May 10-13, pp.53-56

Lucking, W. M. (1990): "On the maximum strength of single bolt fastened joints of graphite/epoxy laminate", Development and Design with Advanced Materials, Sih, G. C., Hoa, S. V., Pindera, J. T. (Editors), Elsevier Science Publishers B. V., pp. 149-154

Madenci, E., Shkarayev, S., Sergeev, B., Oplinger, D. W. and Shyprykevich, P. (1998): "Analysis of composite laminates with multiple fasteners", International Journal of Solids and Structures, Vol. 35, No. 15, pp. 1793-1811

Mangalgiri, P. D. and Dattaguru, B. (1986): "A large orthotropic plate with misfit pin under arbitrary oriented biaxial loading" Composite Structures, Vol. 6, pp. 271-281

Marshall, I. H., Arnold, W. S., Wood, J. and Mousley, R. F. (1989): "Observations on bolted connections in composite structures", Composite Structures, Vol. 13, pp133-151

Matthews, F. L., Roshan, A. A., and Phillips, L. N. (1982a): "The bolt bearing strength of glass/carbon hybrid composites", Composites, July 1982, pp. 225-227

Matthews, F. L., Wong, C. M. and Chryssafitis, S. (1982b): "Stress distribution around a single bolt in fibre-reinforced plastic", Composites, pp. 316-322

Morgan, M. E., and Beckwith, S. W. (1985): "Bolt torque loading and radial gap effects on thick-wall composite joints strength", 30th National SAMPE Symposium March 19-21, 1985, pp. 1321-1334

Murthy, A. V., Dattaguru, B., Narayana, H. V. L., and Rao, A. K. (1990): "An improved iterative finite element solution for pin joints", Computers & Structures, Vol. 36, No. 6, pp. 1121-1128

Murthy, A. V., Dattaguru, B., Narayana, H. V. L., and Rao, A. K. (1991): "Stress and strength analysis of pin joints in laminated anisotropic plates", Composite Structures, Vol. 19, pp. 299-312

Naidu, A. C. B., Dattaguru, B., Mangalgiri, P. D. and Ramamurthy, T. S. (1985) "Analysis of a finite composite plate with smooth rigid pin", Composite Structures, Vol. 4, pp. 197-216

Naik, R. A., and Crews, J. H.(Jr) (1986): "Stress analysis method for a clearance fit bolt under bearing loads", AIAA, Vol. 24, No. 8, pp. 1348-1353

Oakeshott, J. L., and Matthews, F. L. (1994): "Determination of fastener load distribution in double lap composite joints", PD-Vol. 64-2, Engineering Systems Design and Analysis, Volume 2, ASME 1994, pp. 243-251

Oh, J. H., Kim, Y.G., and Lee, D. G. (1997): "Optimum bolted joints for hybrid composite materials", Composite Structures, Vol. 38, No. 1-4, pp. 329-341

Packman, P. F., Hietala, H. J., and Schultz, K. C. (1993): "An experimental and statistical analysis of some fastener anomalies on the bolted joint strength of graphite/epoxy laminates", 38th International SAMPE Symposium, May 10-13, 1993, pp. 66-80

Parida, B. K., Prakash, R. V., Mangalgiri, P. D., and Vijayarya, K. (1997): "Influence of environmental and geometric parameters on the behavior of fastener joints in advanced composites", Composite Materials: Fatigue and Fracture, pp. 432-451

Phillips, L. N. (1989): "Design with advanced composite materials", The Design Council, London

Prabhakaran, R., and Naik, R. A. (1987): "A fiber-optic technique for the measurement of contact angle in a clearance-fit pin loaded hole", Experimental Techniques, April 1987, pp. 20-22

Quinn, W. J., and Matthews, F. L. (1977): "The effect of stacking sequence on the pin-bearing strength in glass fibre reinforced plastic", Journal of Composite Materials, Vol. 11, pp. 139-145

Rahman, M. U., Rowlands, R. E., Cook, R. D., and Wilkinson, T. L. (1984): "An iterative procedure for finite element stress analysis of frictional contact problems", Computers & Structures, Vol. 18, No. 6, pp. 947-954

Rahman, M. U., and Rowlands, R. E. (1993): "Finite element analysis of multiple bolted joints in orthotropic plates", Computers & Structures, Vol. 46, No. 5, pp. 859-867

Raju, I. S. and Crews, J. H. Jr (1982): "Three-dimensional analysis of $(0/90)_s$ and $(90/0)_s$ laminates with a central circular hole", Composites Technology Review, Vol. 4, No. 4, Winter 1982, pp. 116-124

Reddy, J. N. and Pandey, A. K. (1987): "A first-ply failure analysis of composite laminates", Computers & Structures, Vol. 25, pp. 371-393

Reid, R. L., Chen, P., Black, K., and El-Shiekh, A. (1994): "Bearing behavior of 3-D braided carbon/epoxy composite joints", 39th International SAMPE Symposium, April 11-14, 1994, pp. 2013-2022

Rosner, C. N., and Rizkalla, S. H. (1995): "Bolted connections for fiber-reinforced composite structural members: experimental program", Journal of Materials in Civil Engineering, November 1995, pp. 223-231

Rowlands, R. E., Rahman, M. U., Wilkinson, T. L., and Chiang, Y. I. (1982): "Single and multiple bolted joints in orthotropic materials", Composites, pp. 273-279

Rufin, A. C. (1995): "Fastener hole reinforcement in composites using cold expanded inserts", Journal of Composites Technology & Research, Vol. 17, No. 2, pp. 145-151

Saunders, D. S., Galea, S. C. and Deirmendjian, G. K. (1993): "The development of fatigue damage around fastener holes in thick graphite/epoxy composite laminates", Composites, Vol. 24, No. 4, pp. 309-321

Serabian, S. M. (1991): "The effects of nonlinear intralaminar shear behavior on the modelling accuracy of $((0/90)_3/0)_s$ and $((+45/-45))_{3s}$ pin loaded laminates", Journal of Composites Technology & Research, Vol. 13, No. 4, pp. 236-248

Shigley, J. E. (1986): "Mechanical engineering design" McGraw-Hill, Int. Edition, ISBN: 0-07-100292-8

Smith, P. A. (1985): "Aspects of the static and fatigue behaviour of composite laminates, including bolted joints", Ph.D. Thesis, Cambridge University, Engineering Department

Smith, P. A. and Pascoe, K. J. (1985): "Behaviour of bolted joints in $(0/90)_{ns}$ laminates", Technical Report (CUED/C/MATS/TR.121), Cambridge University, Engineering Department

Smith, P. A., Pascoe, K. J., Polak, C., and Stroud, D. O. (1986): "The behaviour of single-lap bolted joints in CFRP laminates", Composite Structures, Vol. 6, pp. 41-55

Soni, S. R. (1981): "Failure analysis of composite laminates with a fastener hole", ASTM Special Technical Publication, Joining of Composite Materials, STP749, 1981

Starikov, R. and Schön, J. (2001): "Quasi-static behaviour of composite joints with protruding-head bolts", Composite Structures, Vol. 51, pp. 411-425

Stockdale, J. H., and Matthews, F. L. (1976): "The effect of clamping pressure on bolt bearing loads in glass fibre reinforced plastics", Composites, Vol. 7, pp. 34-38

Sun, C. T. (1998): "Mechanics of aircraft structures", John Wiley & Sons, New York

Tong, L. (2000): "Bearing failure of composite bolted joints with non-uniform bolt-to-washer clearance", Composites Part A, Vol. 31, pp. 609-615

Tsai, W. S. and Wu, E. M. (1971): "A general theory of strength of anisotropic materials", Journal of Composite Materials, Vol. 5, pp. 58-80

Tsujimoto, Y., and Wilson, D. (1986): "Elasto-plastic failure analysis of composite bolted joints", Journal of Composite Materials, Vol. 20, pp236-252

Tsumara, T., Zako, M., Takano, N. and Tsujikami, T. (1995): "Development of three-dimensional finite element method for composite materials based on damage mechanics", Composites '95:Recent advances in Japan and the United States, pp.69-74

Turvey, G. J. (1998): "Single bolt tension joint tests on pultruded GRP plate – effects of tension direction relative to pultrusion direction", Composite Structures, Vol. 42, pp. 341-351

Walsh, R., Vedula, M., and Koczak, M. J. (1989): "A comparative assessment of bolted joints in a graphite reinforced thermoset vs. thermoplastic", SAMPE Quarterly, July 1989, pp. 15-19

Wang, S., and Han, Y. (1988): "Finite element analysis for load distribution of multi-fastener joints", Journal of Composite Materials, Vol. 22, pp. 124-135

Wang, H. S., Hung, C. L., and Chang, F. K. (1996): "Bearing failure of bolted composite joints. Part I: Experimental characterization", Journal of Composite Materials, Vol. 30, No. 12, pp. 1284-1313

Webber, J. P. H., Graham, U., and Wisnom, M. R. (1997): "Strain distributions around fasteners in laminated plates under biaxial in-plane loading", Journal of Strain Analysis, Vol. 32, No. 3, pp. 167-174

Whitney and Nuismer, (1974): "Stress fracture criteria for laminated composites containing stress concentrations" Journal of Composite Materials, Vol. 8, pp. 253-265

Whitworth, H. A. (1998): "Fatigue evaluation of composite bolted and bonded joints", Journal of Advanced Materials, pp. 25-31

Wilkinson, T. L., Rowlands, R. E., and Cook, R. D. (1981): "An incremental finite element determination of stresses around loaded holes in wood plates", Computers & Structures, Vol. 14, No. 1-2, pp. 123-128

Wilson, D. W. and Pipes, R. B. (1981): "Analysis of the shearout failure mode in composite bolted joints", Composite Structures, Marshall, I. H. (Ed.), Applied Science Publishers Ltd., pp. 34-49

Wilson, D.W. and Tsujimoto, Y. (1986): "On phenomenological failure criteria for composite bolted joint analysis", Composites Science & Technology, Vol. 26, pp. 283-305

Wood, J. (1994): "Finite element analysis of composite structures", Composite Structures, Vol. 29, pp. 219-230

Yamada, S. E. and Sun, C. T. (1978): "Analysis of laminate strength and its distribution", Journal of Composite Materials, Vol. 12, pp. 275-284

Ye, L. (1988): "Role of matrix resin in delamination onset and growth in composite laminates", Composite Science & Technology, Vol. 33, pp. 257-277

Young, W. C. (1989): "ROARK'S formulas for stress and strain", 6th Edition, McGraw-Hill, Inc.

Zhang, K. D. and Ueng, C. E. S. (1984): "Stresses around a pin-loaded hole in orthotropic plates", Journal of Composite Materials, Vol. 18, pp. 432-446

Zhang, K. D. and Ueng, C. E. S. (1988): "A simplified approach for interlaminar stresses around a hole in $[0/90]_s$ laminates", Journal of Composite Materials, Vol. 22, pp. 192-202

Zimmerman, K. B. (1991): "Mechanical fastening of FGRP composites", AIAA, Vol. 29, No. 6, pp.1009-1011

APPENDIX A

FAILURE THEORIES

When considering joint strength of composite laminates either the ultimate strength or first ply failure strength can be used, however, for design purposes it is often preferable to provide conservative strength estimations by using the first ply failure approach. With this method a macromechanical failure theory can be used to predict at what load failure of an individual ply may occur, assuming that the ply in the laminate is the same strength as a single remote ply. The load applied is then assumed to be the maximum allowable strength of the laminate joint.

The macromechanical failure theories available for isotropic materials, such as the maximum normal stress (Rankine), maximum shear stress (Tresca), and maximum distortional energy (Von Mises), have been modified for application to orthotropic materials such as individual composite laminae. The most commonly used failure theories for composite laminates are as detailed below.

Maximum Stress

This is one of the simplest failure theories, which assumes that failure of a ply will occur if any one or more of the individual stress components in material coordinates exceeds the corresponding strength component, hence, no failure will occur as long as the following condition is met:

$$-X_c < \sigma_1 < X_t \tag{A.1}$$

$$-Y_c < \sigma_2 < Y_t \tag{A.2}$$

$$|\tau_{12}| < S \tag{A.3}$$

Where:

σ_1 = direct stress component in the fibre direction

σ_2 = direct stress component in the transverse direction

τ_{12} = shear stress

X_c, X_t = longitudinal compressive and tensile strength respectively of a lamina

Y_c, Y_t = transverse compressive and tensile strength respectively of a lamina

S = shear strength of a lamina

However, this method is not able to predict failure when two or more stress components are just below the strength in their respective directions. This is a shortcoming of this criterion, as interaction effects are known to occur which may initiate failure.

Maximum Strain

This criterion is similar to the maximum stress theory and is probably the most commonly used in industry as it is easy to use and is comparatively more accurate, since allowable strain data is more precise for certain materials compared with allowable stress data. Failure is assumed to occur if any of the strain components exceeds the corresponding allowable strain, hence failure will not occur as long as the following conditions are met:

$$-X_{\varepsilon c} < \varepsilon_1 < X_{\varepsilon t} \tag{A.4}$$

$$-Y_{\varepsilon c} < \varepsilon_2 < Y_{\varepsilon t} \tag{A.5}$$

$$|\gamma_{12}| < S_\gamma \tag{A.6}$$

Where:

ε_1 = principal strain in the fibre direction

ε_2 = principal strain in the transverse direction

γ_{12} = shear strain

$X_{\varepsilon c}$, $X_{\varepsilon t}$ = allowable longitudinal compressive and tensile strain respectively

$Y_{\varepsilon c}$, $Y_{\varepsilon t}$ = allowable transverse compressive and tensile strain respectively

S_γ = allowable shear strain

This criterion suffers the same shortcomings as the maximum stress theory as it does not take interaction effects into consideration.

Tsai-Hill

In an attempt to gain greater accuracy in failure prediction, Azzi and Tsai (1965) used a criterion similar to Von Mises to account for plasticity of metals but adapted it for use with orthotropic composite laminates. Failure is expected to occur if the following relationship is satisfied:

$$\frac{\sigma_1^2}{X^2} - \frac{\sigma_1\sigma_2}{X^2} + \frac{\sigma_2^2}{Y^2} + \frac{\tau_{12}^2}{S^2} = 1 \tag{A.7}$$

The shortcoming of using this method is that it does not distinguish between compressive and tensile strengths, so a decision has to be made as to which strength value is used in the equation. A conservative failure strength may be obtained when using the lower value of strength along each direction. However, if the values of the compressive and tensile strengths for the material are very different, then the results would be more inaccurate, and hence a theory incorporating both tensile and compressive strengths would be more appropriate.

Another shortcoming is that the mode of failure is not identified as it is with the maximum stress and maximum strain criteria.

Hoffman

This criterion is similar to Tsai-Hill but with added terms to enable more accurate prediction of failure for laminae which have different strengths in tension and compression.

$$\left(\frac{1}{X_t} - \frac{1}{X_c}\right)\sigma_1 + \left(\frac{1}{Y_t} - \frac{1}{Y_c}\right)\sigma_2 + \frac{\sigma_1^2}{X_t X_c} + \frac{\sigma_2^2}{Y_t Y_c} + \frac{\tau_{12}^2}{S^2} - \frac{\sigma_1\sigma_2}{X_t X_c} = 1 \tag{A.8}$$

This theory also does not differentiate between failure modes.

Tsai-Wu

The failure criterion given by Tsai and Wu (1971) also differentiates between compressive and tensile strengths and is an attempt to fit experimental data more accurately. Failure is predicted to occur when the following relationship is satisfied:

$$\left(\frac{1}{X_t}-\frac{1}{X_c}\right)\sigma_1+\left(\frac{1}{Y_t}-\frac{1}{Y_c}\right)\sigma_2+\frac{\sigma_1^2}{X_tX_c}+\frac{\sigma_2^2}{Y_tY_c}+\frac{\tau_{12}^2}{S^2}+2*F_{12}\sigma_1\sigma_2=1 \qquad \text{(A.9)}$$

F_{12} is an interaction coefficient, which accounts for the interaction between the two normal stresses. A biaxial test is needed to measure this coefficient and since experimental data are not easily available, an approximation for the coefficient must be taken:

$$F_{12}\cong-\frac{1}{2\sqrt{X_cX_tY_cY_t}} \qquad \text{(A.10)}$$

This method provides a close comparison to experimental data, however it is still unable to provide the failure mode as with the maximum stress and maximum strain criteria.

In a study to compare the different methods of failure prediction, Reddy and Pandey (1987) compared all of the above theories for composite plates under tensile and bending loads. It was concluded that all criteria are equivalent at predicting failure under tensile loading but the Tsai-Hill and maximum strain criteria gave different failure loads and locations to the other theories when transverse loading conditions are applied.

Delamination failure

The previous theories are appropriate for ply failure, however, for delamination failure, Ye (1988) used an equation based on the work by Hashin and Rotem (1974), to predict delamination between each ply.

The Ye delamination criterion predicts that delamination failure will occur if the following equality is satisfied:

When $\bar{\sigma}_3 > 0$:

$$\left(\frac{\bar{\sigma}_3}{Z}\right)^2 + \left(\frac{\bar{\tau}_{13}}{S}\right)^2 + \left(\frac{\bar{\tau}_{23}}{R}\right)^2 = 1 \qquad \text{(A.11)}$$

When $\bar{\sigma}_3 \leq 0$:

$$\left(\frac{\bar{\tau}_{13}}{S}\right)^2 + \left(\frac{\bar{\tau}_{23}}{R}\right)^2 = 1 \qquad \text{(A.12)}$$

Where:

R = interlaminar shear strength

Z = interlaminar normal strength

In previous work such as Zhang & Ueng (1988), Brewer & Lagace (1988) and Raju & Crews (1982), it has been reported that interlaminar stress singularities are known to exist at the hole boundary and between each lamina of angle ply laminates. It is therefore more appropriate to use an average stress criterion rather than a point stress criterion, whereby the stress values are averaged over a small distance away from the stress singularity. The distance from the free edge over which the stress values must be averaged should be determined experimentally.

APPENDIX B

SUBSIDIARY EQUATIONS

Calculation of bolt bending stiffness

The bolt shank bending stiffness can be calculated using the product of Young's modulus and the inertia, where the second moment of area about the neutral axis of bending is given by:

$$I = \frac{\pi d_{bo}^4}{64} \tag{B.1}$$

Equations for washer deflection and plate stiffness (Young, 1989)

The washer through thickness deflection is given by:

$$\delta_{wz} = \frac{L_w d_w^3}{D}\left(\frac{c_a l_b}{c_b} - l_a\right) \tag{B.2}$$

where D is the plate stiffness given by:

$$D = \frac{E t_w^3}{12\left(1 - v^2\right)} \tag{B.3}$$

δ_{wz} = washer through thickness deflection

d_w = washer outside diameter

L_w = load on the washer

c_a, c_b = plate coefficients

l_a, l_b = loading coefficients

t_w = washer thickness